TRP Channels and a Dextran Sulfate Activated Rise in Intracellular Ca^{2+} and Na^{+} in a Subpopulation of Double Positive Thymocytes

DEBORAH ANNE WOHLFAHRT

A thesis submitted for the degree of Doctor of Philosophy of

The Australian National University

July 2019

Declaration

This thesis contains no material which has been accepted for the award of any other degree or diploma in any university. To the best of the author's knowledge, it contains no material previously published or written by another person, except where due reference is made in the text.

Deborah Wohlfahrt

July 2019

Acknowledgements

I wish to express my deep gratitude to my supervisors Christian Stricker and Christopher Parish for their wealth of advice, kind guidance and enthusiasm throughout this project. I especially thank Christian for agreeing to supervise my rather non-neuroscience project. `1I believe we have both been intrigued by TRP channels and thymocytes as we delved into the field of immunology.

I also extend my sincere thanks to Harpreet Vohra and Mick Devoy for their invaluable advice and generous assistance with my flow cytometry problems, and for his valued advice and ideas on aspects of my project, I express my gratitude to Steve Daley.

To the Parish lab members - it was a fantastic opportunity to work alongside you. I enjoyed your company and music choices. I whole-heartedly thank you all, and especially David Simon Davis for his advice, assistance and patient training. Thank you to my friends in the Stricker lab, especially Le Thuy Van Tran whose insightful advice I regard most highly. I learned so much from our discussions over lunch-breaks in the sunshine and I am very grateful for her proof reading this thesis.

A special mention to my cheerleaders Lynne and Emily Raymont for their never-failing support and pep talks that kept me motivated and on track. I am also very grateful to my other family members and friends for all their encouragement and emotional support along the way.

Finally, I gratefully acknowledge the Australian National University for financial support provided by an Australian Government Research Training Program (RTP) Scholarship.

Abstract

This thesis presents the characteristics of the sustained rise of intracellular Ca^{2+} ($[Ca^{2+}]_i$) and Na^+ ($[Na^+]_i$), observed in pre-selection $CD4^+CD8^+$ (double-positive, DP) thymocytes when stimulated with dextran sulfate (DxS) and explores several candidate channels that may be involved in this rise. This $[Ca^{2+}]_i$ rise is proposed to mimic a physiological mechanism that influences early DP thymocyte selection and hence the T cell repertoire.

During thymopoiesis, the patterning of $[Ca^{2+}]_i$ plays a pivotal role in selection of DP thymocytes. In 1987, Tellam & Parish described such a slow and sustained Ca^{2+} rise in DP thymocytes which depended on a transmembrane influx of Ca^{2+}. The channel through which this Ca^{2+} entered remained elusive. Understanding the characterisation of this rise and its underlying signalling and conductance is pivotal to discovering the channel involved.

I have used flow cytometry (FACS) to concomitantly image $[Ca^{2+}]_i$ and $[Na^+]_i$ after DP thymocytes were exposed to 1 μg/ml DxS (500 kDa) using AM-loading of the indicators indo-1 and either ANG-2 or SBFI (5 μM for all). In some instances, Mg^{2+} was monitored with magfluo-4. The rises were evaluated when cells were exposed to activators and blockers of receptors, cell signalling enzymes and channels. In addition, FACS-based immunocytochemistry (ICC) was employed to determine if there was channel expression on the cell surface.

In Chapter 3, I found that the earlier described Ca^{2+} was also accompanied by a Na^+ rise. There was a delay to half-maximal amplitude of 10.8 ± 0.2 min and a rate of ~0.2 per min for both, and an amplitude of 165 ± 11 nM for Ca^{2+}. The one for Na^+ could not be quantified but is likely in the range of several hundred μM suggesting that a non-selective cation channel is involved that predominantly

passes Na^+ over Ca^{2+}. Notably, the DxS rises are prevented by a maintained elevation of $[Ca^{2+}]_i$ >~60 nM, but not by a transient rise. Additionally, the rises were absent if the recording temperature was ≤30°C and if $[Mg^{2+}]_o$ was ≥25 mM.

Activated by DxS, critical elements in the signalling cascade leading to channel opening include CD8β and LFA-1 as the rises were absent in thymocytes from CD8β$^{-/-}$ and LFA-1$^{-/-}$ mice. Furthermore, activation of the Src tyrosine kinase Lck also appears essential as PP2 abolished the rises. Downstream of Lck, both PI_3K and PLC activation is necessary as their inhibition by LY294002 and edelfosine, respectively, abolished the rises. The rises do not involve store release via IP_3 receptors and SOCE, suggesting that either PIP_2 hydrolysis and/or DAG generation lead to channel activation. Both disruption of F-actin polymerization and the tarantula toxin GsMTx4 abolished the rises, suggestive that mechanosensitive stimulation is involved. All these observations indicate that a non-specific cation channel of the TRP family could be involved.

In Chapter 4, commencing with a list of 14 TRP channels as candidates that share a number of the above properties, ICC and flow cytometry experiments are presented that indicate that the DAG-sensitive channels TRPC6, TRPA1 and TRPV1 are expressed and activatable in the membrane of these cells. However, none of these channels underlies the rises, as they were neither blocked by 2-APB, SKF96365, HC030031 or AMG9810, respectively. Rather, I observed that 2-APB potentiated the rises and ruthenium red abolished them, suggestive of involvement of either TRV2, TRPV3 or TRPM6. Since the rises were neither reduced by tranilast (TRPV2 blocker) nor NS8593 (TRPM6 blocker) it strongly suggests an involvement of TRPV3 in the cation rise in DP thymocytes. In support of this notion is the sensitisation by 2-APB and temperature (at 30°C) which when used independently do not cause a rise. But I cannot rule out the possibility that, upon DxS addition, the signalling cascade leading to TRPV3

activation depends on transient activation of a mechanosensitive channel such as piezo1. Such a Ca^{2+} rise, activated by a signalling cascade triggered by the CD8β coreceptors interacting with heparan sulfate on stromal cells, could synergistically enhance TCR signalling and fine tune selection, thus refining the repertoire of T cells.

During thymopoiesis possible inhibition of this mechanism, by fever spikes, may result in increased survival of thymocytes expressing TCRs with a high risk of self-reactivity. Importantly, progressive sialylation of developing T cells appears to negatively regulate the TRPV3 activation mechanism and so, in conditions that decrease sialylation, reactivation of TRPV3 cation influx in mature T cells is likely. Such a change might adversely increase the sensitivity to self-antigens of some T cell clones and lead to the onset of an autoimmune disorder.

1 Table of Contents

List of Figures

List of Tables

List of Appendices

Abbreviations

°C	Degree Celsius
Ab_1	Primary Antibody
Ab_2	Secondary Antibody
AF	Alexa fluor
AA	Arachidonic acid
ACSF	Artificial cerebral spinal fluid
ADPR	Adenosine diphosphate ribose
AM	Acetoxymethyl ester
ANG2 AM	Asante NaTRIUM Green-2 acetoxymethyl ester
APCs	Antigen presenting cells
APC	Allophycocyanin
ARD	Ankyrin repeat domain
ATP	Adenosine 5′-triphosphate
BSA	Bovine serum albumin
B6	C57BL/6 mouse strain
$[Ca^{2+}]_i$	Intracellular calcium concentration
$[Ca^{2+}]_o$	Extracellular calcium concentration
$[Ca^{2+}]_{ER}$	Endoplasmic reticulum calcium concentration
CaM	Calmodulin
CD	Cluster of differentiation
ConA	Concanavalin A
CRAC	Calcium release activated calcium
CHO	Chinese hamster ovary
cTECs	cortical thymic epithelial cells

cTEC^{hi}	cortical thymic epithelial cells that highly express heparan sulfate
DAG	Diacylglycerol
DN	Double Negative ($CD4^-$ $CD8^-$)
DP	Double Positive ($CD4^+$ $CD8^+$)
DxS	Dextran sulfate 500 kDa
ECM	extracellular matrix
EGTA	Ethylene glycol-bis(β-aminoethyl ether)-*N,N,N′,N′*-tetraacetic acid
FCS	Foetal calf serum
FFA	Free fatty acid
Fig.	Figure
FKBP	FK binding protein
FITC	Fluorescein isothiocyanate
HEK-293	Human embryo kidney-293 cell line
HEPES	2-[4-(2-hydroxyethyl)piperazin-1-yl]ethanesulfonic acid
HS	Heparan sulfate
IC_{50}	half maximal inhibitory concentration of a drug
ICAM-1	Intercellular adhesion molecule 1
ICC	Immunocytochemistry
ImmGen	Immunological Genome Project
Indo-1 AM	2-[4-(bis(carboxymethyl)amino)-3-[2-[2-(bis(carboxymethyl) amino)-5-methylphenoxy]ethoxy]phenyl]-1H-indole-6-carboxylic acid-acetoxymethyl
IP_3	Inositol 1,4,5-trisphosphate
IP_3R	Inositol trisphosphate receptor
IR-DIC	Infrared-differential interference contrast

K_d	dissociation constant
kDa	kilodalton
LFA-1	Lymphocyte function-associated antigen-1
LFA-3	Lymphocyte function-associated antigen-3
MHC	Major histocompatibility complex
mAb	Mouse antibody
$[Mg^{2+}]_o$	Extracellular Mg^{2+} concentration
Mm	Mus musculus
mRNA	messenger ribonucleic acid
miRNA	micro ribonucleic acid
mol. wt.	molecular weight
mV	millivolts
$[Na^+]_i$	Intracellular sodium concentration
$[Na^+]_o$	Extracellular sodium concentration
NMDG	N-methyl-D-glucamine
NUDT9-H	Nudix hydrolase motif 9-homology
OAG	1-Oleoyl-2-acetyl-sn-glycerol
p.	Page
PBS	Phosphate buffered saline
PI_3K	Phosphoinositide 3-kinase
PIP_2	Phosphatidylinositol 4,5-bisphosphate
PKC	Protein kinase C
PM	Plasma membrane
PLA	Phospholipase A
PLC-γ	Phospholipase C gamma
PLD	Phospholipase D
PUFA	Polyunsaturated fatty acid
rcf	Relative centrifugal force

RT	Room temperature
RuR	Ruthenium red
SAC	Stretch activated cation (channel)
SBFI AM	Sodium binding benzofurane isophthalate acetoxymethyl
SP	Single Positive
SP CD4	Single Positive $CD4^+$ $CD8^-$
SP CD8	Single Positive $CD4^-$ $CD8^+$
SOCE	Store operated calcium entry
STIM	Stromal interaction molecule
TCR	T-cell antigen receptor
TM	transmembrane
TRP	Transient receptor potential
TRPA	Transient receptor potential ankyrin
TRPC	Transient receptor potential canonical
TRPM	Transient receptor potential melastatin
TRPV	Transient receptor potential vanilloid
VDCC	Voltage dependent calcium channels
V_m	Membrane potential

1 Introduction

1.1 Calcium as a second messenger

In all eukaryotic cells, Ca^{2+} invariably has a vital role as a second messenger molecule. By modulating the activity of Ca^{2+} binding effector molecules such as calmodulin, kinases, phosphatases and transcription factors, Ca^{2+} enables the transduction of signalling pathways that drive diverse cellular functions. These cellular processes include gene expression, cell differentiation, proliferation, cytoskeleton remodelling, motility, cell survival and cell death (reviewed by Berridge *et al.* 2000, Carafoli & Krebs 2016, Clapham 2007a, Lewis 2001, Samanta & Parekh 2017).

1.1.1 Ca^{2+} homeostasis

Ca^{2+} exists in cells in either free or bound form. For cell signalling, the relevant Ca^{2+} is the free form. In thymocytes, (progenitor T lymphocytes, further described in section 1.3) the cell type under investigation in this thesis, the resting free cytosolic Ca^{2+} concentration ($[Ca^{2+}]_i$) is ~100–130 nM (Hesketh *et al.* 1983, Ishida & Chused 1988, Rogers *et al.* 1983, Ross *et al.* 1997, Tellam & Parish 1987, Tsien *et al.* 1982). This is approximately 10^4-fold lower than the concentration of free Ca^{2+} outside the cell ($[Ca^{2+}]_o$ ~1.2 mM; Walser 1961), approximately 10^2-fold lower than free Ca^{2+} concentration in the endoplasmic reticulum (ER; $[Ca^{2+}]_{ER}$ 10–250 μM; Corbett & Michalak 2000), and 5 to 10-fold lower than phosphate buffered Ca^{2+} within the mitochondrial matrix ($[Ca^{2+}]_{mit}$ 0.5–1 μM; Nicholls 2005).

This marked concentration gradient imparts in large driving force on Ca^{2+} to move into the cytosol upon activation of Ca^{2+} permeable ion channels located in the plasma membrane (PM) and the ER membrane. Countering the rise in ($[Ca^{2+}]_i$,

mechanisms that affect the transient binding (buffering) and removal of cytosolic Ca^{2+} rapidly activate. Adenosine triphosphate-dependent enzymatic pumps (ATPase), located on the PM (plasma membrane Ca^{2+} ATPase; PMCA) and the ER membrane (sarco-endoplasmic reticulum Ca^{2+} ATPase; SERCA), and ion transporters, such as sodium-calcium exchangers (NCX) and the mitochondrial Ca^{2+} uniporter (MCU) move Ca^{2+} from the cytosol back to either the extracellular compartment or into cellular organelles. Adding to these extrusion mechanisms, intracellular buffering proteins that bind Ca^{2+} with varying affinity further lower the free Ca^{2+} concentration (Milner *et al.* 1992). A schematic summary of the many mechanisms that may be involved in $[Ca^{2+}]_i$ regulation is presented in Figure 1.7 (p.77) where the role of ion channels and transporters in Ca^{2+} is presented in more detail.

Activation of these mechanisms differentially regulates the pattern of intracellular Ca^{2+} rises. Additionally, these mechanisms crucially maintain $[Ca^{2+}]_i$ homeostasis thereby preventing undesired $[Ca^{2+}]_i$ overload which is well established as cytotoxic and induces cell death (reviewed by Berridge *et al.* 1998, Putney 1999, Raffaello *et al.* 2016, Zhivotovsky & Orrenius 2011).

It is apparent therefore that the characteristics of a $[Ca^{2+}]_i$ rise are determined by the balance between influx, extrusion and buffering mechanisms. Influx into the cytosol via ion channels on both the PM and ER membranes is influenced by their expression (density), open probability, conductance and ion selectivity. These elements may be further modulated by their recruitment into discrete micro- or nanodomains after cytoskeletal rearrangement (Joseph *et al.* 2014).

Relevant to this thesis and highly dependent upon Ca^{2+} is the complex process of maturation of progenitor T cells (thymopoiesis) in the thymus. During thymopoiesis, diverse cellular outcomes are orchestrated by variations in the amplitude of intracellular Ca^{2+} and the temporal and spatial pattern of these rises.

Together, these characteristics become important determinants in the activation of signalling pathways that govern the cell fate (reviewed by Berridge *et al.* 2003, Christo *et al.* 2015, Kurd & Robey 2016).

1.2 The immune system

In higher vertebrates, the ability to defend against invading pathogens is dependent upon the development of an effective immune system, which provides both innate and adaptive immune responses. Belonging to the innate immune system, phagocytic cells, dendritic cells and natural killer cells provide early defence responses without distinguishing between microbes. Enhancing the innate system response, the adaptive immune system can trigger sophisticated and targeted responses, through activation of B and/or T lymphocytes, to defend against specific extracellular or intracellular pathogen invasion, respectively (Punt *et al.* 2018).

Named because they develop in the thymus, T lymphocytes can be broadly grouped according to their function. Cytotoxic T (Tc) cells recognize and mediate killing of infected and/or dysfunctional host cells. Regulatory T (Treg) cells maintain central tolerance by suppressing autoimmune activity and modulating the immune response of activated T cells. While helper T (T_H) cells activate macrophages to destroy ingested pathogens, enhance Tc responses and assist in the activation of B lymphocytes, directing them to produce antigen-specific antibodies (reviewed in Bonilla & Oettgen 2010)

Relatively immature at birth, the immune system (in particular the T cell population of the adaptive immune system) undergoes rapid development and expansion in the early phase of life (Simon *et al.* 2015). Lying behind the sternum, the thymus provides a unique environment for the complex process of T cell development. Accommodating the production of T cells, the thymus increases in

size in early life before undergoing involution and atrophy as the rate of thymopoiesis declines with the approach of puberty (reviewed by Shanley *et al.* 2009). In mice a decrease in thymus size and naïve T cell output is apparent by 12 weeks after birth (Appay & Sauce 2014, den Braber *et al.* 2012, Sempowski *et al.* 2002).

1.3 Thymopoiesis

The process of T cell development begins with the migration of haematopoietic progenitor cells (HPCs) from the bone marrow to the thymus. As illustrated in As illustrated in Figure 1.1A, the HPCs enter the thymic environment at the corticomedullary junction and begin their complex process of differentiation, proliferation and selection with the mature progeny (naïve T cells) egressing to the periphery two to three weeks later (Egerton *et al.* 1990). As they randomly migrate outward from their entry point, through distinct stromal regions to reach the subcapsular region (SCR), the HPCs proliferate and differentiate through four sequential "double negative" (DN) stages. This naming convention indicates that the CD4 and CD8 lineage markers are not yet expressed (negative) on these cells. Rather, the DN1–DN4 stages are defined by the differential expression of other surface receptors such as CD25, CD44 and pre-T cell antigen receptor (TCR) molecules (shown in Figure 1.1B). During their migration through the 3-dimensional network of varying thymic microenvironments, which takes about two weeks, the developing thymocytes dynamically interact with diverse stromal cells. Their exposure to varying endogenous ligands, including neuropeptides, lipids, adhesion molecules and hormones (Juzan *et al.* 1992, Rousseau *et al.* 2015) provides crucial developmental signals that induce activation of transcription factors and gene expression.

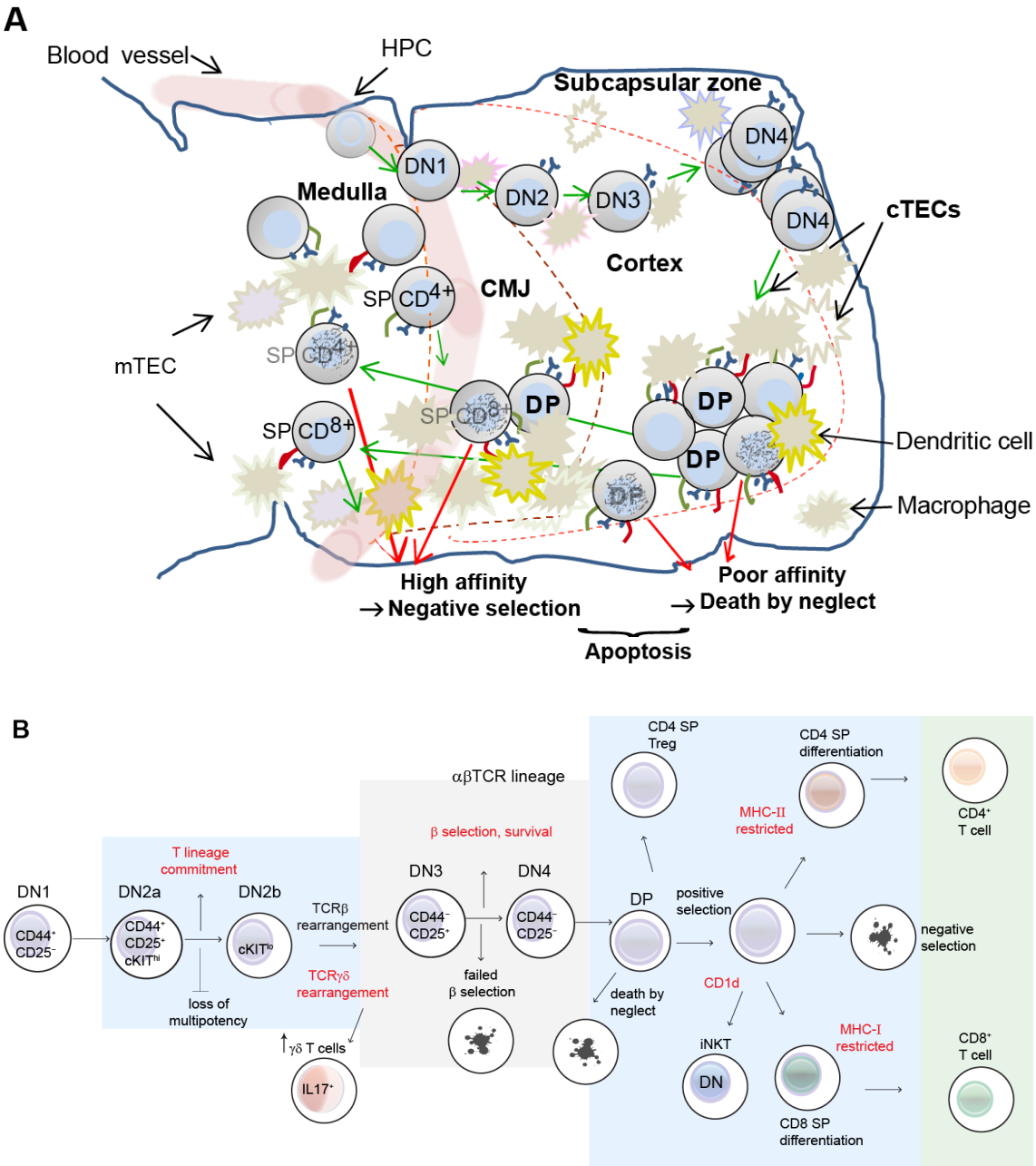

Figure 1.1 Thymopoiesis in a thymic lobe

A. Haematopoietic progenitor cells (HPCs) enter the thymus at the corticomedullary junction (CMJ). Migrating through the cortex to the subcapsular zone, they differentiate through four distinct double negative stages (DN1 - 4). DN4 thymocytes that differentiate to become double positive (DP) thymocytes express both the CD4 and CD8 coreceptor molecules and a T cell receptor complex. Interaction with thymocyte stromal cells including cortical thymic epithelial cells (cTECs), dendritic cells, macrophages and medullary TECs (mTECs), provides stimuli which direct further selection processes. Thymocytes that pass positive selection continue lineage differentiation to become either SP CD8 or SP CD4 cells. Upon further testing, SP thymocytes that are not negatively selected egress the thymus as naïve CD4 or CD8 T cells. B. Thymocyte developmental stages. The expression of the CD4 and CD8 coreceptor molecules distinguishes

double positive (DP) thymocytes. Preceding DP development are four double negative (DN) stages that can broadly be distinguished by expression of CD44 and CD25. Critical check points (red text) include T lineage commitment, TCRγδ rearrangement leading to differentiation of γδTcells, β selection and MHC or CD1d restriction. Distinct from CD4SP and CD8SP thymocytes invariant natural killer T (iNKT) cells engage with MHC-1 like molecule CD1d and become DN.

Not unexpectedly, different Ca^{2+} rises are critical to the transduction of many of these signals. For instance, specific developmental arrests and altered autophagy occur in DN thymocytes deficient in the Ca^{2+} permeable transient receptor potential (TRP) channels TRPM7 (Jin *et al.* 2008a) and TRPV1 (Farfariello *et al.* 2012), respectively. In addition, an altered Ca^{2+} influx observed in phospholipase C-γ 1 (PLC-γ1) deficient thymocytes disturbs differentiation from the DN3 to DN4 stage (Fu *et al.* 2017).

1.3.1 The αβTCR/CD3 signalling complex

At the DN3 stage, precursor thymocytes must pass a critical check point, known as β selection (Figure 1.1B) . This check point ensures the newly formed pre-TCR (comprising a β chain and a pre-Tα chain) is functional (Carpenter & Bosselut 2010). Those that pass, continue to differentiate and proliferate to form a large pool of DN4 thymocytes which express a diverse range of nascent αβTCRs. Depicted in Figure 1.2, the α and β chains that form the αβTCR comprise a proximal constant (c) domain and a distal variable (v) domain. Somatic rearrangement of three gene segments (V, D and J) during development of the α and β chains results in the expression of variable domains that have diverse amino acid sequences (Davis & Bjorkman 1988). The resulting structure determines the affinity of the TCR for peptides/antigens presented on major histocompatibility complex (MHC) molecules (Bonilla & Oettgen 2010). Associated with the αβTCR are CD3 ε, δ, γ and ζ protein chains that form εδ, εγ and ζζ dimers. Altogether, these form the TCR/CD3 signalling complex as shown in Figure 1.2. DN thymocytes that survive through to terminal differentiation,

migrate from the subscapular zone back through the cortical region, differentiating to become preselection-double positive (DP) thymocytes (expressing both CD8 and CD4 coreceptors).

As indicated by their $TCR^{lo}CD4^{+}CD8^{+}$ $CD69^{low}CD5^{low}$ phenotype, preselection DP thymocytes have significantly lower surface expression of αβTCR (Guidos *et al.* 1990) and markers of thymocyte activation (CD69 and CD5; Bhandoola *et al.* 1999) compared to more mature DP and SP thymocytes. However, a heightened sensitivity to TCR stimulation observed in preselection thymocytes enables their activation by low affinity peptide binding. This enhanced response is in part due to participation of the coreceptors and the proposed regulation by the microRNA miR-181a (Davey *et al.* 1998, Li *et al.* 2007).

Depicted in Figure 1.2, the role of the CD8 and CD4 coreceptors is to bind to the MHC class I (MHC-I) and MHC class II (MHC-II) molecules, respectively, and facilitate delivery of the tyrosine kinase Lck to the TCR/CD3 complex (Artyomov *et al.* 2010, Jiang *et al.* 2011, Li & Mariuzza 2013, Stepanek *et al.* 2014, Turner *et al.* 1990). In DP thymocytes, Lck is highly expressed and importantly associated with the cytosolic C-terminal of CD4 and to a lesser extent the CD8 coreceptors (Wiest *et al.* 1993). In thymocytes, sequestration of Lck to the coreceptor molecules has been proposed as a mechanism for ensuring TCR signal activation remains specific to MHC interactions (Van Laethem *et al.* 2007). However, Stepanek *et al.* (2014) argue that very few coreceptors actually couple Lck and that recruitment of coreceptors coupled to Lck to the TCR/CD3 complex provides a rate-limiting step in TCR/CD3 signal initiation.

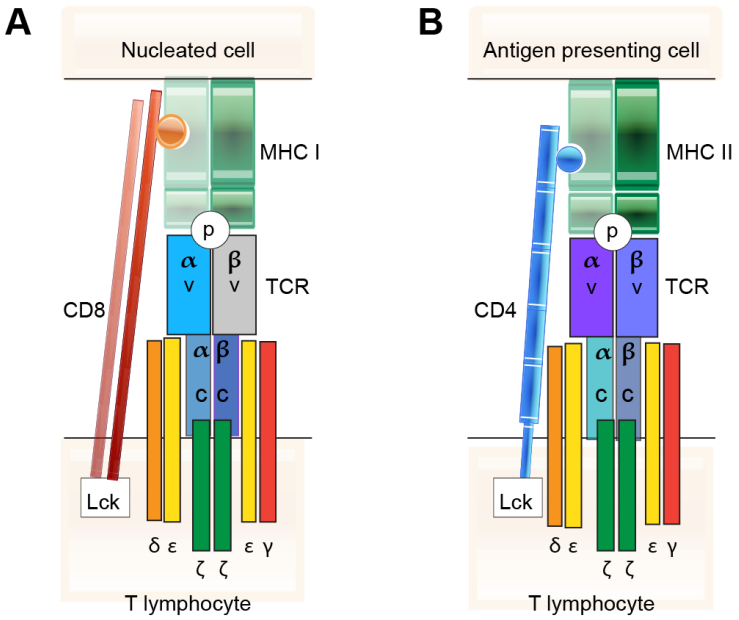

Figure 1.2 Illustration of the αβTCR/CD3 complex–pMHC interactions

Ready for "testing" the newly arranged αβTCR/CD3 complex includes the TCR α and β chains and the CD3 signalling molecules which comprise the γ, δ, ε and ζ chains. The TCR α and β chains both contain variable antigen recognition (v) domains and invariant/constant (c) signalling domains. (A). The interaction of the peptide (p)MHC-I complex with the αβTCR is stabilised by CD8 coreceptor binding to MHC-I. (B). CD4 coreceptor binding to MHC-II enhances αβTCR –pMHC-II interactions during T lymphocyte interaction with APCs. Coupled to the cytosolic tail of CD4 and CD8 is the tyrosine kinase Lck.

1.3.1.1 MHC–αβTRC engagement

Selection of DP thymocytes is dependent upon αβTCR recognition of MHC polymorphic residues in the binding domain (MHC restriction) and on the avidity of peptide engagement (Matzinger *et al.* 1984, Winchester 2008). Expressed on all nucleated cells, MHC-I molecules bind peptide fragments (p) derived from within the cell (pMHC-I) which they present to αβTCRs. This interaction is stabilized by CD8–MHC-I ligation at a site distinct from the αβTCR recognised pMHC-I binding domain (Borger *et al.* 2014). Different from MHC-I, MHC-II molecules are found on antigen presenting cells (APCs) such as macrophages, dendritic cells, B cells and thymic epithelial cells (TECs). Aided by CD4 coreceptor binding, the pMHC-II complex presents peptide fragments

derived from the extracellular milieu to αβTCRs. Associated with stimulation of the αβTCR by pMHC binding (reviewed by Moogk *et al.* 2018), the coreceptor-facilitated Lck phosphorylation of the CD3 chains initiates signal transduction. Subsequent recruitment of ζ-chain-associated protein kinase of 70 kDa (ZAP-70) to CD3 increases phosphorylation of the exposed CD3 immuno-receptor tyrosine-based activation motif domains (ITAMs) and amplifies the αβTCR/ CD3 signalling cascade (reviewed by Bonilla & Oettgen 2010, Lee *et al.* 2015, Palacios & Weiss 2004, Rossy *et al.* 2012).

Engagement of the MHC by the co-receptor molecules augments the stability of αβTCR–pMHC interaction and influences the bond lifetime thereby fine tuning TCR/CD3 reactivity to presented peptides (Hong *et al.* 2018). Furthermore, the CD8–MHC-I engagement has been proposed to facilitate αβTCR–pMHC dependent conformational change in CD3ε (Gil *et al.* 2008) and enhance Lck delivery to the TCR/CD3 complex (Davey *et al.* 1998, Delon *et al.* 1998, Hong *et al.* 2018, Lucas *et al.* 1999, Palmer & Naeher 2009, Stepanek *et al.* 2014, Thome *et al.* 1996). In preselection DP thymocytes, the low sialylation state of the CD8 coreceptor markedly enhances CD8─MHC-I binding and its role in MHC-I–TCR/CD3 activation (Gil *et al.* 2008, Moody *et al.* 2001). However, in the absence of αβTCR–pMHC-I interaction, Grebe *et al.* (2004) suggested that CD8–MHC-I ligation may induce apoptosis in preselection DP thymocytes.

At the DP stage, rigorous testing of the newly formed αβTCR commences to ensure selection of thymocytes that fulfil two criteria. Firstly, they express TCRs that are restricted to binding MHC molecules. Secondly, the binding affinity of the αβTCR to pMHC is both sufficient and self-tolerant. The vast combinatorial diversity in the v domains of the αβTCR chains (approximately 10^{15} permutations; Davis & Bjorkman 1988) means there will be receptors that are not necessarily restricted to binding to MHC molecules and/or receptors that bind

too strongly to MHC molecules. Overall, the "pass rate" of thymocytes is exceedingly low as most thymocytes undergo apoptosis within the thymus (Egerton *et al.* 1990). Approximately 65% of preselection DP thymocytes are predicted to "die by neglect" due to inadequate αβTCR–pMHC binding. In the thymic cortex, this failure to be positively selected is the primary cause of DP thymocyte death (Surh & Sprent 1994, Szondy *et al.* 2012). Of those remaining, a further 91% are likely to undergo apoptosis as a result of negative selection triggered by high affinity αβTCR–pMHC binding (Sawicka *et al.* 2014). While apoptosis more commonly occurs in the medullary region (reviewed by Starr *et al.* 2003b), strong αβTCR–pMHC binding will induce negative selection of DP thymocytes within the thymic cortex (Murphy *et al.* 1990, Surh & Sprent 1994).

1.3.1.2 **Thymic epithelial cell interaction triggers selection signals**

As DP thymocytes randomly migrate through the thymic cortex, they intermittently stop to interact with cortical TECs (cTECs) to receive crucial TCR activation signals which drive positive as well as early negative selection (discussed by Palmer & Naeher 2009). These necessary interactions vary in duration and frequency, from approximately two to four min every 30 min for interactions leading to positive selection (Ross *et al.* 2014) to prolonged interactions of >20 min linked to negative selection (Melichar *et al.* 2013; further described in section 1.4; Figure 1.5). Notably, the intensity of the TCR response influences the amplitude and the patterning of the associated $[Ca^{2+}]_i$ rises (Davey *et al.* 1998). Fluctuations in cytosolic Ca^{2+} ranging from 0.3 to 1 μM have been described (Bhakta & Lewis 2005, Bhakta *et al.* 2005, Melichar *et al.* 2013, Melichar *et al.* 2015, Ross *et al.* 2014). While it is generally agreed that the variation in $[Ca^{2+}]_i$ is critical in the complex processes of positive and negative selection (reviewed in Feske 2007, Feske *et al.* 2015, Vig & Kinet 2009), understanding of the

mechanisms under-pinning these $[Ca^{2+}]_i$ rises (reviewed in section 1.4) remains incomplete.

Mentioned previously, surface expression of the αβTCR in DP thymocytes is about ten-fold lower than that of more mature SP thymocytes (reviewed by Schrum *et al.* 2003). However, in DP thymocytes the αβTCRs are more reactive to low affinity peptides (Davey *et al.* 1998). This sensitisation of the αβTCR–pMHC interactions, which promotes positive selection, is in part facilitated by the CD4 and CD8 coreceptors (Gil *et al.* 2008, Moody *et al.* 2003, Nakayama *et al.* 1990, Simon Davis 2015, Starr *et al.* 2003a), and by the activation of adhesion molecules such as the lymphocyte function-associated antigen-1 (LFA-1) and CD2. These interact dynamically with their respective endogenous ligands expressed on cTECs (Nonoyama *et al.* 1989, Paessens *et al.* 2008). Recognised as adhesion molecules, contemporaneous activation of LFA-1 and CD2 during thymocyte–cTEC interaction may synergistically add to the $[Ca^{2+}]_i$ rises and thereby critically affect the outcome of selection (Danielian *et al.* 1992, Ohno *et al.* 1991, Revilla *et al.* 1997, Teh *et al.* 1997).

1.3.1.3 **Enhancement of TCR/CD3 signalling by LFA-1**

Highly expressed on thymocytes (Fine & Kruisbeek 1991), LFA-1 comprises the α_L and β_2 chains, CD11a and CD18 respectively (Ma *et al.* 2002), which adopt an "inactive" conformational state at rest. In thymocytes, activation of LFA-1 mediates binding to TECs (Singer *et al.* 1990) and significantly biases the commitment to the $CD8^+$ T lymphocyte lineage (Revilla *et al.* 1997). *In vivo* saturation of the CD11a chain by anti-LFA-1α mAb injection was found to selectively decrease the population of CD8 SP thymocytes in treated mice, suggesting that LFA-1 plays a crucial role in the generation of these thymocytes. Perhaps the mechanism by which LFA-1 activation enhances selection is like that which has been described in mature freshly isolated CD8 T cells. In these cells,

prior activation of LFA-1 by adherent antibodies, raised against its CD11a or CD18 chains "primed" the strength of the transduced TCR signal (activated by soluble pMHC monomers) and augmented the subsequent $[Ca^{2+}]_i$ rise (Randriamampita *et al.* 2003).

Under physiological conditions, that is, at 37°C but not 4°C (Moingeon *et al.* 1991), the mechanism activating LFA-1 follows early signalling events downstream of TCR/CD3 activation (Mueller *et al.* 2004). Under tight regulation, the extracellular domain of LFA-1 naturally adopts a folded conformation with low affinity for its major endogenous ligand, intercellular adhesion molecule 1 (ICAM-1). To adopt an activatable extended conformation, LFA-1 requires an inside-out signal (Cairo *et al.* 2006). In thymocytes, the precise molecular mechanisms that regulate LFA-1 activation remain to be characterised. However, studies that investigated the mechanism in Jurkat or mature T lymphocytes suggest that the transduction of the inside-out signal is mediated by at least 4 mechanisms. These are 1) CD4/CD8–Lck kinase activation (Fagerholm *et al.* 2002, Vielkind *et al.* 2005), 2) CD3ε conformational change that allows recruitment of adaptor proteins including the non-catalytic region of kinase domain (Nck; Lettau *et al.* 2014), the SH2 domain-containing leukocyte protein of 76 kDa (SLP-76; Horn *et al.* 2009), the adhesion and granulation-promoting adaptor protein (ADAP; Wang *et al.* 2009, Wu *et al.* 2006) and the Wiskott-Aldrich syndrome protein (WASP); 3) F-actin remodelling regulated by calpain (a Ca^{2+} dependent protease, Stewart *et al.* 1998) activity and talin an integrin–actin binding protein (Cairo *et al.* 2006, reviewed by Hogg *et al.* 2011, Kim *et al.* 2003, Lub *et al.* 1997) and 4) increased cytosolic Ca^{2+} (Guo *et al.* 2018, Liu *et al.* 2018, van Kooyk *et al.* 1993). Such a signalling mechanism is shown in Figure 1.4 (p. 51) where these signalling molecules are proposed to be activated during thymocyte–cTEC interaction without αβTCR–MHC engagement.

Once in an extended conformation, LFA-1 activation by ICAM-1 or by anti-LFA-1 Ab triggers a complex outside-in signalling cascade. Also not well characterised in thymocytes, the transduction of the outside-in signal in other T lymphocytes reportedly entails 1) Src kinase phosphorylation of adaptor proteins including C10 regulator of kinase (Crk; Roy *et al.* 2018), ADAP (Suzuki *et al.* 2007, Wang *et al.* 2009), SLP-76 (Baker *et al.* 2009); 2) localised formation of "actin-clouds" (Suzuki *et al.* 2007); 3) recruitment and activation of focal adhesion kinase (FAK) and proline-rich tyrosine kinase 2 (PYK-2; Rodriguez-Fernandez *et al.* 1999); and 4) enhanced activation of effector molecules including Vav, a guanine nucleotide exchange factor that crucially regulates actin polymerization (Kong *et al.* 1998), phosphoinositide 3 kinase (PI_3K) and PLC-γ1 (Kim *et al.* 2009a, Sánchez-Martín *et al.* 2004).

Activation of LFA-1 signal transduction is proposed to facilitate TCR activation. In conditions of suboptimal TCR stimulation, Kim *et al.* (2009a) showed that LFA-1 interaction with ICAM-1 resulted in a $[Ca^{2+}]_i$ rise (Figure 1.3A, black trace) that involved PLC-γ1 activation, but was independent of store operated Ca^{2+} entry (SOCE). This $[Ca^{2+}]_i$ rise was abolished in WT cells preincubated with anti-LFA-1 mAb and in LFA-$1^{-/-}$ T cells (Figure 1.3A, orange and green, respectively). Additionally, Kim *et al.* (2009a) showed that the LFA-1 enhanced Ca^{2+} influx was abolished by inhibiting the Src kinase and significantly reduced following pre-treatment with the PI_3K and PLC-γ1 inhibitors, respectively. Without TCR stimulation, they found the addition of anti-LFA-1 mAb was not sufficient to evoke a Ca^{2+} rise (Figure 1.3A, grey trace), most likely because LFA-1 remained in a folded inactive state. They conclude that essentially in conditions of suboptimal TCR stimulation, synergistic signal transduction via activated LFA-1 augments activation of PLC-γ1 and PI_3K signalling cascades and increases the $[Ca^{2+}]_i$ rise. This synergistic $[Ca^{2+}]_i$ rise potentially lowers the threshold for TCR signalling activation (Wang *et al.* 2008, Wulfing *et al.* 1998). In DP thymocytes

such a mechanism could promote positive selection downstream of poor avidity pMHC –TCR interaction.

1.3.1.4 **TCR/CD3 signalling may be enhanced by CD2**

Further to LFA-1 enhancement of T-lymphocyte signalling, an additive $[Ca^{2+}]_i$ rise associated with CD2 activation perhaps negatively regulates DP thymocyte sensitivity to TCR positive selection signals (Bierer *et al.* 1988, Teh *et al.* 1997). Distinct from LFA-1 activation, in T lymphocytes, CD2 adhesion and signal transduction activity have been shown to be independent of TCR signalling, Ca^{2+} and temperature (Meuer *et al.* 1984, Moingeon *et al.* 1991). Independent of TCR stimulation in T lymphocytes, cross-linking anti-CD2 mouse antibody (mAb) has been shown to evoke a sustained $[Ca^{2+}]_i$ rise (Figure 1.3B) that comprised both intracellular and extracellular components, suggestive of activation of a SOCE mechanism (Ledbetter *et al.* 1988, van Kooyk *et al.* 1993).

In Jurkat cells, ligation of CD2 to the endogenous glycoprotein CD48 (mice; CD58/LFA-3 humans) commonly expressed on cTECs and APCs, has been shown to promote signal transduction via activation of protein tyrosine kinases including Fyn, Pyk2 (Sunder-Plassmann & Reinherz 1998), and spleen tyrosine kinase (Syk; Umehara *et al.* 1998). These then lead to an $[Ca^{2+}]_i$ rise (Bachmann *et al.* 1999, Vollger *et al.* 1987). Although preselection DP thymocytes express lower levels of CD2 than mature thymocytes (Duplay *et al.* 1989), its colocation with LFA-1 (Altin *et al.* 1994) perhaps enables the synergistic activation of Lck, Fyn and Syk (Danielian *et al.* 1992, Lin *et al.* 1998) and enhanced recruitment and activation of PI_3K and PLC-γ1 (Dietsch *et al.* 1994, Espagnolle *et al.* 2007, Kivens *et al.* 1998, Shimizu *et al.* 1995). There is evidence that thymopoiesis is subtly altered in $CD2^{-/-}$ mice. Sasada and Reinherz (2001) found in these mice that the T cell repertoire of the peripheral pool was decreased compared to that of the WT mice and they proposed that this change reflected altered thymocyte selection.

However, this disruption of thymopoiesis appeared to precede DP differentiation, and whether CD2-dependent parallel signalling has a role in directing TCR/CD3 signalling in preselection DP thymocytes remains unknown.

1.3.1.5 αβTCR reactivity modulated by glycosylation of CD8

In the thymus the variable expression and secretion of glycosaminoglycans (GAGs) by different stromal cell types is likely to support the formation of distinct microenvironments that facilitate thymocyte maturation (Simon Davis 2015, Werneck *et al.* 2000, Werneck *et al.* 1999). GAGs are linear polysaccharide chains which often covalently attach to a core protein, forming a large family of proteoglycans. Found intracellularly, on cell surfaces and in the extracellular matrix, these structurally diverse and sometimes highly sulfated macromolecules are essential to normal cell function (reviewed by Bishop *et al.* 2007, Gandhi & Mancera 2008). Perhaps the best studied GAG is the ubiquitously expressed heparan sulfate (HS).

1.3.1.5.1 Heparan sulfate

Covalently bound to a core glycoprotein, HS is proposed to have a role in multiple responses in the immune system, including the modulation of the TEC–thymocyte adhesion (Werneck *et al.* 1999), the initial expression of the TCR, CD4 and CD8 coreceptors in early thymocyte development (Wrenshall *et al.* 1993), immune cell migration and their activation (reviewed by Simon Davis & Parish 2013). The polyanionic nature of HS enables multiple interactions with many classes of proteins. Such interactions are commonly electrostatic in nature (Ori *et al.* 2011). In their comprehensive study of the rat HS interactome, Ori *et al.* (2011) conclude that heparan sulfate binding proteins (HSBPs) are strongly associated with transduction of extracellular cues to intracellular signalling pathways that lead to a diverse range of biological responses, including cell adhesion and

possible modulation of the kinetics of some ion channels. Specifically, in lymphocytes, 234 candidate HSBPs have been proposed based on the detection of a "consensus" HS-binding motif. Of these candidates, 54 are found in the PM (Simon Davis & Parish 2013). Notably, in DP thymocytes, increased mRNA expression has been described for some candidate HSBPs. These include the coreceptor chains CD8β, CD4, the protein tyrosine phosphatase receptor CD45, and an adhesion G-protein coupled receptor E5 (CD97). A list of these, their proposed function and the mRNA expression level in DP thymocyte subpopulations is provided in Appendices 1 and 2, respectively (pp. 349 & 351).

1.3.1.5.2 **Dextran sulfate (DxS)**

Just as extracellular GAGs interact with and influence activation of cell surface receptors and membrane lipid dynamics (Huster *et al.* 1999, reviewed by Sahoo & Schwille 2013), for many years it has been recognised that high molecular weight (mol. wt.) sulfated polysaccharides, such as DxS, may also trigger cellular responses in lymphocytes (Palacios *et al.* 1982, Sasaki & Suchi 1967, Sugawara & Ishizaka 1982). The addition of 0.1 mg/ml DxS (50 kDa) has been shown to promote mitogenic activity in mouse peripheral T cells, but notably the presence of irradiated autologous adherent cells was necessary (Palacios *et al.* 1982). Relevant to this thesis, it is assumed that DxS likely cross-links with PM proteins which results in the subsequent activation of HSBPs, most crucially CD8β, and perhaps with other polyanionic binding sites, such as those identified on CD4 (Lederman *et al.* 1989, Parish *et al.* 1990), CD2 (Warren & Parish 1990) and LFA-1 (Vermot-Desroches *et al.* 1991).

1.3.1.6 **HS causes rosetting on cTECs in preselection DP thymocytes**

HS proteoglycans (HSPGs) were found to be variably abundant on cell surface extracts purified from cTEC like cells (Werneck *et al.* 1999). More specifically, in

thymic slices prepared from C57BL/6 mice, Simon Davis (2015) identified multiple "hot spots" stained with an anti-HS mAb suggesting a high local concentration of HS. Restricted to the thymic cortical region, these focal cTECs (hereafter described as $cTEC^{hi}$) had about a 20-fold higher anti-HS mAb binding compared to other cTECs (Simon Davis 2015). It is hypothesised that HS on these cTECs binds to CD8 coreceptors on preselection DP thymocytes at a location distinct from the MHC-I binding site. This HS–CD8 binding in addition to MHC promotes the formation of stable rosette-like structures, where multiple thymocytes form clusters with a single cTEC (Kyewski *et al.* 1982, Oliveira-dos-Santos *et al.* 1998). Further supporting a role for CD8, the ability to form stable thymocyte–$cTEC^{hi}$ rosettes was markedly impaired in $CD8\alpha^{-/-}$ and $CD8\beta^{-/-}$ thymocytes (Simon Davis 2015).

In a series of elegant experiments, DP thymocyte–$cTEC^{hi}$ congregates (described as rosetting) have been experimentally formed and the associated Ca^{2+} rises quantified using flow cytometry (Simon Davis 2015). Consistent with earlier findings (Hare *et al.* 2003), Simon Davis (2015) found rosette formation was significantly enhanced by αβTCR–pMHC engagement. Specifically, the stability and number of rosettes was markedly higher in samples where thymocytes were mixed with WT cTECs, compared to those where thymocytes were mixed with MHC-I/II deficient cTECs. Furthermore, a significant and sustained $[Ca^{2+}]_i$ rise was observed in DP thymocytes rosetting on WT cTECs compared to non-rosetting thymocytes (Figure 1.3C; black and grey, respectively). Significant to this thesis, in the absence of TCR–MHC-I/II binding, while reduced, rosette formation was not completely abolished (Figure 1.3C; red) compared to non-rosetting thymocytes (Figure 1.3C; pink). The formation of rosettes under these conditions was associated with a small amplitude $[Ca^{2+}]_i$ rise which reached a plateau after about 10 min, suggesting the existence of an alternate $[Ca^{2+}]_i$ source. Independent of TCR–MHC-I/II interaction, this $[Ca^{2+}]_i$ rise was possibly evoked

by the activation of surface receptors, notably CD8 and perhaps the integrins LFA-1 and CD2 upon binding to the respective ligands expressed on cTECs (Kanner *et al.* 1993, Simon Davis 2015). While the role for CD2 in enhancing preselection DP–cTEC^{hi} binding has not been determined, there is evidence that CD2 plays a significant role in thymocyte–erythrocyte autorosetting.

While a mechanism of enhanced signal transduction evoked by HS–CD8β chain binding remains to be identified, it is notable that independent of TCR–pMHC engagement, the CD8β chain has been found to physically interact with the CD3δ and to a lesser extent CD3ε and γ chains (Gil *et al.* 2008, Suzuki *et al.* 1992). This interaction is proposed as a mechanism for inducing a conformational change of CD3 and therefore an important early step in signal transduction and positive selection (reviewed by Bettini *et al.* 2014, Ma *et al.* 2017, Xu *et al.* 2008). Whether this conformational change requires an increase in $[Ca^{2+}]_i$ in the TCR/CD3 microdomain and precedes CD3 phosphorylation remains a topic of debate (Gagnon *et al.* 2012, Gil *et al.* 2005, Shi *et al.* 2013).

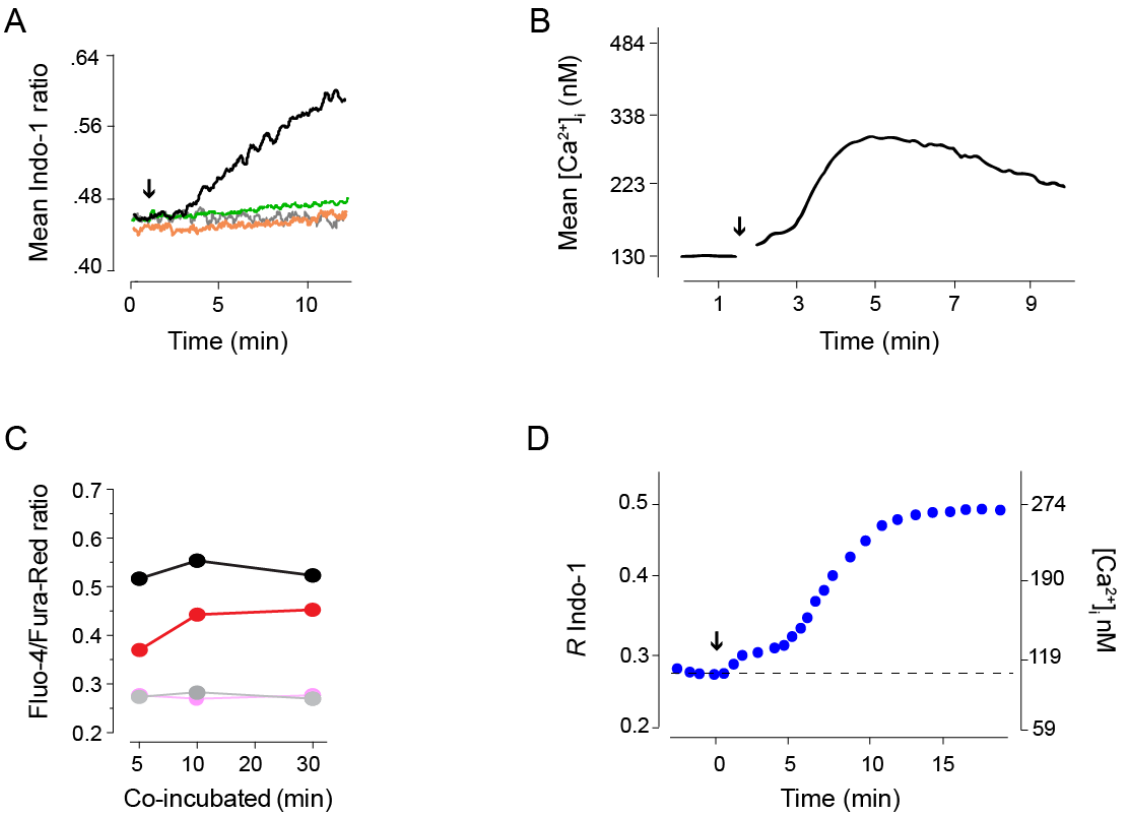

Figure 1.3 $[Ca^{2+}]_i$ rises induced by costimulatory receptor activation

Time courses of $[Ca^{2+}]_i$ rises evoked in thymocytes in conditions of suboptimal TCR activation. (A) Ca^{2+} responses in $CD8^+$ T lymphocytes following the addition of plasma membrane vesicles expressing the endogenous ligand ICAM-1 and peptide loaded MHC molecules (arrow). The $[Ca^{2+}]_i$ rise is observed in WT T lymphocytes (black), but not when the cells were LFA-$1^{-/-}$ T lymphocytes, or treated with anti LFA-1Ab or where the peptide did not bind to the TCR (green, orange and grey respectively; adapted from Kim *et al.* 2009a). (B) $[Ca^{2+}]_i$ rise observed in T cells incubated for 5 min with mAb against CD2 and cross-linked by goat anti-mouse Ig Ab at 1.5 min (adapted from Ledbetter *et al.* 1988). (C) Monitoring of $[Ca^{2+}]_i$ in preselection DP thymocytes mixed with $cTEC^{hi}$. WT thymocytes rosetting on WT $cTEC^{hi}$ show a sustained $[Ca^{2+}]_i$ rise (black) compared to non-rosetting ones (grey). $[Ca^{2+}]_i$ rise in WT thymocytes rosetting on MHC-I/II$^{-/-}$ cTECs (red) and in non-rosetting ones (adapted from Simon Davis 2015). (D) The addition of 1 µg/ml DxS (arrow) to a thymocyte suspension evokes a delayed $[Ca^{2+}]_i$ rise that is specific to DP thymocytes (adapted from Tellam & Parish 1987).

Investigating the characteristics of thymocyte autorosetting (Parish *et al.* 1984) reported that rosetting receptors also bound with high affinity to sulfated poly-saccharides such as heparin. Preincubation with fucoidan and dextran sulfate competitively prevents this phenomenon. Adding to this observation, Simon

Davis (2015) found rosetting between cTEC^{hi} –preselection DP thymocytes was also significantly inhibited by prior addition of dextran sulfate or HS mimetics like heparin to the cell suspension. It is likely these HS mimetics and DxS competitively bind to rosetting receptors, preventing HS interaction with HSBPs, in particular CD8. Furthermore, dependent upon low CD8 sialylation (Simon Davis 2015), the addition of DxS$^{500\ kDa}$ (DxS) to a thymocyte suspension evokes a $[Ca^{2+}]_i$ rise (as shown in Figure 1.3D, adapted from Tellam & Parish 1987). First observed in 1987, this DxS $[Ca^{2+}]_i$ rise was found to be specific to DP thymocytes (Tellam & Parish 1987, Weston *et al.* 1991). In this thesis, it is postulated that the cross-linking of multiple surface receptors, including CD8, by DxS, mimics an endogenous mechanism activated in preselection DP thymocytes during their interaction with cTEC^{hi}. Because this observation is central to the research presented in this thesis, the characteristics of this DxS $[Ca^{2+}]_i$ rise are reviewed in greater detail in section 1.5.

1.3.1.6.1 **Proposed DP thymocyte–cTEC^{hi} signalling mechanisms**

For some early selecting DP thymocytes, cTEC^{hi} rosetting may provide a mechanism by which selection signalling pathways are adjusted consequent to $[Ca^{2+}]_i$ rises and that is dependent upon HS evoked CD8β chain activation. During preselection DP thymocyte–cTEC^{hi} interaction, numerous surface receptors are most likely activated as they engage their endogenous ligands. Considering just CD8–HS binding, physical interaction between CD8β and CD3 and binding of the adhesion molecules LFA-1 and CD2 to ICAM-1 and CD48 respectively, Figure 1.4 illustrates a proposed DP thymocyte–cTEC^{hi} interaction and possible signalling mechanisms which may lead to $[Ca^{2+}]_i$ rises.

As illustrated in Figure 1.4, downstream of Lck and Syk activation, phosphorylation and activation of crucial linker/adaptor proteins by these kinases promotes formation of a membrane raft domain around the membrane

bound protein "linker for activation of T cells" (LAT; reviewed by Horejsi *et al.* 2010, Zhang *et al.* 1998). This macromolecular signalling complex provides scaffolding for the recruitment and activation of the enzymes PLC-γ1 (Zhu *et al.* 2003) and phosphoinositide 3 kinase (PI_3K; Shim *et al.* 2011). Hydrolysis of phosphatidylinositol-4,5-bisphosphate (PIP_2) by PLC-γ1 leads to a transient increase in the potent second messenger molecules inositol 1,4,5-trisphosphate (IP_3) and membrane bound diacylglycerol (DAG). The former has the potential to bind to IP_3 receptors (IP_3R) on the ER to cause release of Ca^{2+} from stores (Streb *et al.* 1983). The latter can alter the local lipid composition in the PM or as a signalling molecule activate PKC (Szamel *et al.* 1989). The enzymatic activity of PI_3K dynamically alters the concentration of PIP_2 and phosphatidyl-inositol-3,4,5-trisphosphate (PIP_3) within the local PM. Cellular imaging studies show that PIP_2 and PIP_3 localise to discrete microdomains in the PM. This restriction of lipid diffusion is thought to enable generation of local gradients, thereby enhancing the role of PIPs as regulatory molecules of PM proteins like ion channels (Hilgemann 2007, Wang & Richards 2012). Notably, dynamic changes in the local concentration of PIP_2 and PIP_3, and the generation of a broad range of endogenous lipid metabolites downstream of DAG, has been recognised as an important mechanism which can affect $[Ca^{2+}]_i$ (reviewed in Ciardo & Ferrer-Montiel 2017, Cordero-Morales & Vásquez 2018, and Taberner *et al.* 2015).

How HS-enhanced autorosetting influences the DP thymocyte selection outcome remains a matter for further investigation. However, I note that a deleterious structural modification of the HS molecule (specifically in TECs) was found to increase the TCR repertoire of the peripheral CD8 T cell pool (Simon Davis, personal communication). In accordance with Grebe *et al.* (2004), this preliminary finding may suggest that in the absence of adequate TCR–MHC-I engagement, the role of this $[Ca^{2+}]_i$ rise is perhaps to induce "death by instruction" in a subpopulation of preselection MHC-I restricted DP thymocytes. Facilitation of

rosetting by cTEC expressed HS binding to the thymocyte CD8 coreceptor might be required to promote a sustained stop signal in preselection thymocytes expressing poor affinity TCR.

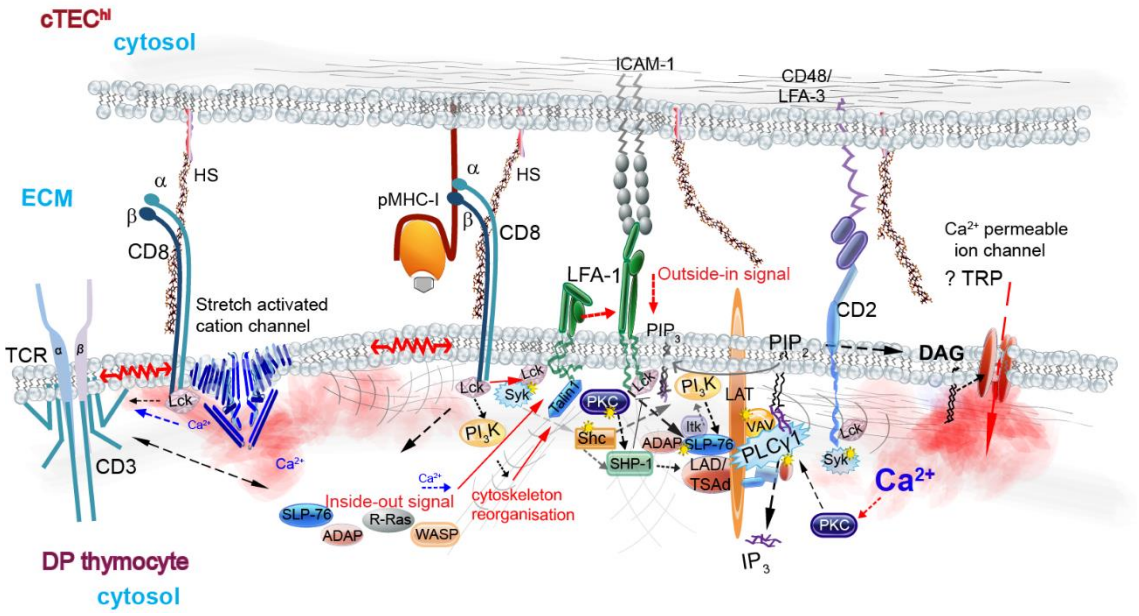

Figure 1.4 A proposed HS priming mechanism involving CD8

Proposed mechanism for Ca^{2+} priming of the TCR signalling cascade during $cTEC^{hi}$ (HS high) interaction. Without αβTCR–MHC engagement, HS binding of CD8 activates Lck signalling pathways and applies mechanical load on the PM which may be sufficient to transiently activate TCR associated stretch activated cation channels. Ca^{2+} influx, Lck activation of adaptor molecules includingSLP-76 and cytoskeleton reorganisation leads to LFA1 conformational change and signalling. Synergistic Lck and LFA1 signalling promotes formation of the LAT signalosome and PLC-γ1 activation. PLC-γ1 hydrolysis of PIP_2 leads to DAG production, PKC activation. Downstream of DAG production a non-selective cation channel promotes a sustained $[Ca^{2+}]_i$ rise. ECM: extracellular matrix; Adaptor molecules: SLP-76:SH2 domain-containing leukocyte protein of 76 kDa; ADAP: adhesion and degranulation-promoting adaptor protein; WASP: Wiskott-Aldrich syndrome; Shc; Src homology domain containing. Cytoskeleton associated adaptor: talin1. Effector molecules: Lck, Syk: spleen tyrosine kinase; Itk: IL2-inducible T cell kinase; SHP-1: Src homology region 2 domain containing phosphatase; PKC: protein kinase C; stretch activated cation channel perhaps from TRP family or Piezo1.

1.3.1.7 **Sialylation of surface receptors modulates αβTCR reactivity**

As DP thymocytes continue to undergo positive selection and differentiation toward either $CD4^+$ or $CD8^+$ T cell lineage, there is associated upregulation of the TCR. In the $CD8^+$ population, this upregulation which has the potential to increase the reactivity to low affinity antigens, is countered by progressive glycosylation of the CD8 coreceptor (Daniels *et al.* 2001, Gil *et al.* 2008, Starr *et al.* 2003a). Physical modification of the CD8β structure by the addition of terminal sialic acid residues hinders CD8–MHC-I molecule interaction and hence impairs its role in stabilising weak affinity TCRs–pMHC-I interactions (Casabó *et al.* 1994, Li & Mariuzza 2013). Reducing the TCR–pMHC dwell time results in diminished signalling and provides a mechanism for tuning tolerance to self-peptides (Daniels *et al.* 2001). The added sialylation of CD8β has also been shown to inhibit HS binding to the coreceptor (Simon Davis 2015) and hence may act to negatively regulate rosette formation in positively selected thymocytes.

DP thymocytes that are positively selected continue to transition to become either $CD4^+$ or $CD8^+$ lineage single positive (SP) thymocytes. The lineage lines are restricted to binding either MHC-I or -II molecules, respectively (reviewed by Shah & Zúñiga-Pflücker 2014). During this period (~3 days; Jin *et al.* 2008b), the avidity of the αβTCR binding to the pMHC complex continues to be stringently tested. In addition, reactivity of the receptor to low affinity peptides decreases as sialylation of the surface receptors, in particular CD8, is progressively increased (Moody *et al.* 2001, Moody *et al.* 2003, Starr *et al.* 2003a). At the end of selection, it is critical that the repertoire of naïve $CD4^-CD8^+TCR^{hi}$ cytotoxic T cells, or $CD4^+CD8^-$ TCR^{hi} helper T cells exiting the thymus has the potential to respond to foreign antigen presented on MHC molecules but shows tolerance and hence minimal reactivity to self-peptide-MHC engagement.

1.4 Ca^{2+} rises associated with thymocyte selection

In DP thymocytes, different patterns of $[Ca^{2+}]_i$ rises have been associated with different selection outcomes (Bhakta & Lewis 2005, Fu *et al.* 2009, Kane & Hedrick 1996, Kim *et al.* 2009a, Lo *et al.* 2012, Melichar *et al.* 2015, Ohno *et al.* 1991, Teh *et al.* 1997). This is supported by data presented in Figure 1.5.

1.4.1 Negative selection involves large amplitude $[Ca^{2+}]_i$ rises

In panel A (adapted from Fu *et al.* 2009), $[Ca^{2+}]_i$ responses were measured using flow cytometry in OT-1 transgenic (tg) thymocytes loaded with the Ca^{2+} indicator Indo-1, when stimulated with the peptide tetramers of known avidity to OT-1 tgTCRs. The strong response of the tgTCRs to the OVA peptide (epitope of ovalbumin) is associated with a large $[Ca^{2+}]_i$ rise (top) after exposure to normal extracellular Ca^{2+} at 2 min. This suggests that the rise in this case is largely carried by a transmembrane Ca^{2+} influx. Note that there is a much smaller rise immediately after the ova peptide is added to a nominally 0 mM Ca^{2+} solution, suggesting that with high affinity peptides, there is some contributing store release (see also below). The outcome of this type of Ca^{2+} rise was negative selection.

1.4.2 Positive selection involves a small, cumulative $[Ca^{2+}]_i$ increase

Variants of the ova epitope with less affinity to the OT-1 tgTCR are used from top to bottom with the top 4 resulting in negative and the bottom 5 in positive selection (Fu *et al.* 2009). Notably, in this *in vitro* study, the $[Ca^{2+}]_i$ rises associated with negative selection have an initial high peak amplitude, which declines slowly over minutes but remains well above resting $[Ca^{2+}]_i$. In contrast, when thymocytes were exposed to low avidity antigens (bottom 5 panels) in this reduced system, the positive selecting $[Ca^{2+}]_i$ rises increased slowly over time (5 min) and notably did not reach the amplitude triggered by high avidity antigens.

1.4.3 TCR–pMHC interaction duration reflects selection outcome

What is not captured in this figure is the much briefer duration of individual $[Ca^{2+}]_i$ rises that strongly correlate with periods of thymocyte migration arrest during which cell-cell interaction occurs (Bhakta & Lewis 2005). Figure 1.5B (adapted from Melichar *et al.* 2013) depicts $[Ca^{2+}]_i$ amplitude changes in individual DP thymocytes, detected using two-photon laser-scanning microscopy, as they migrated through a thymic slice, which likely represents a more biologically relevant environment. Not unexpectedly, $[Ca^{2+}]_i$ remained at resting level in HY^{CD4}tg thymocytes (sensitive to an endogenous male peptide) seeded into a thymic slice from MHC $I^{-/-}$ mice, a mutation that limits thymocyte–TEC interaction (non-selecting; Figure 1.5Bi). Without TCR–MHC interaction, these thymocytes will not receive survival signals and are predicted to die by neglect (Surh & Sprent 1994). When the same line of thymocytes was seeded onto a thymic slice derived from either a male (Figure 1.5Bii) or female mouse (Figure 1.5Biii), the duration and amplitude of the resulting $[Ca^{2+}]_i$ rise were distinctly different. In the case of male peptides with high affinity to the TCR, the interaction with TEC (red line) were long lasting (>20 min) and the $[Ca^{2+}]_i$ was elevated throughout. During this time, summation of signalling responses triggered by repeated applied force transduced by TCR–pMHC–CD8 bond formation and disengagement induces enhanced $[Ca^{2+}]_i$ signalling (Pryshchep *et al.* 2014) which leads to negative selection. However, when exposed to female peptides (reduced affinity), the interactions were short lived (<5 min) with concomitant short rises above background $[Ca^{2+}]_i$ (dashed line).

1.4.4 A SOCE mechanism triggers negative selection

Aside from the differences in duration and amplitude, the mechanisms of the Ca^{2+} rise driving negative selection are also distinctly different from that associated with positive selection (Fu *et al.* 2013). In the absence of extracellular

Ca^{2+} (Figure 1.5A, top), negative selection is also associated with a rapid Ca^{2+} rise of >550 nM (Nakayama *et al.* 1992) that includes ER store release (see also above). This suggests that a signalling cascade activates ER store release followed by store operated Ca^{2+} entry (SOCE), resulting in a subsequent large Ca^{2+} influx from the extracellular space. Certainly, in STIM deficient thymocytes, Oh-hora *et al.* (2013) found negative selection was reduced in favour of positive selection outcomes.

In mature T cells, activation of the "classical" SOCE channels (STIM1/Orai1) is considered the primary mechanism for Ca^{2+} rise downstream of TCR activation (Feske *et al.* 2005). Highly selective for Ca^{2+} (P_{Ca}:P_{Na} >1000:1), functional STIM1/Orai channels are present in thymocytes, but the mechanisms which might differentially regulate their activity are poorly understood. In tumour derived Jurkat T cells (human $CD4^+$ leukemic T cells), the transient receptor potential vanilloid channel 2 (TRPV2) has been shown to positively modulate STIM1/Orai activity. Specifically, in cells transfected with a dominant-negative TRPV2 channel, Sauer and Jegla (2006) found that the previously observed SOCE downstream of TCR activation was absent in WT cells. Whether a similar mechanism is in place in thymocytes remains to be resolved.

1.4.5 **SOCE is not required for positive selection**

While large amplitude $[Ca^{2+}]_i$ rises coupled to SOCE play a central role in negative selection, this mechanism of "bulk" Ca^{2+} entry is likely inappropriate for positive selection (Oh-hora *et al.* 2013). Rather, positive selection is triggered by repeated small amplitude $[Ca^{2+}]_i$ rises of 200 to 550 nM and an associated gradual elevation in background $[Ca^{2+}]_i$ over many hours (Nakayama *et al.* 1992, Ross *et al.* 2014). These transient rises do not appear to evoke detectable store release (Oh-hora *et al.* 2013), perhaps because signal transduction in positively selecting events is associated with delayed phosphorylation of LAT (Daniels *et al.* 2006).

The amplification of the signal may be insufficient to overcome the tight regulation of IP_3R activation by reversible tyrosine phosphorylation (Cui *et al.* 2004, Jayaraman *et al.* 1996) and binding of adaptor proteins, including Bcl-2 (Chen *et al.* 2004, Foyouzi-Youssefi *et al.* 2000, Rong *et al.* 2008, Rong *et al.* 2009, Zhong *et al.* 2006), thymocyte-expressed positive selection-associated 1 (Tespa 1; Wang *et al.* 2012) and thymocyte-expressed molecule involved in selection (Themis; Fu *et al.* 2013). The expression of anti-apoptotic proteins Bcl-2 and Bcl-X_L is topographically regulated and their effect on thymocyte survival is likely to be complex. In DP thymocytes, a notable increase in Bcl-X_L expression is proposed to down-regulate expression of the IP_3R and so modulate Ca^{2+} homeostasis (Li *et al.* 2002a) and repress programmed cell death (Chao *et al.* 1995). While a 3-fold down-regulation of Bcl-2 is proposed to increase the susceptibility of DP thymocytes that fail positive selection, to programmed cell death. Intriguingly, within the DP population, a subset population (10–20%) scattered throughout the cortex has been shown to maintain high expression of Bcl-2 protein and these thymocytes are resistant to glucocorticoid induced death (Chao *et al.* 1995, Gratiot-Deans *et al.* 1993, Veis *et al.* 1993).

1.4.6 TCR–MHC independent Ca^{2+} rises

Interestingly even in non-selecting thymic slice environments, sporadic Ca^{2+} rises in DP thymocytes have been recorded (shown in Figure 1.5C; adapted from Bhakta *et al.* 2005). Occurring in approximately 15% of seeded thymocytes the authors proposed that these might be evoked by spontaneous integrin-mediated signal transduction. As mentioned previously, during thymocyte–TEC interaction and in the absence of TCR stimulation, CD8–MHC-I interaction alone caused apoptosis (Grebe *et al.* 2004). While the authors did not examine the $[Ca^{2+}]_i$, other studies have reported that antibody cross-linking with an extracellular CD8 epitope lead to increased tyrosine phosphorylation of Lck (Irie *et al.* 1998,

Veillette *et al.* 1989). This, together with an increase in $[Ca^{2+}]_i$, perhaps via mechanical and/or Src kinase mediated activation of a Ca^{2+} permeable ion channel (Hisatsune *et al.* 2004, Jin *et al.* 2004, Vazquez *et al.* 2004, Xu *et al.* 2003), could provide the inside-out signal sufficient to induce a conformational change of LFA-1 to its receptive state. In conditions of suboptimal TCR stimulation, ligation of surface receptors such as CD2 and LFA-1 with their endogenous agonists present on the TECs has been shown to evoke $[Ca^{2+}]_i$ rises, most likely via synergistic enhancement of signal transduction and activation of different kinases, including the tyrosine kinases Lck, Syk and Fyn (Danielian *et al.* 1992, Kim *et al.* 2009a, Nonoyama *et al.* 1989, Paessens *et al.* 2008, Umehara *et al.* 1998, Walk *et al.* 1998, Zhao & Iwata 1995). In the case of preselection DP thymocyte–$cTEC^{hi}$ interaction, activation of CD8 by HS binding (Simon Davis 2015) may further enhance signalling, potentially leading to activation of more than one Ca^{2+} mobilising mechanism and resulting in an enhanced Ca^{2+} rise, as illustrated in Figure 1.4. With regard to the current research, the $[Ca^{2+}]_i$ rise induced by the addition of DxS is thought to be enabled by activation of such a synergistic signalling pathway.

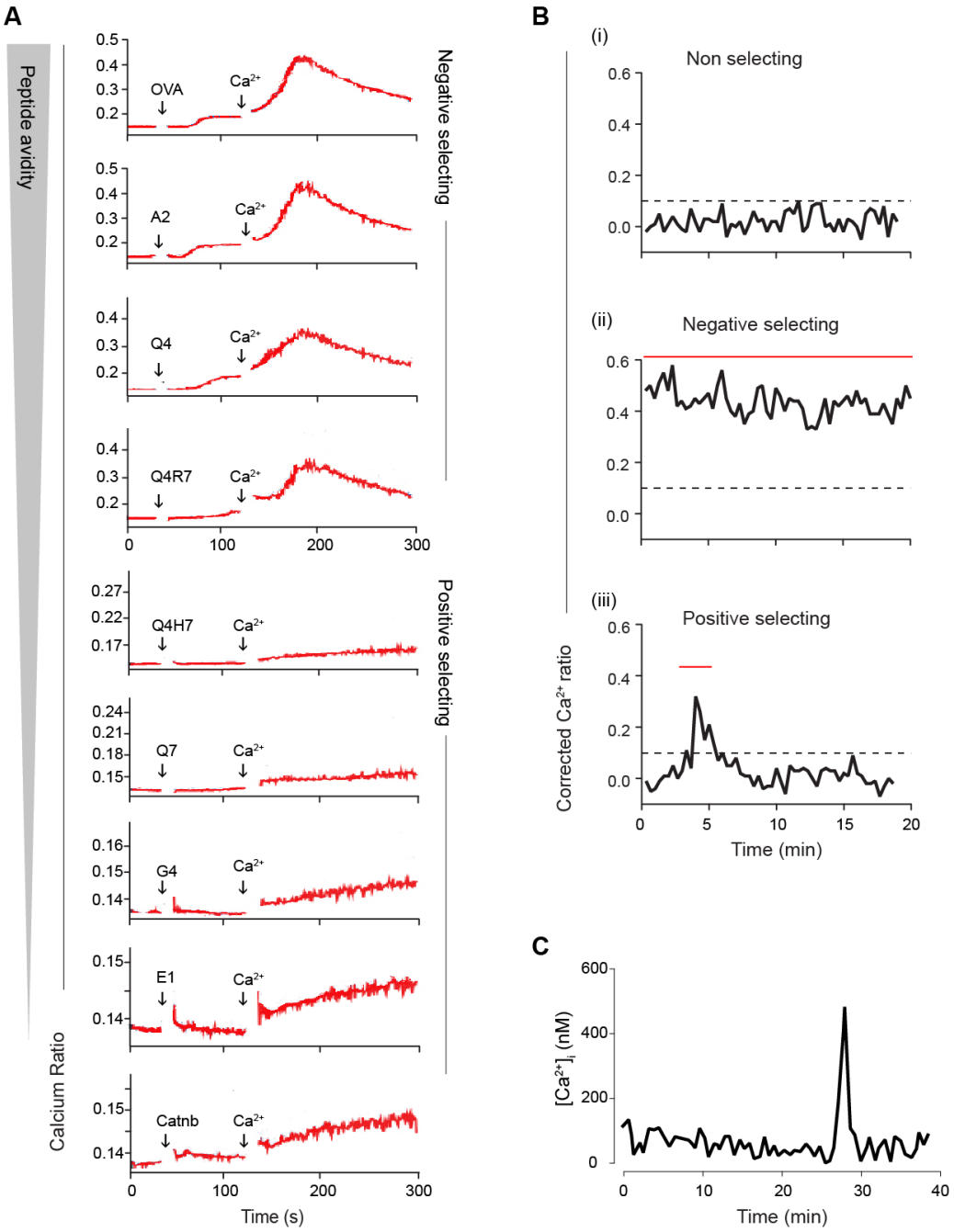

Figure 1.5 Selection associated Ca^{2+} fluxes in DP thymocytes

(A) Ca^{2+} time courses measured using flow cytometry in OT-1 thymocytes responding to the addition of antigen peptides OVA–Catnb (from top to bottom). In all samples, the $[Ca^{2+}]_o$ was initially kept nominally 0 mM and was restored to normal after 2 min. Note the change in scale of the abscissa from top to bottom. (B) Plots of Ca^{2+} ratio in individual thymocytes under (i) non-selecting, negative (ii) and positive (iii) conditions. The red line indicates period of thymocyte-TEC interaction. Dashed line indicates the upper limit of background $[Ca^{2+}]_i$ under resting conditions. (C) Spontaneous $[Ca^{2+}]_i$ rise occurring during a non-selecting condition.

1.5 The "Tellam-Parish" Ca^{2+} rise

Central to this thesis is the study by Tellam and Parish (1987) who described a sustained $[Ca^{2+}]_i$ rise that was induced in thymocytes following the addition of 0.1 mg/mL DxS, but not by the addition of other smaller mol. wt. polysulfated polysaccharides. The rise was carried by an influx of Ca^{2+} across the PM and seemed independent of ER store release as EGTA chelation of $[Ca^{2+}]_o$ abolished it. Subsequent investigations found this DxS induced $[Ca^{2+}]_i$ rise was specific to glucocorticoid-sensitive DP thymocytes (Weston *et al.* 1991), indicative of preselection DP thymocytes (Ohoka *et al.* 1996). As shown in Figure 1.3D, DxS added to a thymocytes in a spectroscopy cuvette resulted in a biphasic $[Ca^{2+}]_i$ rise. This rise comprised a small increase shortly after the addition of DxS followed approximately 4 min later by a significantly larger $[Ca^{2+}]_i$ rise of 165 ± 11 nM (Tellam & Parish 1987), which slowly reached a sustained maximum after 15 min.

However, distinct from DxS, the addition of 0.1 mg/mL heparin (12.5 kDa) or 0.1 mg/mL DxS (5 kDa) to DP thymocytes in suspension elicited only a negligible $[Ca^{2+}]_i$ increase (Tellam & Parish 1987). This observation suggests that activation of other surface receptors and adhesion molecules may be involved in causing the $[Ca^{2+}]_i$ rise. It appears that in contrast to heparin and low mol. wt. DxS (5 kDa), the significantly larger DxS molecule interacts not only with CD8β but potentially also binds and/or cross-links with other surface receptors.

1.6 Overview of Ca^{2+} handling mechanisms in thymocytes

As proposed earlier, to modulate the resting $[Ca^{2+}]_i$ and shape Ca^{2+} rises downstream of thymocyte–TEC interaction there must be a range of Ca^{2+} handling mechanisms in place (Badou *et al.* 2013, Feske 2013, Matza *et al.* 2016). *In vivo*, multiple signalling receptors may be activated during thymocyte–TEC interaction, leading to synergistic enhancement of signal transduction via

activation of different kinases. These include the tyrosine kinases Lck, Syk and Fyn (Danielian *et al.* 1992, Nonoyama *et al.* 1989, Paessens *et al.* 2008, Umehara *et al.* 1998, Walk *et al.* 1998, Zhao & Iwata 1995), protein kinase C (PKC) isoforms and the phosphatase CD45, which together potentially result in the activation of more than a single Ca^{2+} mobilising target (reviewed by Kotturi *et al.* 2006, Shiroo *et al.* 1992).

An increasing number of ion channels and transporters some of which are Ca^{2+} permeable, have been positively identified in thymocytes though, often, their functional role remains unclear. While different patterns of Ca^{2+} rises are required during thymopoiesis, knowledge of the molecular nature of the respective Ca^{2+} rises involved in positive selection, negative selection and in the mechanism underpinning death by neglect or "death by instruction" (Grebe *et al.* 2004) remains incomplete. In the next sections, I will review some of the ion channels and transporters proposed to have roles in thymopoiesis and also channels, not specifically identified in thymocytes, but considered as potential candidates in the DxS $[Ca^{2+}]_i$.

1.6.1 Ion channels and transporters identified in thymocytes

Table 1.1 lists functional Ca^{2+} permeable channels, ion transporters/exchangers and Na^+, K^+ and Cl^--selective channels reportedly present in thymocytes that potentially affect $[Ca^{2+}]_i$ homeostasis and/or mediate distinct $[Ca^{2+}]_i$ signals.

1.6.1.1 Voltage-gated cation channels

Included are several channels that activate in response to local changes in PM potential, and as indicated by their name, these voltage-gated channels, K_V, Ca_V and Na_V are highly selective for K^+, Ca^{2+} and Na^+, respectively. Upon reaching a threshold voltage these channels undergo a rapid conformational change that opens the pore and allows the flow of ions down the electrochemical gradient.

As in excitable cells, K_V channels have a role in restoring the resting membrane potential (V_m) following depolarisation and so can modulate the influx of both Ca^{2+} and Na^+ through other open channels. However, it is notable that prolonged or repeated depolarisation will in activate $K_V1.3$ (reviewed by Cahalan *et al.* 2001).

Ca_V channels have been well described in excitable cells (Hille 2001). While a few voltage-dependent Ca^{2+} channels (typically T- and some L-type) can be activated at low voltage that is not far from the resting membrane voltage which is typically around -60 mV, most Ca_V channels (N-, P/Q- R- and most L-type) require considerable membrane depolarisation (typically ≥-25 mV) to stimulate their gating. However, in lymphocytes this dependency on voltage-gating may be lost. Recent evidence suggests that the L-type channels expressed in T lymphocytes are structurally distinct and may be insensitive to membrane depolarization. As a consequence of alternative pre-mRNA splicing, $Ca_V1.1$ and $Ca_V1.4$ channels are made up of subunits with a disrupted "voltage sensing" domain. Consequently, these channels are not significantly gated by membrane depolarisation (reviewed by Davenport *et al.* 2015, Kotturi & Jefferies 2005, Matza *et al.* 2016). Rather, constitutive activity of these channels is thought to be inhibited by binding of the calcium sensing molecule STIM 1 at the channel C-terminal region (Park *et al.* 2010, Wang *et al.* 2010, Zinchenko *et al.* 2009).

Table 1.1 Ion channels and transporters detected in thymocytes

Channel type	gene	Ion permeability	
Na_V	*Scn4b* *Scn5a* ($Na_V1.5$)	Na^+	(Lo *et al.* 2012)
K_{Ca}	*Kcnn4* ($K_{Ca}3.1$)	K^+	(Mahaut-Smith & Mason 1991)
K_V	*Kcna3* ($K_V1.3$) *Kcna1* ($K_V1.1$)	K^+	(Freedman *et al.* 1995, Kazama *et al.* 2012, Koni *et al.* 2003, Koo *et al.* 1997, Lewis & Cahalan 1988, McKinnon & Ceredig 1986)
CIC	*Clcn2* *Cln3* *TMEM16a*	Cl^-	(Koni *et al.* 2003) (Suzuki *et al.* 2014)
Ca_V	*Cacna1c* ($Ca_V1.2$) *Cacna1d* ($Ca_V1.3$) *Cacna1f* ($Ca_V1.4$) *Cacnb1* *Cacnb2* *Cacnb3*	Ca^{2+}	(Jha *et al.* 2015, Jha *et al.* 2009) (Omilusik *et al.* 2011)
CRAC	*Orai/STIM*	Ca^{2+}	(Oh-hora *et al.* 2013)
IP_3R	*Itpr1* *Itpr2* *Itpr3*	Ca^{2+}	(Khan *et al.* 1996, Khan *et al.* 1992b, Ouyang *et al.* 2014)
Purinoceptor	*P2rx1* *P2rx2* *P2rx6* *P2rx7*	NSC	(Chvatchko *et al.* 1996, Courageot *et al.* 2004, Delfino *et al.* 2011, Freedman *et al.* 1999, Lépine *et al.* 2006, Nagy *et al.* 2000)
TRP	*Trpm7*	NSC	(Jin *et al.* 2008a)
	Trpm2	NSC	(Gasser & Guse 2005)
	Trpm4	Na^+	(Launay *et al.* 2004)
	Trpa1	NSC	(indirect; Hurne *et al.* 2002, Koh *et al.* 1998)
	Trpv1	NSC	(Amantini *et al.* 2004, Farfariello *et al.* 2012)
	? Trpv6	Ca^{2+}	(Peng *et al.* 1999)
iGluRs	*Grin1* NMDAR	NSC	(Affaticati *et al.* 2010)
nAChR	*? Chrna1* *Chrna9*	NSC	(Toyabe *et al.* 1997)
NCX	*Slc8a1*	$3Na^+$: Ca^{2+}	(Echevarria-Lima *et al.* 2003)
Na/K-ATPase	*Atp1a1* *Atp1a3*	$3Na^+$: $2K^+$	(Mann *et al.* 2001, Rodrigues-Mascarenhas *et al.* 2009)

1.6.1.2 **Voltage-independent Ca^{2+} permeable channels**

Also listed in Table 1.1 are the voltage-independent cyclic nucleotide gated (CNG) channels and transient receptor potential (TRP) channel family. Typically, these channels do not require a depolarisation for activation, although some TRP channels display non-classical voltage sensitivity (reviewed by Bertin & Raz 2016). Instead, their activation may be due to locally experienced factors like the metabolic state, availability of 2nd messengers, temperature and mechanical load. Distinct from Cav channels, TRP and CNG are typically cation-selective and consequently, may have only a partial conductance for Ca^{2+} (Cahalan & Chandy 2009, Ramsey *et al.* 2006, Robert *et al.* 2011, Varnum & Dai 2015).

1.6.1.3 **Ligand-gated Ca^{2+} permeable channels**

Other non-selective cation channels reportedly expressed in thymocytes are the ionotropic glutamatergic (iGluR), purinergic (P2XR) and nicotinic acetylcholine (nAChR) receptors. Activation of these channels depends upon agonist ligand (glutamate, adenosine triphosphate and acetylcholine, respectively) binding at the receptor site, to induce a conformation change in the protein that gates the pore (Burnstock & Boeynaems 2014, Fujii *et al.* 2017).

1.6.1.4 **2nd messenger-gated channels**

In thymocytes the generation of second messenger signalling molecules, including IP_3, DAG and Ca^{2+} facilities activation of 2nd messenger-gated channels expressed on the ER/mitochondrial membrane as well as the PM. IP_3 triggered activation of IP_3R located in the ER membrane and Ca^{2+} mediated ryanodine receptor activation results in ER Ca^{2+} release and subsequent activation of SOCE channels, most notably Orai channels. Debatably, some canonical TRP (TRPC) and vanilloid TRP (TRPV) channels also function as SOCE channels (DeHaven *et al.* 2009). While the STIM/Orai channel complex and TRPV6 are highly selective

for Ca^{2+}, TRPC channels are non-selective cation channels with variable selectively for divalent *vs.* monovalent cations (reviewed by Gees *et al.* 2011). Since TRP channels are thought to be involved in the DxS $[Ca^{2+}]_i$ they are reviewed in more detail in section 1.7.2.

1.6.1.5 **Ca^{2+} activated K^+ channels**

Thought to be important in enabling sustained Ca^{2+} entry through activated SOCE channels in T-lymphocytes (reviewed by Chandy *et al.* 2004), the Ca^{2+} activated K^+ channel $K_{Ca}3.1$ is also expressed by thymocytes. Located on the PM, channel gating is regulated by the Ca^{2+} sensing protein calmodulin which is tightly bound in the $K_{Ca}3.1$ C-terminal region. Co-located with Ca^{2+} permeable channels, $K_{Ca}3.1$ activation is triggered when a rise in $[Ca^{2+}]_i$ results in Ca^{2+}–calmodulin binding (K_d ~300 nM; reviewed by Cahalan *et al.* 2001). The consequent K^+ efflux via this intermediate conductance channel induces a repolarization, effectively lowering V_m and so increasing the electrical driving force for Ca^{2+} to enter the cell.

1.6.2 **Crucial channels in thymopoiesis**

Our understanding of channels crucial to thymocyte maturation is far from complete. Ca^{2+} signalling during thymopoiesis is likely to be complex, highly variable and dependent upon orchestration by multiple channels that may well be differentially expressed at distinct stages of development and in response to different signalling pathways. Of the channels listed in Table 1.1, a few have been identified as having a critical role in thymopoiesis (see sections below). In general, mutations affecting the function of these channels has been shown to alter the outcome of thymocyte maturation, *e.g.* reducing the size and/or altering the ratio of $CD8^+$ and $CD4^+$ lineage cells in the peripheral T-cell population.

1.6.2.1 **TRPM7$^{-/-}$ causes impaired DN3 differentiation**

Notably, deletion of the transient receptor potential melastatin 7 (TRPM7) channel results in a partial block of thymocyte maturation beyond the DN3 phase and significant reduction of the DP and CD4 SP populations (Jin *et al.* 2008a). TRPM7 forms an unusual channel–kinase complex (discussed further in 1.7.3.3.4) and is proposed to play a role in Mg^{2+} homeostasis. However, in the TRPM7 deficient thymocytes cellular Mg^{2+} was not apparently disturbed. Rather, these authors observed a change in thymic architecture and mTEC maintenance. As development of the varied thymic microenvironments is crucially influenced by thymocyte–TEC cross-talk, perhaps as observed in developing lung fibroblasts (Wei *et al.* 2009), a loss of TRPM7-evoked "Ca^{2+} flickers" similarly impairs thymocyte migration and adhesion. Typical of TRP family channels, TRPM7 is gated by multimodal mechanisms, including direct activation by membrane stretch (Numata *et al.* 2007). It is well established (reviewed by Takahama 2006) that thymocyte–stromal cell interactions across varied thymic microenvironments are pivotal to thymocyte maturation. Failure to receive the necessary development signals from stromal cells will disrupt thymocyte proliferation and differentiation (reviewed by Dzhagalov & Phee 2012, van Ewijk *et al.* 2000, van Ewijk *et al.* 1994).

1.6.2.2 **Kv1.1 and 1.3 channels indirectly modulate Ca^{2+} entry**

While not permeable to Ca^{2+}, the voltage-gated K^+ channels, $K_V1.1$ and $K_V1.3$ also play a role in early thymopoiesis and are proposed to indirectly modulate Ca^{2+} entry. Specifically, Freedman *et al.* (1995) showed the addition of dentrotoxin and charybdotoxin ($K_V1.1$ and $K_V1.3$ antagonists, respectively) significantly reduced DN thymocyte proliferation and decreased the DP population in fetal thymic organ cultures. In T lymphocytes, $K_V1.3$ channels activate at >-50 V_m and reach half maximal activation at ~-30 mV (Hajdu *et al.* 2003, McKinnon & Ceredig 1986).

As V_m in T lymphocytes is maintained between -50 to -70 mV (reviewed by Cahalan & Chandy 2009, Ishida & Chused 1993) it is likely a small number $K_V1.3$ channels are readily activated. Comparable to the V_m value (-50 mV) proposed by Cahalan and Chandy (2009), I found the resting V_m in thymocytes to be 49.5 ± 12.5 mV, n = 15. This value was obtained from patch clamp experiments conducted as part of my honours research project in 2012 (Feakes 2012). Not unexpectedly, in T lymphocytes, inhibition of these K^+ channels, which normally maintain the electronegative resting membrane potential by efflux of K^+ (Hess *et al.* 1993), causes membrane depolarisation which consequently reduces Ca^{2+} influx (Hess *et al.* 1993, Liu *et al.* 2002).

Surprisingly however, thymocyte proliferation and development is normal in $K_V1.3^{-/-}$ mice. In the $K_V1.3$ deficient thymocytes, Koni *et al.* (2003) found Cl^- conductance was increased by 50-fold which, they suggest, restored the normal V_m. This compensatory mechanism indirectly supports the role of K_V channels in maintaining normal V_m, a requirement for normal Ca^{2+} influx (Hess *et al.* 1993) and DN thymocyte proliferation and differentiation.

1.6.2.3 **$Ca_V(\beta2)^{-/-}$ causes impaired DN differentiation**

Disrupted differentiation from the DN3 to DN4 stage has been reported in thymocyte precursors deficient in the β2 regulatory subunit of voltage-gated Ca^{2+} channels ($Ca_V\beta2$; Jha *et al.* 2015). In DN thymocytes it appears the β2 regulatory subunit combines with the 1.2 or 1.3 isoform of the Ca_V pore forming α subunit to create functional channels. Consequently, the abundance of $Ca_V1.2$ and $Ca_V1.3$ channels was found to be reduced in $Ca_V\beta2$ deficient thymocytes. Examining the effect on thymopoiesis, Jha *et al.* (2015) found the DP population and consequently the peripheral T cell pool were substantially depleted. This perhaps reflects an alteration of the crucial biphasic Ca^{2+} signals associated with β-selection. Whether these channels continue to have roles in DP selection

processes and/or death by instruction/neglect is not known particularly as expression of the α and β subunits of Ca_V varies markedly between DN, DP and SP thymocytes and T lymphocytes (Badou *et al.* 2013, Badou *et al.* 2006, Jha *et al.* 2015, Matza *et al.* 2016, Omilusik *et al.* 2011).

1.6.2.4 **Ca_V1.4 and Na_V1.5 regulate CD4 lineage selection**

L-type Ca_V1.4 (Omilusik *et al.* 2011) and the TTX insensitive voltage-gated Na^+ channel Na_V 1.5 ($Scn5a^{-/-}$ and $Scn4\beta^{-/-}$; Lo *et al.* 2012) have been shown to be important for lineage dependent differentiation in thymopoiesis. Analysis of the SP CD4 and SP CD8 in thymocytes deficient in either of these channels showed a significant decrease in the number of SP CD4 cells, while the SP CD8 population was not markedly affected. In these thymocytes, TCR activated Ca^{2+} signalling was shown to be significantly reduced however, SP CD8 differentiation again appeared relatively unchanged. Interestingly, McRory *et al.* (2004) found very few cells in the thymus positively stained for Ca_V1.4 protein. This might indicate that, rather than being expressed by DP thymocytes, Ca_V1.4 channel activity may be required at a later developmental stage where it crucially regulates CD4 lineage differentiation.

1.6.2.5 **Orai/STIM channels are not critical for thymocyte maturation**

While the SOCE channels STIM/Orai (Feske *et al.* 2005) and Ca_V1 channels (particularly Ca_V1.4 channels which contain a unique α_{IF} and β4 subunits) have been shown to play crucial roles in mature T cell survival and function, thymocytes deficient in these genes show only subtle changes in development (Kotturi & Jefferies 2005, Oh-hora *et al.* 2013, Omilusik *et al.* 2011). Perhaps this reflects different and limited expression of these channels in the thymocyte PM compared to naïve and mature T cells (Badou *et al.* 2006, Kotturi & Jefferies 2005, McRory *et al.* 2004).

The expression profile of *Orai* and *Stim* isoforms vary at distinct stages of T cell maturation (as shown in Fig. 1.6, an extract from the BioGPS database; Barrett *et al.* 2013, Edgar *et al.* 2002). This phenomenon may reflect the apparent difference in dependence on STIM/Orai channels for normal function. In the BioGPS database the median value (M) is derived from the gene expression profile from an array of normal mouse embryonic and mature tissues, cell lines and organs. In each case, the gene expression profile is shown relative to the median value which was determined from the expression profile from a diverse range (96) of normal tissues, organs, and cell lines obtained from naïve male C57BL/6 mice and hybridized to MOE_2 arrays.

Notably, in thymocytes the expression profile of *Stim2* is higher than that of *Stim1* (Figure 1.6B). An increase in STIM2 protein perhaps also provides an additional mechanism for inhibition of Orai channel Ca^{2+} influx during early T cell development. What cannot be deduced from the Bio GPS data and remains to be investigated, is the relative expression in thymocytes of the *Stim2* spice variants: *Stim2α* and *Stim2β*. Distinct from STIM1 and STIM2α, STIM2β has been shown to block Orai channel activation and hence negatively modulate SOCE (Rana *et al.* 2015).

Related to Orai channel activation, IP_3R-mediated Ca^{2+} release has also been shown to play crucial role in directing thymopoiesis and programmed cell death (Khan *et al.* 1996, Ouyang *et al.* 2014). However, the significant redundancy within the IP_3R genes (*Itpr1, Itpr2 & Itpr3*) ensures normal DP thymocyte development; such that, Ouyang *et al.* (2014) found transition from the DN4 to DP stage was significantly disrupted only when all 3 genes were conditionally knocked out.

Aside from the well-described role the IP_3Rs play in the release of Ca^{2+} from the ER (reviewed by Fedorenko *et al.* 2014), in thymocytes ~30% of IP_3Rs are enriched

with sialic acid and proposed to be located at the PM. Distinct from the ER located receptor, the PM associated IP_3R has a higher affinity for inositol 1,3,4,5-tetrakisphosphate (IP_4) (Khan *et al.* 1992b). Proposed roles for these PM bound IP_3Rs are facilitation of the $[Ca^{2+}]_i$ plateau phase observed in lymphocytes after a proliferative stimulus (Khan *et al.* 1992a) and regulation of apoptosis in thymocytes via modulation of capacitive Ca^{2+} influx (Khan *et al.* 1996).

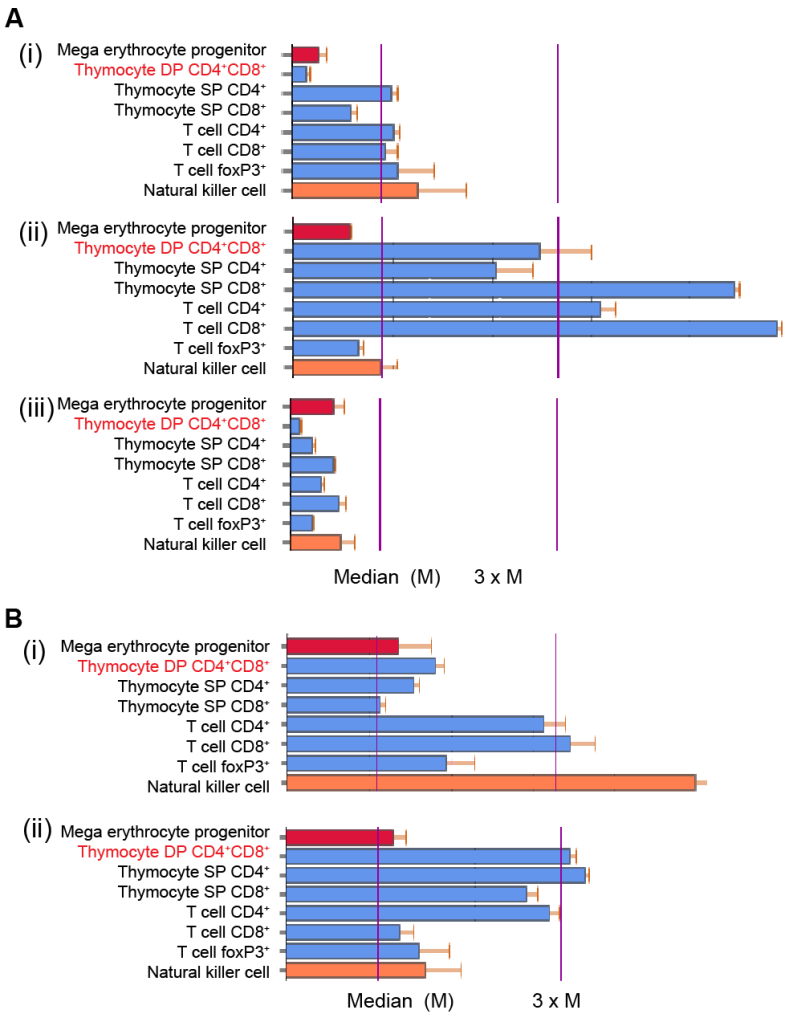

Figure 1.6 Relative Orai expression profile in T lymphocyte populations

mRNA expression data detailed in the BioGPS database (dataset: GeneAtlas MOE430, gcrma) which shows the variation in expression of *Orai* and *Stim* isotopes during T cell maturation. A. (i) *Orai1:* probe set 1424990_at; (ii) *Orai2:* probe set 1424990_at; (iii) *Orai3:* probe set 1424990_at. B. (i) *Stim1*: probe set 1436945_x_at; (ii) *Stim2:* probe set 1441024_at.

1.6.3 Channels linked to thymocyte apoptosis

Channels reported as having a role in thymocyte death, have in general been determined through the application of either glucocorticoids or adenosine 5'-triphosphate (ATP; or its analogue). Studying the effect of 0.1 μM dexamethasone on rat thymocytes, Khan *et al.* (1996) noted a 20-fold increase in IP_3R (type 3) protein at the PM, an associated Ca^{2+} rise and induced apoptotic changes. Significantly, in thymocytes transfected with antisense IP_3R3 mRNA the dexamethasone evoked changes were abolished. Based on these findings the authors propose that that the PM IP_3R3 provided a mechanism for Ca^{2+} entry that lead to cell apoptosis. Notably, their results do not rule out the possibility that another channel was responsible for the Ca^{2+} flux.

For instance, canonical transient receptor potential channels (TRPC; further reviewed in 1.7.3) contain regulatory IP_3R/calmodulin (CaM) binding site within their C-terminal region (Kiselyov *et al.* 1998, Kwon *et al.* 2007, Tang *et al.* 2001, Yuan *et al.* 2003). While the expression of TRPC channels in thymocytes remains to be determined, they have been reported in other T lymphocytes and so may provide an IP_3R-dependent mechanism for Ca^{2+} influx (Kim *et al.* 2006, Vazquez *et al.* 2006). While the involvement of TRPC channels in apoptotic signalling pathways remains undefined, it is noted that, TRPC3 and TRPC6 activation have been linked to apoptosis in septic T- lymphocytes.

1.6.3.1 P2X receptors

While purinoreceptors (P2XRs) do not play a role in glucocorticoid mediated thymocyte death (Jiang *et al.* 1996), their ligand activation by extracellular ATP has been linked to thymocyte apoptosis. P2X1, -X2, -X6 and -X7 channels are reportedly expressed in thymocytes (see Table 1.1). Located in the PM, these ligand-gated channels are rapidly activated by extracellular ATP and commonly

are permeable to Ca^{2+}, Na^{+} and K^{+}. In thymocytes, apoptosis can be induced upon activation of P2X7R (Courageot *et al.* 2004, Le Stunff *et al.* 2004) and perhaps P2X1R (Ross *et al.* 1997). Investigating the mechanism involved, Shoji *et al.* (2014) found in mature murine T cells, non-selective pannexin1 channels (Panx1) modulated the Ca^{2+} influx observed in response to P2X7R activation. But notably, in T cells obtained from $Panx1^{-/-}$ mice, the ATP induced Ca^{2+} was not abolished. While this functional role was studied using mature T cells, Locovei *et al.* (2007) have provided evidence of functional Panx1 channels in thymocytes. These large pore forming channels are described as having variable conductance, that ranges from 50–500 pS depending upon the activating stimuli. In their high conductance state Panx1 channels may allow ATP efflux which in turn provides a feedback stimulus that acts on the P2XR and promotes Ca^{2+} waves (reviewed by Whyte-Fagundes & Zoidl 2018).

Adding further complexity to the ATP activation of thymocyte purinoreceptors and the resultant Ca^{2+} driven apoptotic response (reviews by Alves *et al.* 1999, and Burnstock & Boeynaems 2014) the mechanism may also be specific to the stage of thymocyte development (El-Moatassim *et al.* 1989, Ross *et al.* 1997).

1.6.4 Transporters, exchangers and channels that can modulate $[Ca^{2+}]_i$

As mentioned earlier, $[Ca^{2+}]_i$ rises associated with activation of Ca^{2+} permeable channels, are countered by the activation of ion transporters which may be facilitated by the transmembrane flux of ions besides Ca^{2+} via Na^{+}, K^{+} or Cl^{-} channels. Figure 1.7 schematically illustrates how the interplay between channels and transporter activity might modulate $[Ca^{2+}]_i$. Active ion transport is facilitated by Ca^{2+}-ATPase pumps on the PM and ER (PMCA and SERCA, respectively). Deriving energy from ATP hydrolysis, these pumps remove Ca^{2+} from the cytosol into the extracellular milieu or the ER lumen by transporting Ca^{2+} against its concentration gradient.

In thymocytes, the moderate constitutive leak of Ca^{2+} from the ER is normally balanced by Ca^{2+} reuptake via the SERCA pump. Pharmacological inhibition of SERCA, using drugs such as cyclopiazonic acid (CPA) or thapsigargin, provides evidence of the leak and is a commonly used method to induce depletion of $[Ca^{2+}]_{ER}$. This protocol enables investigation of the relationship between the ER store release and various Ca^{2+} entry mechanisms via channels or transporters.

Transport of Ca^{2+} is commonly enabled by Na^+/Ca^{2+} antiporters, which are also referred to as exchangers. Of the 3 genes encoding sodium-calcium exchangers (*Slca8a1–Slca8a3*), *Slca8a1* (NCX1) has the highest expression in DP thymocytes (>3 x median expression; probeset:1420210_at; dataset: GeneAtlas MOE430, gcrma; BioGPS data base). NCX uses the concentration gradients of Ca^{2+} and Na^+ to couple transport (in opposing directions) of 1 Ca^{2+} against 3 Na^+ producing a net ion flux that is electrogenic. Importantly, the direction of the ion exchange is not fixed and NCX activity may shift between "forward" and "reverse" modes depending upon ion concentrations and V_m. The extrusion of Ca^{2+} and influx of Na^+ during forward (exit) mode causes a depolarization, while the reverse (entry) mode which brings Ca^{2+} into the cytosol and extrudes Na^+ results in a hyperpolarization. Having a markedly higher maximal rate than the PMCA, activation of the NCX can rapidly alter V_m, thereby altering the electrochemical driving force and affecting the $[Ca^{2+}]_i$ and also $[Na^+]_i$ (reviewed by Blaustein & Lederer 1999, Verkhratsky *et al.* 2017).

In activated human peripheral T cells and Jurkat cells, Wacholtz *et al.* (1993) found that pharmacological block of NCX activity reduced the movement of Ca^{2+} across the PM and so reduced the expected TCR-induced increase in $[Ca^{2+}]_i$. Based on their findings they proposed that in T lymphocytes reverse mode NCX activity may sustain a $[Ca^{2+}]_i$ rise. However contrary to their results, Donnadieu

and Trautmann (1993) found no evidence to support reverse mode NCX activity in these cells.

In murine thymocytes evidence for functional NCX activity is reported by Echevarria-Lima *et al.* (2003). Their research demonstrated reverse mode activation of the NCX, when the Na^+ gradient was pharmacologically lowered by the addition of ouabain (Echevarria-Lima *et al.* 2003), which blocks the sodium-potassium ATPase (Na-K-ATPase; preventing K^+ influx and Na^+ extrusion at a ratio of 2:3). However, activation of this mode under physiological conditions remains to be determined. The use of drugs such as YM244769 and SN-6, which preferentially inhibit the NCX reverse mode, may provide more information on a role for NCX in facilitation of sustained $[Ca^{2+}]_i$ rises.

Additional to NCX, sodium-potassium-calcium exchangers (NCKX) co-transport Ca^{2+} and K^+ across the PM using energy derived from the ion gradients of Na^+ and to some extent K^+. In DP thymocytes, expression of the genes encoding NCKX exchangers (*Slc24a1-Slc24a4*) does not exceed the median value and a functional role for NCKX in thymocytes is uncertain. The transport of 4 Na^+ counter to 1 Ca^{2+} plus 1 K^+ results in the net movement of one positive charge and like the NCX, NCKX activity also produces a change in V_m (reviewed in Altimimi & Schnetkamp 2007).

The local electrogenesis of such transporters can alter V_m, and consequently vary the transmembrane ionic driving force acting on Ca^{2+}. Responsible for setting the $[Na^+]_i$, the Na^+-K^+-ATPase actively exchanges 3 cytosolic Na^+ ions for 2 extra-cellular K^+ ions. This acts to lower V_m and maintain the gradient for Na^+ and also Ca^{2+} to enter the cell (Skou & Esmann 1992). In T lymphocytes, Ishida and Chused (1993) found inhibition of the Na^+-K^+-ATPase with ouabain, or removal of $[K^+]_o$, caused a depolarisation of T lymphocytes. Similarly, margatoxin or charybdo-toxin induced inhibition of K_V channels in lymphocytes causes a depolarization

and attenuates the amplitudes of $[Ca^{2+}]_i$ rises necessary for T cell activation and DP thymocyte differentiation (Koo *et al.* 1997, Leonard *et al.* 1992).

Additional to these transporters, there are Ca^{2+} transporters located on the inner mitochondrial membrane. Importantly, these transporters can modify oscillations in $[Ca^{2+}]_i$. Activation of the mitochondrial Ca^{2+} uniporter (MCU), Na^+-Ca^{2+} exchangers (NCLX) and Ca^{2+}-H^+ antiporter facilitates the sequestration and release of Ca^{2+} into and from mitochondria. This mitochondrial "buffering" of $[Ca^{2+}]_i$ rises enables the slow tuning their amplitudes and decays (Santo-Domingo & Demaurex 2010).

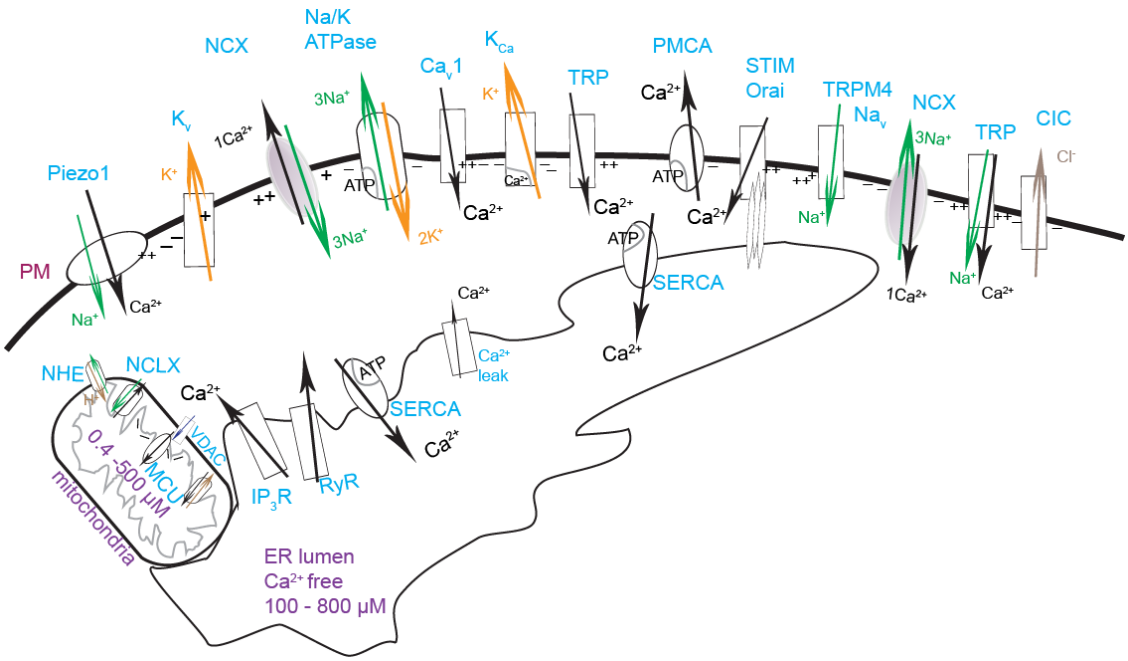

Figure 1.7 Mechanisms involved in $[Ca^{2+}]_i$ homeostasis

Schematic drawing of movement of ions via a broad range of ion channels, SERCA and PMCA Ca^{2+} pumps, NCXs (working in forward or reverse mode), mitochondrial Ca^{2+} uniporter (MCU) voltage-dependent anion channel and sodium-hydrogen exchanger (NHE). The interplay of these ionic mechanisms enables the removal of cytosolic Ca^{2+} against the concentration gradient into the ER, mitochondria and extracellular space. The movement of monovalent ions (Na^+, K^+, H^+ and Cl^-) across the various membranes via activated channels and or transporters locally alters the membrane voltage potential and modulates the driving force acting on Ca^{2+} influx.

1.6.4.1 **Regulation of channels and transporters by membrane lipids**

Increasing evidence suggests that in addition to being an important secondary messenger molecule, PIP_2 and other membrane lipids such as cholesterol, arachidonic acid (AA) and eicosanoids crucially regulate activation of numerous ion channels and transporters (Hofmann *et al.* 1999, Lemonnier *et al.* 2008, Lichtenegger *et al.* 2018, Lucas *et al.* 2003, reviewed by Morales-Lázaro & Rosenbaum 2017, Trebak *et al.* 2003, Woo *et al.* 2008, Zarayskiy *et al.* 2007), many of which raise $[Ca^{2+}]_i$ that trigger cellular responses (reviewed in Balla 2009, Hansen 2015, Hilgemann *et al.* 2001, Hille *et al.* 2015, Klein *et al.* 2014, Levitan *et al.* 2014, and Rohacs 2014, Rousseau *et al.* 2015). The formation of discrete membrane rafts rich in these lipids enables often complex modulation of channel activity through the association of lipids and protein/channel complexes and/or cytoskeleton-PM interaction (discussed by Horejsi *et al.* 2010, Lukacs *et al.* 2007, Morales-Lázaro & Rosenbaum 2017, Raucher *et al.* 2000, Suh & Hille 2008, Tolstykh *et al.* 2017). Modulated by lipid raft formation (Barbat *et al.* 2007) and downstream of TCR/CD3 Src tyrosine kinase activation, promotes $PI_3K\delta$ (Swat *et al.* 2006) and PLC-γ1 activation (Rameh *et al.* 1998) and subsequent hydrolysis of PIP_2. This discretely alters lipid concentrations of PIP_2, PIP_3 and DAG in localised domains of the PM (Loew 2007, Reddy & Bazan 1987, Tolstykh *et al.* 2017, Vazquez *et al.* 2010).

In many cell types including T lymphocytes, rapid phosphorylation of DAG by diacylglycerol kinases is thought to curb initial DAG induced signalling. However, subsequent activation of PKC and promotion of phospholipase D (PLD) and phosphatidic acid (PA) can result in a second and more sustained increase in DAG and long lasting activation of PKC (reviewed by Nishizuka 1992, Outram *et al.* 2002, Szamel *et al.* 1989).

Beyond this, subsequent hydrolysis DAG by DAG lipase and parallel cytosolic phospholipase A_2 ($cPLA_2$) enzymatic activity leads to the production of AA, a major regulatory lipid which can also have signalling properties. In turn, oxidization of AA via either the lipoxygenase, cyclooxygenase or cytochrome-P450 metabolic pathway gives rise to a multitude of eicosanoids (Rousseau *et al.* 2015) which also have potent signalling properties. Figure 1.8A schematically illustrates how the generation of the lipid signalling molecules DAG and AA downstream of activation of PLC-γ1, PKC, PLD_3 and PLA_2 and how the relative increase of these lipids within the cell over time (Fig1.8B) may lead in activation of DAG and AA sensitive TRP channels and sustained Ca^{2+} entry (adapted from Nishizuka 1992, and Szamel *et al.* 1989).

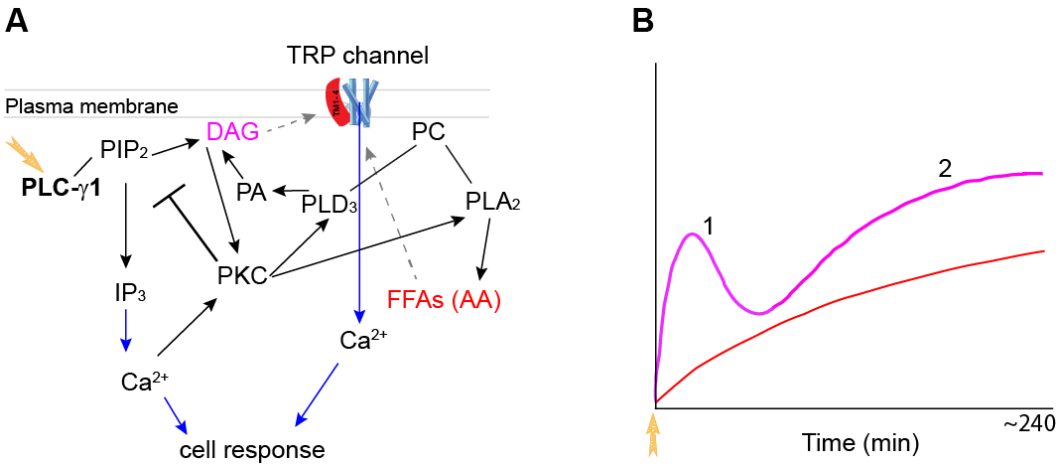

Figure 1.8 DAG and AA generation downstream of PLC activation

A. Schematic overview of how production of DAG and AA downstream of PIP_2 hydrolysis by PLC-γ1, and phosphatidylcholine (PC) hydrolysis by phospholipase D_3 (PLD_3) and PLA_2 may promote activation of TRP channels leading to Ca^{2+} entry. Downstream of PKC activation by DAG, activation of PLD_3 promotes ongoing DAG production via phosphatidic acid (PA). Production of free fatty acids (FFA), notably AA, by activated PLA_2 may further modulate TRP channel activity and Ca^{2+} influx. Rises in $[Ca^{2+}]_i$ can influence various cellular responses. B. Provides a schematic time course of DAG (pink) and AA (red) production over time. The first distinct rise(1) in DAG is in response to activation of PLC-γ1 (yellow arrow), while a second rise (2) occurs following PLD_3 activation. Shown in (A) PLD_3 and PLA_2 activation occurs following production of DAG and Ca^{2+} dependent PKC activation and subsequent hydrolysis of PC leads to increased AA production over time. Adapted from Nishizuka (1992).

Not surprisingly, many of these lipid mediators have been proposed as direct and indirect regulators of ion channel gating, in particular channels belonging to the large TRP family (reviewed in Bang *et al.* 2012, Caires *et al.* 2017, Ciardo & Ferrer-Montiel 2017, Eijkelkamp *et al.* 2013, Hwang *et al.* 2000, Sisignano *et al.* 2014, Taberner *et al.* 2015, Vazquez *et al.* 2010) and also Piezo channels (Borbiro *et al.* 2015).

1.6.4.1.1 **Modulation of ion channels by GAGs including DxS**

For this thesis, DxS was commonly used to evoke the specific Ca^{2+} rise in DP thymocytes (described in Section 1.5). While direct channel gating by DxS is not considered the primary mechanism for initiating this Ca^{2+} entry, it is noted that HS and other large sulfated polysaccharides, including DxS, can directly modify the activity of some ion channels. Specifically, both HS and DxS have been found to affect AMPA receptors in rat hippocampal neurons. Specifically, direct polysaccharide–AMPA receptor interaction was shown to enhance channel opening time and subsequently potentiate Ca^{2+} entry (Chicoine & Bahr 2007, Chicoine *et al.* 2004, Suppiramaniam *et al.* 2006). Additionally, externally applied heparin has an agonistic effect on Ca_V1 channels (in rabbit skeletal muscle cells; Knaus *et al.* 1992, Knaus *et al.* 1990). While AMPA receptors are reportedly involved in integrin-mediated adhesion in T cells (Ganor *et al.* 2003), their presence in DP thymocytes has not been established. However, L-type Ca^{2+} channels have been identified on thymocytes (Omilusik *et al.* 2011) and so perhaps might be potential binding targets of GAGs.

1.7 Overview of channels that may enable the DxS $[Ca^{2+}]_i$ rise

Investigating the DxS $[Ca^{2+}]_i$ rise, Tellam and Parish (1987) showed the Ca^{2+} influx was not altered by membrane depolarisation (induced by increasing $[K^+]_o$ to 60 mM) or by the addition of 3 μM nifedipine (a Ca_V1 type channel antagonist).

Additional to these results, pharmacological blocking experiments undertaken in 2012 (as my honours research project; outlined in Appendix 3; p.353) rule out Ca_V2 and 3 type voltage-gated Ca^{2+} channels, ligand gated receptors (specifically the P2XR, iGluR, PM bound IP_3R and nAChR) and the cyclic nucleotide gated channel CNGA1 as likely candidates. Rather, a Piezo channel and/or channels from the TRP family were considered potential candidates, in particular channels proposed to be mechanosensitive, modulated by Src kinase and membrane lipids.

1.7.1 **Piezo channels**

The recently identified Piezo channel family is small, having two members identified as Piezo1 and Piezo 2 (Coste *et al.* 2010). Comprising >2500 amino acid residues these proteins share approximately 54% sequence homology (MmPiezo; BLASTP 2.8.1; Altschul *et al.* 2005) and their deletion results in embryonic lethality (Dubin *et al.* 2012, Li *et al.* 2014). Formed from three subunits, these non-selective cation channels bear little resemblance to other known channels (Coste *et al.* 2012, Ge *et al.* 2015, Wang *et al.* 2018). While the Piezo2 structure is yet to be determined, a recently reported cryo-electron microscopy structure for Piezo1 predicts the presence of 38 transmembrane (TM) helices in each subunit. Surrounding the central pore region, three large extended arms containing six repeated 4-TM domains are predicted to curve the lipid bilayer. This results in formation of a dome like structure that is sensitive to mechanical displacement (Guo & MacKinnon 2017, Liang & Howard 2018). Sensing changes in lateral membrane tension these channels are directly gated by membrane deformation/flattening and lateral tension induced by pressure or stretch (Coste *et al.* 2010, Cox *et al.* 2016, Guo & MacKinnon 2017, Lewis & Grandl 2015, reviewed by Wu *et al.* 2017a).

In the literature, Piezo2 does not appear to have a significant role in immune system function. Rather, its proposed role is to facilitate somatosensory transduction in dorsal root ganglia sensory neurons and mechano-transduction in Merkel-cells (Coste *et al.* 2010, Woo *et al.* 2014). *Piezo2* expression in DP thymocytes (as provided in the ImmGen database, "abT cells group" and shown here in Figure 1.9B) is at least 10-fold lower than *Piezo1* expression.

1.7.2 **Piezo1 channel**

Piezo1 has been proposed to play a role in stem cell lineage differentiation (Li *et al.* 2014, Pathak *et al.* 2014) perhaps having an essential role in facilitating intracellular signalling (Gottlieb & Sachs 2012). Specifically in epithelial cells, Piezo1 activation of R-Ras (a small GTPase) was implicated in regulating an inside-out signalling pathway that activates endogenous β1 integrins and hence facilitate cell adhesion (McHugh *et al.* 2010).

In response to mechanical strain, the channel activates rapidly (<1 ms; Gottlieb *et al.* 2012) and has a single channel conductance of ~30 pS (Coste *et al.* 2010, Gottlieb *et al.* 2012). It also inactivates rapidly (τ = 16.0 ± 1.2 ms; Zhao *et al.* 2016) via a mechanism involving the extracellular carboxy (C) terminal domain and inner pore helix (Wu *et al.* 2017b) and remains inactivated in the continued presence of the ongoing force stimulus (Gottlieb *et al.* 2012, Wu *et al.* 2017a). Permeable to both mono and divalent cations, the selectivity filter slightly favours Ca^{2+} (Zhao *et al.* 2016); however, the conductance of Ca^{2+} is lower. Ca^{2+} permeation appears to be retarded by hydration shell–pore interactions (15 pS for Ca^{2+} *vs*. 36 pS for Na^{+} at -80 mV; Gnanasambandam *et al.* 2015). Unlike Orai and L-type Ca_V

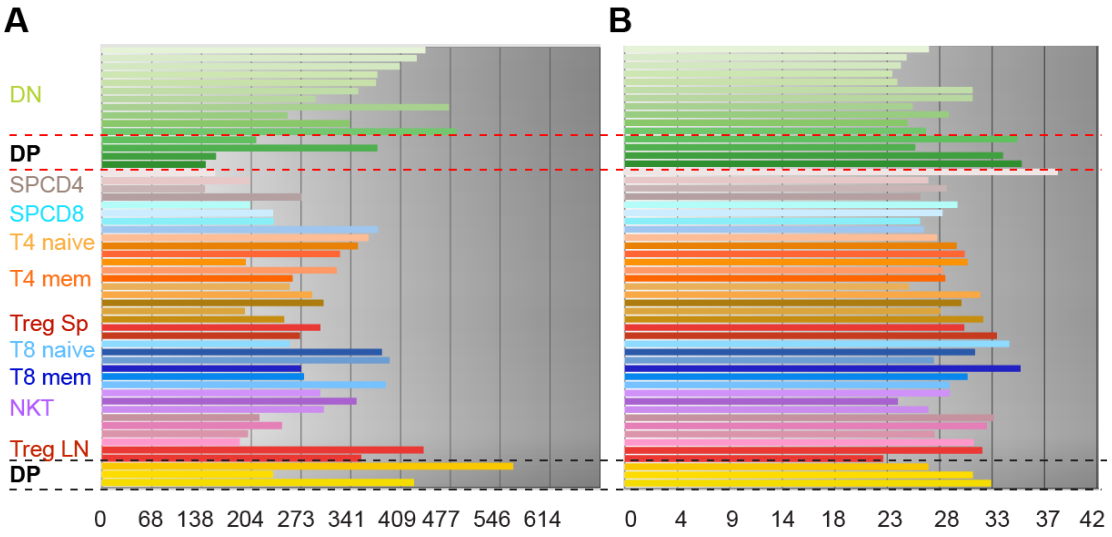

Figure 1.9 *Piezo1* and *Piezo2* expression in αβT lymphocyte populations

Screen shots of the relative mRNA expression of *Piezo1 (Fam38a)* and *Piezo2 (Fam38b)* transcripts in mice. The expression is predicted by the arbitrary numbers of transcripts given along the abscissa, where typically >120 indicates true expression (more than 95% probability), while <47 suggests the gene expression is unlikely or silent (Ericson *et al.* 2019). In descending order, the four DP subpopulations framed by dashed red lines are all, blasts, small resting and 69^+ early positive selection. The three DP subpopulations framed by the dashed black lines are DP 69^- preselection, DP 69^+ early positive selection, and DP early positive selection. Data for *Piezo1* (A; Probe set: 10582376) and *Piezo2* (B; Probe set: 10459363).

channels which have pore diameters of 6 and 6.2 Å, respectively and acid residues that coordinate shedding of the Ca^{2+} ion hydration shell as it moves through the selectivity filter (Cataldi *et al.* 2002, Rothberg *et al.* 2013), the pore diameter of Piezo 1 is predicted to be larger (~8 Å) and to allow permeation of hydrated Ca^{2+}.

Primarily gated by tensile forces, Piezo1 activity may also depend upon the presence of PIP_2 (Borbiro *et al.* 2015) and it can be inhibited by a phosphatidylserine redistribution to the outer leaflet of the PM (Tsuchiya *et al.* 2018). In addition, channel activity may be complexly modulated by membrane voltage (Moroni *et al.* 2018), by mechano-protective forces provided by cytoskeletal proteins, and by localisation to "stiffer" cholesterol-rich lipid rafts

which facilitate transmission of membrane tension to increase channel gating (Cox *et al.* 2016, Gnanasambandam *et al.* 2015, Qi *et al.* 2015).

1.7.2.1 **Piezo1 channels in thymocytes**

In thymocytes, the expression of Piezo1 and whether it plays a role in thymocyte selection is yet to be determined. However, in mature T cells, Piezo1 channel activation and consequent localised Ca^{2+} flux is proposed to have an important role in promoting TCR activation and signalling (Liu *et al.* 2018). The Immunological Genome Project (ImmGen) database, which primarily derives its data from Affymetrix Gene microarray profiling (Heng & Painter 2008, Painter *et al.* 2011), indicates that, unlike *Fam38b* (Piezo2) the relative expression of *Fam38a* (Piezo1) mRNA expression is high in the abT cells group, *i.e.* lymphocytes that express an αβTCR (Figure 1.9). Within the DP populations (outlined by the red dashed lines) a spike in expression is noted in the DP blast population. Likewise, a spike in expression is observed in the DP $CD69^-$ subset (outlined by the black dashed lines). As CD69 expression is an early indicator of TCR activation, appearing within 2 hours of TCR stimulation (Davey *et al.* 1998) the DP $CD69^-$ population is likely to represent preselection thymocytes. The presence of Piezo1 protein in thymocytes is yet to be identified, and while the mRNA observation is promising (Tian *et al.* 2004), it does not necessarily infer of translation to Piezo1 channel expression and localisation to the PM.

Recently it has been shown that sequential application of a 10–50 pN tensile force to the TCR but not to other surface receptors such as LFA-1 results in significant localised $[Ca^{2+}]_i$ increase (Kim *et al.* 2009b, Liu *et al.* 2014). While identification of the Ca^{2+} source was not within the scope of these papers, Liu *et al.* (2018) have since proposed that it is this mechanosensitive Piezo1 channel that facilitates this Ca^{2+} entry in T cell receptor signalling and activation. It is generally agreed that the TCR acts as a mechanoreceptor however the mechanism of transduction of

mechanical force to chemical signalling is not fully understood (Hu & Butte 2016, Kim *et al.* 2009b, Li *et al.* 2010).

Tangential forces in the range of 50 pN incurred during interaction of αβ chains of the TCR with the pMHC are proposed to exert torque on the CD3εγ and CD3εδ subunits necessary to trigger TCR signalling (Kim *et al.* 2009b). Transfer of this mechanical force to the cell membrane is suggested to involve the conformational rearrangement of the CD3ζζ juxtamembrane regions (Lee *et al.* 2015). Notably, the Ca^{2+} flux immediately associated with mechanically loading of the TCR is not dependent on the cytoskeletal arrangement when the applied force is cyclical (Hu & Butte 2016, Wahl *et al.* 2017). This finding suggests that the activation of a SAC channel, proposed to be Piezo1 in mature T-cells, is sensitive to changes in lateral membrane tension.

Of interest to this research, Doucey *et al.* (2003) reported that the CD3δ subunit couples the raft associated CD8 to the TCR complex and is required for positive selection of $CD8^+$ lineage T cells. Specifically, this coupling is dependent upon the CD3δ interaction with the cytosolic tail of the CD8β chain (Doucey *et al.* 2003). Perhaps during preselection DP thymocyte–$cTEC^{hi}$ rosetting, this physical association provides a mechanism whereby extracellular binding of HS to the CD8 coreceptor, enhances transmembrane/intracellular CD8β mediated CD3δ conformational change, and so adjusts the transduction of concomitant pMHC-I stimulated TCR/CD3 signalling. It remains to be determined if HS (or indeed DxS) bound CD8 coreceptors induce CD3δ changes that produce torque sufficient to be detected by subunits of the CD3 receptor and facilitate a $[Ca^{2+}]_i$ rise, perhaps via Piezo1 channel activation, similar to the rise reported by Kim *et al.* (2009b).

1.7.3 Transient receptor potential channels

Belonging to an evolutionary ancient family of channels, the mammalian TRP family comprises 28 channels which structurally contain elements reminiscent of voltage-gated K^+ channels (reviewed by Gees *et al.* 2010, Kalia & Swartz 2013). While there is still much to be learnt about the physiological function of this family of channels, one proposed role for a number of these channels is to regulate immune cells (reviewed in Khalil *et al.* 2018, Majhi *et al.* 2015, Vaeth & Feske 2018).

1.7.3.1 TRP channel overview

Following the detection of an abnormal electroretinogram in a *Drosophila melanogaster* mutant (Cosens & Manning 1969), a novel Ca^{2+} channel, comprising the putative integral membrane "*trp* protein" (Montell & Rubin 1989), was proposed as the mechanism responsible for this transient electrical response (Hardie & Minke 1992, Hardie & Minke 1993). Since then, the mammalian TRP channel family has expanded to include 28 channels. Based on sequence homology these channels have been further grouped into 7 subfamilies. Reviewed by Nilius and Owsianik (2011), these designated subfamilies are: TRPC (the first discovered 'canonical'; 7 members with TRPC2 being a pseudogene in humans), TRPV (vanilloid; 6 members), TRPA (ankyrin; 1 member), TRPM (melastatin; 8 members) and the more distantly related TRPP (polycystin; 3 members) and TRPML (mucolipin; 3 members). The phylogenetic relationship between TRPC, TRPV, TRPA1 and TRPM channels is shown in Appendix 4 (p.355).

These cation specific channels comprise 4 subunits and may be configured as a homomeric or a heteromeric complex assembled from subunits from one or, on occasion, different subfamilies (Bai *et al.* 2008, Chu *et al.* 2004, Fischer *et al.* 2014,

Li *et al.* 2006, Ma *et al.* 2010, and reviewed by Zheng 2013). Each subunit has 6 putative TM regions with the channel pore and pore loop formed between the TM5 and TM6 regions (described by Gaudet 2008 and references therein).

Mostly, the permeability ratios for divalent and monovalent cations differ between TRP channels (depicted by Gees *et al.* 2010; adapted in this thesis as Figure 1.10, Schrapers *et al.* 2018). Exceptions to this non-selective cation permeability are the Ca^{2+} dependent TRPM4 and M5 channels, which conduct only monovalent cations (Launay *et al.* 2002, Nilius *et al.* 2005, Prawitt *et al.* 2003) and TRPV5 (originally described as ECaC) and V6 (originally CAT1), which are highly selective for Ca^{2+} (P_{Ca}:P_{Na} >100; Nilius *et al.* 2000, Yue *et al.* 2001). Adding complexity to the understanding of TRP channel permeability, alternative splicing sites within the pore region have been predicted to alter pore selectivity (Oberwinkler *et al.* 2005) and result in prolonged channel activation (reviewed by Ferreira & Faria 2016).

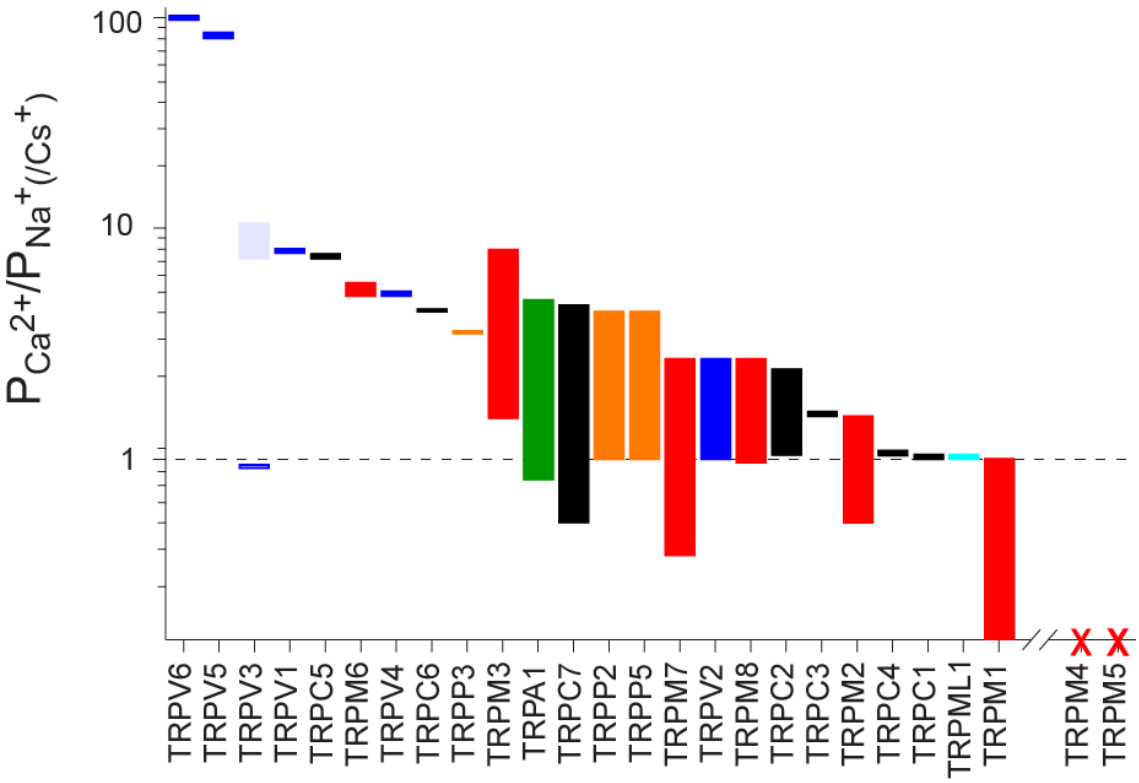

Figure 1.10 Ca^{2+}:Na^+ selectivity in TRP channels

Summary plot of reported Ca^{2+} to Na^+ selectivity for different TRP channels. Here TRPV6 and TRPV5 (blue, on the left) are shown to be ~100 fold more selective for Ca^{2+} over Na^+. In contrast, the red crosses (on the right) indicate TRPM4 and TRPM5 channels are virtually impermeable to Ca^{2+}. The broad bands, shown for many of the channels, reflect the large variation in ion permeability reported in the literature (adapted from Gees *et al.* 2010, TRPV3 P_{Ca}/P_{Na} ~0.5, Schrapers *et al.* 2018).

1.7.3.2 **Diverse functional domains modulate TRP channels**

In addition to the diversity of ion selectivity of TRP channels, between the subfamilies moderate structural variation occurs within the intracellular amino- (N) and carboxy (C) -termini (Figure 1.11). Domains of note are the

—tandem ankyrin repeats (that vary in number from 2 to ~18), which have roles in mechano-transduction and competitive Ca^{2+}–CaM/ATP binding (Erler *et al.* 2004, Gaudet 2008, Lee *et al.* 2006, Mosavi *et al.* 2002, Phelps *et al.* 2010, Sotomayor *et al.* 2005),

—coiled-coil motifs, which direct channel assembly and protein-protein interaction (Engelke *et al.* 2002, Tsuruda *et al.* 2006),

—proline-rich regions, which provide a binding site for Src homology 3 (SH3) domains found in proteins such as PLC-γ1 (Gaudet 2008, Yuan *et al.* 2003),

—IP_3R/CaM binding sites (reviewed by Eder *et al.* 2007, Tang *et al.* 2001) with a conserved "TRP box" motif, both of which reportedly regulate channel gating (Rohacs *et al.* 2005),

—the PSD-95/Discs-large/Zona occludens (PDZ) sequence, which forms a protein scaffold motif that regulates macromolecular complex formation (reviewed by Harteneck 2003),

—Ca^{2+} binding EF hand motifs (helix-loop-helix protein structures) that regulate channel activity in a Ca^{2+}-dependent manner (Doerner *et al.* 2007, Kramer 2016),

—ER retention domains (Erler *et al.* 2004, Tsuruda *et al.* 2006), and

—unique enzymatic domains located in the C-terminal of TRPM6 and TRPM7 (a Mg^{2+}- dependent atypical α-kinase; Ryazanova *et al.* 2004) and TRPM2 (an adenosine diphosphate ribose pyrophosphatase; Sumoza-Toledo & Penner 2011).

As indicated, these distinct domains facilitate subunit assembly, promote channel trafficking and cellular localisation, provide cytoskeleton anchoring sites, enhance protein-protein and lipid interaction, modulate gating via Ca^{2+} sensitisation, modulate channel phosphorylation and detect physical stimuli (Doerner *et al.* 2007, Garcia-Elias *et al.* 2015, Nilius *et al.* 2008, Schindl & Romanin 2007, Taberner *et al.* 2015, described by Venkatachalam & Montell 2007, Zheng *et al.* 2018). Adding to the functional diversity imparted by the cytosolic domains, variation in *Trp* mRNA splicing (Fischer *et al.* 2014, Kim *et al.* 2012, Lis *et al.* 2005, Oberwinkler *et al.* 2005, Zhou *et al.* 2013) plus the formation of heteromeric channels that exhibit distinctly different properties from their homomeric counterparts (Cheng *et al.* 2012, Fischer *et al.* 2014, Li *et al.* 2006) affords a broad range of characteristics to the TRP channels and imparts a vast capacity to respond to a broad range of activating mechanisms.

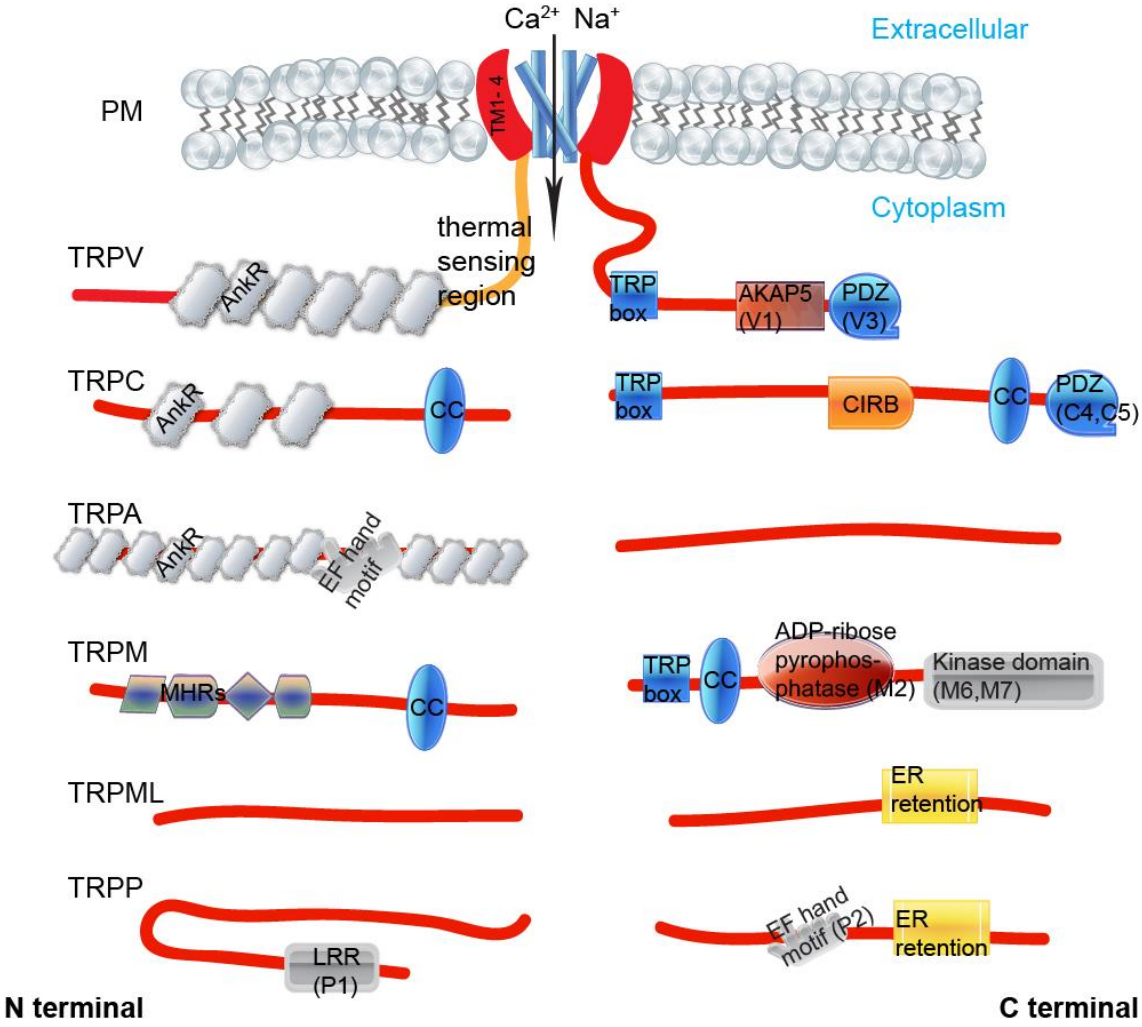

Figure 1.11 Variations in C- and N-termini in TRP channels

Cartoon of intracellular domains identified in the 6 TRP channel subfamilies- TRPV, TRPC, TRPA, TRPM, TRPML and TRPP. The ankyrin repeats (AnkR) in the N terminal regions of TRPA1 > TRPVs > TRPCs may enable mechanosensitivity, while coiled coil (CC) domains may enhance subunit binding. The conserved EWKFAR motif recognized as the 'TRP box' domain regulates gating of TRPVs, TRPCs and TRPMs. TRPC, TRPA1 and TRPP channel activity is also modulated by a Ca^{2+}-dependent CaM and IP_3 receptor binding (CIRB) site or the EF hand motif. While TRPM channel insertion into the PM may be regulated by the melastatin homology domain (MHR), localisation of TRPML and TRPP is regulated by ER retention and leucine rich repeat (LRR) regions. PSD-95/Discs-large/Zona occludens (PDZ) regions and A-Kinase Anchoring Protein 5 (AKAP5) as protein binding regions facilitate macromolecular formation.

1.7.3.3 **Overview of TRP channel activation mechanisms**

A remarkable variety of physical and chemical stimuli have been reported as channel activators or inhibitors, making them important local sensors of the intracellular and extracellular environment with key roles in most physiological processes (reviews by Clapham 2003, Gees *et al.* 2010, Vrenken *et al.* 2016). Activating stimuli include 1) ligand binding, 2) thermal stimuli that range from cold through to noxious heat (reviewed in Baez *et al.* 2014), 3) non-canonical membrane voltage sensing (Palovcak *et al.* 2015), 4) intra and/or extracellular pH change (Dhaka *et al.* 2009), 5) changes in $[Ca^{2+}]_i$ (Launay *et al.* 2002, Zurborg *et al.* 2007), 6) change in concentration of membrane-contained lipids (such as PIP_2; Imai *et al.* 2012, Lucas *et al.* 2003, Nilius *et al.* 2006, Xie *et al.* 2011), polyunsaturated fatty acids (PUFAs, *eg*. AA; Sanaki *et al.* 2017) and epoxyeicosatrienoic acids (Watanabe *et al.* 2003b), 7) stress induced increase of reactive oxygen species (reviewed by Simon *et al.* 2013), and 8) physical stimuli induced by mechanical force or osmotic pressure fluctuation (Sato *et al.* 2013). Figure 1.12 provides a schematic summary of the polymodal gating regulation of TRPC, TRPV1, TRPA1 and TRPM channels.

In addition, posttranslational protein modification such as N-glycosylation (Dietrich *et al.* 2003, Egan *et al.* 2016, Voolstra & Huber 2014, Xu *et al.* 2006) and hydroxylation (Nagarajan *et al.* 2017), as well as phosphorylation (Yao *et al.* 2005) and the formation of macromolecular signalling complexes by some TRP channels (Adebiyi *et al.* 2011, Bandyopadhyay *et al.* 2008, Huber *et al.* 1996, Kim & Saffen 2005, Zhang *et al.* 2008) can further alter their gating properties (Hu *et al.* 2009, Palovcak *et al.* 2015, reviewed by Zheng 2013). The identification of TRP channel "networks", which involve dozens of interacting proteins, including CaM, IP_3R, homer, FKBP, STIM1, PIP_3, PKA, Src family kinases, and caveolin-1, highlights the complexity of their activation (discussed in Ambudkar & Ong

2007, Cerny & Huber 2011, Chun *et al.* 2014, Kiselyov *et al.* 2005 and references therein).Despite this enormous variation in activating mechanisms, it is notable that the activity of all TRP channels can be negatively regulated by $[Ca^{2+}]_i$ in a concentration dependent manner (reviewed in Gordon-Shaag *et al.* 2008). Not surprisingly, the mechanism of Ca^{2+} sensitisation is often complex. Notably, an increase in $[Ca^{2+}]_i$ initially increases activity of TRPA1 (Hasan *et al.* 2017), TRPC5 (Gross *et al.* 2009), TRPC6 (Shi *et al.* 2004), TRPV4 (Strotmann *et al.* 2003), TRPM2 (EC_{50} = 340 nM; McHugh *et al.* 2003), TRPM4 and TRPM5 (Ullrich *et al.* 2005). While the mechanism of sensitisation is not fully understood, Ca^{2+} dependent activation of effector molecules such as kinases, phosphatases or calmodulin have been proposed as important modulatory components in this process (reviewed in Hasan & Zhang 2018, Zhu 2005).

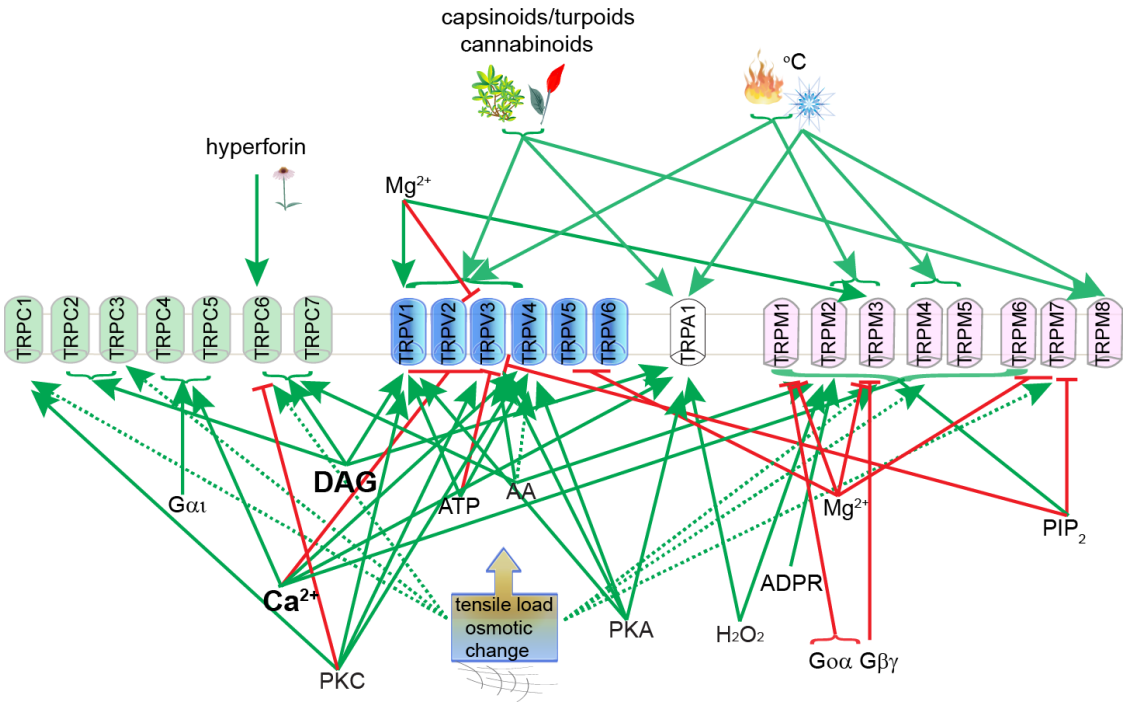

Figure 1.12 TRP channel activators and inhibitors

Schematic review of some of the reported various polymodal and non-specific stimuli that promote activation/ sensitisation or inhibition/ desensitisation of TRPC,TRPV, TRPA and TRPM channel gating. Green lines indicate activating while red indicates inhibitory.

Additional to Ca^{2+} regulation, TRP channel activity is also commonly regulated by Mg^{2+} (reviewed by Bouron *et al.* 2015). In common with most cells, the free $[Mg^{2+}]_i$ in thymocytes is ~1 mM (Rink *et al.* 1982). Notably, activated TRPV3, -V6, -M1, -M6 and -M7 inward currents are reportedly suppressed by $[Mg^{2+}]_i$, at concentrations of 2 mM (IC_{50}), 1 mM, 1.7 mM, 510 μM (IC_{50}) and 165 μM (IC_{50}), respectively (Chokshi *et al.* 2012b, Luo *et al.* 2012, Rampino & Nawy 2011, Voets *et al.* 2003, Voets *et al.* 2004). While the open probability of TRPV1 and TRPM3 channels is potentiated by $[Mg^{2+}]_o$ and >2 mM $[Mg^{2+}]_i$, respectively (Grimm *et al.* 2003, Yang *et al.* 2014).

Physical stimulation is another gating mechanism identified in a number of TRP channels, and interestingly, Liu and Montell (2015) propose that most TRP channels are sensitive to mechanical force. Within the literature there is considerable debate if these are mechanoreceptors. This may in part be due to the experimental challenge to distinguish between direct and indirect mechano-sensitivity. As Liu and Montell (2015) argue, distinct from direct gating, forces transduced via the lipid membrane and/or the cytoskeleton (which promote channel gating) may arise downstream of a signalling cascade. Certainly in TRPA1 channels, the long ankyrin repeat region (14–18), which is proposed to act as a "spring mechanism", may provide a force sensitive component for channel gating (Zayats *et al.* 2013). When transfected in HEK293 cells, exogenous TRPA1 channels were reportedly gated by a pharmacologically induced change in the composition of the lipid bilayer and the subsequent alteration in the PM curvature (Startek *et al.* 2018). In contrast, HEK cells expressing exogenous TRPV1 channels (which contain <10 ankyrin repeats) did not respond to a similar membrane deformation (Hill & Schaefer 2007). If not directly gated by force through membrane curvature changes, physical interaction with the elements of the cytoskeleton may provide the necessary link that imparts mechanosensitivity to TRPV1 and other proposed mechanosensitive channels like TRPV2, -V4, -C1, -

C5, -C6, -M3, -M4 and -M7 (Goswami & Hucho 2008, Maroto *et al.* 2005, Shen *et al.* 2015, Wei *et al.* 2009).

1.7.3.3.1 TRPC channel activating characteristics

It is commonly accepted that TRPC channels are gated by signalling downstream of the G-protein coupled receptors linked to Gq. This results in the activation of various isotypes of PLC to produce IP_3 and DAG. However, the mode of operation remains a debated topic, with evidence suggesting that due to store release by IP_3, they may function as either SOCE and/or receptor operated Ca^{2+} entry (ROCE) channels (Antigny *et al.* 2017, Jungnickel *et al.* 2001, Lièvremont *et al.* 2004, Ong *et al.* 2007, Plant & Schaefer 2005, Thakur *et al.* 2016, Trebak *et al.* 2003, Vannier *et al.* 1999, Vazquez *et al.* 2001, Zagranichnaya *et al.* 2005, Zarayskiy *et al.* 2007). These divergent findings are perhaps the outcome of different experimental methodologies including the cell type studied (native *vs.* transfected immortal cell line) or the expression level of the channel protein. With the aim of clarifying the involvement of the ER Ca^{2+} depletion in activation of TRPC channels, DeHaven *et al.* (2009) examined the responses in HEK-293 cells variably transfected with *Stim1* and *2*, *Orai* and *Trpc* cDNA and siRNA. In contrast to previous studies, they found no evidence of involvement of the ER Ca^{2+} sensor STIM1 in TRPC channel activation, thus ruling out SOCE.

Supporting ROCE, TRPC2, -C3, -C6 and -C7 channels have been found to be directly activated by the other molecule in the hydrolysis of PIP_2, namely DAG (Hofmann *et al.* 1999, Lemonnier *et al.* 2008, Lichtenegger *et al.* 2018, Lucas *et al.* 2003, Trebak *et al.* 2003). In addition, mechanical stress is also a proposed mechanism for activation of TRPC6, -C1 and -C3 (Anderson *et al.* 2013, Formigli *et al.* 2009, Maroto *et al.* 2005, Spassova *et al.* 2006). However, evidence for this mode of activation is not robust (Gottlieb *et al.* 2008). Being a pseudogene in primates, TRPC2 is less frequently studied and there is no evidence for TRPC2

mechanosensitivity. However, as with other channels, changes in membrane lipid composition and/or cytoskeleton rearrangement downstream of PLC and PI_3K activation might indirectly gate TRPC2 (discussed by Liu & Montell 2015).

Less well understood are the gating mechanisms of TRPC4 and TRPC5 channels (Thakur *et al.* 2016). As with the other TRPC channels, stimulation of Gq proteins promotes TRPC4 and TRPC5 channel activation. However, the mechanism is not dependent on second messenger molecules downstream of PLC activation. Rather, a complex mechanism has been proposed where TRPC4 and TRPC5 channel activation involves direct gating by Gαi-protein in a PIP_2 and $[Ca^{2+}]_i$ dependent manner (Jeon *et al.* 2012, Thakur *et al.* 2016, Tsvilovskyy *et al.* 2009, Zholos *et al.* 2004).

An often reported distinctive feature of TRPC4 and 5 activation is potentiation by micromolar concentrations of lanthanides (summarised in Plant & Schaefer 2005). Considered as non-specific TRP channel inhibitors (reviewed in Bouron *et al.* 2015), sub-millimolar concentrations of La^{3+} and Gd^{3+} have been employed to block TRPC1, -C3, -C6, and -C7 (Halaszovich *et al.* 2000, Inoue *et al.* 2001, Okada *et al.* 1999). However, results from their use on native cells need to be considered with great caution as they also potently interact with NCX and SERCA (Fujimori & Jencks 1990), and may change the mechanical properties of the PM by interacting with anionic lipids (Ermakov *et al.* 2001), sulphates, phosphates and bicarbonates.

1.7.3.3.2 **TRPV activating channel characteristics**

TRPV channels are without doubt polymodal receptors, responding to a multitude of diverse stimuli which may be further regulated by phosphorylation (reviewed by Park *et al.* 2017, Yao *et al.* 2005). Sharing <50% homology (Hu *et al.* 2009), TRPV1, -V2 and to a lesser extent -V3 and -V4 (Huang *et al.* 2011) are

considered thermo-TRPs, opening in response to a range of threshold temperatures as described below in Table 1.2 (Caterina *et al.* 1999, Caterina *et al.* 1997, Liu *et al.* 2011, Peier *et al.* 2002, Smith *et al.* 2002, Watanabe *et al.* 2002). In contrast, TRPV5 and TRPV6, which share ~80% sequence homology, are not thermosensitive but rather, reflecting their high selectivity for Ca^{2+}, are considered important channels contributing to Ca^{2+} homeostasis (Nijenhuis *et al.* 2005).

Table 1.2 Threshold temperatures for TRPV channel activation

Channel	Temperature threshold (°C)
TRPV4	~25
TRPV3	~40 prior to gating sensitisation ~33 after gating sensitisation
TRPV1	~40
TRPV2	~52

While a conserved heat sensing region has been proposed in the N-terminal membrane proximal domain (MPD) of TRPV1, -V2, -V3 and -V4 (Yao *et al.* 2011), a single residue variation in the MPD loop region imparts use-dependent heat sensitivity to the TRPV3 channel (Liu & Qin 2017). TRPV3 has an exceptionally high value for Q_{10} (>20) and hence a very high sensitivity to temperature, particularly around physiological temperature (Xu *et al.* 2002). However, this temperature sensitivity appears to be complex and requires structural changes that substantially alter the gating mechanism (Liu & Qin 2017, Liu *et al.* 2011) and its role in thermoregulation may be minimal (Huang *et al.* 2011). Apart from the thermal sensing region, distinctly different thermal gating regions have been identified in TRPV1 and TRPV3. Specifically, these residues are located in the C

terminal of TRPV1 (Brauchi *et al.* 2007, Brauchi *et al.* 2006), but in the outer pore region within the helix of the sixth TM region adjoining the extracellular loop in TRPV3 (Grandl *et al.* 2008).

In addition to their different thermal sensitivity, TRPV1–4 channels are also differently regulated by Ca^{2+}. TRPV1, -V3 and -V4 can all bind Ca^{2+}-CaM in the N terminal ankyrin repeat domain (ARD) and C terminal regions. However, the response to this Ca^{2+} dependent interaction varies between these channels. Specifically, following CaM binding, TRPV1 and -V3 channels undergo rapid desensitisation while TRPV4 activity is potentiated, at least initially (Liu *et al.* 2011, Numazaki *et al.* 2003, Phelps *et al.* 2010). Similarly, TRPV1, -V3 and -V4 (but not 2) are differently regulated by intracellular ATP through competitive binding at the ARD CaM binding site. When bound, ATP reduces TRPV3 sensitisation, but conversely enhances the sensitivity of TRPV1 and -V4 (Phelps *et al.* 2010).

Distinct from TRPV1, -V3 and -V4, TRPV2 lacks an ARD-binding site for CaM and intracellular ATP (Phelps *et al.* 2010). However, TRPV2 channels also undergo Ca^{2+} dependent desensitisation. A potential CaM binding domain has been identified within the C-terminus of human TRPV2 (Holakovska *et al.* 2011); however, its role in channel desensitisation has not been determined. Rather, the proposed mechanism leading to TRPV2 desensitisation is Ca^{2+}-dependent hydrolysis of PIP_2 (Mercado *et al.* 2010).

The "vanilloid" designation was adopted following identification of the first member in this family (TRPV1) as a capsaicin (vanilloid) sensitive receptor (Montell *et al.* 2002, Szallasi & Blumberg 1996). Whilst this vanilloid sensitivity is not conserved across this subfamily, TRPV channels in general respond to a variety of pungent plant derived alkaloids, cannabinoids, inflammatory mediators (such as AA and/or its metabolites), osmolarity changes and acidic pH. Notably these stimuli are predicted to induce channel gating via different

activation sites (Belmonte & Viana 2008, Brauchi *et al.* 2007, Cao *et al.* 2012, Cui *et al.* 2012, Grandl *et al.* 2008, Hwang *et al.* 2000, Ignatowska-Jankowska *et al.* 2009, Watanabe *et al.* 2003b).

Interestingly, the broadly used synthetic channel modulator 2-APB, which was first described as an inhibitor of IP_3R (Maruyama *et al.* 1997), has been used to differentiate TRPV1, -V2, -V3 and -V4. *In vitro* results indicate that TRPV1, -V2 and -V3, but not TRPV4, are sensitive to 2-APB (Hu *et al.* 2004). Notably, the addition of 100 μM 2-APB potently activates TRPV1 and -V2 currents in HEK-293 cells, but in distinct contrast, the current activation in TRPV3 was minimal (Hu *et al.* 2006). Significantly, this poor response to 2-APB can however be uniquely potentiated if the TRPV3 channel is additionally activated by mechanisms downstream of purinergic $G_{q/11}$-protein coupled receptor stimulation (Doerner *et al.* 2011), by the addition of AA (Hu *et al.* 2006), or by priming the channel with thermal stimuli. It appears that converging and repeated stimuli, including PIP_2 hydrolysis (Doerner *et al.* 2011) and intracellular protonation (Cao *et al.* 2012), uniquely sensitise TRPV3 channels. This sensitisation can reduce the temperature threshold and increase the probability of channel opening (Chung *et al.* 2004, Liu & Qin 2017, Liu *et al.* 2011).

The sensitivity of TRPV1 and -V3 to warm temperatures (~39–40°C) makes these channels ideal participants in sensing fever and stimulating the immune response. Certainly, CD8 naïve T cells cultured under the temperature of mild febrile show enhanced antigen-induced TCR activation compared to cells maintained at 37°C (Gothard *et al.* 2003, Mace *et al.* 2011, Mace *et al.* 2012, Smith *et al.* 1978). While a role for TRPV channels is yet to be established, it is conceivable that contemporaneous Ca^{2+} entry via thermally activated TRPV channels could synergistically potentiate TCR signalling in a manner similar to that observed downstream of LFA-1 activation (Kim *et al.* 2009a).

Studying a lipopolysaccharide fever model, Lai *et al.* (1998) found that addition of 1 μM capsaicin (a known potent TRPV1 agonist) to peripheral blood T cells caused a significant release of the inflammatory mediator substance P. While the mechanism underlying its release was not determined in this study, the authors note that other studies have reported that substance P release was evoked by an influx of Ca^{2+} triggered by capsaicin. Suggestive of activation of a capsaicin sensitive channel, the presence of functional capsaicin-sensitive channels TRPV1 and TRPV6 (Chow *et al.* 2007) has been detected in T lymphocytes.

1.7.3.3.3 **TRPA1 channel activating characteristics**

As indicated above, TRPA1 has a complex relationship with TRPV1. In addition to the proposed cross-talk between co-expressed TRPA1 and TRPV1 channels (Bertin *et al.* 2017, Schwartz *et al.* 2011, Staruschenko *et al.* 2010, Zhou *et al.* 2013), Fischer *et al.* (2014) argue that these proteins can form a functional heteromeric channel. In transfected HEK-293 cells, these authors found that the activation of TRPA1/TRPV1 heterotetramers were reminiscent of that of TRPV1, but the presence of the TRPA1 subunit suppressed channel gating.

Like TRPVs, TRPA1 can be activated by a number of capsinoids (Shintaku *et al.* 2012), allicin (Macpherson *et al.* 2005) as well as a range of highly reactive electrophilic chemicals. Commonly derived from plants, these alkaloids include nicotine, camphor, mustard oil, menthol, cinnamaldehyde, carvacrol, eugenol and thymol. Interestingly, the later five compounds are all reported agonists of TRPV3 (Bang & Hwang 2009, Wang & Wang 2017). Dependent upon the concentration, a number of these alkaloids elicit a bimodal response (Alpizar *et al.* 2013), which may be a consequence of off-target binding (Alvarez-Collazo *et al.* 2014) or reflect co-activation of the gating mechanism by Ca^{2+}-binding to the N-terminal EF hand domain (Doerner *et al.* 2007, Zayats *et al.* 2013). At low $[Ca^{2+}]_i$

the current is potentiated, but at high $[Ca^{2+}]_i$ channel closure ensues (Nagata *et al.* 2005).

Additional to this Ca^{2+}-dependent enhancement of ligand activation, TRPA1 is also directly activated by elevated $[Ca^{2+}]_i$ (EC_{50} ~0.9 μM; Doerner *et al.* 2011, Zurborg *et al.* 2007), DAG (Bandell *et al.* 2004), AA derivatives (Motter & Ahern 2012), miRNA-711 (Han *et al.* 2018) and reactive oxygen species such as H_2O_2 (Andersson *et al.* 2008, Bessac *et al.* 2008). In some species, including *Mus musculus* (reviewed by Laursen *et al.* 2015), TRPA1 can be activated by temperatures below ~17°C (Chen *et al.* 2013, Story *et al.* 2003). It has also been observed with mouse TRPA1 but, in this case, this sensitivity was dependent upon point mutations within the sixth ankyrin repeat (Jabba *et al.* 2014).

1.7.3.3.4 **TRPM activating characteristics**

Of all the TRPM channels, the characteristics and regulatory mechanisms of TRPM1 are least well understood. First identified in melanocytes, this channel plays a role in cell differentiation and proliferation (Fang & Setaluri 2000). TRPM1 is also, predominantly expressed in retinal bipolar cells. In these cells, it forms a macromolecular complex with mGluR6 and GPR179 (an orphan G-protein coupled receptor, that binds HSPGs). Here its activity is suppressed by the presence of activated Goα and G$\beta\gamma$ proteins (Orlandi *et al.* 2013, Shen *et al.* 2012) and by $[Mg^{2+}]_i$. The formation of this complex and recruitment of regulator of G protein signalling (RGS) proteins, is proposed to provide a highly sensitive platform that enables discrete spatiotemporal cation influx and signal transduction (Orlandi *et al.* 2013). The alleviation of the voltage-independent $[Mg^{2+}]_i$ inhibition of TRPM1, by DAG activated PKCα, is thought to further enhance the signal transmission (Rampino & Nawy 2011). Without these inhibitory mechanisms, TRPM1 is thought to be constitutively active, and while it is permeable to Ca^{2+} it preferentially conducts Na^+ (Koike *et al.* 2010).

When expressed in HEK293 cells, TRPM1 functions as an ionotropic steroid receptor, a role previously identified in TRPM3, its closest relative (Harteneck 2013, Lambert *et al.* 2011, Wagner *et al.* 2008). Like TRPM1, the functional characterisation of TRPM3 is incomplete. Likely because, in both, the expression of multiple slice variants may modulate translocation to the PM, and markedly alter pore selectivity and function (Fruhwald *et al.* 2012, Oberwinkler *et al.* 2005, Xu *et al.* 2001). Nevertheless, the available evidence suggests that, TRPM3 is also inhibited by Gβγ-protein subunits (Quallo *et al.* 2017) and in common with other TRPM members, it is sensitive to mechanical and thermal stimuli.

In common with TRPA1 and -V4, TRPM4, -M5 and -M8 channels are reported to be sensitive to cool temperatures (15–25°C). While, TRPM2 and -M3 are more similar to TRPV3 and -V1, in that they are activated by innocuous (~35°C) and noxious temperatures (~40°C), respectively (reviewed in Alexander *et al.* 2011, Castillo *et al.* 2018, Diaz-Franulic *et al.* 2016, Vriens *et al.* 2011). Interestingly, similar chemical activation has also been reported for some of these channels, specifically for compounds like menthol (bimodial action on TRPA1; Karashima *et al.* 2007, TRPV3 agonist; Macpherson *et al.* 2006, TRPM8 agonist; McKemy *et al.* 2002), citral (biomodal action on TRPV1, -V3, -A1 and -M8; Stotz *et al.* 2008) and icilin (TRPA1 and -M8 agonist; Story *et al.* 2003).

Significantly, TRPM channels are also regulated by PIP_2 which, in general, positively modulates channel activation (Badheka *et al.* 2015, Bousova *et al.* 2015, Brauchi *et al.* 2007, Gwanyanya *et al.* 2006, Holendova *et al.* 2012, Liu & Liman 2003, Rohacs *et al.* 2005, Runnels *et al.* 2002, Toth & Csanady 2012, Tóth *et al.* 2015, Xie *et al.* 2011). However, as also observed for other TRP channels, intracellular Ca^{2+}-binding may affect these channels in a complex way (reviewed in Hasan & Zhang 2018, Toth & Csanady 2012) and may, in part, explain variable results, including the inhibition of TRPM7 by PIP_2 (Langeslag *et al.* 2007). Not

unexpectedly, binding sites for PIP_2 and the Ca^{2+}-binding protein S100A1 have been identified in the N-termini of TRPM1; however, their regulatory effect on TRPM1 activity is uncertain (Jirku *et al.* 2015, Jirku *et al.* 2016).

Like most other TRP channels TRPM6 and -M7 are nonselective cation channels, but notably they are permeable to Mg^{2+} and are considered important in Mg^{2+} homeostasis. Unlike all other channels in this family, the ion-conducting pores of TRPM6 and -M7 are covalently coupled to an atypical serine/threonine kinase at their C-terminal. This motif is referred to as "chanzyme" as it links the ion channel with the enzymatic activity. Just how these distinct components affect channel activity is not well understood. While an independent function has been proposed (Clark *et al.* 2006, Krapivinsky *et al.* 2014, Matsushita *et al.* 2005, Romagnani *et al.* 2017), other studies have demonstrated bidirectional functional interaction. Notably, the kinase domain modulates the ion channel stability and activation, and the Mg^{2+} influx regulates the enzymatic activity of the kinase (Cai *et al.* 2018, Cao *et al.* 2009, Demeuse *et al.* 2006, Krapivinsky *et al.* 2017, Thebault *et al.* 2008, van der Wijst *et al.* 2014).

Sharing 52% sequence homology, these non-redundant proteins (Jin *et al.* 2008a, Woudenberg-Vrenken *et al.* 2011) can form homomeric channels (Li *et al.* 2006). However, without overexpression, endogenous TRPM6 may preferentially assemble with TRPM7 to facilitate surface expression (Cai *et al.* 2017, Chubanov *et al.* 2004, Schmitz *et al.* 2005). Both channels are reported to be constitutively active (Monteilh-Zoller *et al.* 2003, Runnels *et al.* 2001, Suzuki *et al.* 2018, Voets *et al.* 2004) and are highly selective to divalent cations with ion permeation favouring $Zn^{2+} > Ba^{2+} > Mg^{2+} > Ca^{2+}$ (reviewed by Bouron *et al.* 2015, Gees *et al.* 2011). Interestingly, these cations also negatively regulate channel activity, perhaps by means of electrostatic hindrance of PIP_2 association with the channel and/or a voltage-dependent permeation block (Chokshi *et al.* 2012b, Kozak & Cahalan

2003, Langeslag *et al.* 2007). Linked to their Mg^{2+} conductance, TRPM6 and -M7 channels are believed to be key regulators of cellular Mg^{2+} (Chubanov *et al.* 2016, Mandt *et al.* 2011, Ryazanova *et al.* 2010, Schlingmann *et al.* 2002, Schmitz *et al.* 2014, Stritt *et al.* 2016). In the immune system, Mg^{2+} deficiency has been linked to delayed PLC-γ1 phosphorylation and IP_3 production in human T cells (Li *et al.* 2011), and increased apoptosis in rat thymocytes (Gunther *et al.* 1984, Malpuech-Brugere *et al.* 1999).

Like TRPM6 and -M7, TRPM2 has been described as a chanzyme. However, this may be incorrect since Iordanov *et al.* (2016) recently reported that the putative "catalytic" *Nudix-box* domain (NUDT9-H) has no functional enzymatic activity. Rather, TRPM2 may be a ligand-gated channel. Potently activated by ADPR binding to the NUDT9-H region (Perraud *et al.* 2005), TRPM2 channels can be synergistically activated by reactive oxygen species such as H_2O_2 and β-nicotinamide adenine dinucleotide (NAD^+), and also modulated by $[Ca^{2+}]_i$ and 30 μM AA (Csanády & Törőcsik 2009, Hara *et al.* 2002, Sano *et al.* 2001, Zhang *et al.* 2018). Its sensitivity to the redox status of the cell has resulted in TRPM2 activity being commonly linked to mediation of cell death following hypoxia/anoxia (Fonfria *et al.* 2005, Hara *et al.* 2002, Perraud *et al.* 2005).

1.7.3.4 **Pore dilation**

First described for some ionotropic ATP (purinergic) receptors (P2X), sustained activation of TRPV1–V4, TRPA1 and perhaps TRPM8 appears to lead to changes in the pore configuration, which allows the diffusion of large molecular weight solutes across the PM such as N-methyl-D-glucamine (NMDG) or the fluorescent cationic dyes FM1-43 and YO-PRO-1 (Banke *et al.* 2010, Chen *et al.* 2009, Chung *et al.* 2008, Kittaka *et al.* 2017, Meyers *et al.* 2003, Munns *et al.* 2015, Zubcevic *et al.* 2018). Banke *et al.* (2010) proposed that the "pore dilation" mechanism involved conformational changes to the selectivity filter regulated by $[Ca^{2+}]_o$. Added to this, Cao *et al.* (2013) indicated that allosteric coupling between the selectivity filter and a lower gate, regulated by the S4-S5 and S6-TRP box linker domains provided a mechanism to expand the diameter of the lower gate. However, they did not actually detect pore dilation in the static TRPV1 configurations derived from cryo-electron microscopy.

Countering the concept of pore dilation, Li *et al.* (2015) argue that at least in P2X channels, these larger molecular weight solutes are always able to permeate the pore. They suggest the apparent change in selectivity was not due to pore dilation; rather, it was caused by a time-dependent change in intracellular ion concentrations and was perhaps a consequence of the electrophysiological recording technique. So, while the pore dilation phenomenon is not clearly established, it is apparent that the selectivity of some TRP channels may alter during prolonged activation.

1.7.3.5 **Limitations to understanding TRP channel function**

The task of investigating a role for TRP channels in native cells such as lymphocytes is complicated by 1) the variation in the biophysical properties of TRP channels described in native cells from different tissues as well as native cells from different species (Belmonte & Viana 2008, Chen *et al.* 2013, Grubisha *et al.* 2014, McIntyre *et al.* 2001, Saito & Tominaga 2017), 2) the likelihood that TRP channels from one or more subgroup are expressed in a cell (Dong *et al.* 2012, Khalil *et al.* 2018), and 3) the general paucity of potent and selective modulating chemicals. Disambiguation is likely a challenge when interpreting results.

1.7.3.5.1 **TRP channel pharmacology is complex**

Distinct from the pharmacology used to inhibit or activate voltage-gated channels, very few drugs have been identified as selective and potent modulators of TRP channel activity. To some extent, this issue stems from the fact that, following the discovery of the first TRP channel in *Drosophila* (Cosens & Manning 1969), sequence homology was the predominant method used to discover new TRP channels and in mammals the TRP family rapidly grew to include 28 channels by 1990. With increased understanding of the channel structure, it appears their multimodal activation characteristics (discussed in 1.7.3.3) can direct distinct activation pathways (Grandl *et al.* 2008, Nilius & Szallasi 2014, Zheng 2013, Zheng *et al.* 2018). This synergistic activation in response to distinct stimuli has made identification of drugs that target specific TRP channel activity difficult (reviewed by Gavva *et al.* 2008, Holzer & Izzo 2014, Moran 2018, Wu *et al.* 2010). Consequently, the pharmacological tools used to characterise these channels are often highly non-specific chemicals, such as 2-aminoethoxydiphenyl borate (2-APB), ruthenium red (RuR), lanthanides, flufenamic acid and plant derived cannabinoids (reviewed by Alexander *et al.* 2011, Belmonte & Viana 2008, Clapham 2007b, Guinamard *et al.* 2013).

For example, a summary of 2-APB and RuR targets is provided in Table 1.3. In most cases, the effect on the listed target channel has been described in mouse cells. In general, with regard to non-selective TRP channels, concentrations of 2-APB, varying from 10 to 500 μM have been reported to 1) inhibit TRPC2, -C3, -C5, -C6, -C7 (Lievremont *et al.* 2005, Viitanen *et al.* 2013, Xu *et al.* 2005), TRPM2 and -M3 (Mortadza *et al.* 2017, Pang *et al.* 2012, Togashi *et al.* 2008); 2) indirectly inhibit TRPM7 channel activation (Chokshi *et al.* 2012a); and 3) activate TRPA1 (Zhou *et al.* 2013), TRPM6 (Li *et al.* 2006) and TRPV1, -V2, and -V3 (Hu *et al.* 2004, Juvin *et al.* 2007). Its complex pharmacology also results in concentration dependent inhibitory or activating effects on Orai channel activity (Amcheslavsky *et al.* 2015, Prakriya & Lewis 2001) and inhibition of IP_3R activation (Missiaen *et al.* 2001, Simkus & Stricker 2002).

Similarly as detailed in Table 1.3, RuR whilst commonly used to investigate TRPV channels has many other targets, including ryanodine receptors (RyR) located on the ER membrane (Ma 1993) and mitochondrial calcium uniporters. Specifically, in mouse pancreatic acinar cells, Wu *et al.* (2000) showed slow inhibition of the RyR following internal perfusion of 100 μM RuR. While in permeabilised rat mast cells, RuR has also been shown to potently inhibit mitochondrial Ca^{2+} uptake (Hajnóczky *et al.* 2006, Moore 1971). Importantly and relevant to my extracellular application, this inhibitory effect was not observed in intact rat mast cells and human hepatoma cells. The hexavalent nature of RuR is believed to slow its movement across the intact PM (Hajnóczky *et al.* 2006).

Table 1.3 Pharmacological effects of 2-APB and ruthenium red

Listed are channels, that are targeted by 2-APB and RuR and in most cases have been described in mouse tissue.
‡www.guidetopharmacology.org/GRAC/LigandDisplayForward?tab=biology&ligandId=2433;
*www.guidetopharmacology.org/GRAC/LigandDisplayForward?tab=biology&ligandId=2432;
∞www.guidetopharmacology.org/GRAC/LigandDisplayForward?tab=biology&ligandId=2426

	Agonist activity	**Antagonist activity**	**Non-channel target**
2-APB	TRPV1, 2, 3 ‡ TRPM6 (Suzuki *et al.* 2017) TRPM7 (>1 mM; Li *et al.* 2006, Nadler *et al.* 2001)	TRPC1, 2, 3, 4, 5, 6, 7 ‡ TRPM7 (Li *et al.* 2006), TRPM2, 3, 8 (IC_{50}=1,100,12 μM; Zholos 2010) TRPV6 (Singh *et al.* 2018) IP_3R (Maruyama *et al.* 1997) SERCA (Missiaen *et al.* 2001) thermally activated STIM1/Orai (Liu *et al.* 2019)	Directly scavenges extracellular ROS (Morihara *et al.* 2017)
RuR		TRPV1, 2, 3, 4, 6, A1, * TRPM1 (10 μM; Shen *et al.* 2009) TRPM6 (Voets *et al.* 2004) TRPM8 (20 μM; Zholos 2010) Piezo1(5.4 μM; Coste *et al.* 2012) Catsper1, 2, 3, 4 * MCU (Moore 1971); Ca_V (Cibulsky & Sather 1999); RyR (Wu *et al.* 2000); VDAC1 (Israelson *et al.* 2008)	Binds sialic acid residues (rat; Wieraszko 1986) Inhibits Ca^{2+}–CaM binding (bovine; Sasaki *et al.* 1992); Inhibits tubulin assembly, induces disassembly (bovine; Deinum *et al.* 1985)

1.7.3.5.2 **Characteristics vary between native and exogenous channels**

Much of the research investigating TRP channel function has been undertaken in expression systems. Typically, cultures of human embryonic kidney (HEK) 293 or Chinese hamster ovary (CHO) cells are transfected with vectors containing the DNA coding sequence for the TRP channel(s) of interest. Additional to the ectopic gene expression often forcing high protein content in typically monomeric configuration, it is notable that these cell lines also contain a number of endogenous channels, including TRP and Piezo1 (Amarouch *et al.* 2013, Berjukow *et al.* 1996, Bugaj *et al.* 2005, Dubin *et al.* 2017, He & Soderlund 2010, Vaca & Sampieri 2002).

Specifically, in immune system studies, TRP channel function has mostly been investigated using tumour-derived cell lines such as Jurkat T cells (derived from human CD4 leukemic T cells), CTLL-2 lymphocytes (cloned from C57BL/6 mouse CD8 T cells; Gillis & Smith 1977) and EL4 thymoma cells (originally derived from a carcinogen-induced C57BL/6 mouse lymphoblast tumour). Since the expression profile of ion channels may not be comparable (Kunert-Keil *et al.* 2006, Vandewauw *et al.* 2013, Wenning *et al.* 2011), the translation of results from immortal cell lines and expression systems to native cell function or to different tissue types, different mouse strains and/or different species may be problematic (Riccio *et al.* 2002). In CD4 T lymphocytes, Wenning *et al.* (2011) found a significant difference in the expression profile of TRP channels in Jurkat T-cells compared to native human CD4 T cells. Similarly, TRPM2 expression also differed between activated Jurkat cells and native peripheral T lymphocytes. Specifically, Kotturi and Jefferies (2005) observed mRNA expression gradually decreased in Jurkat cells compared to a two-fold increase noted for T cells.

In addition to the variation in expression, the properties of channels studied in heterologous overexpression systems may significantly differ from those in

native cells. For instance, Grubisha *et al.* (2014) found TRPV3 pharmacology was significantly different between recombinant rat cell lines and native channels present in a mouse keratinocyte cell line. In contrast to the activation demonstrated by exogenous TRPV3, the activation of native TRPV3 channels required the addition of markedly higher concentrations of agonists and/or exposure to disparate stimuli which act synergistically. It is likely that variation in the presence of interacting proteins and lipids between cell types alters the biophysical properties of TRP channels. Consequently, our understanding of the characteristics which influence endogenous TRP channels function in native cells is far from complete and, in thymocytes particularly, there is a scarcity of research on this topic.

While evidence of mRNA expression is not necessarily indicative of functional protein expression, it nevertheless is noteworthy that murine thymocytes contain mRNA that encodes TRPC2 and -C6, TRPM1, -M2, -M4, -M5, -M6 and -M7 and TRPV2, -V3 and -V4 (shown as Figure 1.13; adapted from Inada *et al.* 2006). This data provided a starting point for determining potential candidate channels that might play a role in the DxS induced $[Ca^{2+}]_i$ rise observed in DP thymocytes (Weston *et al.* 1991). The following sections provide a more focused review of the literature; outlining characteristics specific to TRPC, TRPV, TRPM and TRPA1 channels and current evidence which suggests their functional role in T lymphocyte development, activation and death.

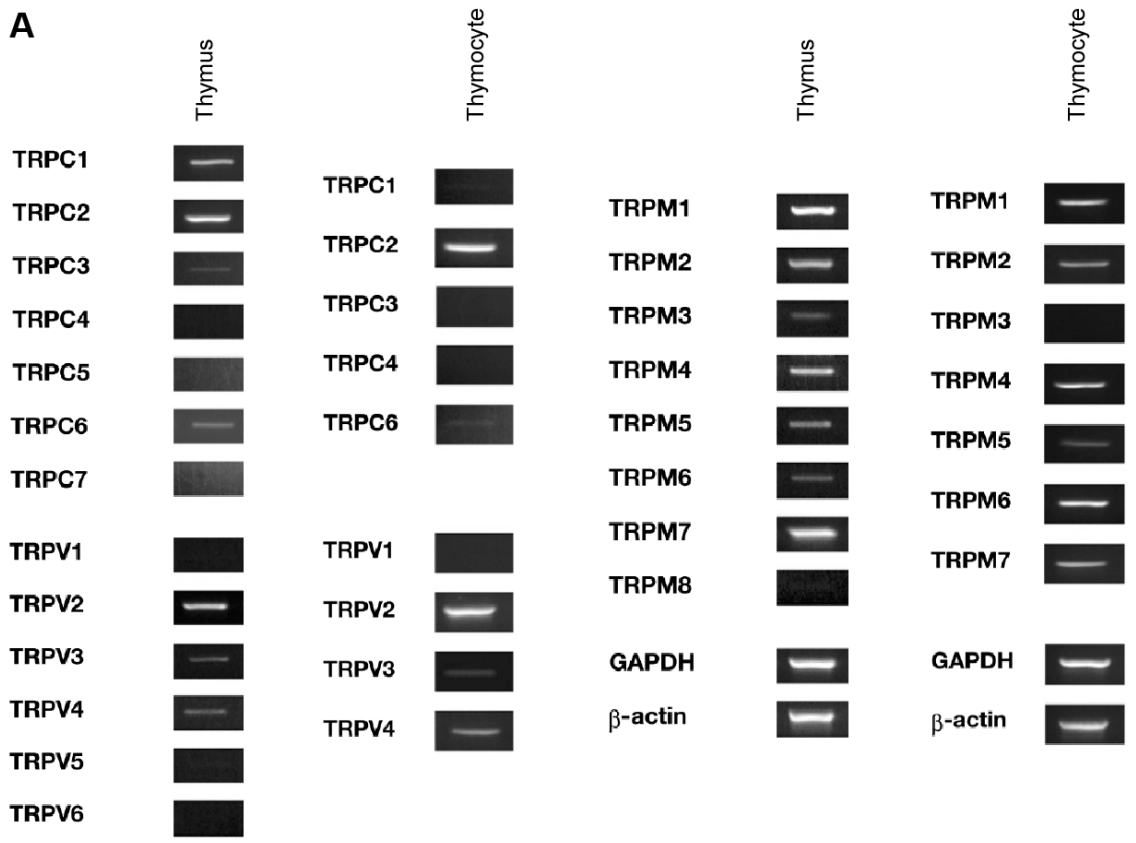

B

Trpc1	*Trpc2*	*Trpc3*	*Trpc4*	*Trpc5*	*Trpc6*	*Trpc7*	*Trpv1*	*Trpv2*	*Trpv3*	*Trpv4*	*Trpv5*	*Trpv6*	*Trpa1*	*Trpm1*	*Trpm2*	*Trpm3*	*Trpm4*	*Trpm5*	*Trpm6*	*Trpm7*	*Trpm8*
(+)	+	−	−	−	(+)	−	ND	+	+	+	−	−		+	+	−	+	+	+	+	ND

Figure 1.13 TRP mRNA expression during T cell development

(A) RT-PCR results showing mRNA expression of *Trp* genes and (house keeper) *GAPDH* and *β-actin* genes in both the thymus and isolated thymocytes from 8–12 week C57BL/6 male mice (sourced from Inada *et al.* 2006). (B) Summary the expression of *Trp* genes in thymocytes isolated by flow cytometry. Purified mRNA was amplified by RT-PCR using gene specific primer sets (+) faintly present; + present; − not detected; ND not determined (reported by Inada *et al.* 2006).

1.7.3.6 **Proposed TRP channel roles in T lymphocytes**

Without doubt, TRP channels are polymodal "receptors". They respond to multiple disparate stimuli that may synergistically potentiate the channel activity, thereby acting as potential coincidence detectors of intra- and extra-cellular events and integrators of diverse activation signals (reviewed by Belmonte & Viana 2008, Hu *et al.* 2009, Palovcak *et al.* 2015, reviewed by Zheng 2013). Associated with an increased understanding of their function, there has been a rise in research papers reporting crucial roles for TRP channels in immune system development and function and, pathophysiological processes (reviews by Bertin & Raz 2016, Minard *et al.* 2018, Nilius *et al.* 2007, Vaeth & Feske 2018, Yang *et al.* 2009). However, to date the role of TRP channels in thymocytes is not well defined, and channels identified in immortal lymphocyte T cell lines and mature T cells may not necessarily be present or even have the same role in native thymocytes.

1.7.3.6.1 **TRPCs in T lymphocytes**

In human T lymphocytes, TRPC3 activation has been shown to enhance TCR dependent Ca^{2+} signalling in Jurkat T cells and naïve CD4 T cells (Pang *et al.* 2012, Philipp *et al.* 2003, Wenning *et al.* 2011). Specifically, Philipp *et al.* (2003) showed that a mutation of *TRPC3* in human T cells reduced Ca^{2+} rise following TCR stimulation.

Using a Jurkat cell line, Carrillo *et al.* (2012) presented evidence of TRPC6 possibly forming a heteromeric TRPC3/6 channel which was activated by DAG. Notably, they observed that the TRPC3/6 opening was abolished following a methyl-β-cyclodextrin-induced depletion of membrane cholesterol. As cholesterol is an important regulator of lipid raft integrity and cytoskeletal F-actin arrangement (Chubinskiy-Nadezhdin *et al.* 2013), the observed TRPC3/6 channel inhibition is

likely caused by diffusion of key modulating proteins and lipids away from the signalling domain and perhaps also actin cytoskeleton remodelling. Shown to interact with both cholesterol and TRPC6 is the integral protein podocin which may provide a regulatory "switch" enabling channel activation by either DAG or mechanical stress (Anderson *et al.* 2013, Huber *et al.* 2006). While not studied in thymocytes, it is interesting to note that in DP thymocytes, >10-fold expression of *Nphs2* (podocin) has been detected (detailed in the BioGPS database, dataset: GeneAtlas MOE430, gcrma, probeset: 1437605_at).

T lymphocytes harvested from Wistar rat peripheral blood also express TRPC6 > TRC3 > TRPC1. In response to induced sepsis, upregulation of TRPC6 and TRPC3 was associated with enhanced T cell apoptosis (Wu *et al.* 2015). In a mouse CD8 T cell line, Kim *et al.* (2009a) have suggested that LFA-1 dependent Ca^{2+} influx is via a DAG-activated TRPC channel. Subsequent to LFA-1/ICAM-1 interaction, this Ca^{2+} influx (shown earlier in Figure 1.3A) was found to be downstream of PLC-γ1 activation and significantly was independent of ER Ca^{2+} release. Interestingly, somewhat reminiscent of the Ca^{2+} influx under investigation in this thesis, this LFA-1/ICAM-1 associated Ca^{2+} influx has a delayed onset of approximately three minutes, which may indicate the involvement of a complex signalling mechanism and perhaps may include translocation of the channel from the endosome to the PM. It is important to note that these authors did not identify the channel involved. Reviewing the DAG sensitive TRPCs in thymocytes, it appears *Trpc2* is highly expressed and to a lesser extent *Trpc6* (Fig. 1.13; Inada *et al.* 2006). However, the presence of any DAG activated TRPC channel in mouse T cells and more specifically murine thymocytes is yet to be clarified.

Furthermore, as DAG has also been proposed to activate TRPA1 (Bandell *et al.* 2004) and TRPV1 (Woo *et al.* 2008) channels, and since its metabolite AA is an

endogenous agonist of TRPV3 and TRPV4 channels (Hu *et al.* 2006, Watanabe *et al.* 2003b), it may be argued that the influx observed down-stream of LFA-1 activation may have been caused by one of these channels and not necessarily a TRPC channel. In contrast to the lack of evidence for TRPC channels in thymocytes, functional TRPV and TRPA1 channels, however, have been detected in various T lymphocytes, including thymocytes (Bertin *et al.* 2014, Bertin *et al.* 2017, Majhi *et al.* 2015).

1.7.3.6.2 **TRPVs in T lymphocytes**

In mouse and human peripheral T cells the thermo-sensitive TRPV channels, *i.e.* TRPV1, -V2, -V3 and -V4 have been detected in both the PM and cytosol under resting conditions (Majhi *et al.* 2015). Additionally, Vassilieva *et al.* (2013) have reported the presence of the TRPV5 and TRPV6 proteins in peripheral lymphocytes. However, their expression level was markedly lower than that observed in tumour derived Jurkat T cells, where they are thought to play a role in tumour growth. In thymocytes, the presence of TRPV channel proteins has been less well established. While all thermo-sensing *Trpv* genes have been detected in murine thymocytes, with *Trpv2* showing the highest expression profile (Fig. 1 13; Inada *et al.* 2006), TRPV1 and perhaps TRPV6 (Peng *et al.* 1999) are the only channels so far detected.

Within the TRPV family, the most extensively investigated member is TRPV1. Perhaps because of this, it is also the most commonly detected TRPV channel in T lymphocytes, including thymocytes, where it is predominantly found in cells of the $CD4^+$ lineage. Functional TRPV1 channels identified in CD4 T cell lines from mouse, rat and human peripheral blood are generally thought to play a role in promoting cell activation and enhancing the inflammatory responses (Baker *et al.* 2016, Bertin *et al.* 2014, Saunders *et al.* 2007, Spinsanti *et al.* 2008). However, activation of TRPV1 channels detected in Wistar rat DN and SP CD4 populations

and in C57BL/6 mouse DP^{dull} thymocytes with low CD4 and CD8 expression appears to modulate the differentiation of these populations by mediating autophagy and apoptosis. In DP^{bright} thymocytes (*i.e*. cells with high CD4 and CD8 expression), it is notable that TRPV1 expression was found to be negligible (Amantini *et al.* 2017, Amantini *et al.* 2004, Farfariello *et al.* 2012).

Additional to TRPV1, expression of TRPV2, -V3 and -V4 has been detected in human and murine primary T cells (Majhi *et al.* 2015, Saunders *et al.* 2007, Spinsanti *et al.* 2008). In mouse splenic T cells, TRPV4 and TRPV1 proteins reportedly co-localise with the CD4 coreceptor (Bertin *et al.* 2014, Chen *et al.* 2017a), and the activation of either of these channels was found to regulate mitogenic activity after either TCR/CD3 activation or cell stimulation with the mitogen ConA (Bertin *et al.* 2014, Majhi *et al.* 2015).

As mentioned earlier, TRPV2 activity appeared to positively regulate SOCE downstream of TCR activation (Sauer & Jegla 2006). However, this was determined in Jurkat T cells and, therefore, a similar role for TRPV2 in thymocytes may not be present. Furthermore, although the expression of *Trpv2* in thymocytes appears high (Inada *et al.* 2006), to date, functional TRPV2 channels have only been identified in cells from thymocyte–acute lymphoblastic leukemia (T-ALL) where these channels were likely involved in volume regulation (Dobrovinskaya *et al.* 2015). Thus, with the exception of TRPV1, expression of functional TRPV2, -V3 and/or -V4 channels in thymocytes remains to be established.

Commonly colocalised with TRPV1, TRPA1 channels are sensitive to many of the stimuli known to also activate TRPV channels. This raises the question if TRPA1 is also present in thymocytes.

1.7.3.6.3 **TRPA1 in T lymphocytes**

The commonly reported co-expression and interaction of TRPV1 and TRPA1 channels observed in sensory neurons (Malin *et al.* 2011, Patil *et al.* 2010) has recently been confirmed in primary human CD4 T cells. In these cells, the proposed function of TRPA1 is to inhibit TRPV1 activation and thereby to suppress T cell activation (Bertin *et al.* 2017). To date, no evidence of TRPA1 in mouse T lymphocytes has been reported. Notably, while it does not reflect an absence of the protein, it is interesting that in rat peripheral blood lymphocytes *Trpa1* expression was found to be negligible (Trevisan *et al.* 2014). Inada *et al.* (2006) in their paper examining the expression profile of *Trp* genes in mouse lymphocytes did not include *Trpa1*. However, data available in the BioGPS and ImmGen databases show slight upregulation of *Trpa1* in DP thymocytes. Compared to the median determined from the RNA expression profile in a large range of mouse tissues, organs, and cell lines, TRPA1 expression is slightly increased in DP and SP CD8 thymocytes (Figure 1.14).

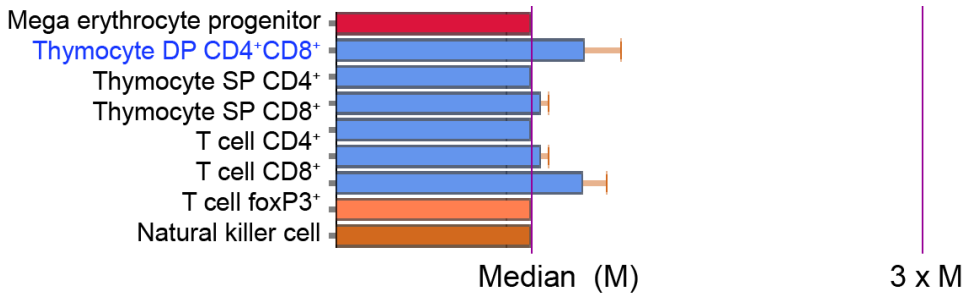

Figure 1.14 Relative expression profile of murine *Trpa1* in T lymphocytes

Plot of the relative mRNA expression of *Trpa1* during T cell maturation compared to the median determined from the RNA expression profile in a large range of mouse tissues, organs, and cell lines (BioGPS probe set 1457164_at).

The presence of TRPA1 channels in mouse thymocytes and splenic T cells has been presumed based on changes in lineage differentiation when treated with cinnamaldehyde, a TRPA1 channel agonist (Bandell *et al.* 2004, Fernandes *et al.*

2012, Horváth *et al.* 2016, Koh *et al.* 1998). Specifically, compared to untreated thymocytes, the addition of cinnamaldehyde to murine thymocytes in single cell suspension augmented DP thymocyte differentiation to CD4 SP and CD8 SP, without apparently affecting their viability (Koh *et al.* 1998). This response was greatest in DP thymocytes that had higher forward scatter (indicative of larger diameter) and low side scatter measured by flow cytometry. Smaller DP thymocytes with increased side scatter (indicative of increased granularity) did not respond as strongly. Investigation of the mechanism triggered by the addition of cinnamaldehyde was beyond the scope of this research and notably, at the time of writing, the TRPA1 channel was yet to be identified (Jaquemar *et al.* 1999). However, with the knowledge that cinnamaldehyde activates TRPA1 channels (IC_{50} = 9.5 μM; Macpherson *et al.* 2006), Koh *et al.* (1998) results could indicate that functional TRPA1 channels are expressed during a discrete stage of thymocyte development. Equally, these findings may be due to an alternate target effect of the cinnamaldehyde such as activation of TRPV3 (0.5–5 mM; Macpherson *et al.* 2006) or inhibition of L-type Ca^{2+} channels (Alvarez-Collazo *et al.* 2014).

1.7.3.6.4 **TRPMs in lymphocytes**

Detection of *Trpm1, Trpm2, Trpm4, Trpm6* and *Trpm7* mRNA in thymocytes has been reported (Fig. 1 13; Inada *et al.* 2006). Aside from *Trpm7* which is moderately expressed in DP thymocytes, it is notable that extraordinarily high expression of *Trpm1* in T-lymphocytes has been reported, particularly in cells that express CD8 (Figure 1.15A & B).

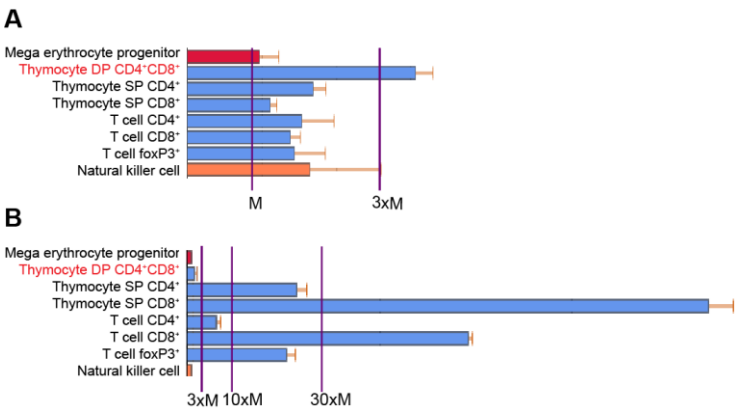

Figure 1.15 *Trpm7* and *Trpm1* expression in T lymphocytes

(A) mRNA expression of *Trpm7* during T cell maturation compared to the median determined from the RNA expression profile in a large range of mouse tissues, organs, and cell lines (BioGPS dataset: GeneAtlas MOE430, gcrma) probe set 1431355_s_at. (B) mRNA expression of *Trpm1*, probe set 1437455_at.

However, except for TRPM7 and perhaps TRPM2, the presence of other functional TRPM channels specifically in thymocytes remains to be established. Specifically, a loss of function in the TRPM7 ion pore significantly disturbs thymopoiesis, with a large percentage of TRPM7$^{-/-}$ DN thymocytes failing to differentiate to the DP stage (Jin *et al.* 2008a, Romagnani *et al.* 2017). While the mechanism causing this partial block was not determined, in activated T-cells and DT40 B lymphocytes, the loss of TRPM7 channel function reportedly impaired migration and curtailed IP_3R signalling, respectively (Kuras *et al.* 2012, Sahni & Scharenberg 2008). Notably, these are also critical requirements for thymocyte maturation to the DP stage (Juntilla & Koretzky 2008, reviewed in Savino *et al.* 2000). Furthermore, the proposed regulation of SOCE by TRPM7 channel activity would provide a crucial mechanism for regulation of Ca^{2+} homeostasis in immune cells and hence have an important role in setting an initial equilibrium within the immune system, including during thymopoiesis (Beesetty *et al.* 2018, Brandao *et al.* 2013, Faouzi *et al.* 2017, Mendu *et al.* 2018, Nadolni & Zierler 2018).

While not yet investigated in thymocytes, functional TRPM2 channels have been detected in both Jurkat and murine CD4 T cells (Beck *et al.* 2006, Gasser *et al.* 2006, Melzer *et al.* 2012, Sano *et al.* 2001). Additionally, in human primary CD4 T cells, Wenning *et al.* (2011) found the expression of TRPM4 increased following Ab stimulation of CD3. In the absence of stimulating antigen, T lymphocytes can be activated by an $[Ca^{2+}]_i$ rise triggered by the addition of ConA. In Jurkat cells, this ConA-induced increase in $[Ca^{2+}]_i$ has been linked to a rise in cytosolic ADPR that facilitates TRPM2 channel activation (Gasser *et al.* 2006, Pang *et al.* 2012). Of note, Buttgereit *et al.* (1997) observed that the addition of ConA to a rat thymocyte suspension evoked a concurrent influx of Na^+ and Ca^{2+} from across the PM. Furthermore, they found that the rise in $[Na^+]_i$ and $[Ca^{2+}]_i$ was downstream of increased cellular oxidative phosphorylation and associated substrate oxidation reactions (Buttgereit *et al.* 1993). While they did not identify the mechanism of cation entry, their findings may arguably suggest that thymocytes also express functional TRPM2 channels.

As with TRPM2, functional TRPM4 channels are expressed in Jurkat and mature T lymphocytes; however, their presence in thymocytes has not been determined. In CD4 lineage helper type 1 and 2 cells, TRPM4 channel activation plays a significant role in differential regulation of Ca^{2+} signals. However, as TRPM4 is a non-selective for Ca^{2+}, the proposed mechanism of $[Ca^{2+}]_i$ oscillations involves Na^+ driving depolarization which is sufficient to reduce the driving force on Ca^{2+} entry through neighbouring Ca^{2+}-permeable channels (Launay *et al.* 2004, Takezawa *et al.* 2006, Weber *et al.* 2010). It is notable that in *Trpm4*$^{-/-}$ mice, the thymus size and the number of mature CD4 and CD8 T cells were comparable to those from WT mice (Barbet *et al.* 2008). However, these broad observations do not exclude a role for TRPM4, as having a comparable number of mature T cells may not necessarily equate to a comparable TCR repertoire.

1.8 Summary

A crucial outcome of thymopoiesis is the egress of naïve T cells bearing TCRs that enrich the repertoire of the peripheral T cell pool; specifically, increasing the capacity for foreign antigen recognition while at the same time retaining tolerance of self-antigens. During thymopoiesis, testing of the diverse TCRs occurs during interactions between thymocytes and distinct populations of thymic stromal cells. These interactions facilitate activation and transduction of various signalling pathways that often depend on Ca^{2+}. Perhaps as a reflection of the relatively small number of functional Ca^{2+}-permeable channels thus far identified in DP thymocytes, our understanding of Ca^{2+} entry mechanisms involved in thymopoiesis, particularly during positive selection, is incomplete. Based on the available evidence of mRNA expression, it may be that DP thymocytes variably express a multiplicity of channels, including Piezo1 and TRP channels, to orchestrate distinct $[Ca^{2+}]_i$ rises and regulate Ca^{2+} homeostasis. While there is sparse evidence of functional expression of these channels, the mechanisms of gating, modulation and sensitisation of such channels, reported in current literature, can provide some useful information towards the identification of (a) specific channel(s).

Relevant to this thesis, a subpopulation of cTECs (*i.e.* $cTEC^{hi}$) has been found to promote rosetting of preselection DP thymocytes and induce a small $[Ca^{2+}]_i$ rise in these thymocytes. The formation of $cTEC^{hi}$–thymocyte rosettes is enabled by HS engagement of minimally sialylated CD8 coreceptors at a binding site that is distinct from the MHC-I binding site. In activated DP thymocytes, the progressive sialylation of their surface receptors, including CD8, is thought to impede further rosette formation. *In vitro* DP–$cTEC^{hi}$ rosette formation can also be blocked by prior application of DxS or HS to the cell suspension. It is thought

that competitive binding to the CD8 coreceptor occludes the binding site for the endogenous HS expressed.

The functional role of the $[Ca^{2+}]_i$ rise associated with preselection DP thymocyte rosetting is yet to be clarified. However, the transduction of signalling pathways activated by TCR stimulation is likely modulated by resting $[Ca^{2+}]_i$ and a concomitant $[Ca^{2+}]_i$ rise. Hence, a synergistic $[Ca^{2+}]_i$ increase when added to either a moderately strong or a negligible TCR response may alter the selection in preselection DP thymocytes that express marginally self-reactive TCR or have poor TCR-MHC avidity, respectively.

In this thesis, DxS is used to evoke a consistently observed $[Ca^{2+}]_i$ rise in DP thymocytes (Tellam & Parish 1987). This $[Ca^{2+}]_i$ rise is hypothesised to mimic the Ca^{2+} influx evoked by the interaction of preselection DP thymocytes with $cTEC^{hi}$. To evoke the $[Ca^{2+}]_i$ rise, it was necessary to use large MW (500kDa) DxS which may suggest that the mechanism might involve extensive cross-linking of surface receptors and thereby impart mechanical tension. Considering the time course of the Ca^{2+} influx, with its delayed onset and slow rise, channel activation is predicted to be downstream of one or several signalling cascades, rather than by direct gating by DxS.

1.8.1 **Aims of study**

The overall aim of this thesis is to identify the Ca^{2+} permeable channel(s) activated in preselection DP thymocytes following the addition of DxS. To expand the focus in regard to function, I also aimed to identify some crucial signalling mechanisms upstream of channel activation. Recognising that DxS is not a biological ligand, it nonetheless provides an experimental paradigm that allows the investigation of signalling mechanisms and candidate channels using broad pharmacological testing in the context of flow cytometry.

To assist in the principal aim of identifying the Ca^{2+} permeable ion channel, there were a number of experimental objectives. These were as follows:

In Chapter 3, I will

1. determine if the channel is selectively permeable to Ca^{2+},

2. identify membrane receptors expressed by DP thymocytes that may be crucial to the signal transduction,

3. identify intracellular molecular components necessary for transduction of the signal cascade which leads to the channel activation, and

4. identify candidate channels based on pharmacological properties and activation characteristics.

And in Chapter 4, I will

5. investigate these "target" channels using pharmacological testing and immunocytochemistry.

1.8.2 **Thesis structure**

Chapter 1 of this thesis presents a review of literature considered to be pertinent to the aim of this thesis which is identifying mechanisms that induce a $[Ca^{2+}]_i$ rise in DP thymocytes following the addition of DxS. In Chapter 2, I provide details of the experimental protocols used in monitoring $[Ca^{2+}]_i$, $[Na^+]_i$ and $[Mg^{2+}]_i$ in murine DP thymocytes, the drugs used in the pharmacological testing and the method I devised for analysing data from flow cytometry. Chapter 3 presents the results of experiments which examine the 1) characteristics of the DxS induced $[Ca^{2+}]_i$ and $[Na^+]_i$ rises and 2) elements of the signalling cascade that appear essential/sufficient for the activation of the Ca^{2+} rise. Based on these results and the knowledge about Ca^{2+}-permeable channels described in Chapter 1, Chapter 3

includes a list of candidate channels that may be involved in the DxS $[Ca^{2+}]_i$ rise. Chapter 4 presents the results of pharmacological experiments which aim to clarify which candidate channels contribute to the DxS $[Ca^{2+}]_i$ rise. In Chapter 5, I summarise, discuss and contextualise the findings made in the previous chapters, identify limitations of the research and present directions for further investigation.

2 Materials and Methods

This chapter details the common materials and general methods that have been used in the experiments described in this thesis. Specific concentrations and protocols for blocking and/or activation of specific signalling pathways or candidate channels are given in the respective Materials section in Chapters 3 and 4.

2.1 Animals

Mice aged from four to ten weeks were used in this project. C57/BL/6-NCrlAnu and C57BL/6-Jackson mice were bred at the Animal Services Division of the Australian National University, while 129SvEv and 129SvEvTRPC1,3,6,7 KO mice were obtained from the Australian BioResources Pty. Ltd. with the kind permission of Professor Gary Housley, UNSW. These quadruple TRPC channel KO mice were bred from mixed C57BL/6J:129SvEv strains carrying single TRPC KO alleles and originally generated at the NIEHS, Research Triangle Park, NC, USA ($TRPC1^{-/-}$; Dietrich *et al.* 2007, $TRPC6^{-/-}$; Dietrich *et al.* 2005, $TRPC3^{-/-}$; Hartmann *et al.* 2008, $TRPC7^{-/-}$; Perez-Leighton *et al.* 2011). In these transgenic mice the respective channel has been made non-functional due to a mutation in the channel pore region. CD8β KO mice (Casey Crooks & Littman 1994) were used with the kind permission of Professor Christopher Parish, JCSMR. These mice, bred at the APF/ANU, were originally sourced from Professor Alfred Singer, NIH, USA. CD11a KO mice (strain: ENU15NIH:036:a:B6:G17) were used with the kind permission of Dr. Anselm Enders, JCSMR. The thymus from a single TRPA KO mouse, was kindly provided by Dr. E. Kheradpezhouh, JCSMR This animal was initially sourced from Professor Stuart Brierley, University of Adelaide, SA.

The animals were housed and transported in accordance with the guidelines laid out by the ANU Animal Experimentation Ethics committee. All mice were humanely euthanised by CO_2 asphyxiation in accordance with the animal welfare regulations.

2.2 Biochemicals

2.2.1 Solutions

Commonly used chemicals for making up buffer solutions and media were sourced from various suppliers and are listed in Appendix 5 (p. 356). The recipes for commonly used solutions are detailed in Table 2.1.

HEPES buffered saline (HBS) was prepared according to the experimental requirements following the recipe described in Table 2.1. Importantly, the pH of HBS is temperature dependent, such that increasing the temperature of HBS from 7–19–37°C shifts the measured pH from 7.59 to 7.38 and 7.19, respectively. To minimise the impact of this pH shift when cells were warmed from 19 (RT) to 37°C (physiological, for flow cytometry experiments), separate aliquots of HBS were prepared on the day of the experiment. One was warmed to 37°C and pH adjusted to pH 7.3 ± 0.05, using either NaOH 1 M or HCl 1M as required. The pH of the other was similarly adjusted with the sample at RT. The osmolarity of both solutions was measured by a freezing point depression osmometer (Micro-Osmometer Autocal Type 13, Roebling) and adjusted by the addition of milliQ to 295 ± 5 mOsmol.

Table 2.1 Buffer solutions used for single thymocyte suspension

Medium/ solution	Composition (mM, unless otherwise stated)
Dulbecco's Phosphate Buffered Saline (PBS)	Ca^{2+}/Mg^{2+}-free. Sigma-Aldrich, St. Louis, MO
F15 MEM	F15 MEM powder 9.61 g/l, $NaHCO_3$ 2.2 g/l, in milliQ®. pH adjusted to 7.1 with HCl or NaOH prior to sterile filtering (Corning bottle cap filter 0.22 μM) which raises pH 0.1 - 0.3
HEPES buffered saline (HBS)	HEPES 10, NaCl 140, KCl 5, $CaCl_2$ 1.8, $MgCl_2$ 1.0, D-glucose 10, in milliQ®, titrated with NaOH to pH~ 7.3, ~ 295 mOsmol
HEPES buffer Na^+ free	NMDG 140, KCl 5, $MgCl_2$ 1.0**,** $CaCl_2$ 1, D-glucose 10, HEPES 10, in milliQ®, pH ~ 7.3 adjusted with HCl, ~ 295 mOsmol
HEPES buffer Mg^{2+} free	NaCl 140, KCl 5, $CaCl_2$ 2.8, D-glucose 10, HEPES 10, in milliQ®, HCl pH ~ 7.3 adjusted with HCl or NaOH, ~ 295 mOsmol
HEPES buffer Ca^{2+} free	NaCl 140, KCl 5, $MgCl_2$ 2.8, D-glucose 10, HEPES 10, in milliQ®, HCl pH ~ 7.3 adjusted with HCl or NaOH, ~ 295 mOsmol
HEPES buffer with Ba^{2+}	HEPES 10, NaCl 140, KCl 5, $BaCl_2$ 1.8, $MgCl_2$ 1.0, D-glucose 10, in milliQ®, titrated with NaOH to pH~ 7.3, ~ 295 mOsmol
RPMI 1640	Gibco® Life Technologies Carlsbad, CA
Phosphate buffered saline (PBS)	NaCl 150, $NaPO_4$ 50, in milliQ® titrated to pH 7.3

2.2.1.1 **FACs buffer**

In flow cytometry experiments, cell samples were suspended in HBS rather than the commonly used FACs buffer solution of PBS supplemented with fetal calf serum (FCS)/or BSA 5%. This was done to avert the complication of adsorption of chemicals like latrunculin B and hematoporphyrin onto albumin (Kinoshita *et al.* 1988, Spector *et al.* 1989).

2.2.2 **Inhibitory and activating chemicals**

In investigating the role of potential signal transduction molecules and involvement of candidate ion channels together with their selectivity, and transporters, a variety of chemicals was employed. A list of these chemicals can be found in Table 2.2 which provides the common name, International Union of Pure and Applied chemistry (IUPAC) nomenclature, catalogue number and the manufacturer.

In general, stock solutions were prepared and stored in accordance with the supplier's recommendation. Chemicals were prepared to the maximal recommended solubility using either DMSO or milliQ, aliquoted and stored at either -80, -20 or -4°C depending on recommendation. Immediately prior to their use the stock solutions were diluted with HBS to the desired concentration. Hence, the concentration of the DMSO solvent was generally reduced to <0.01% (vol/vol). Details of their application and concentrations used will be described in greater detail in sections 3.2 and 4.2.

2.2.3 **Antibodies**

The primary (Ab_1) and secondary antibodies (Ab_2) and concentrations used in various flow cytometry and immunocytochemistry (ICC) experiments are listed in Table 2.3, Table 2.4 and Table 2.5. Purchased from Alomone Labs, the polyclonal anti-TRP channel Ab_1s have been validated to some extent by other

researchers. Specifically, the specificity of the anti-TRPA1 Ab has been verified in TRPA1 KO mice (Sullivan *et al.* 2015) while the anti-TRPC6 Ab has been validated using shTRPC6 knockdown methods in human cancer cells (Diez-Bello *et al.* 2019). Notably, this anti-TRPC6 (raised against aa residues 573-586 from rat TRPC6) cannot be validated in TRPC6$^{-/-}$ mice, where a targeted deletion of exon 7 results in expression of non-functional TRPC6 channel (specifically Trpc6tm1Lbi; Dietrich *et al.* 2005) but still contains the epitope (Riazanski *et al.* 2015). However, it has been shown to inhibit WT channel function. In electrophysiology experiments Gonzales *et al.* (2014) found addition of the anti-TRPC6 Ab significantly reduced the channel current.

Regarding the remaining extracellular Abs listed in Table 2.4, the specificity of the anti-TRPM6 has been verified by mock transfected HEK cells (Suzuki *et al.* 2017) while Yang *et al.* (2017) used the host IgG as a negative Ab control for anti-TRPC7 binding. Like the TRPC6 KO, the non-functional TRPC7 channel expressed in the TRPC1,3,6,7 KO mice used in my research, still contains the epitope that binds this anti-TRPC7 Ab. Hence, thymocytes from these animals do not provide a means to validate the Ab specificity. As for the anti-TRPV Abs, only the specificity of Abs for the immunogen, *i.e.* peptide sequence derived from the TRP protein on which the Ab was generated, has been reported (Majhi *et al.* 2015).

2.2.4 Cell-permeant cation sensitive fluorophores

For this project, the cell-permeant fluorescent indicator dyes listed in Table 2.7 were purchased in order to monitor intracellular changes in Ca^{2+}, Na^{+} or Mg^{2+}. The acetoxymethyl (AM) moiety conjugated to these fluorophores enables ready loading into thymocytes. Considering the excitation wavelengths of these probes (see Table 2.7), concurrent monitoring of Ca^{2+} and Na^{+} or Ca^{2+} and Mg^{2+} is possible where 4-(6-carboxy-2-indolyl)-4′-methyl-2,2′-(ethylenedioxy)-dianiline-*N*,*N*,*N*′,*N*′-tetra-acetic acid tetrakis (acetoxymethyl) ester (indo-1-AM) and Asante

NaTRIUM green 2™ acetoxymethyl (ANG2-AM) or indo-1-AM and Mag-fluo-4-AM have been loaded simultaneously.

Excited by UV light, indo-1 and the sodium binding benzofurane isophthalate acetoxymethyl (SBFI-AM) are both described as ratiometric probes. Using an excitation wavelength of 355 nm, indo-1 undergoes a distinct shift in emission fluorescence upon Ca^{2+} binding (F_{405}/F_{475}), with the peak emission wavelength shifting from ~475 nm (λ_2) when in its unbound to ~405 nm (λ_1) when Ca^{2+} is bound; however there is >30% spectral overlap. In contrast, SBFI requires a shift in the excitation wavelength to best detect the intracellular Na^+ levels, with maximal excitation at 380 in its Na^+ free state and at 340 nm in the bound state (F_{340}/F_{380}). Both ANG-2 and Mag-fluo-4 only increase the fluorescence intensity as they bind Na^+ or Mg^{2+}/Ca^{2+}, respectively.

With all acetoxymethyl conjugated fluorophores it is expected that intracellular esterases will cleave the AM moiety thereby converting the fluorophore to an active ionic form and at the same time trapping the dye within the cell. Nevertheless, there will be some leakage from the cell over time which can be delayed by keeping the cells at a low temperature prior to requirement. Leakage of indo-1 from thymocytes has been shown to be less than 3% over a two-hour period (Schrek *et al.* 1967, Tellam & Parish 1987).

Table 2.2 Chemicals used to assess the DxS $[Ca^{2+}]_i$ mechanism

Common name; IUPAC name	**(Cat. No.); Source**
2-APB; 2-aminoethoxydiphenylborane	(1224); TOCRIS Bioscience, Tocris House, Bristol BS11 0QL, UK
A967079; (NE)-*N*-[(E)-1-(4-fluorophenyl)-2-methylpent-1-en-3-ylidene]hydroxylamine	(A-225); Alomone Labs, Jerusalem BioPark, Jerusalem 9104201 Israel
ATP; Adenosine 5′-triphosphate disodium salt	(A-2383); Sigma Aldrich St Louis, MO, USA.
Arachidonic acid; (5Z,8Z,11Z,14Z)-icosa-5,8,11,14-tetraenoic acid	(90010); Cayman chemical, Ann Arbor, MI, USA.
AMG9810; 3-(4-tert-butylphenyl)-*N*-(2,3-di hydro-1,4-benzodioxin-7-yl)prop-2-enamide	(14715); Cayman chemical
Amphotericin B; (35*S*)-33*R*-[(3-amino-3,6-di deoxy-β-D-mannopyranosyl)oxy]-1,3,5,6,9,11,17,37-octahydroxy-15,16,18-trimethyl-13-oxo-14,39-dioxabicyclo[33.3.1]nonatriaconta-19,21,23,25,27,29,31-heptaene-36*R*-carboxylic acid	(11635); Cayman chemical
Cyclopiazonic acid(CPA); (2*R*,3*S*,9*R*)-5-acetyl-4-hydroxy-8,8-dimethyl-7,16-diaza-pentacyclo [9.6.1.0^(2,9).0^(3,7). 0^ (15,18)] octadeca-1(17),4,11(18),12,14-pentaen-6-one	(C-750); Alomone Labs
Dextran sulfate 500 kDa (DxS) *	(D6001); Sigma-Aldrich. St Louis, MO, USA.
Edelfosine; 1-*O*-octadecyl-2-methyl-*sn*-glycero-3-phosphocholine	(3022); TOCRIS Bioscience
EGTA; Ethylene glycol-bis(2-aminoethyl ether)-*N*,*N*,*N*′,*N*′-tetraacetic acid	(E-4378); Sigma-Aldrich
FFA; flufenamic acid; 2-[[3-(Trifluoromethyl) phenyl]amino]benzoic acid	(F9005); Sigma-Aldrich
Gadolinium chloride	(93-6416); STREM chemicals, Newburyport, MA, USA

Gö6983; (3-[1-[3-(Dimethylamino)propyl]-5-methoxy-1*H*-indol-3-yl]-4-(1*H*-indol-3-yl)-1*H*-pyrrole-2,5-dione	(2285); Tocris Bioscience
GSK2193874; 3-([1,4′-Bipiperidin]-1′-ylmethyl) -7-bromo-*N*-(1-phenylcyclopropyl)-2-[3-(trifluoromethyl)phenyl]-4-quinoline carboxamide	(5016); Tocris
GsMTx4; M-theraphotoxin-Gr1a	(STG-100); Alomone Labs
H-89; (N-[2-3-(4-bromophenyl)prop-2-enyl amino ethyl]isoquinoline-5-sulfonamide	(BML-EI196); ENZO life Sciences, Farmingdale, NY USA
HC-030031; 2-(1,3-dimethyl-2,6-dioxo purin-7-yl)-*N*-(4-propan-2-ylphenyl)acetamide	(11923); Cayman chemical
Hyperforin (1*R*,5*S*,6*R*,7S)-4-hydroxy-6-methyl-1,3,7-tris(3-methylbut-2-en-1-yl)-6-(4-methyl pent-3-en-1-yl)-5-(2-methylpropanoyl)bicyclo [3.3.1]non-3-ene-2,9-dione	(75650);Cayman chemical
Ionomycin (4*R*,6*S*,8*S*,10*Z*,12*R*,14*R*,16*E*,18*R*,19*R*, 20*S*,21*S*)-11,19,21-Trihydroxy-4,6,8,12,14, 18,20-heptamethyl-22-[(2*S*,2′*R*,5*S*,5′*S*)-octa hydro-5′-[(1*R*)-1-hydroxyethyl]-2,5′-dimethyl [2,2′-bifuran]-5-yl]-9-oxo-10,16-docosadienoic acid calcium salt	(Asc-370); Ascent Scientific, Islip, NY, USA
Magnesium chloride ($MgCl_2$)	(296); Ajax Chemicals Pty. Ltd. Auburn, NSW AUS
Nordihydroguaiaretic acid; 4-[4(3,4-dihydroxy phenyl)-2,3-dimethylbutyl]benzene-1,2-diol	(70300); Cayman chemical
NMDG; *N*-methyl-D-glucamine	(M2004); Sigma-Aldrich
Neuraminidase type II digestion enzyme *	Sigma-Aldrich, St Louis, MO.
Norgestimate; ((17α)-17-(Acetyloxy)-13-ethyl-18,19-dinorpregn-4-en-20-yn-3-one 3-oxime)	(N686000); Toronto Research Chemicals, North York, ON. CAN
NS8593; *N*-[(1*R*)-1,2,3,4-tetrahydronaphthalen -1-yl]-1*H*-1.3-benzodiazol-2-amine	(N2538) Sigma-Aldrich

OAG; 1-oleoyl-2-acetyl-*sn*-glycerol	(62600); Cayman chemical
PP2; 3-(4-chlorophenyl)-1-(1,1-dimethylethyl)-1*H*-pyrazolo[3,4-d] pyrimidin-4-amine	(13198); Cayman chemical
Pyr3; ethyl 1-[4-(trichloroprop-2-enamido) phenyl]-5-(trifluoromethyl)-1*H*-pyrazole-4-carboxylate	(3751); TOCRIS Bioscience
Ruthenium red; (RuR) $[(NH_3)_5RuORu(NH_3)_4ORu(NH_3)_5]Cl_6$	(11103-72-3); Sigma-Aldrich
SKF96365; 1-(β[3-(4-methoxyphenyl)propoxy] -4-methoxyphenethyl)-1*H*-imidazole hydrochloride	(10009312); Cayman chemicals
SN-6; 1-methyl-4-([4-((4-[(1-methylpyridin-1-ium-4-yl)amino]-phenyl)-carbamoyl)phenyl] amino)quinolin-1-ium	(2184); TOCRIS Bioscience
Tetrodotoxin (TTX); Octahydro-12-(hydroxy methyl)-2-imino-5,9:7,10a-dimethano-10a*H*-[1,3]dioxocino[6,5-*d*]pyrimidine-4,7,10,11,12, -pentol	(1078); TOCRIS Bioscience
Tranilast; 2-[3-(3,4-dimethoxyphenyl)-prop-2-enoylamino]benzoic acid	(13044); Cayman chemical
Xestospongin C (XestC); (1*R*,4a*R*,11*R*,12a*S*,13*S*, 16a*S*,23*R*,24a*S*)-Eicosahydro-5*H*,17*H*-1,23: 11, 13-diethano-2*H*,14*H*-[1,11]dioxacycloeicosino [2,3-b:12,13-*b*']dipyridine	(1280); TOCRIS Bioscience
YM-244769; *N*-[(3-aminophenyl)-methyl]-6-[4-[(3-fluorophenyl)methoxy]-phenoxy]-pyridine-3-carboxamide	(4544); TOCRIS Bioscience
YM-58483 or BTP2; *N*-[4-[3,5-bis(trifluoromethyl)pyrazol-1-yl]phenyl]-4-methylthiadiazole-5-carboxamide	(3939); TOCRIS Bioscience

* Kindly supplied by D. Simon Davis

Table 2.3 Primary extracellular antibodies for staining live thymocytes

Fluorochrome conjugated antibodies used to identify/gate CD4 and CD8 thymocyte populations in flow cytometry experiments. Allophycocyanin (APC), Fluorescein isothiocyanate (FITC), AlexaFluor®647 (AF647), Cyanine 7™ (Cy7)

Specificity	**Isotype**	**Clone**	**Conjugate**	**Final conc (μg/mL)**	**Source**
CD4	Rat IgG2b,κ	GK1.5	APC	0.5	BioLegend
CD4	Rat IgG2a,κ	RM4-5	FITC	0.5	BD Pharmingen™
CD8a	Rat IgG2a,κ	53-6.7	FITC	1.0	BioLegend
CD8a	Rat IgGa,κ	53-6.7	AF647	0.4	BD Pharmingen™
CD8a	Rat IgGa,κ	53-6.7	APC-Cy7	0.4	BD Pharmingen™

Table 2.4 List of primary antibodies (Ab_1) for immunocytochemistry

Primary extracellular anti-TRP channel antibodies used in immunocytochemistry/flow cytometry experiments.

Anti-	Immunogen	Host, clonality	Lot	(μg/ml); dilution	Source (Cat #)
TRPC6	2nd extracellular loop aa573-586r	Rabbit, polyclonal	ACC120 AN0750	(0.85); 1:100	Alomone (ACC-120)
TRPC7	2nd extracellular loop aa504-516h	Rabbit, polyclonal	ACC066 AN0102	(0.8); 1:100	Alomone (ACC-066)
TRPV2	1st extracellular loop aa413-428r	Rabbit, polyclonal	ACC039 AN0202	(0.6); 1:75	Alomone (ACC-037)
TRPV3	1st extracellular loop aa464-478h	Rabbit, polyclonal	ACC033 AN0225	(0.85); 1:100	Alomone (ACC-033)
TRPV4	3rd extracellular loop aa647-662r	Rabbit, polyclonal	ACC124 AN0402	(1); 1:100	Alomone (ACC-124)
TRPA1	1st extracellular loop aa747-760h	Rabbit, polyclonal	ACC037 AN1402	(8.5); 1:100	Alomone (ACC-037)
TRPM6	1st extracellular loop aa802-815m	Rabbit, polyclonal	ACC046 AN0225	(8.5); 1:100	Alomone (ACC-046)
TRPC2 peptide	Isoform 4 aa 475-525		D1216	(4) 1:50	SantaCruz (sc162356P)
TRPC2	2ndextracellular loop	Goat, polyclonal	H1313	1:50	SantaCruz (sc162356)

Alomone Labs, Har Hotzvim Hi-Teck Park, Jerusalem, Israel
Santa Cruz Biotechnology Inc., CA, USA

Table 2.5 List of secondary antibodies (Ab_2)

Secondary fluorochrome-conjugated anti-IgG antibodies used to detect primary anti-TRP channel antibodies in immunocytochemistry/flow cytometry experiments.

Immunogen specificity	Host, clonality	Conjugate	Lot	µg/mL	Sourced from (Code #)
Goat IgG (H&L)	Donkey polyclonal	FITC	127414	7.5	Jackson Immuno-Research (705-096-147)
Rabbit IgG (H&L)	Donkey polyclonal	FITC	35762	7.5	Jackson Immuno-Research (711-095-152)

Jackson ImmunoResearch Laboratories, Inc., West Grove, PA, USA

Table 2.6 Buffers and reagents used for immunocytochemistry

Blocking buffer	PBS + 5% donkey
Primary antibody buffer (Ab_1B)	PBS + 1% donkey
Secondary AbB (Ab_2 B)	PBS
Wash buffer	PBS + 0.1% donkey
Fixing agent	4% paraformaldehyde

Table 2.7 Intracellular cation sensitive fluorescent dyes

Details of the fluorescent indicator dyes used to monitor intracellular ions. Ex/Em λ are the reported maxima.

Indicator (Cat. No.)	Binds	~K_d (mM)	Working range (mM)	Conc loaded (μM)	Ratiometric	λ Maxima: Ex/Em (nm)	Source
Indo-1-AM (50043-1)	Ca^{2+} free bound	250 (nM)†		5	yes	346/475 330/400	Biotium Hayward CA 94545 USA
Asante NaTRIUM Green-2-AM (C3512)	Na^+	32‡	3.75–120‡	5	no	517/540	TEFLabs Austin TX USA.
SBFI-AM (sc-215841)	Na^+ free bound	10*-20.7‡	10–120‡	5	yes	380/510 340/510	SantaCruz Biotechnology CA USA
Mag-fluo-4-AM (M14206)	Mg^{2+} Ca^{2+}	4.7 ~20 μM		1	no	494/527	ThermoFisher Scientific

†(Grynkiewicz *et al.* 1985); ‡(Iamshanova *et al.* 2016); *(Roder & Hille 2014)

2.3 Thymocyte preparation

Freshly acquired murine thymocytes were used in all experiments. The survival rate of DP thymocytes in suspension deteriorates significantly over 24 hours (Outram *et al.* 2002), therefore all experiments using live cells were conducted on the same day. An attempt was made to culture a comparable DP cell line from a murine thymoma cell line EL4, following the protocol described by Echevarria-Lima *et al.* (2005). These authors reported that a small percentage of cultured EL4 cells could be driven to express CD4 and CD8 coreceptor molecules when 75 μM indomethacin was added to the cell culture media. Notably, expression of the coreceptors was the endpoint of their experiment. For my requirement, too few cells positively stained for both coreceptors and in general the viability of the cells compared to a control EL4 cells was reduced. Furthermore, the EL4 "DP" cells did not respond to the addition of DxS.

2.3.1 Preparation of a single cell suspension

Following CO_2 asphyxiation, the thorax was opened, and the thymus removed while taking care not to rupture the heart or major blood vessels. The thymus was placed in 10 mL of ice-cold Minimum Essential Medium (MEM) in a 10 mL centrifuge tube (Technoplas). The contents were then poured into a 70 μm nylon strainer (BD Falcon™) placed in a 10 cm diameter cell culture dish. To dissociate the thymus, it was gently mashed using the plunger from a 3 mL syringe. Using a transfer pipette, the flow-through was returned to the 10 mL tube. The sample was centrifuged (300 g, 5 min, 4°C) and the supernatant discarded. The cells were washed twice, each time resuspending the pellet in 10 mL of ice-cold phosphate buffered saline (PBS) and centrifuging as before. The pellet was then resuspended in 1 mL of MEM and the cell concentration was determined.

The cell concentration was determined manually or with an automatic cell counter and viability analyser (Beckman Coulter VI-CELL™ XR, Beckman Coulter Inc, Ontario CA). To manually count, 10 µl of the cell suspension was first diluted in PBS (1:50). From this suspension, a 50 µl aliquot was further diluted with 50 µl of 0.1% trypan blue (1:2; BDH Poole Chemicals, London UK). Approximately 20 µl of the stained suspension was pipetted to fill the wells of a haemocytometer (Reichert Bright, Buffalo NY USA). The cell count was on a light microscope (BX40, Olympus Optical, Tokyo, Japan) at 40x magnification and the cell count per mL was calculated by multiplying the count/square by 10^6. For automatic cell counting, 490 µl PBS was added to a 4 mL polystyrene (PS) cup to which 10 µl of the cell suspension was then added. This sample was then run on the VI-CELL™ XR instrument.

2.3.1.1 **Loading of fluorescent indicators**

Stock solutions (2 mM) of the ion-sensitive indicators were prepared with dimethyl sulfoxide (DMSO). Aliquots of 2.5–5 µL were stored at -20°C protected from light. When added to the cell suspension, the final concentration was 5 µM for Ca^{2+}- and Na^{+}- or 1 µM, for Mg^{2+}-sensitive dyes. While thymocytes have been shown to be more sensitive to DMSO than splenic lymphocytes (Schrek *et al.* 1967), the 0.5% solvent concentration (when two fluorophores are simultaneously loaded) is not expected to have a significant cytotoxic effect within the time frame of the experiments, as they found that the mean survival of murine thymocytes incubated with 8% DMSO for 4 hours remained at 98.9 ± 4.3%.

Prior to loading, the cell concentration was adjusted to 3 x 10^7 cells/mL by the addition of MEM that was not supplemented with FBS. Once the fluorophore was added, the tube/s was/were wrapped in foil to minimise photobleaching of the fluorophore and incubated for 30–60 min at 37°C in 5% CO_2 followed by storage on ice for 20 min. Supporting the indo-1 AM loading concentration used

in this research, an examination of loading concentrations, undertaken by Tellam and Parish (1987), found incubation with 5 μM indo-1 AM for 1 h was not toxic to thymocytes suspended at 2.5 x 10^7 cells/ml. Furthermore, these authors found that it did not notably alter basal $[Ca^{2+}]_i$ and it provided a "practical fluorescence signal".

2.3.1.2 **Antibody staining**

When staining thymocyte surface markers, such as CD4 and CD8, the antibodies were added to the cell suspension immediately following the incubation required to load the cation-sensitive dyes. The fluorochrome conjugated antibodies and the concentrations used in staining of CD4 and CD8 are described in Table 2.3. The undiluted antibodies were added to the cell suspension which was then incubated at 4°C for 20 min. Following this incubation, residual dye and unbound antibodies were removed from suspension by washing twice with 8 mL of ice-cold PBS, centrifuged (300 g, 5 min, 4°C) and the supernatant discarded. Following the final wash, the pellet was resuspended in 1 mL HBS (pH 7.3 at 7 or 19°C), a cell count was done, and the concentration diluted to 25 x 10^6 cells/mL

The samples were immediately taken for measurement on the flow cytometer. To study the DxS-induced ionic rises, thymocytes were used on the day of preparation.

2.3.1.3 **Method for preparing depleted $[Ca^{2+}]_o$ cell suspension**

Prior to pre-warming the sample, 100 μl of cells suspended in normal HBS were diluted with 400 μl of Ca^{2+} free HEPES buffer, nominally reducing $[Ca^{2+}]_o$ to ~0.36 mM. The Ca^{2+} was then chelated by adding 1 mM EGTA to the cell suspension. Using the Maxchelator program the estimated free Ca^{2+} was calculated to be ~42 nM (http://web.stanford.edu/~cpatton/CaEGTA-NIST.htm).

2.3.2 Monitoring intracellular Ca^{2+}, Na^{+} and Mg^{2+} time course

Commonly, $[Ca^{2+}]_i$ and $[Na^{+}]_i$ were monitored simultaneously. However, in some experiments $[Mg^{2+}]_i$ instead of $[Na^{+}]_i$ was monitored. On such occasions, $[Ca^{2+}]_i$ and $[Mg^{2+}]_i$ were concurrently monitored. A BD LSRFortessa cytometer supported by BD FACSDiva™ software version 6.2 (Becton, Dickinson and Company, Franklin Lakes, NJ) was used to measure and record the time course of $[Ca^{2+}]_i$, $[Na^{+}]_i$ and $[Mg^{2+}]_i$. Table 2.8 provides the details of the lasers, detectors and filter set configuration used to excite and detect emissions from cation sensitive fluorescent indicator dyes and Ab conjugated fluorophores (used to stain for CD4 and CD8).

2.3.2.1 Ca^{2+} detection using indo-1

As detailed in Table 2.8, the indo-1 fluorescence signal was detected using 379/28 nm and 505LP 530/30 nm emission filter sets for indo-1 bound and indo-1 free, respectively. Two distinct emission peaks were readily measurable. Considering the 30 % spectral overlap of indo-1, this configuration results in a small "spill" of emission light into both bound (0.3%) and free (6.2%) "channels". It also minimises the detection of uncleaved indo-1-AM fluorescence at ~480–500 nm (Lückhoff 1986).

2.3.2.2 Na^{+} detection using SBFI

As detailed in Table 2.7, unlike for indo-1, SBFI is optimally excited by 2 wavelengths and detected at a single wavelength. These physical properties make SBFI a far from ideal dye to use in flow cytometry using a single laser. As well, in contrast to the considerable separation of the indo-1 emission peaks (>100 nm), there is significant spectral overlap of bound and free SBFI. Nevertheless, using the 355 nm laser to excite SBFI and the detection filter sets described in Table 2.8 differentiation of emission from free and bound dye was possible.

Manual compensation was undertaken to reduce the spectral overlap of 0.7 and 3.8% into bound and free, respectively.

Table 2.8 LSRFortessa instrument configuration

Details of the instrument set up used to excite and detect emission signals from intracellular cation sensitive fluorescent dyes and Ab conjugated fluorochromes used for detection of coreceptor expression.

Fluorescent indicator or fluorochrome	Laser (nm)	Detector	Dichroic mirror Long pass (nm)	filter /band pass (nm)
Indo-1 free	UV (355)	A	None	379/28
Indo-1 bound		B	505	530/30
SBFI free	UV (355)	A	None	379/28
SBFI bound		B	None	450/50
ANG-2	Blue (488)	D	550	575/26
ANG-2	Blue (488)	E	505	530/30
Mag-fluo-4	Blue (488)	E	505	530/30
APC	Red (633)	C	None	670/14
FITC	Blue (488)	E	505	530/30
AF647	Red (640)	C	None	670/14
APC-Cy7	Red (640)	A	750	780/60

2.3.2.3 Na^+ detection using ANG-2

Since in most instances, absolute values in $[Na^+]_i$ were not required, a concentration change can still be monitored with a non-ratiometric dye like ANG-2 (detailed in Table 2.8). Although optimally excited by 517 nm, ANG-2 can

be sufficiently excited with a 488 nm laser. The peak amplitude of ANG-2 emission is at ~540 nm, and it increases with $[Na^+]$. When used alone, the ANG-2 fluorescence signal was best detected using a 505LP 530/30 nm filter set.

2.3.2.4 **Simultaneous measurement of $[Na^+]_i$ and $[Ca^{2+}]_i$**

As both SBFI and indo-1 dyes have similar emission spectra, they cannot be used to simultaneously monitor $[Ca^{2+}]_i$ and $[Na^+]_i$ changes. To simultaneously monitor the two, cells were loaded with ANG-2-AM and indo-1-AM. The detection of indo-1 emission was done the same way as indicated above, but to gain better spectral separation, ANG-2 emission was measured at a longer wavelength "channel", namely after passing a 550LP and a 575/26 nm filter set. Using this filter set decreased unwanted detection of leaked indo-1 (free) into the ANG-2 signal from ~47 to ~32%, which was further reduced by manual compensation.

2.3.2.5 **Simultaneous measurement of $[Ca^{2+}]_{ER}$ and $[Mg^{2+}]_i$**

With the intent of monitoring $[Mg^{2+}]_i$ changes in DP thymocytes, cells were loaded with Mag-fluo-4-AM. Mag-fluo-4 has a high sensitivity to Mg^{2+}, with a K_d of ~4.7 mM. However, it is also a low affinity Ca^{2+} dye (K_d = 22 μM) and since it also readily loads into the ER, it has been used to monitor $[Ca^{2+}]_{ER}$ (Li *et al.* 2011).

Similar to ANG-2, Mag-fluo-4 was chosen as it can be detected simultaneously with indo-1. The excitation/emission wavelength maxima for this non-ratiometric dye is 494/527 nm. In the experiments illustrated here, the LSRFortessa 488 nm laser and 505 LP 530/30 filter set were used for excitation and emission detection.

When Mag-fluo-4 (5 μM) was loaded for 1 h at 37°C, it had readily entered the ER and bound Ca^{2+}. This confounded the $[Mg^{2+}]_i$ detection without first depleting the stores. Even with depleted stores, Mag-fluo-4 detection of $[Mg^{2+}]_i$ was poor.

Reducing the dye loading to 30 min and its concentration to 1 μM did not alter ER uptake much. In thymocytes, this dye appears better suited for monitoring ER store Ca^{2+} rather than cytosolic Mg^{2+}.

2.3.2.6 **Recording conditions**

Following the setup for each dye in regard to excitation, emission filter sets and numerical compensation for spectral overlap, a template was saved in FACS Diva. New experiments were run from such saved templates. At the commencement of a new session, the voltage settings were checked to ensure optimal detection of each fluorescence signal.

To enable experiments to be conducted at 37 ± 0.5°C, a double-layer Perspex sheath was specially made to encase a 5 mL test tube (Round Bottom Falcon®) when fitted on the LSRFortessa sample injection port. Fluid from the water bath was pumped through this sheath, keeping the sample at ~37°C throughout the experiment.

Aliquots of HBS (pH adjusted for 37°C) were pipetted into a 5 mL polystyrene test and placed into a water bath set at 37°C. As required, 100 μL of the cell suspension (kept at RT, *i.e.* 19°C) was pipetted into a 400 μL HBS sample (or 1:5 dilution). This dilution brought the cell concentration to ~5 x 10^6 cells/mL. The sample was left to equilibrate with the bath temperature for 5 min. Following pre-warming, the tube was inserted into the Perspex sheath. During the experiment the sample was removed to add relevant chemicals and briefly vortexed before placing it back into the sheath on the cytometer. On average, the duration of the removal was ~15 s.

In this thesis, samples from single cell suspensions were acquired at a rate of ~800 events/s. Dye loading was checked by the addition either 2 μM ionomycin or 20 μM amphotericin B (AmpB) to saturate with Ca^{2+} or Na^+, respectively.

2.3.2.7 **Gating hierarchy for data acquisition and analysis**

BD FACSDiva software was used for acquisition setup and data acquisition. The gating hierarchy commonly used for acquisition and for data analysis using the FlowJo® V8–V10 analysis software (Tree Star Inc. Ashland, OR) are shown in Figure 2.1. Panel A (i–iv) shows the protocol used to monitor Ca^{2+} (or Na^{+}, when cells were loaded with SBFI). Panel B (i–iii) shows the gating hierarchy for experiments that monitored indo-1 simultaneously with ANG2 (or indo-1 with Mag-fluo-4). In these plots the density of the observed events is represented by a colour code running from blue to red (maximum). The aim of the initial gate is to identify the thymocyte population based on the relative cell size and internal complexity of the cell, while at the same time eliminating dead cells and debris. As shown in Figure 2.1A-i & B-i, the live cell population of interest was gated (black circle) by forward scatter area (FSC-A; estimation of size) and side scatter area (SSC-A; estimation of granulation). Aggregates/doublets were excluded from this population by gating FSC-A and FSC-height (FSC-H; Figure 2.1-ii). Next, specific populations of interest, that is DP or $CD8^{hi}$ thymocyte populations, were defined by gating on CD4 CD8 expression (DP) or CD8 expression and ANG-2 fluorescence intensity as shown in Figure 2.1A-iii & B-iii, respectively.

As illustrated in Figure 2.1A-iii, DP thymocytes form the largest population group and when using indo-1 or SBFI alone, cells were stained with anti-CD4 and anti-CD8α fluorochrome conjugated Abs to capture this population. In contrast, when cells were loaded with both indo-1 and ANG2, only CD8α staining was added. With this reduced staining it was only necessary to compensate for the fluorescence spill-over of indo-1 free (λ_2) into ANG2. It was decided that gating on thymocytes expressing the CD8α coreceptor, thus capturing small populations of pre-DP CD8 SP thymocytes and differentiated SP $CD8^{+}CD4^{-}$ as well as the predominant DP population, would adequately identify

DxS responders. During acquisition the ratio of indo-1 and ANG2 fluorescence was monitored over time as shown in Figure 2.1A-iv & B-iv.

The FlowJo® V8–V10 kinetics platform was used to create the graphs shown in Figure 2.1A-v & B-v. These graphs plot the median fluorescence of events in each time interval which was 1–3 s depending upon duration of the acquisition.

2.3.3 Estimating the $[Ca^{2+}]_i$ and $[Na^+]_i$

$[Ca^{2+}]_i$ and $[Na^+]_i$ were determined based on fluorescence values obtained using either a LSRFortessa™ (BD Biosciences, San Jose, CA, USA) or a Tecan microplate reader (Infinite® M200 Pro, Männedorf, Switzerland configured with Version 3.40 01/15 infinite firmware).

2.3.3.1 Determination of $[Ca^{2+}]_i$ in indo-1 loaded cells

The intracellular Ca^{2+} concentration was estimated using the following equation (Grundler *et al.* 2001).

$$\left[Ca^{2+}\right]_i = K_d \frac{1 - R_{min}/R}{R_{max}/R - 1} \cdot \frac{S_{f2}}{S_{b2}}, \qquad \text{(Eq. 1)}$$

where K_d is the dissociation constant of indo-1. At 37°C, this value is 250 nM (Grynkiewicz *et al.* 1985). R is the bound/free indo-1 ratio measured during the DxS $[Ca^{2+}]_i$ plateau. R_{max} is the ratio measured (as before) under saturating Ca^{2+} conditions, induced by adding the Ca^{2+} ionophore ionomycin (3 μM) to cells suspended in normal HBS ($[Ca^{2+}]_o$ = 1.8 mM). R_{min} was obtained by the addition of ionomycin to cells suspended in low Ca^{2+}-HBS plus 1 mM EGTA to clamp $[Ca^{2+}]_o$ to ~40 nM. S_{f2}/S_{b2} is the measured median fluorescence intensity (from 60 s of recorded data) under saturating *vs.* Ca^{2+} depletion conditions in λ_2, *i.e.* the emission detected after passing the 530/30 filter set.

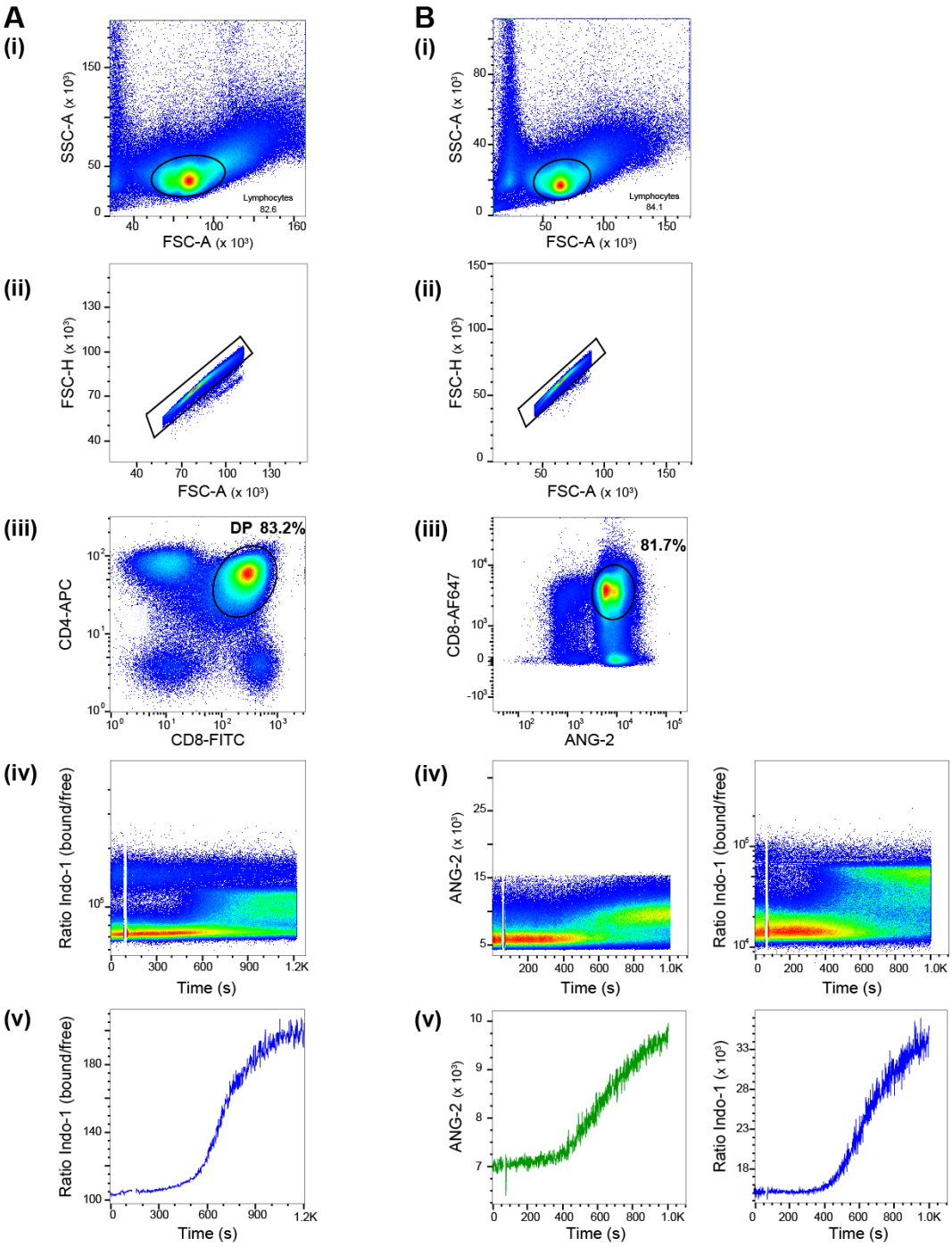

Figure 2.1 Gating hierarchy for acquisition and analysis

A(i). The thymocyte population (black circle) is identified based on based on forward and side scatter area properties (FSC-A and SSC-A). A(ii). This selected population is further defined using FSC-H plotted against FSC-A to exclude aggregates. (iii) The DP thymocyte population is identified by APC and FITC (conjugated to anti-CD4 and anti-CD8 mAb, respectively) fluorescence detection. The number indicates the percentage of thymocytes contained within the gate (circle). (iv). The ratio of indo-1 (bound/free) is plotted over time for the DP thymocytes. Hiatus indicates the time when DxS was added to the sample with no detection. (v) A kinetics

plot determined from (iv) based on the median indo-1 ratio fluorescence from >600 events/s (blue). B(i-iv). Shows the hierarchy gating applied when both $[Ca^{2+}]_i$ and $[Na^+]_i$ are measured. (i - ii) As described in A(i–ii). (iii) Here a $CD8^{hi}$ thymocyte population is identified by AF647 (conjugated to anti-CD8 mAb) fluorescence is plotted against that of ANG-2 (black circle). (iv) Density plots based on ANG-2 fluorescence intensity and ratio of indo-1 against time. (v). $[Na^+]_i$ and $[Ca^{2+}]_i$ kinetics plots are derived from the events in (iv) based on the median fluorescence from >600 events/s. Consistent throughout this thesis, the control DxS plots are colour coded blue for Ca^{2+} and green for Na^+.

2.3.3.2 **Determination of $[Na^+]_i$ using ANG-2**

2.3.3.2.1 ANG-2 calibration

ANG-2 calibration was done using a Tecan microplate reader. Thymocytes were loaded with 1 μM ANG-2-AM following the protocol described above (2.3.1.1). To prepare samples for ANG-2 calibration, prior to the final wash the cell suspension was divided into two 10 ml Falcon tubes and following centrifugation the pellets were resuspended at a concentration of 10^6 cells/mL, one in *N*-methyl-D-glucamine (NMDG) HEPES solution and the other in HBS. NMDG is used here as a replacement for Na^+. A range of $[Na^+]$ solutions from 0–140 mM was made by serially diluting the NMDG-HEPES buffer with HBS as required. Using a Corning 96 well flat bottom polystyrene plate, 160 μl from each calibration solution was pipetted into wells and 40 μl of cells (suspended in NMDG-HEPES buffer) were added to each. This resulted in a set of $[Na^+]_o$ values ranging from 0–112 mM. To equilibrate $[Na^+]_i$ with $[Na^+]_o$, the samples were incubated for 15 min at 37°C with 20 μM amphotericin B (AmpB).

Prior to loading the plate, the Tecan microplate reader temperature was brought to 37°C and the optimal excitation at of 515 nm and emission at 550 nm (bandwidth 9 and 20 nM, respectively) was set. The fluorescence at each $[Na^+]$ was measured. These values were then normalised to the maximal value and plotted as illustrated in Figure 2.2A. K_d was estimated by fitting a sigmoidal function to these data points. In the example illustrated, the K_d was 37 ± 4 mM.

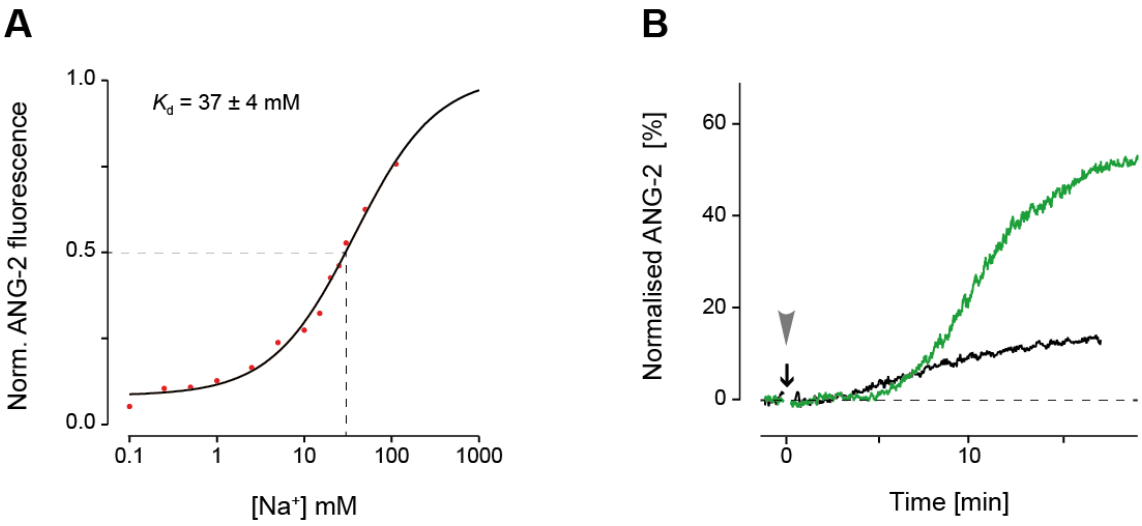

Figure 2.2 ANG-2 calibration curve

Plot of normalised fluorescence *vs*. $[Na^+]_i$ for ANG-2 measured in thymocytes incubated with AmpB. The data points were fitted with a sigmoidal curve to yield K_d (dashed lines). (B) Time courses of $[Na^+]_i$ when either DxS or ConA was added at $t = 0$ min (green and black, respectively).

Using this value, the intracellular $[Na^+]_i$ could be estimated using equation 2 (Iamshanova *et al.* 2016)

$$\left[Na^+\right]_i = K_d \frac{F - F_{min}}{F_{max} - F}, \qquad \text{(Eq. 2)}$$

where F is the ANG-2 detected fluorescence intensity, F_{min} is the emission signal detected when AmpB was added to thymocytes suspended in a Na^+ free NMDG-HEPES buffer. F_{max} was obtained by adding 20 μM AmpB to cells suspended in 140 mM Na^+-HBS. F was obtained at the plateau (~15 min) after adding DxS. These experiments were done using a BDFortessa cytometer.

I note here that the accurate estimation the DxS Na^+ rise using the plate reader was confounded by cell death and consequent loss ANG-2 caused by incubation with AmpB. Therefore, given that the change is within the linear range of the dye

(see above), an estimation of the amplitude was made by bracketing it against the Na^+ rise induced by ConA, which has been reported by Segel *et al.* (1979) to be ~6 mM (Figure 2.2B).

2.3.4 Preparation of peripheral T cells

For peripheral T cells, following dissection of the thymus, the lymph nodes were also removed and transferred to ice-cold MEM solution. A single cell suspension was prepared following the same protocol as described for thymocytes (section 2.3.1). Two aliquots of 0.5 mL were prepared, and both were loaded with 5 μM SBFI-AM. Additionally, one sample had neuraminidase (from *V. cholerae*, final concentration 0.1 U/mL) added, while the other served as a control sample. The two tubes were wrapped in aluminium foil and incubated at 37°C in 5% CO_2 as described earlier.

2.3.5 Immunocytochemistry

On day 1, a single cell suspension (3 x 10^7 cells/mL) was prepared following the method in section 2.3.1. Two aliquots were made and Alexa Fluor®647-CD8α (1:500) was added to one to stain $CD8^+$ thymocytes. Both samples were incubated 4°C for 20 min and then centrifuged (300 *g*, 5 min, 4°C). The supernatant was discarded, and the pellets were resuspended in 1 mL HBS pre-warmed to 37°C. Following a cell count, the concentration was diluted to 10^7 cells/mL. Aliquots of 150 μL from each sample were transferred to wells on a 96-round bottom plate.

The cells were fixed by the addition of 50 μL of 4% paraformaldehyde (final concentration 1%) and incubated for 1 h at 4°C. Next, the cells were washed twice with 200 μL PBS per well. The plate was centrifuged (150 *g*, 10 min, 4°C) and the supernatant was removed. Following a second wash, the pellets were resuspended in 100 μl PBS/ 5% normal donkey serum to block nonspecific sites. The plate was wrapped in foil and left overnight at 4°C. Also incubated overnight

at 4°C were the anti-TRP Ab_1–blocking peptide (BP) solutions. These solutions, prepared at a ratio of 1 μg peptide per 1 μg antibody, were placed on a rocker to facilitate Ab_1–BP binding.

All other Ab solutions were prepared on the following morning. Ab_1 and Ab_2 dilutions (detailed in Table 2.4 and 2.5) were made in PBS/ 1% donkey serum and PBS, respectively and placed on ice, while the plate was centrifuged (150 *g*, 10 min, 4°C). The Ab_1 solutions, Ab_1–BP or PBS/ 1% donkey serum were then added to the relevant wells and, to facilitate Ab binding, the plate was placed on a rocker for 1 h at RT. Subsequently, unbound Ab_1 was removed by washing the cells 3 times, as described above, before adding either the Ab_2 solutions or PBS to the relevant wells. The plate was placed on a rocker, leaving the cells to incubate with the Ab_2 for 1 h at RT. As before, unbound Ab_2 were removed by washing 3 times with 200 μL washing buffer and centrifuged as before. After the final wash, the pellets were resuspended in 100 μL sterile PBS, and the plate was stored at 4°C prior to analysis using flow cytometry.

2.3.5.1 **Analysis of anti-TRP Ab binding using flow cytometry**

The samples were run at RT on a BD LSR™II cytometer supported by FACSDiva™ software. The fluorochromes FITC and AF647 were excited using 488 and 633 nm lasers and detected using 505LP 530/30 and 660/20 filter sets, respectively. At the commencement of a new session, the voltage settings were checked to ensure optimal detection of each fluorescence signal.

As described in Gating hierarchy for data acquisition and analysis, the cell population of interest was identified based on forward and side scatter properties (Figure 2.3A-i) and to exclude debris and aggregates (A-ii). Contour plots, as shown in Figure 2.3B, were used to display the density of events relative to FITC (conjugated to the Ab_2) and AF647 (conjugated to anti-CD8α Ab) fluorescence

intensity. The contour plots of CD8α against TRP channel expression are shown in Figure 2.3. From left to right, the four plots show the relative density and frequency of i) unstained cells, used to detect background unspecific autofluorescence, ii) anti-CD8α-AF647 plus Ab_2 (without Ab_1) stained cells, used to detect unspecific Ab_2 binding, iii) anti-CD8α-AF647 plus Ab_1–BP (anti-TRP Ab preincubated with antigen peptide) plus Ab_2 stained cells, used to check the specificity of the Ab_1 for the immunogen it was raised against, and iv) anti-CD8α-AF647 plus Ab_1 plus Ab_2 stained cells which detect binding of the primary anti-TRP channel antibody. To visually screen for the likely presence of each TRP channel, a threshold for detection of Ab_1 binding in $CD8^{hi}$ cells was set in plot (iii) by positioning the vertex of a quadrant gate (red) to the right of the population density. This quadrant gate was copied into plots i, ii and iv.

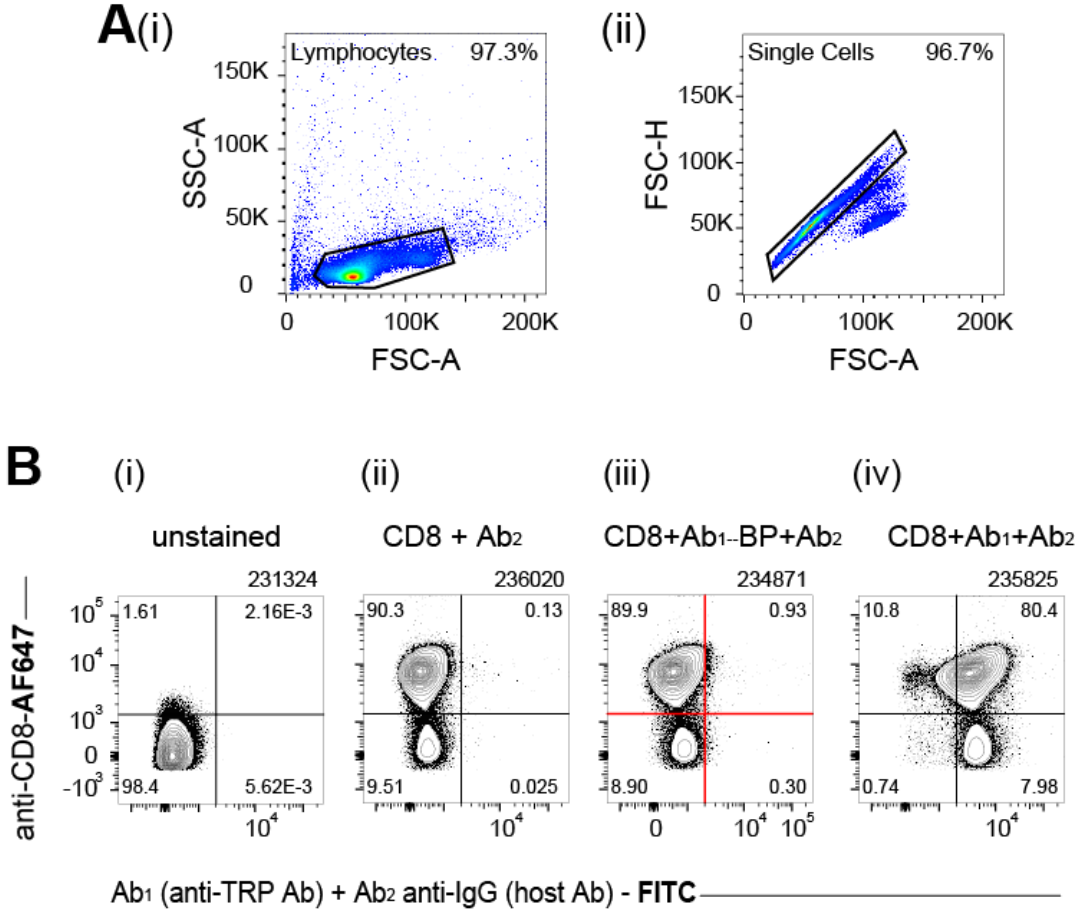

Figure 2.3 Gating protocol to assess possible presence of TRP channel

(A) Dot plots with gating hierarchy used to distinguish the cell population of interest (i) and exclude aggregates (ii). (B) Contour plots showing cell populations relative to the detection of surface expression of CD8 (conjugated AlexaFluor®647) and a TRP channel (in this case TRPV3). Ab_1 binding was detected by Ab_2 staining (donkey anti-rabbit IgG conjugated to FITC). The quadrant gate (red) applied in plot (iii) was copied to the other plots.

As before, the data files were analysed using the FlowJo® V8–V10 analysis software (Tree Star Inc. Ashland, OR).

2.4 Data analysis

Additional data analysis was done in Igor Pro (Versions 7 and 8; Wavemetrics, Oregon). Time series data from FlowJo kinetics plots were saved into an Excel file and imported into Igor Pro.

2.4.1 Analysis of flow cytometry time course plots

The ratio of bound over free indo-1 (R) was used to determine the relative change in Ca^{2+}. In general, this data was normalised for the ratio before the start of the experiment (F_0) averaged over 30 s and set to zero (Figure 2.4). The subsequent change in fluorescence (ΔF) was then plotted as a time course during the experiment, with DxS typically added at t = 0. FACS data for Na^+ and Mg^{2+} fluorescence were analysed in a similar manner. The peak amplitude was equally determined as the mean over 30 s symmetrically around the peak, or typically over the last 30 s. The delay of the onset (red) of the respective rise was determined by fitting a Boltzmann equation of the following form

$$f_B = max / \left(1 + \exp^{a \cdot (t_{half} - t)}\right)$$

to the time course, with max the value of the relative peak, t_{half} the time at half-maximal amplitude and a the rate of rise.

The difference (in percentage) between two peak amplitudes in a set of experiments when, for example, the rise was blocked, was normalised to that of the corresponding rise with DxS (100% - control rise, blue). This is shown in Figure 2.4 (y-axis on the right) and, as an example, that when PLC was blocked (black). In this case, the difference is indicated by the red line and corresponds to ~80%.

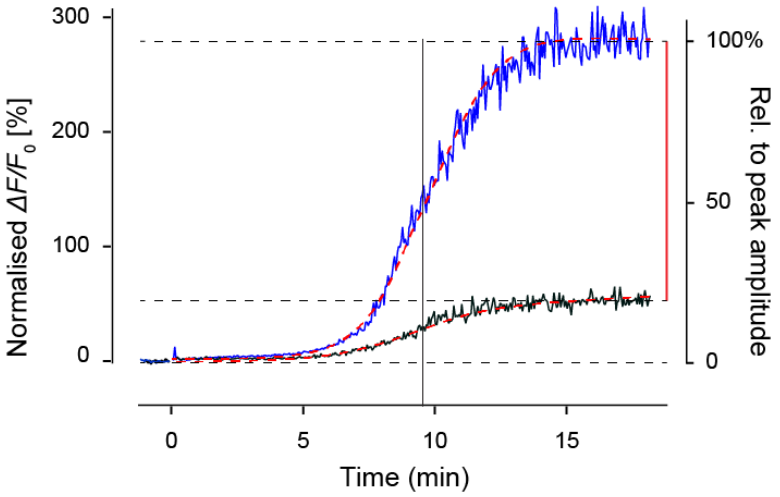

Figure 2.4 Time courses of normalised $\Delta F/F_0$ caused by DxS

Percentage difference (red) between DxS treated sample (blue, control) and one with an inhibitory drug added (black). Time to half maximal amplitude (t_{half}, black line) was determined by fitting a sigmoid to the data sets (red dash).

2.4.2 Statistical comparisons

Summary data is typically reported as mean ± standard error of the mean (S.E.M) with the number of experiments (n) provided. In the case of n = 3, a box plot is given with the top and bottom representing the 25th and 75th percentile. The line within the box represents the median and is typically colour coded with blue for Ca^{2+} and green for Na^{+}. Where n > 3, whiskers are added to the same box indicating the range from the minimum to maximum value.

Significance level was set at 0.05. The statistical significance of the differences of means for a minimum of at least 3 separate experiments was determined by Student's *t*-test (unpaired, two-tailed). In Figures, where asterisks used to indicate the level of significant difference, the p_t value is <0.05 (∗), <0.01 (∗∗), <0.001 (∗∗∗) and <0.0001 (∗∗∗∗). Based on an acquisition rate of ≥800 events/s during flow cytometry experiments, following the removal of noise, the resultant kinetics plots generally are derived from 600 ± 23 events/s (n = 40 randomly opened experiments). A minimum of three repetitions was considered sufficient to determine if the samples were significantly different.

The statistical significance of the differences between two distributions of ICC samples in control and when exposed to DxS was determined using the Kolmogorov-Smirnov statistic.

3 Characterisation of the DxS $[Ca^{2+}]_i$ rise and mechanisms

3.1 Introduction

Distinct from the small transient Ca^{2+} flickers that are linked to thymocyte motility, thymocyte arrest and associated cell–cell interactions result in sustained $[Ca^{2+}]_i$ oscillations with large amplitude (Bhakta *et al.* 2005, Melichar *et al.* 2013, Ross *et al.* 2014). In 1987, Tellam & Parish described a sustained $[Ca^{2+}]_i$ rise that was induced in DP thymocytes (Weston *et al.* 1991) following the addition of DxS, but not by the addition of other smaller mol. wt. polysulfated polysaccharides. This rise was dependent upon influx of Ca^{2+} across the PM and seemingly independent of Ca^{2+} store release. Recently, Simon Davis (2015) proposed that the DxS $[Ca^{2+}]_i$ rise may mimic the $[Ca^{2+}]_i$ response observed in preselection DP thymocytes–$cTEC^{hi}$ rosette formation. Significantly, rosette formation was markedly inhibited by the addition of anti-CD8β mAb, in CD8β deficient thymocytes, and when DxS or heparin mimetics were added to the WT thymocyte–$cTEC^{hi}$ suspension (Simon Davis 2015). This suggests that in thymocyte–cTEC suspensions, HS binding to the CD8 coreceptor was crucial to triggering a signalling cascade that led to activation of a Ca^{2+}-permeable channel.

Without rosetting, 0.1 mg/mL heparin (a highly sulfated HS analogue) added to a thymocyte suspension was not sufficient to induce a $[Ca^{2+}]_i$ rise (Simon Davis 2015). This fact suggests that activation of other surface receptors and adhesion molecules during rosetting facilitates this $[Ca^{2+}]_i$ rise. It also suggests that in contrast to heparin, the significantly larger molecule DxS must interact with other surface molecules in addition to CD8β. Interestingly, while αβTCR–MHC-I interactions have been shown to enhance the $[Ca^{2+}]_i$ rise associated with rosetting, Simon Davis (2015) observed TCR/CD3 signalling via ZAP-70 activation was not

necessary in facilitating the DxS $[Ca^{2+}]_i$ rise. In thymocytes derived from ZAP-70 deficient mutant mice, he found that the DxS $[Ca^{2+}]_i$ rise was unchanged. While this finding rules out the involvement of the ZAP-70 signalling pathway, it does not necessarily exclude any CD3 involvement with DxS. Upstream of ZAP-70 phosphorylation of the CD3ζ chains, avid physical association between the CD8 coreceptor β chain and CD3δ may facilitate a conformational change in CD3 in response to CD8β stimulation (Doucey *et al.* 2003). Associated with this conformational change is the proposed SLP-76 recruitment of the adaptor protein Nck to the CDε chain (Barda-Saad *et al.* 2004, de la Cruz *et al.* 2011). In turn, Nck engages phosphorylated SLP-76, ADAP and WASP to the inside-out signalling cascade required for LFA-1 activation and to the LAT-nucleated macromolecular signalling complex, a necessary step in the orchestration of PLC-γ1 activity (Gil *et al.* 2002).

Notably, in thymocytes derived from SLP-76 deficient mice the DxS $[Ca^{2+}]_i$ rise was found to be significantly diminished (Simon Davis 2015) suggesting a crucial role for this adaptor protein. While SLP-76 is best phosphorylated by ZAP-70, it may also be phosphorylated by Lck (Y423/426; Wardenburg *et al.* 1996). This may be sufficient to allow suboptimal TCR stimulation to evoke an LFA-1 dependent $[Ca^{2+}]_i$ rise like the one described by Kim *et al.* (2009a; Figure 1.3A; black trace).

If the DxS $[Ca^{2+}]_i$ rise mimicked a physiological $[Ca^{2+}]_i$ rise which functions to modify or fine tune the selection processes by "priming" of some preselection thymocytes, then identifying the mechanisms which are activated upstream of the DxS-induced Ca^{2+} influx will add to our understanding of T cell development by revealing critical features of selection. Furthermore, exploring the characteristics and mechanisms which modulate the DxS-induced Ca^{2+} influx observed in DP thymocytes may help to identify the ion channel(s) involved.

In this chapter, I am presenting results which further characterize the DxS $[Ca^{2+}]_i$ rise described. I will show that the addition of DxS results not only in a Ca^{2+} but also in a concomitant $[Na^+]_i$ rise and that activation of the transmembrane flux is indeed independent of Ca^{2+} release from ER stores. The DxS mediated signalling mechanism is proposed to mimic the HS signalling pathways described in 1.3.1.6.1 (p. 52) and depicted in Figure 1.4. Therefore, in this chapter I also present the results from flow cytometry experiments which aimed to identify crucial receptors, kinases and other proteins that facilitate the transduction of the relevant signalling pathways leading to subsequent activation of an unspecific cation permeable channel or channels sustaining the two rises. Results from this chapter will be used in narrowing down a list of putative channel(s) presented in the following chapter.

3.2 Materials

Details of the solutions and chemicals commonly used in cell preparation and flow cytometry experiments can be found in Chapter 2. Table 3.1 provides details of the concentrations of the various chemicals used and when they were added to the sample. Unless otherwise stated, DxS was added to the cell suspension after at least one minute of recording. In control experiments where the effect of the chemical without the addition of DxS was tested, the chemicals were also added to the cell suspension at $t = 0$ min and at the concentrations stated in Table 3.1.

Table 3.1 List of chemicals

Chemical	Putative target	Mechanism	Protocol	Conc. (μM)
Caffeine	Phosphor-diesterase	inhibits degradation of cAMP	5 min pre-incub.	400
ConA	TCR/CD3 crosslinker	mitogenic activator	15 min pre-incub. at 37°C	10 μg/ml
CPA	SERCA	inhibitor	Added at *t* = 0 min	20
EGTA	$[Ca^{2+}]_o$	chelator	Added at *t* = -1 min	5 mM or 100
Edelfosine	PLC	inhibitor	Added at *t* = -1 min	1
FFA	TRPC3	inhibitor	5 min pre-incub. or at 12 min	100
Gö6983	PKC	inhibitor	Added at *t* = -3 min	0.1
GsMtx4	SAC channels	inhibitor	Added at *t* = -5 min	3.5
H-89	PKA	inhibitor	Added at *t* = -15 min	0.5
Ionomycin	Raises $[Ca^{2+}]_i$	ionophore	Added at *t* = 15 min	2
Latrunculin B	F-actin	inhibits polymer formation	55 min pre-incub. at RT + 5 min at 37°C	1
LY294002	PI_3K	inhibitor	30 min pre-incub. at 37°C	50

PP2	Lck inhibitor	inhibitor	10 min pre-incub. at 37°C	0.1
Pyr3	Orai, TRPC3	inhibitor	5 min pre-incub. or at 12 min	5
SN-6	NXC	inhibitor	Added at *t* = -1 min	3
Tetrodotoxin	Na_V	pore blocker	Added at *t* = -1 or 0 or 5 min	1, 5 or 10
Xestospongin C	IP_3R	inhibitor	15 min pre-incub. at 37°C	2
YM244769	NCX	inhibitor	Added at *t* = -1 min	0.5
YM58483 (BTP2)	Orai1-3	inhibitor	Added at *t* = -1 min	1

3.3 Characteristics of the DxS-induced cation influx

3.3.1 Reproduction of DxS $[Ca^{2+}]_i$ rise in DP thymocytes

In investigating the characteristics of the $[Ca^{2+}]_i$ rise, the first step was to determine if the properties of the $[Ca^{2+}]_i$ rise detected by flow cytometry were comparable to that described by Tellam and Parish (1987) which was based on measurements by a spectrometer.

After pre-warming the sample cells to 37°C for 5 min in a water bath, the addition of 100 μg/mL DxS to a thymocyte suspension resulted in a robust rise in $[Ca^{2+}]_i$, which started after ~5 min, slowly reached a peak after 15 min (Figure 3.1A, blue), and maintained a plateau for at least another 15 min (not shown). Here, the relative change in $[Ca^{2+}]_i$ is plotted over time after the addition of DxS at *t* = 0 min (grey arrowhead) and after normalising for the baseline to be zero.

The black trace shows a typical time course for a control sample when no DxS was added to the suspension. The ochre trace was obtained when 5 mM EGTA was added to the suspension (normal HBS) before the addition of DxS (t = -1 min), indicating that the rise is dependent upon a transmembrane Ca^{2+} influx into the thymocytes and that the background Ca^{2+} in these cells is dependent on a Ca^{2+} leak either across the PM or from stores. The peak amplitude of this $[Ca^{2+}]_i$ rise was well within the linear range of the indo-1 dye as determined by the addition of 2 μM ionomycin during the plateau period (Figure 3.1D, black arrow), which still resulted in a ~5-fold increase of the normalised ratio.

The $[Ca^{2+}]_i$ concentration of the DxS induced rise, as detected by flow cytometry, was estimated using Eq. 1 (see Methods 2.3.3.1) and compared with the result reported by Tellam and Parish (1987). Based on a resting $[Ca^{2+}]_i$ of ~110 nM (Hesketh *et al.* 1983, Ross & Cahalan 1995, Tellam & Parish 1987), the DxS $[Ca^{2+}]_i$ rise was found to be 165 ± 11 nM (n = 5). This value is not different to that reported by Tellam & Parish (1987; 146 ± 23 nM, n = 11, p_t = 0.28). For comparison, their figure is redrawn here (Figure 3.1B), where in blue, the Ca^{2+} rise is shown as measured on the Perkin Elmer LS-5 luminescence spectrometer and in ochre, after 5 mM EGTA had been added to the suspension. On the left, R indo-1 is plotted and on the right, the respective estimated Ca^{2+} concentration.

Notably, in the original time course, there was a small initial Ca^{2+} rise within about 2 min, which was also abolished when the $[Ca^{2+}]_o$ was chelated with EGTA (see Fig.3.1B, ochre; Tellam & Parish 1987). This small early rise was not apparent in the traces obtained with flow cytometry.

In agreement with the later findings reported by Weston *et al.* (1991), the $[Ca^{2+}]_i$ rise was indeed restricted to thymocytes in the DP population as shown in Figure 3.1C (blue). A smaller, highly variable rise was observed in CD8 SP thymocytes (grey). This finding was inconsistent and most likely an artefact of population

gating (Figure 3.1C, inset), which may have included early transitional $CD4^{int}$ $CD8^{hi}$ thymocytes in this population. An even smaller rise was seen in CD4 SP cells (pink), but the $[Ca^{2+}]_i$ in the DN subset (red) was no different to the control when no DxS was added (black). With the exception of the early rise not present in cytometry data, the findings so far are consistent with the idea that there was no difference between the rise measured with the cytometer *vs*. that with the spectrometer and suggests that with my methods, the same Ca^{2+} rise was tracked reliably.

3.3.2 The DxS $[Ca^{2+}]_i$ rise measured early *vs*. late was comparable

As most cytometry experiments were conducted over a period of three to four hours, it was important to determine if the DxS $[Ca^{2+}]_i$ rise could still be reliably activated in samples that were "freshly" prepared *vs*. ones that had been stored on ice for more than two hours. It was noticed that keeping the cells on ice for prolonged periods caused a gradual increase in the resting $[Ca^{2+}]_i$ evidenced by the fact that during a subsequent experiment there was an increased *R* of indo-1 fluorescence. In these samples, the amplitude of the DxS $[Ca^{2+}]_i$ rise was also noticeably smaller. However, keeping the cells at RT (~19°C in the cytometry facility) alleviated this problem.

Over a period of four hours, and when the cell suspension was stored at RT, no significant difference was found between the indo-1 *R* obtained from early and late samples (Figure 3.1E; $n = 26$; $p_t = 0.89$). In this figure, one of two samples was measured early (left) and the other late (right). The respective values for the same preparation are joined by a line with the respective box-and-whisker plots overlaid.

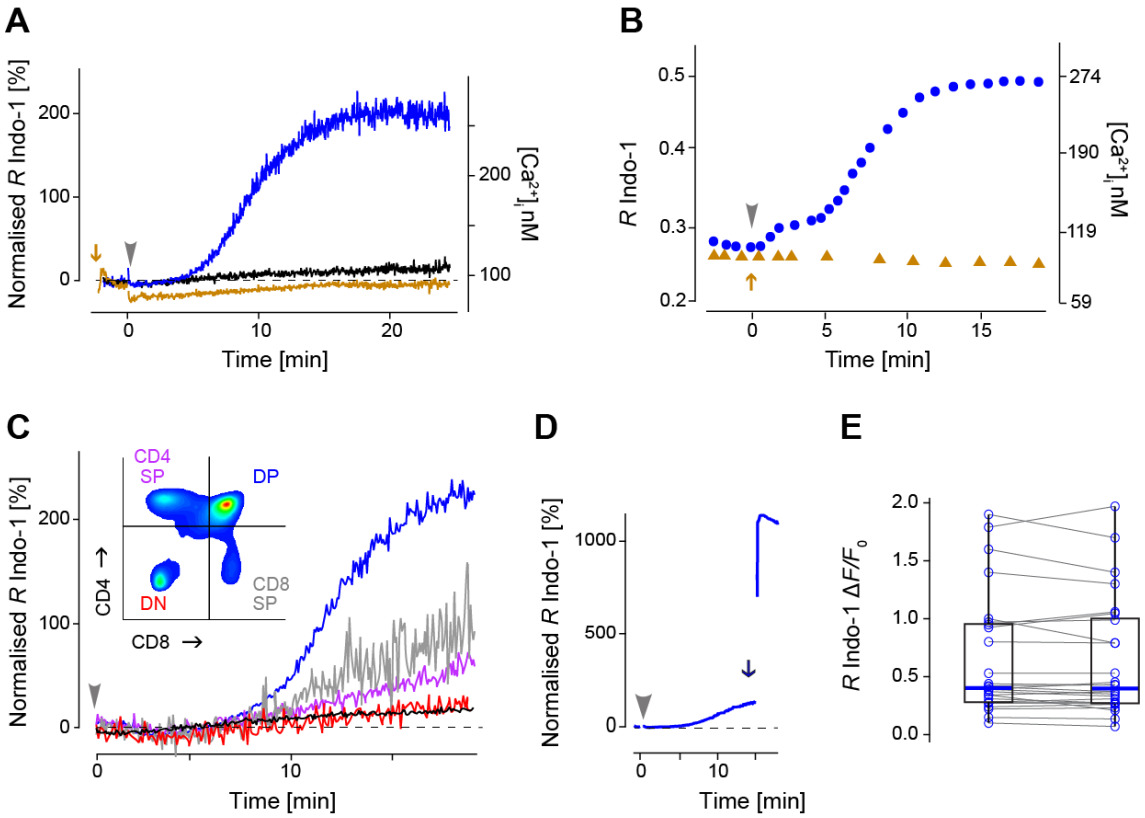

Figure 3.1 Characterisation of the DxS $[Ca^{2+}]_i$ rise

(A) Time courses of DxS $[Ca^{2+}]_i$ under normal conditions (blue) when DxS was added at $t = 0$ (grey arrowhead). Controls without DxS (black) and with DxS in the presence of 5 mM EGTA extracellularly (ochre). (B) Time courses obtained in a spectrometer by Tellam and Parish (1987) for DxS (blue) and in the presence of 5 mM EGTA (ochre). (C) $[Ca^{2+}]_i$ time courses evoked by DxS added at $t = 0$ (grey arrow) for the 4 different thymocyte populations based on low *vs.* high gating on CD4 and CD8 (inset) with DP cells (blue), CD8 SP (grey), CD4 SP (pink) and DN (red). Control without DxS in black. (D) Time course of DxS $[Ca^{2+}]_i$ under normal conditions (t = 0 min) with subsequent addition of 2 μM ionomycin at $t = 15$ min (black arrow). (E) Plots of peak amplitudes ($n = 26$) of $[Ca^{2+}]_i$ from the same preparation obtained early (left) and late (right) with data pairs joined by a line and box-and-whisker plot superimposed.

Importantly results presented in 3.3.1–3.3.3, show that the DxS induced $[Ca^{2+}]_i$ rise is repeatable and consistent over experimental sessions lasting up to 4 h. In the following sections I demonstrate how the 'DxS related' results may be altered by subtle changes in the background $[Ca^{2+}]_i$. caused by drugs or changes in temperature. These stimulatory mechanisms may include thermally activated STIM1 (Xiao *et al.* 2011) or drugs such as the mitogen Concanavalin A, or channel inhibitors such as Pyr3, and flufenamic acid which evoke a sustained rise in

$[Ca^{2+}]_i$. Depending upon when these stimuli are applied, they either abolish or potentiate the DxS induced $[Ca^{2+}]_i$ rise.

3.3.3 The mechanism is sensitive to elevated background $[Ca^{2+}]_i$

In addition to being very sensitive to temperature, the mechanism is also dependent on background $[Ca^{2+}]_i$. Significantly, while investigating the relationship between the rises induced by ConA and DxS , I noticed that a stable elevation of the background $[Ca^{2+}]_i$ by ~60 nM prior to the addition of DxS occluded any subsequent DxS Ca^{2+} rise. As also found by Tellam and Parish (1987), the addition of 10 μg/ml ConA during the plateau phase of the DxS $[Ca^{2+}]_i$ rise still evoked a transient additive $[Ca^{2+}]_i$ rise (Figure 3.2A; red arrowhead on blue). However, this time course was not only faster than when added on its own (Figure 3.2A; red arrow at t = 0 min, red), but also much smaller. This suggests that ConA causes a rise via a different mechanism, but that the two are not necessarily independent of each other. In addition, I have also been able to show that in contrast to the DxS rise, ConA can still evoke a much smaller Ca^{2+} transient under conditions when $[Ca^{2+}]_o$ is nominally 0 mM with 100 μM EGTA (red arrowhead on ochre). This suggests that ConA involves Ca^{2+} release from stores.

The unexpected finding, however, was that, under conditions when cells were pre-incubated with ConA for 15 min, the DxS $[Ca^{2+}]_i$ rise (blue, without ConA as control) was abolished (Figure 3.2B; brown). Note that in contrast to most other figures, I am presenting this data without normalisation of R (raw). This is to clarify that background $[Ca^{2+}]_i$ was elevated before the addition of DxS by about 60 nM. This experiment was repeated 5 times and the block was highly significant (p_t <0.0001). This finding suggests that prior elevation of $[Ca^{2+}]_i$ can occlude the transmembrane DxS rise.

Furthermore, this Ca^{2+}-dependent block of the DxS $[Ca^{2+}]_i$ rise was consistently observed following application of several chemicals including Pyrazole 3 (Pyr3, a potent and selective TRPC3 antagonist), flufenamic acid (FFA), capsazepine, NS8593 and norgestimate. Shown in Figure 3.3C (yellow), preincubation with 5 μM Pyr3 (5-butyl-1*H*-pyrazole-3-carboxylic acid) promoted a persistent elevation in background $[Ca^{2+}]_i$ and prohibited the expected Ca^{2+} influx caused by adding DxS (yellow, $n = 8$, $p_t < 0.0001$). Likewise, the sustained rise in background $[Ca^{2+}]_i$ triggered by the addition of 100 μM FFA (2-[[3-(Trifluoromethyl)phenyl] amino] benzoic acid) also abolished the DxS influx (Figure 3.3D, aqua; $n = 4$, $p_t < 0.0001$). Notably, as observed with ConA, the addition of Pyr3 or FFA late (*i.e.* after the rise onset, Figure 3.3C & D insets, black), caused an additive $[Ca^{2+}]_i$ rise. Interestingly, the time courses of these rises were different, suggesting activation of other channels. Together, these findings indicate that the DxS $[Ca^{2+}]_i$ rise may be 1) modulated by mechanisms involved in store Ca^{2+} release and SOCE activation, such as IP_3R activation or STIM1 binding, or 2) the channel or its signalling components may themselves be inhibited by $[Ca^{2+}]_i$.

As stock solutions of chemicals, such as Pyr3 and NS8593 (*N*-[(1*R*)-1,2,3,4-tetra-hydronaphthalen-1-yl]-1*H*-1.3-benzodiazol-2-amine), were made using DMSO as the solvent, I confirmed that 1% DMSO did not elevate the background $[Ca^{2+}]_i$ or alter the DxS rise (Figure 3.3E, black and pink). Notably, when used in experiments, stock solutions were diluted by a factor $\geq 10^3$, and DMSO was not considered likely to confound the results.

3.3.4 **The mechanism is temperature sensitive**

Another factor affecting reproducibility was variation in recording temperature. Therefore, to monitor if the temperature remained within physiological range (37 ± 1°C), a Brannan immersion thermometer was placed into the water bath. Significantly, the DxS-induced Ca^{2+} rise could not be activated under conditions

where the pre-warm and acquisition temperatures were ≤30°C (Figure 3.2F, light blue; n = 7, p_t <0.0001). Furthermore, maintaining cells on ice raises the background $[Ca^{2+}]_i$ compared to cells held at RT and at 37°C. This is depicted in Figure 3.2F (inset) which shows $[Ca^{2+}]_i$ in cells, when monitored at 4°C, then RT

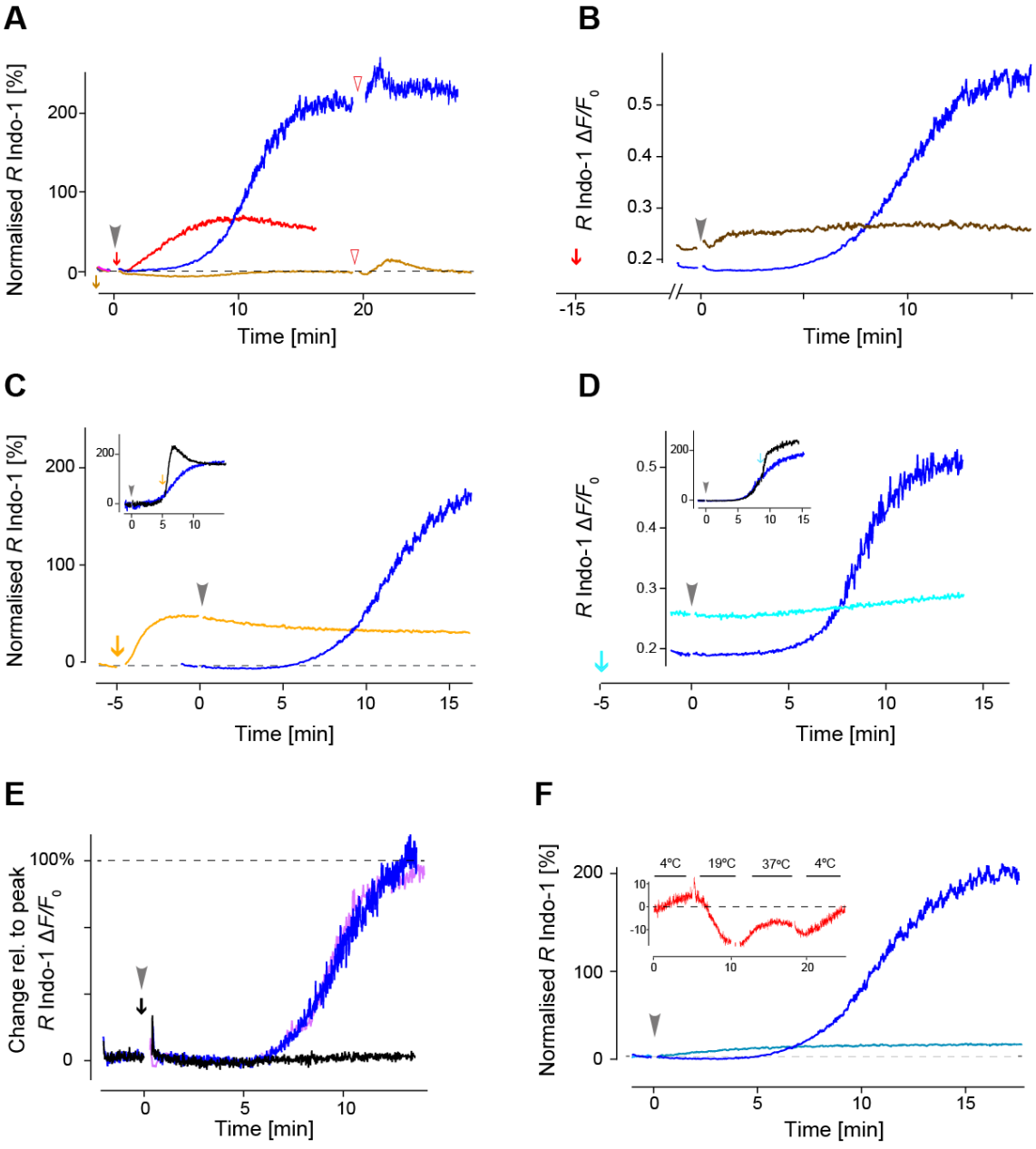

Figure 3.2 $[Ca^{2+}]_i$ and thermal inhibition of the DxS rise

(A) Time courses of DxS $[Ca^{2+}]_i$ (blue) with addition of 30 µg/mL ConA at the peak of the DxS rise (t = 20 min; red arrowhead), without DxS but with ConA alone (red with red arrow at t = 0), and with DxS (in Ca^{2+} free-HBS) and in the presence of 100 µM EGTA (ochre) and subsequent

addition of ConA at t = 20 min. (B). Raw ratio of $\Delta F/F_0$ given for normal DxS rise (blue) and when pre-incubated with ConA for 15 min (red arrow, brown trace). (C) Time courses of DxS $[Ca^{2+}]_i$ under normal conditions (blue) when DxS was added at t = 0 (grey arrowhead) and when preincubated with Pyr3 (yellow arrow, trace) for 5 min prior to the DxS addition. Inset: Pyr3 added at the onset of the DxS Ca rise (t = 5 min, black). (D) Raw ratio of $\Delta F/F_0$ given for normal DxS $[Ca^{2+}]_i$ under control conditions (blue) with DxS added at t = 0 (grey arrowhead) and when also preincubated with FFA for 5 min (aqua arrow, trace). Inset: FFA added during the DxS rise at t = 8 min (black). (E) Time course of DxS induces $[Ca^{2+}]_i$ under control conditions (blue) and in the presence of 1% DMSO (purple). Black trace indicates $[Ca^{2+}]_i$ after addition of only DMSO at t = 0 min. (F) Time courses of DxS $[Ca^{2+}]_i$ under normal conditions (blue) when DxS was added at t = 0; when the sample was prewarmed and acquired at 30°C (light blue), and when the temperature was raised to 40°C at t = 8 min (black arrow, trace). Inset: Time course $[Ca^{2+}]$i, in cells monitored at 4°C, then RT from t = 5 min, then 37°C from t = 11 min then 4°C from t = 17 min (red).

(removed from ice bath at t = 5 min). At t = 11 min, the sample was placed in the heating jacket and warmed to 37°C and finally returned to the ice bath at t = 17 min. This observation suggests that the ion channel(s) and/or the signalling cascade involved have a complex temperature sensitivity.

3.3.5 SOCE via STIM/Orai channel activation is not involved

The classically described SOCE channels, comprising STIM/Orai subunits, are expressed in DP thymocytes (Gwack *et al.* 2008). Of the three *Orai* isoforms, *Orai2* mRNA has the highest expression (see Appendix 6; p.357). Notably, the ability of Orai2 to form heteromeric Orai1/Orai2 channels may result in alteration of the Orai channel characteristics during early positive selection reducing their activation (Bertin *et al.* 2014, Vaeth *et al.* 2017, Vig & Kinet 2009).

Pharmacologically induced emptying of $[Ca^{2+}]_{ER}$ by the inhibition of the SERCA pump with cyclopiazonic acid (CPA) is a common *in vitro* method used to activate STIM/Orai channels. In thymocytes, the depletion of $[Ca^{2+}]_{ER}$ following the addition of 20 μM CPA rapidly activates them. Using the low affinity dye Mag-fluo-4 to monitor $[Ca^{2+}]_{ER}$ (Diercks *et al.* 2017, Gerasimenko *et al.* 2014), I provide evidence of a considerable ER Ca^{2+} leak in these cells. As shown in Figure

3.3A, the addition of 20 μM CPA at $t = 0$ min resulted in a small transient increase immediately followed by a large decrease in Mag-fluo-4 fluorescence (black), distinctly different to the maintained fluorescence in the control sample (purple). This suggests that when the SERCA pump is blocked, *i.e.* when replenishment of the store is prevented, the fast and large drop in $[Ca^{2+}]_{ER}$ can only be explained by a persistent Ca^{2+} leak.

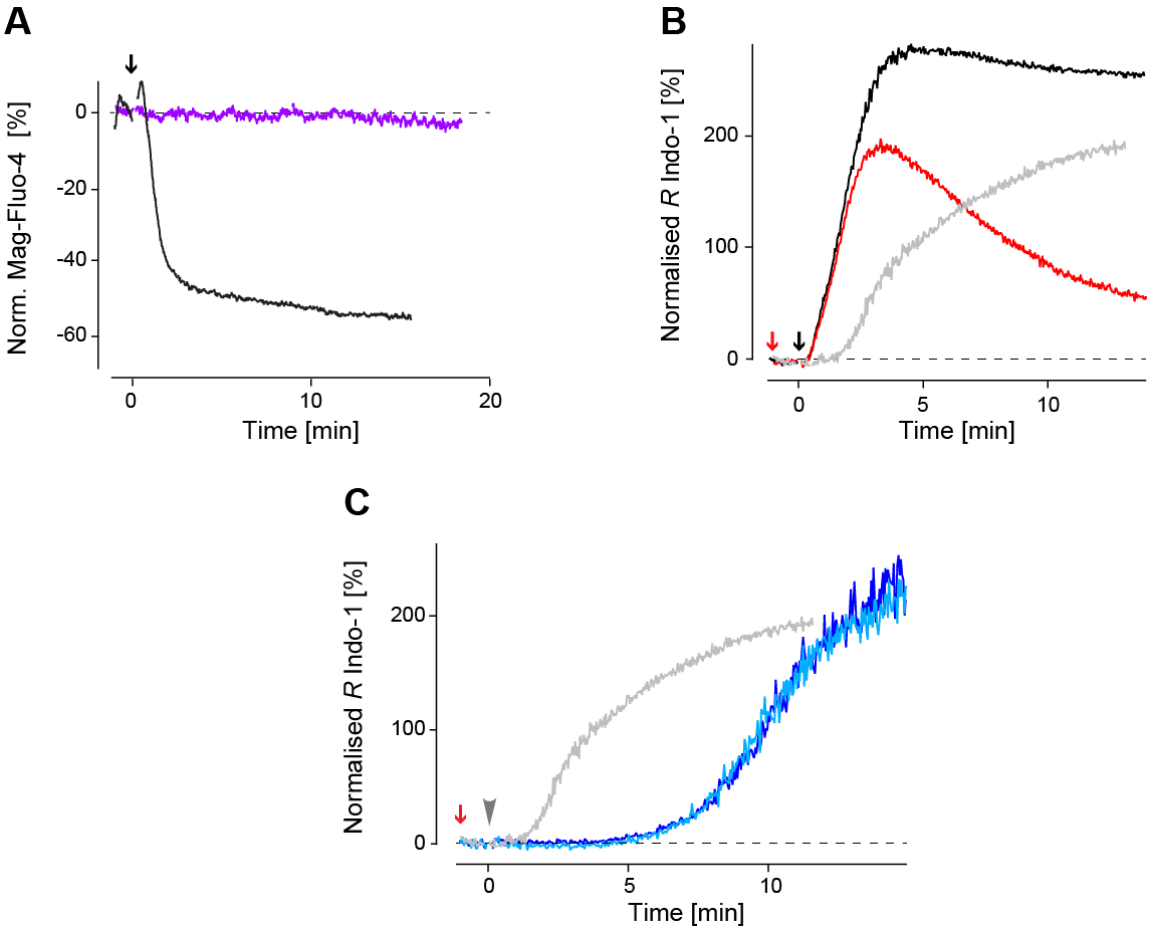

Figure 3.3 The DxS $[Ca^{2+}]_i$ rise is independent of store operated STIM/Orai activation.

(A) Mag-fluo-4 fluorescence during control (pink) and after the addition of CPA to the sample at $t = 0$ (black) suspended in a nominally Ca^{2+} free solution. (B) Normalised indo-1 fluorescence when SOCE channels were activated by 20 μM CPA (black) and after the addition of 1 μM YM58483 (red) to block Orai channels, isolating Ca^{2+} release from the ER. The calculated difference between black and red indicates the Ca^{2+} influx through Orai channels (grey). (C) Time course of

the DxS induced Ca^{2+} rise with or without YM58483 (red arrow/aqua trace and blue, respectively). Added for comparison is the SOCE component from E (grey).

Because the usage of Mag-fluo-4 with a K_d of 20–25 μM for Ca^{2+} precludes the monitoring of the much smaller $[Ca^{2+}]_i$ changes with DxS, the involvement of SOCE was then tested with indo-1. In Figure 3.3B, the addition of 20 μM CPA to the sample at $t = 0$ caused a $[Ca^{2+}]_i$ increase with much shorter latency, faster rise and larger amplitude. It reached a peak after ~4 min followed by a small decay afterwards (black). This rise was very different to that seen with DxS and is likely caused by activation of SOCE channels, perhaps STIM/Orai. YM58483 (also known as BTP2) has been described as an indirect inhibitor of Orai channel activation (Ishikawa *et al.* 2003, Mercer *et al.* 2010, Zitt *et al.* 2004). In Jurkat cells, Ishikawa *et al.* (2003) found that this chemical had an IC_{50} of ~150 nM, and importantly, concentrations up to 3 μM did not affect the resting $[Ca^{2+}]_i$. I therefore chose 1 μM to test if Orai channels were involved. The results as depicted in Figure 3.3B (red) show that Orai channels could be significantly inhibited after pre-incubation of the sample in 1 μM YM58483; *i.e.* the Ca^{2+} rise caused by CPA was curtailed (red). To get an idea as to how much Ca^{2+} was the result of SOCE, the arithmetic difference between the total Ca^{2+} rise caused by CPA and after Orai channels were blocked is illustrated in grey. It shows that SOCE is delayed and rises much slower but is still considerably faster than that by DxS. In addition, while these channels were blocked (Figure 3.3C), the addition of DxS still caused a $[Ca^{2+}]_i$ rise (light blue), indistinguishable from the case when no YM58483 was present (blue, $n = 4$, $p_t = 0.98$). This line of evidence suggests that SOCE via Orai channels is not involved in the DxS $[Ca^{2+}]_i$ rise.

However, these results do not entirely rule out activation of a non-selective cation channel. For example, a number of TRP channels are reportedly modulated by STIM1 and IP_3R (Albarran *et al.* 2014, Horinouchi *et al.* 2012, Jardín *et al.* 2009,

Yuan *et al.* 2007). If this were the case, then there should also be a concomitant $[Na^+]_i$ rise in these cells.

3.3.6 Concomitant $[Na^+]_i$ rise

To investigate whether the addition of DxS also led to a rise in $[Na^+]_i$, cells were loaded with either 5 μM of the ratiometric Na^+-sensitive dye SBFI-AM or 5 μM ANG-2-AM. Using the latter dye, it is possible to also image Ca^{2+} simultaneously with 5 μM indo-1-AM.

The addition DxS still evoked the same delayed $[Ca^{2+}]_i$ rise (blue; axis on the left) but also caused a $[Na^+]_i$ rise (green; axis on the right) with very similar time course (Figure 3.4A). Fitting sigmoidal functions to both the Ca^{2+} and Na^+ time courses revealed that the t_{half} values of the two rises were not different (10.8 ± 0.2 *vs.* 10.9 ± 0.2 min; $n = 50$, $p_t = 0.14$), but the rate of the $[Na^+]_i$ rise was marginally faster (0.19 ± 0.01 *vs.* 0.21 ± 0.01 min^{-1}, $p_t < 0.0001$).

As with Ca^{2+}, compared to the other three populations, DP thymocytes showed the largest $[Na^+]_i$ rise (Figure 3.4B). Moreover, this rise was also only seen around physiological temperature. Like the Ca^{2+} results, the DxS-induced Na^+ rise could not be activated under conditions where the pre-warming and acquisition temperatures were ≤30°C (Figure 3.4C, light green; $n = 7$, $p_t < 0.0001$). As observed for $[Ca^{2+}]_i$ (Simon Davis 2015), a much lower DxS concentration (1 μg/mL) was also still sufficient to activate the $[Na^+]_i$ rise.

I noticed that the background SBFI fluorescence without stimulation decayed slowly with time (Figure 3.4B, black). This is likely caused by inappropriate single wavelength excitation (Borin & Siffert 1990) and perhaps also intracellular acidification associated with use of the HEPES buffer (Cowan & Martin 1995), reducing the emission of SBFI fluorescence (Diarra *et al.* 2001, Iamshanova *et al.* 2016). Unlike with SBFI, detection of background ANG-2 fluorescence was stable

throughout (Figure 3.4D, grey). As for Ca^{2+} imaging, there was no significant difference between the relative ANG-2 $\Delta F/F_0$ values obtained from samples measured early or late (Figure 3.4C; n = 19, 0.336 ± 0.038 *vs.* 0.324 ± 0.039, p_t = 0.82).

To get an estimate of the $[Na^+]_i$ accumulation, I calibrated ANG-2 as illustrated in Figure 2.2A, and found a value of 37 ± 4 mM for its K_d, comparable to that reported by Iamshanova *et al.* (2016; 34 mM). Using this and an estimated a background $[Na^+]_i$ value of 9.4 mM (Harootunian *et al.* 1989) the DxS induced Na^+

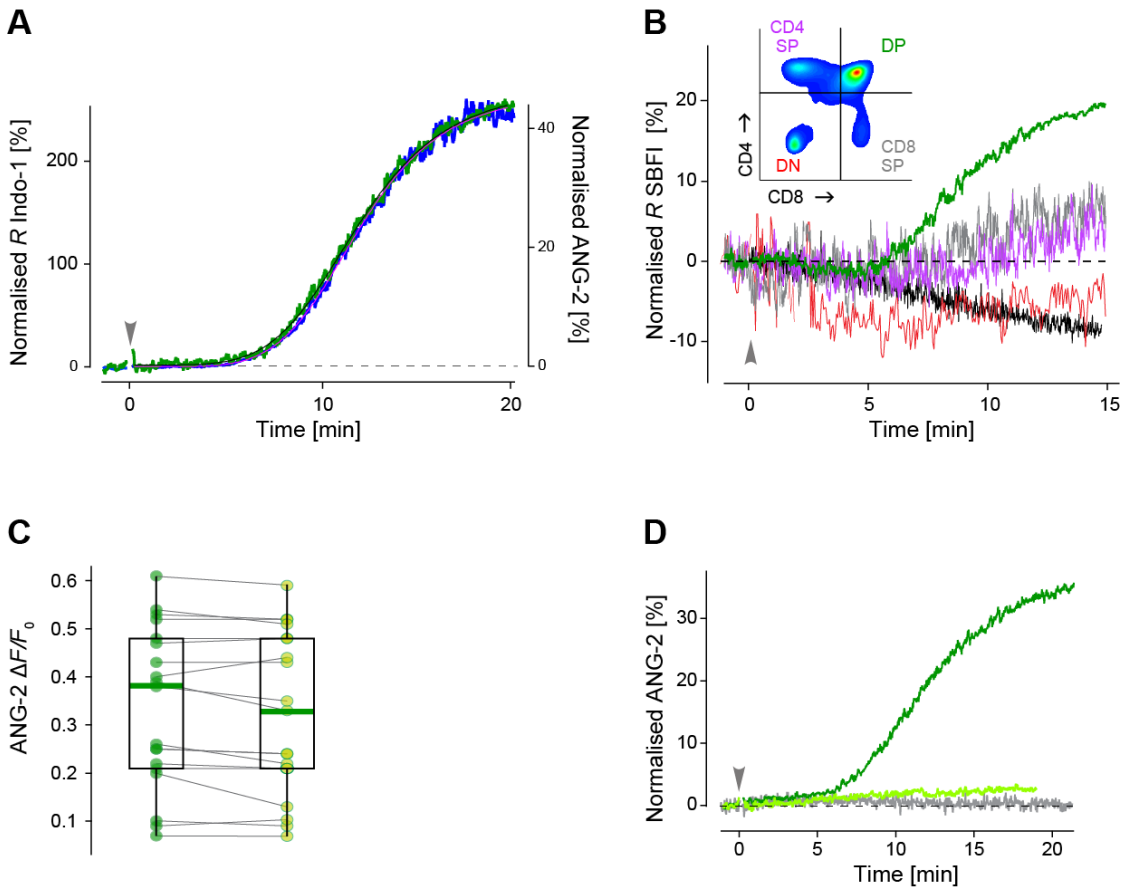

Figure 3.4 The relationship between Na^+ and Ca^{2+} influx.

(A) Time courses of the normalised $[Ca^{2+}]_i$ rise after DxS (blue; left axis) and that of $[Na^+]_i$ detected with ANG-2 (green; right axis) overlayed with the respective fits (Ca^{2+} pink, Na^+ black). (B) DxS evoked $[Na^+]_i$ rises in the 4 thymocyte populations (inset) using SBFI (DP green, CD4 SP pink, CD8 SP grey, DN red, no stimulus control black). (C) Individual results and overlaid box-and-whisker plots of relative ANG-2 $\Delta F/F_0$ measured early (left) and late (right). Paired experiments

are joined by a line. (D) Time courses of DxS $[Na^+]_i$ under normal conditions (green) when DxS was added at $t = 0$ and when the sample was both prewarmed and acquired at 30°C (light green). No stimulus control in grey.

rise was estimated to be 20 ± 3.4 mM. Since this value was surprisingly large, I wanted to obtain an independent estimate based on the $[Na^+]_i$ rise caused by ConA (Figure 2.2B), which had been measured to be ~6 mM (Segel *et al.* 1979). As the increase in fluorescence of ANG-2 is ~3-fold higher in DxS than in ConA this means that DxS raised $[Na^+]_i$ by 19.8 ± 5.0 mM ($n = 5$), consistent with my previous estimate. This indicates that within the about 10 min of the Na^+ rise, there is a large concentration change most likely associated with a significant depolarisation and conductance change.

Like the $[Ca^{2+}]_i$ rise, the $[Na^+]_i$ rise did not occur when the sample was prewarmed and acquired at 30 rather than 37°C (Figure 3.4D, light green; $n = 7$, $p_t < 0.0001$). These data show that concomitant with the $[Ca^{2+}]_i$ rise, there is a $[Na^+]_i$ rise with a similar time course and properties. These two observations are consistent with the idea that the underlying influx may be via a non-selective cation channel (one channel hypothesis) or a set of two channels with similar activation properties (two channel hypothesis).

Since the Na^+ influx could be the result of Ca^{2+} clearance via the NCX, an important consideration was to check if perhaps the $[Ca^{2+}]_i$ rise was dependent on a Na^+ influx.

3.4 Relationship between $[Ca^{2+}]_i$ and $[Na^+]_i$

3.4.1 $[Ca^{2+}]_i$ rise is partially dependent on Na^+ influx

Because Ca^{2+} homeostasis is not independent of that of Na^+, particularly under conditions when NCX is involved, the relationship between the Na^+ rise and Ca^{2+} rise was investigated using both Na^+ substitution and the pharmacological block of NCX.

When $[Na^+]_o$ was replaced with the organic cation NMDG, the resultant DxS $[Ca^{2+}]_i$ rise was ~45 % smaller than that during control (Figure 3.5A & B, grey; n = 7, p_t <0.001). Fitting a sigmoid curve to each trace (red), I found the half rise and rate values were not significantly different (n = 3; p_t = 0.87 and 0.95, respectively). This data suggests that there is likely a role for NCX in reverse mode by transporting 3 Na^+ ions out and adding one to the $[Ca^{2+}]_i$ influx, most likely as the rise begins to plateau.

However, it needs to be pointed out that the cation NMDG may also alter the charge interaction of DxS with the thymocyte membrane. To rule this possibility out, NCX was pharmacologically blocked. Both YM244769 (IC_{50} ~70 nM) and SN-6 (IC_{50} ~3 μM) selectively inhibit all NCX isoforms by preferentially blocking the reverse mode (Iwamoto *et al.* 2004, Iwamoto *et al.* 2007).

When added to the cell suspension without DxS, neither 0.5 μM YM244769 nor 3 μM SN-6 significantly affected background $[Ca^{2+}]_i$ over time (n = 11; p_t = 0.1). Significantly, when either of these NCX inhibitors were added prior to DxS, the peak amplitude $[Ca^{2+}]_i$ rise was reduced by ~45% (n = 6, p_t <0.001), as shown in Figure 3.5G. This reduction was comparable to that seen with NMDG (p_t = 0.9), suggesting that altered charge screening near the membrane surface is not a major confounding factor. The effect on the peak amplitude of the $[Na^+]_i$ rise was

highly variable, but overall not significantly different to the control rise (Figure 3.5C; n = 8, p_t = 0.4).

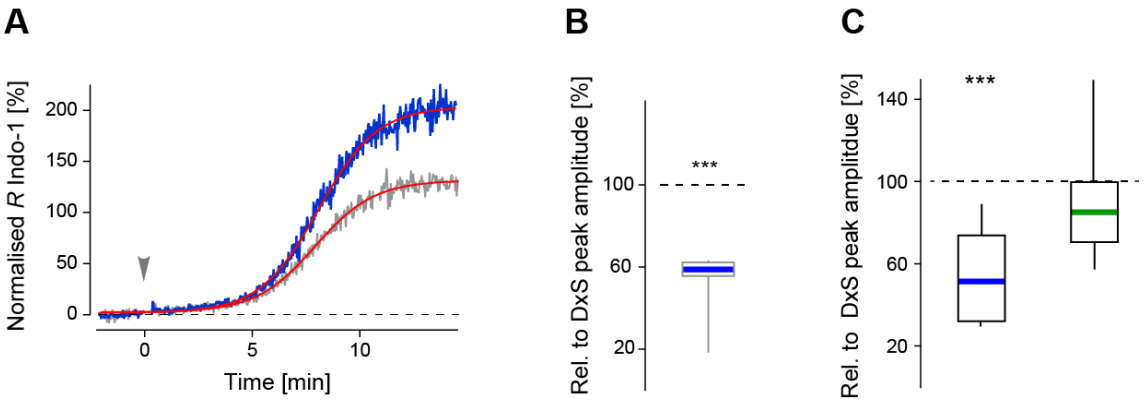

Figure 3.5 The Ca^{2+} rise is not dependent upon Na^+ entry

(A) Time course of the normalised $[Ca^{2+}]_i$ rise after DxS (blue) and when $[Na^+]_o$ was replaced by NMDG (grey), fitted sigmoid curve (red). (B) Peak amplitude of DxS $[Ca^{2+}]_i$ rise when $[Na^+]_o$ was replaced by NMDG normalised to control (dashed line). (C) Box-and-whisker plots of relative peak amplitudes of $[Ca^{2+}]_i$ (blue) and $[Na^+]_i$ (green) in the presence of SN6 or YM244769 with the control value indicated by the dash. *** for p <0.001.

This finding was unexpected as blocking NCX reverse mode should have resulted in Na^+ accumulation over time. It is likely explained by the fact that the exchange by NCX is much smaller than the change caused by Na^+ influx. These data lend support to the idea that about 40% of the Ca^{2+} amplitude is caused by reverse mode activity of NCX. Having established that the Ca^{2+} influx was dependent to some extent on Na^+ influx, in the next set of experiments, I tested the converse, namely if the $[Na^+]_i$ rise depended on Ca^{2+} influx.

3.4.2 $[Na^+]_i$ rise does not depend on Ca^{2+} influx

If the $[Na^+]_i$ rise depended on a Ca^{2+} influx, chelation of $[Ca^{2+}]_o$ with EGTA should have abolished it. As illustrated in Figure 3.6A & B when compared to control (green), the time course and amplitude of the DxS $[Na^+]_i$ rise remained unaltered (ochre; n = 10, p_t = 0.96). While this finding is consistent with activation of a non-

selective cation channel (one channel hypothesis), an alternative explanation is that Na^+ rose because of a concomitant activation of a voltage-dependent Na^+ channel (two channel hypothesis). To rule this possibility out, Na_V were blocked with various concentrations of tetrodotoxin (TTX), a pan-Na_V blocker.

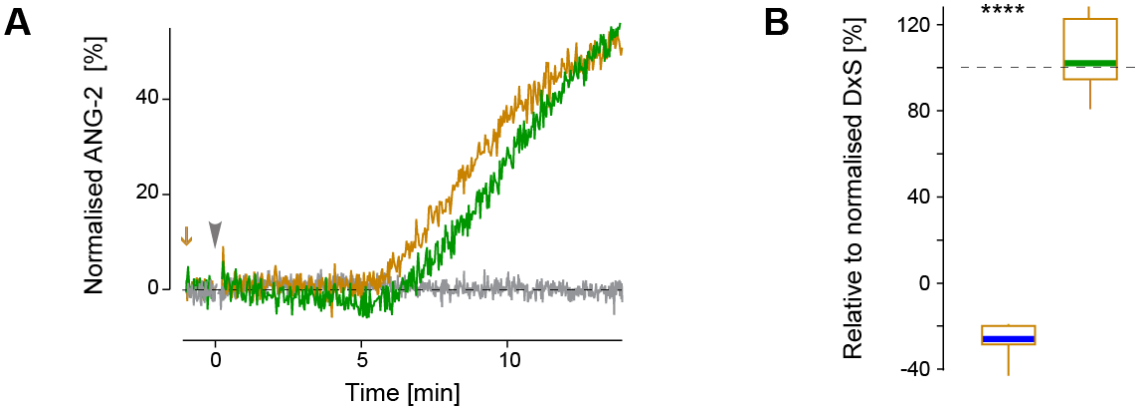

Figure 3.6 DxS $[Na^+]_i$ rise does not depend on $[Ca^{2+}]_o$

(A) DxS $[Na^+]_i$ rise measured with ANG2 when $[Ca^{2+}]_o$ was chelated with 100 μM EGTA (ochre) compared to control DxS $[Na^+]_i$ rise (green). No stimulus control in grey. (B) Box-and-whisker plots of peak amplitudes of DxS $[Ca^{2+}]_i$ (blue) and $[Na^+]_i$ (green) when Ca^{2+} was chelated extracellularly with EGTA (ochre) relative to that of control (100%, dash). Notably, in the presence of EGTA, $[Ca^{2+}]_i$ is below normalised 0. This can be explained by the constitutive Ca^{2+} leak from stores and active transport of Ca^{2+} from the cell.

3.4.3 Na_V channels are not involved in $[Na^+]_i$ rise

In 2012, Lo et al proposed that a $Na_V1.5$ channel facilitated the Ca^{2+} influx in positively selecting DP thymocytes and consequently played an essential role in selection, particularly for CD4 SP development. In their experimental protocol, the authors did not monitor $[Na^+]_i$. However, they did show that addition of 1 μM TTX significantly reduced the $[Ca^{2+}]_i$ rise. Notably, the rise was not completely abolished. This was perhaps because $Na_V1.5$ channels are quite resistant to TTX (IC_{50} ~3 μM, Cribbs *et al.* 1990, Onkal *et al.* 2008).

To investigate Na_V channel involvement, concentrations of 1, 5 and 10 μM TTX were applied either with DxS (t = 0) or, because TTX sterically impedes Na^+

permeation through the open channel pore (Lipkind & Fozzard 1994), it was also added after the onset of the $[Na^+]_i$ rise (*i.e.* when channels have started to open; *t* = 7 min). The results of such experiments are shown in Figure 3.7A. Here the representative Na^+ time course plots are presented for a set of experiments with and without 1 or 5 μM TTX. In both instances, the time courses more or less overlapped. Whisker plots shown in Figure 3.7B indicate there was no statistically significant difference in either the DxS $[Ca^{2+}]_i$ (n = 8, p_t = 0.59) or $[Na^+]_i$ rise (n = 5, p_t = 0.5) when the TTX was added (combined 1 or 5 μM data). Furthermore, the addition of 10 μM TTX, thought to be sufficient to block TTX-resistant Nav1.5 channels (Fraser *et al.* 2004), also did not significantly alter the DxS $[Ca^{2+}]_i$ rise (n = 3, p_t = 0.66). These findings indicate that Nav channel activation was not necessary for the DxS $[Ca^{2+}]_i$ rise and further support an argument for a non-selective cation channel.

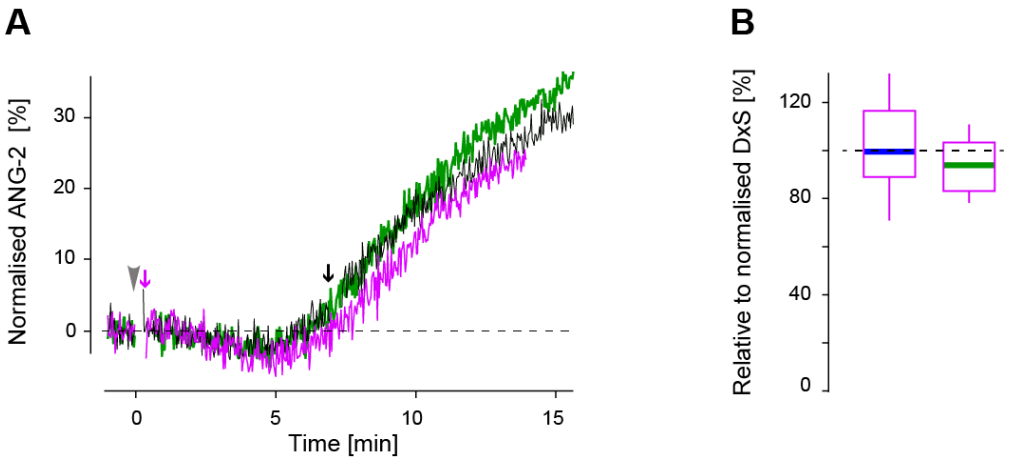

Figure 3.7 DxS $[Na^+]_i$ rise does not depend Nav channels.

(A) Time courses of DxS induced change in ANG2 fluorescence in the presence of 5 μM (pink, added at *t* = 0) or 1 μM TTX to block Nav channels (black, added at *t* = 7 min) against that without (green). (B) Respective box-and-whisker plots of the relative peak amplitudes of $[Ca^{2+}]_i$ (blue) and $[Na^+]_i$ rise (green) in the presence of TTX, with the control peak value indicated by the dash.

3.4.4 Elevated $[Mg^{2+}]_o$ blocks both rises

Interestingly, I found both the DxS Ca^{2+} and Na^+ rises were reduced by $[Mg^{2+}]_o$ in a concentration dependent manner. Shown in Figure 3.8A, compared to control (blue), the addition of 30 mM Mg^{2+} 1 min before DxS abolished the $[Ca^{2+}]_i$ rise (black, $n = 3$, $p_t < 0.0001$), while the addition of 10 mM Mg^{2+} (C, grey) led to a partial reduction. The $[Na^+]_i$ rises were similarly affected, though notably the addition of 30 mM Mg^{2+} (Figure 3.8B, black, $n = 3$, $p_t < 0.001$) caused a small rise in $[Na^+]_i$, perhaps indicative of Mg^{2+}/Na^+ antiporter activity (Gunther & Vormann 1992). This data indicates that there is likely a Mg^{2+}-sensitive channel involved in the cation rise.

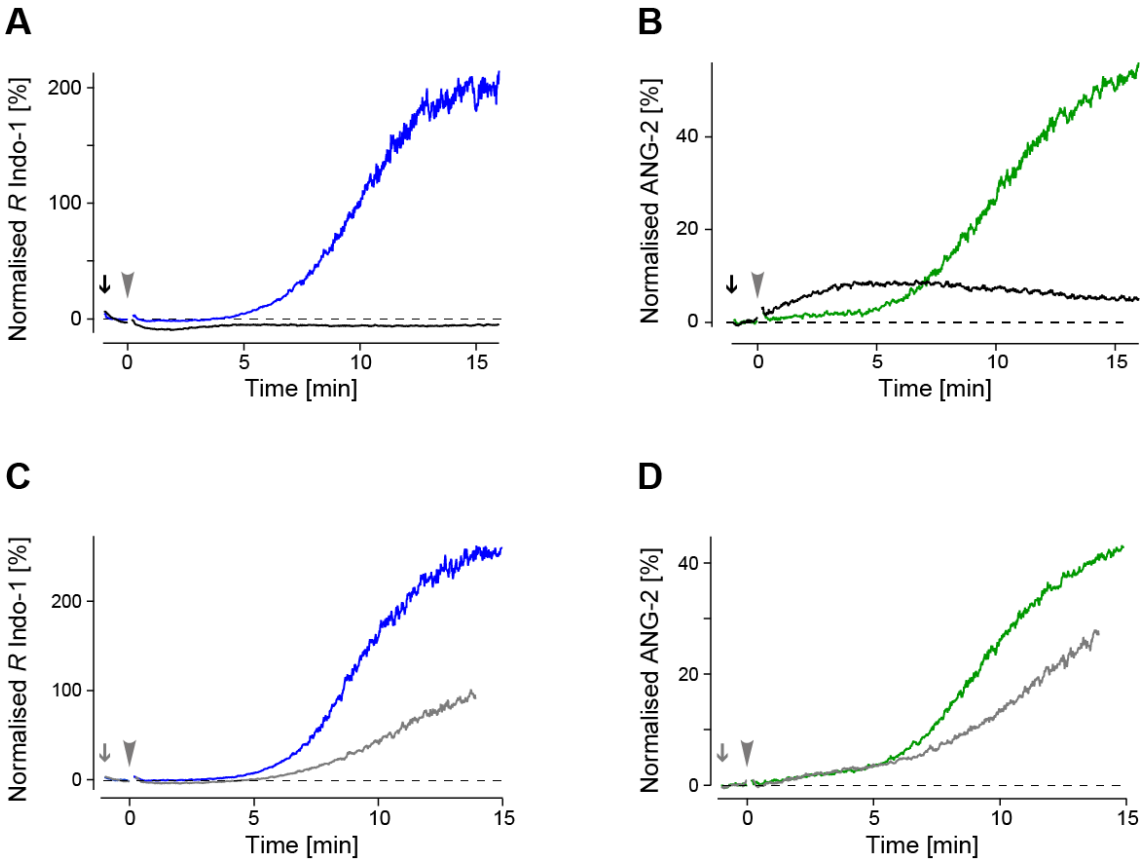

Figure 3.8 Increased $[Mg^{2+}]_o$ reduces the Ca^{2+} and Na^+ influx

(A) Time course of the DxS $[Ca^{2+}]_i$ rise in control (blue) and when 30 mM Mg^{2+} were added at t = -1 min (black arrow/trace). (B) As in (A) but for $[Na^+]_i$ with the control green. (C and D) Same as in (A) and (B) but for 10 mM Mg^{2+} (grey).

3.4.5 Elevated background $[Ca^{2+}]_i$ also abolishes the Na^+ influx

As described in 3.3.3, elevated background $[Ca^{2+}]_i$ prohibited the DxS $[Ca^{2+}]_i$ rise. I therefore checked if such a rise also occluded the $[Na^+]_i$ rise. To elevate background $[Ca^{2+}]_i$, I used ConA. Unlike the relatively fast-onset and transient $[Ca^{2+}]_i$ rise observed by the addition of 30 µg/ml ConA on its own (see Figure 3.2A), using ANG-2 revealed a small gradual $[Na^+]_i$ rise (Figure 3.9A, red). This is likely explained by NCX activity as a consequence of the concomitant Ca^{2+} load. As in Figure 3.2A, ConA was applied during the plateau phase at t = 20 min (Figure 3.9A, red arrowhead), but in contrast to the Ca^{2+} response, there was no small transient increase with $[Na^+]_i$ (green). Even with $[Ca^{2+}]_o$ chelated with 100 µM EGTA, no change was seen either (ochre).

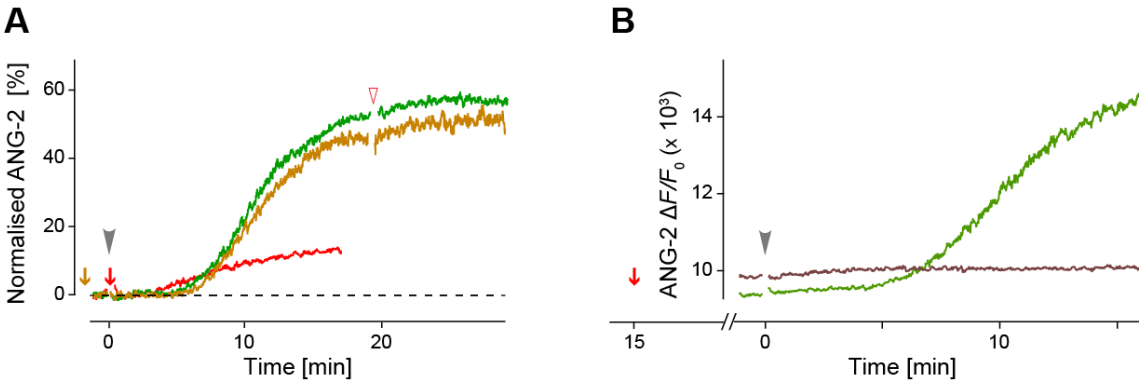

Figure 3.9 DxS $[Na^+]_i$ is abolished by increased background $[Ca^{2+}]_i$

(A) Time courses DxS $[Na^+]_i$ under control (green) and when extracellular Ca^{2+} was chelated with EGTA (ochre). At the time of the red arrowhead, ConA was added. Time course of $[Na^+]_i$, when ConA but no DxS was added at t=0 min (red). (B) Time course of raw $\Delta F/F_0$ when DxS was added at t = 0 min during control and after pre-incubation with ConA for 15 min (brown).

As previously observed when monitoring $[Ca^{2+}]_i$ (Figure 3.2B), I found preincubation with ConA abolished any further DxS induced $[Na^+]_i$ rise (Figure 3.9B, brown). Similarly, in this plot I have not normalised to the control $\Delta F/F_0$ in order to make an elevated background $[Na^+]_i$ visible. The control $[Na^+]_i$ rise is shown in green, and when the sample was pre-incubated for 15 min in ConA

(brown). This time course indicates that after pre-incubation, not only $[Ca^{2+}]_i$ but also background $[Na^+]_i$ was elevated. Notable though is the fact that there is no $[Na^+]_i$ rise following addition of DxS (Figure 3.9B; brown). This was the case in all such experiments (n = 7, p_t <0.0001). This indicates that activation of the non-specific cationic influx is prevented by a prior rise in background $[Ca^{2+}]_i$ and/or $[Na^+]_i$.

The findings so far suggest that the addition of DxS to DP thymocytes activates a non-selective cation influx. In addition, a rise in background $[Ca^{2+}]_i$ by ~60 nM and/or $[Na^+]_i$ prevents its activation. In the presence of a small and sustained elevation in background $[Ca^{2+}]_i$, this apparent inhibition raises the question if the block is due solely to the increased Ca^{2+} and/or Na^+ or if the activation of the influx is negatively modulated by changes in STIM1 or IP_3R, that are associated with $[Ca^{2+}]_{ER}$ release.

The fact that the influx occurs via a non-specific ion channel would support many TRP channels as potential candidates. Since most TRP channels are modulated by intracellular signalling cascades (reviewed by Numata *et al.* 2011), it was necessary to investigate the involvement of cell signalling prior to the Ca^{2+} influx.

3.5 Molecular mechanisms upstream of the cation influx

3.5.1 PLC activation is required

To determine if PLC activity was necessary upstream of the rise activation, edelfosine (1-octadecyl-2-methylglycero-3-phosphorylcholine), an ether lipid analogue, was used to inhibit the activation of all isoforms (Horowitz *et al.* 2005). Since both PLC-γ1 and -β2 isoforms are moderately expressed in these cells, the precise target remains unclear. The cell suspension was pre-incubated with 1 μM edelfosine for 1 min. As shown in Figure 3.10A & B and summarised in C for $[Ca^{2+}]_i$ and $[Na^+]_i$ (blue and green respectively), the addition of edelfosine prior to DxS resulted in a significant inhibition in both the Ca^{2+} (pink; n = 4, p_t <0.0001) and Na^+ influx (n = 4, p_t <0.01). Furthermore, comparison of the two mean inhibitions revealed that there was no difference between them (p_{pt} = 0.4). These data suggest that the activation of PLC is critically involved in generating the DxS Ca^{2+} and Na^+ influx. Notably, 30 μM edelfosine (IC_{50} = 9.6 μM, Powis *et al.* 1992) caused an extreme rise in $[Ca^{2+}]_i$ and loss of the indo-1 signal (Figure 3.10A inset).

3.5.2 Not modulated by $[Ca^{2+}]_{ER}$ depleted STIM1 activation or IP_3R

In thymocytes, depletion of Ca^{2+} in the ER normally occurs when PLC-γ1 generates IP_3 that then activates IP_3Rs. This in turn can lead to STIM1-dependent activation of SOCE channels. The subsequent Ca^{2+} influx then replenishes the $[Ca^{2+}]_{ER}$ via the SERCA pump uptake, altogether homeostatically maintaining $[Ca^{2+}]_{ER}$.

In section 3.4.4, I showed that the DxS activated rise was not due to STIM/Orai or a TRPC3 channel. While STIM1 is generally associated with SOCE, it can also function as a regulatory mechanism in ROCE. For instance, STIM1 regulates translocation of receptor-operated TRPC6 channels to the PM (Albarran *et al.* 2014), and its association with TRPA1 negatively modulates STIM1/Orai

interaction (Albarrán *et al.* 2013). In addition, IP_3R binding on the C terminus of TRPC and TRPV4 channels has been shown to modulate channel activity (Garcia-Elias *et al.* 2008, Zhang *et al.* 2001). Therefore, investigation of a potential role for STIM1 and/or IP_3R activation in regulating a second messenger-activated channel was still warranted.

Previously, I have shown that $[Ca^{2+}]_{ER}$ could be depleted by concurrently blocking both Orai channels and the SERCA pump. This protocol was again used to examine if store release and associated STIM1 activation significantly altered the DxS rise.

Figure 3.10D shows the effect over time of concurrent inhibition of Orai channel by 1 μM YM58483 and the SERCA activity by 20 μM CPA (red). With STIM1-dependent transmembrane Ca^{2+} influx (via Orai channel, activation) and Ca^{2+} sequestration into the ER blocked, $[Ca^{2+}]_i$ initially rapidly rose followed by an exponential decay back to background $[Ca^{2+}]_i$, and after ~10 min was indistinguishable from baseline $[Ca^{2+}]_i$. I note that there was no concomitant $[Na^+]_i$ rise. This observation is consistent with the appreciable constitutive Ca^{2+} leak from ER stores mentioned above (section 3.3.5), which depletes $[Ca^{2+}]_{ER}$ to activate SOCE (Camello *et al.* 2002, Foyouzi-Youssefi *et al.* 2000).

Having depleted $[Ca^{2+}]_{ER}$ and likely induced a conformational change in STIM1, DxS was added in an experiment at $t = 0$ min. As shown in Figure 3.10D, this still resulted in subsequent rises in Ca^{2+} (light blue) and Na^+ (light green), which were not different to the normal DxS rises, respectively ($n = 6$, $p_t = 0.11$; $n = 3$, $p_t > 0.07$). These rises also had a similar delay of ~5 min. This suggests that both DxS rises remained largely unchanged. I note that within ~6 min of depleting stores, $[Ca^{2+}]_i$ had returned to close to the background level, which likely "re-enabled" the subsequent rises. This suggests that most likely increased background $[Ca^{2+}]_i$ is solely responsible for blocking channel activation or the preceding signalling

cascade. These data provide evidence that both rises are not significantly modulated by activation of STIM1 by $[Ca^{2+}]_{ER}$ depletion. However, a role for thermally activated STIM1 (Liu *et al.* 2019, Xiao *et al.* 2011) in regulation of this cation rise cannot be discounted and remains to be determined.

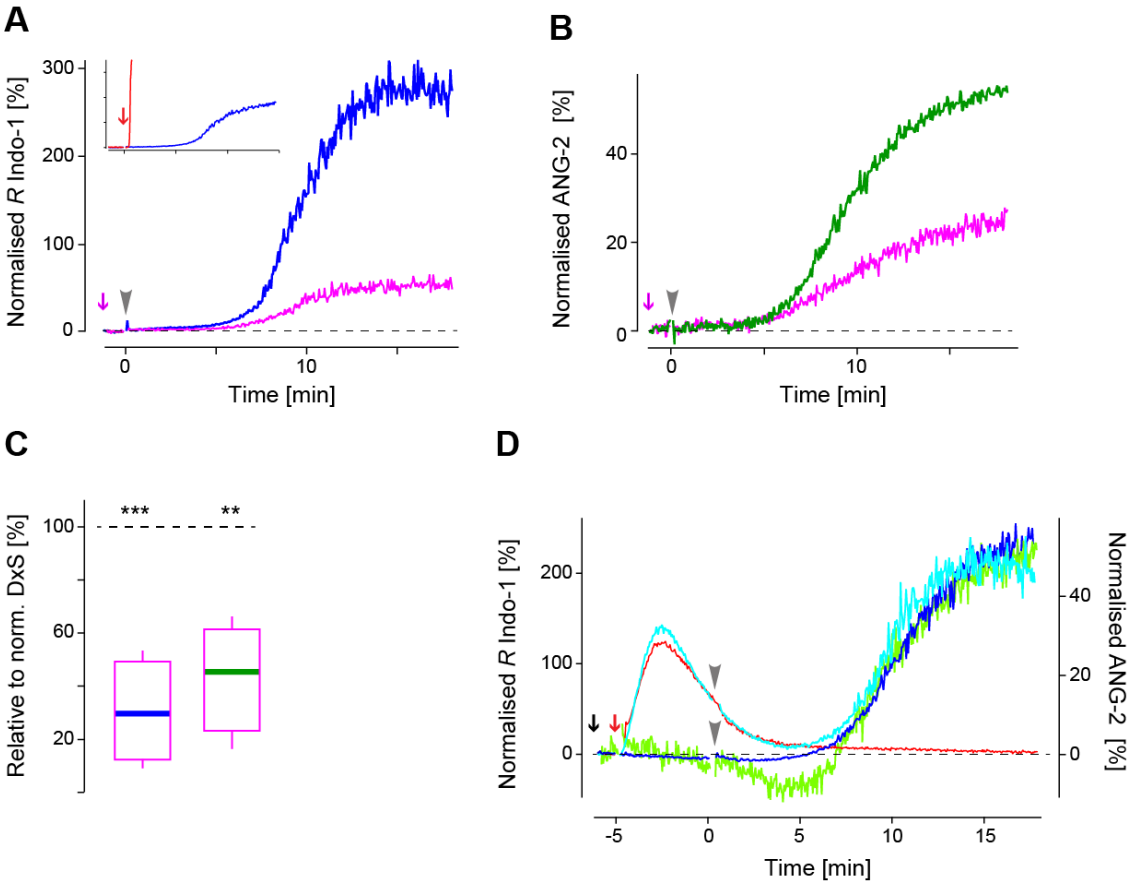

Figure 3.10 Activation of PLC-γ1 is required, but not SOCE

(A) Time course plots of the DxS $[Ca^{2+}]_i$ rise control (blue) and when incubated with edelfosine (pink arrow/trace). Inset: 30 μM edelfosine added at $t = 0$ min caused massive rise and then loss of indo-1 emission detection. (B) As in (A) but monitoring the DxS $[Na^+]_i$ rise; control (green) and pre-treated with edelfosine (pink). (C) Box-and-whisker plot (pink) summarising the effect of added edelfosine on the DxS $[Ca^{2+}]_i$ rise and DxS $[Na^+]_i$ rise. (D) Time course plots of the DxS $[Ca^{2+}]_i$ rise when DxS was added at $t = 0$ min (grey arrowhead). Control DxS $[Ca^{2+}]_i$ rise (blue) and when Orai channels were inhibited (1 μM YM58483, black arrow) and the ER store depleted (CPA 20 μM, red arrow, aqua trace). Appended in this plot is the DxS $[Na^+]_i$ rise when treated with YM58483 + CPA (black & red arrows, respectively) before adding DxS at $t = 0$ min (grey arrowhead; light green). Also shown is a time course (red) of the $[Ca^{2+}]_i$ rise when YM58483 and CPA were added (black & red arrow, respectively).

To demonstrate if IP_3R activation were involved, the IP_3R antagonist xestospongin C (XestC) was used. Initially identified as a selective inhibitor of IP_3Rs with an IC_{50} of 358 nM (Gafni *et al.* 1997), its pharmacology is debated as to its target(s). While it has been argued that XestC inhibits the SERCA pump rather than IP_3R (Castonguay & Robitaille 2002, De Smet *et al.* 1999, Solovyova *et al.* 2002), Ta *et al.* (2006) concluded, based on data acquired by specifically monitoring $[Ca^{2+}]_{ER}$, that XestC inhibited IP_3R activity but did not inhibit the SERCA pump. Notably, inhibition of IP_3R by XestC slowly increases with time due to the slow on-rate (De Smet *et al.* 1999). Therefore, samples were first pre-incubated with 2 μM XestC at 37°C for 10 min. To control for the longer incubation time, the control samples were likewise pre-warmed.

The addition of 2 μM XestC to thymocytes by itself did not produce a $[Ca^{2+}]_i$ rise (Figure 3.11B, black; $n = 4$, $p_t = 0.99$), suggesting that it did not significantly inhibit the SERCA pump. In samples pre-incubated with XestC prior to DxS ($n = 4$), the characteristics of the rises, including the $[Ca^{2+}]_i$ and $[Na^+]_i$ peak amplitudes (shown in Figure 3.11A), were not significantly different compared to the normalised DxS control (Ca^{2+}: $p_t = 0.6$; Na^+: $p_t = 0.3$). This result may indicate that IP_3R activation was not significantly involved in both rises. An alternative and simpler explanation is that XestC failed to inhibit IP_3R.

To rule this possibility out, a large Ca^{2+} rise was evoked by norgestimate. In thymocytes, the addition of 15 μM norgestimate resulted in an immediate Ca^{2+} rise consistent with SOCE (Figure 3.11B, grey). Reportedly, this occurs via activation of a steroid sensitive receptor which in turn activates a Src tyrosine kinase signalling cascade to stimulate PLC-γ1 (Boonyaratanakornkit *et al.* 2001). To provide evidence that this was the case, I used PP2 (1-tert-butyl-3-(4-chlorophenyl)pyrazolo[4,5-e]pyrimidin-4-amine), a pan-Src kinase inhibitor (Hanke *et al.* 1996, Irie *et al.* 1998). Pre-incubation for 10 min at 37°C with 300 nM

PP2 largely abolished the rise seen with norgestimate (Figure 3.11B, pink), lending support to the idea that norgestimate acted via Src kinase to stimulate PLC-γ1. To identify the contribution of Orai channels to the Ca^{2+} influx, the addition of 1 μM YM58483 together with norgestimate inhibited the sustained rise, whilst leaving a transient rise (red). The IP_3R contribution was revealed when a sample exposed to the same blockers was pre-incubated with XestC (ochre). Together, these results suggest that 2 μM XestC was capable of blocking IP_3R, albeit not completely, and consequently rules the simple explanation out.

Furthermore, they support the argument that the DxS rises are dependent upon PLC-γ1 activation but do not require IP_3R activation nor modulation by store Ca^{2+} depletion activation of STIM1.

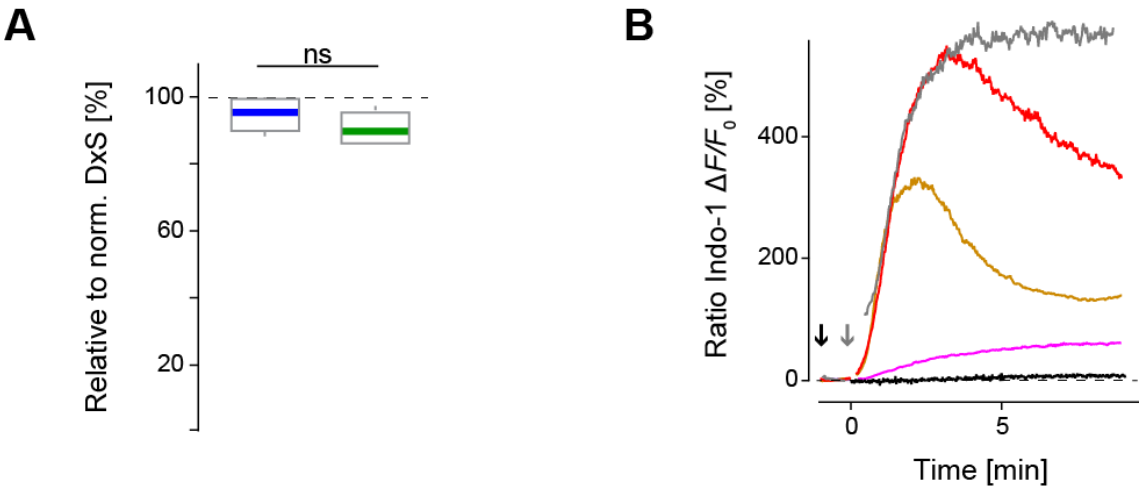

Figure 3.11 Activation of IP_3R not required

(A) Box-and-whisker plots (grey) summarising the effect of XestC on the DxS $[Ca^{2+}]_i$ (blue) and $[Na^+]_i$ (green) rise amplitude. The dashed line at 100%, denotes the normalised DxS peak amplitude. (B) Time course plots comparing the $[Ca^{2+}]_i$ influx from store release with and without SOCE channel activation following the addition of norgestimate (grey arrow/trace) and when also treated with YM58483 (black arrow, red). Time course of $[Ca^{2+}]_i$ following incubation with XestC prior to addition of YM58483 with norgestimate (ochre) and when pre-incubated with PP2 prior to adding norgestimate (grey arrow, pink). Black trace shows the effect of 2 μM XestC added at t = 0 min on $[Ca^{2+}]_i$.

Having looked so far at a few mechanisms upstream of the non-specific cation influx, in the following I would like to turn the focus around to investigate mechanisms downstream of DxS binding to surface molecules. As mentioned previously, DxS potentially interacts with multiple targets on the surface of DP thymocytes. Consequently, more than one signalling pathway may turn on.

3.5.3 **Role for CD8β**

Recent evidence suggests that DxS competitively binds to the CD8 coreceptor, particularly the CD8β chain, at a heparan sulfate binding region. Comparing the response in DP thymocytes obtained from CD8β$^{-/-}$ with that of WT mice, Simon Davis (2015) demonstrated that the interaction of DxS with CD8β was crucial for the initiation of the signalling pathway that resulted in the sustained $[Ca^{2+}]_i$ rise.

I confirmed these findings for Ca^{2+} under the conditions used in this thesis and extended them to include Na^+ imaging. Consistent with his findings, not only the DxS $[Ca^{2+}]_i$ was strongly inhibited, but also the $[Na^+]_i$ rise was much reduced in cells from CD8β$^{-/-}$ mice (Figure 3.12A & B, red). In this data set and similar to the reduction observed for Ca^{2+} (n = 6, p_t <0.0001), the mean Na^+ rise was 23.7 ± 3.2% of that observed in WT litter mates (n = 3, p_t <0.0001). However, it is interesting to note that while the DxS $[Ca^{2+}]_i$ and $[Na^+]_i$ rises were both much reduced, neither was completely abolished (Figure 3.12C, red boxes; n = 6, p_t <0.0001 and n = 4, p_t <0.0001, respectively). This suggests that DxS likely cross-linked (an)other target(s) on the PM, sufficient to partially activate both influxes.

Furthermore, restriction of the rises to the DP population could be explained by the low level of CD8 coreceptor sialylation (Simon Davis 2015). As thymocytes differentiate to become mature CD8 T cells, the stabilisation of TCR–MHC-I interaction by CD8–MHC-I binding is reduced by increased sialylation of the CD8β coreceptor (Moody *et al.* 2003). This sialylation also appears to prohibit

activation of the signalling cascade initiated by DxS binding as reducing CD8β sialylation, by prior treatment of mature T cells with neuraminidase (type II from *V. cholera*), re-established the DxS $[Ca^{2+}]_i$ rise in CD8 but not CD4 T cells (Simon Davis 2015).

I therefore checked if cleavage of sialic acid by pre-incubation with neuraminidase for 1 h not only re-established the $[Ca^{2+}]_i$ rise in mature peripheral CD8 lymphocytes, but if this rise was also accompanied by a $[Na^+]_i$ rise. This is illustrated in Figure 3.12E, where in this case, peripheral T cells when exposed to DxS do not show a $[Na^+]_i$ rise (olive). But when pre-incubated with neuraminidase, DxS was capable of evoking a similar rise in mature CD8 (aqua) but not CD4 T cells (data not shown). These results confirm that CD8β sialylation is a critical repressor of downstream signalling.

As the DxS was not abolished in CD8$\beta^{-/-}$ thymocytes (Figure 3.12A & B), I next checked the involvement of LFA-1. Shown in Figure 1.3A (Kim *et al.* 2009a), activation of this integrin has been shown to evoke a SOCE independent Ca^{2+} influx in conditions of sub-optimal TCR activation.

3.5.4 **Role of LFA-1**

Notably, this cell adhesion molecule reportedly plays a crucial role in the development of CD8 but not CD4 lineage cells (Revilla *et al.* 1997). Therefore, the contribution of LFA-1 to the DxS rises was investigated using thymocytes prepared from mice either deficient in the CD11a chain of LFA-1 or WT littermates.

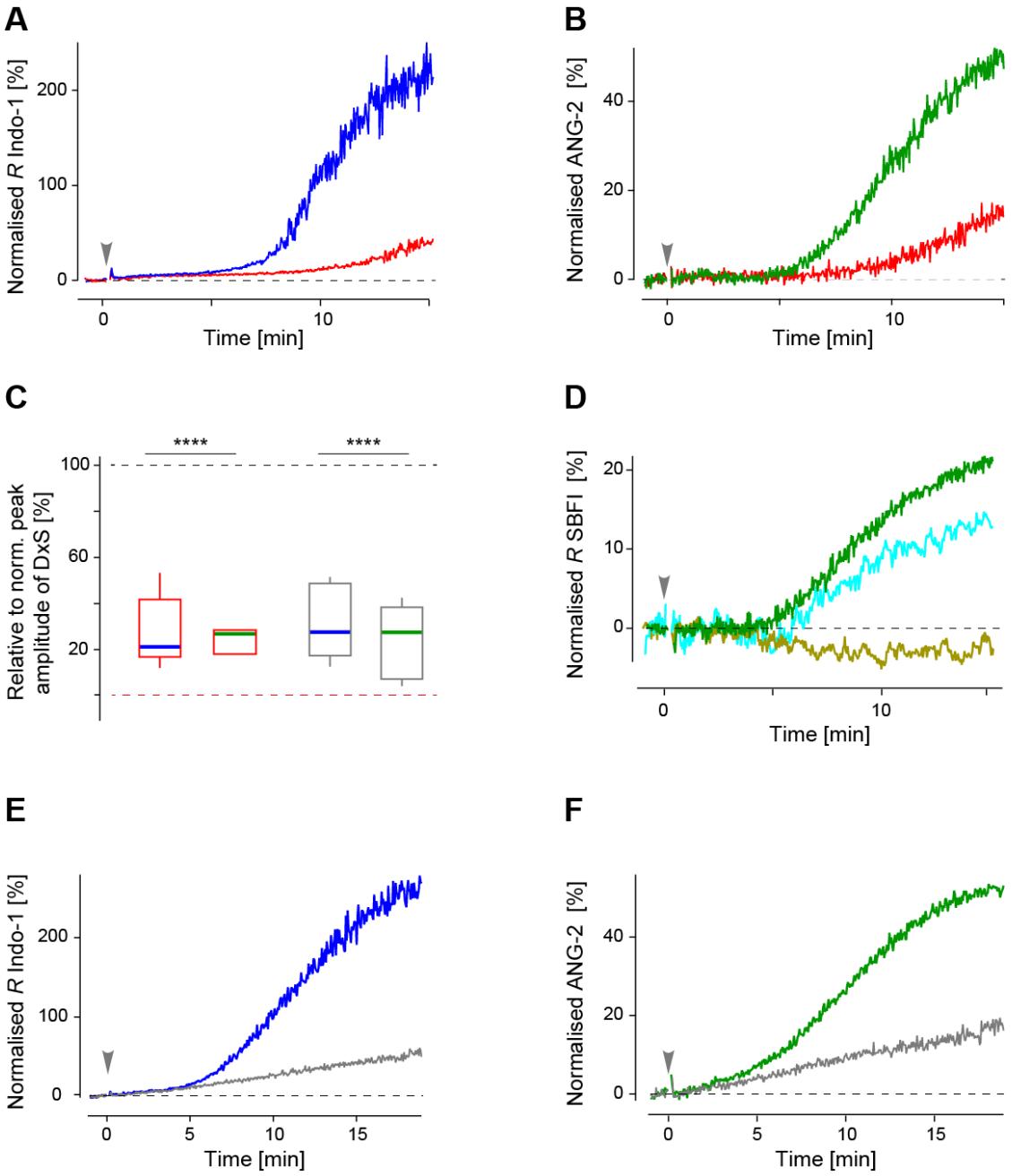

Figure 3.12 CD8 and LFA-1 are required.

(A) DxS $[Ca^{2+}]_i$ rises in cells from a WT (blue) and CD8β$^{-/-}$ mouse (red). (B) Same as in (A) but for $[Na^+]_i$. (C) Box-and-whisker plots for DxS $[Ca^{2+}]_i$ rise (blue) and the DxS $[Na^+]_i$ (green) in CD8β$^{-/-}$ (red) and LFA-1 deficient cells (grey), with the control DxS peak amplitude indicated by the grey dashed line. **** p <0.0001 (D) Time courses of DxS $[Na^+]_i$ rise normalised for the peak amplitude in DP thymocytes (green), mature peripheral CD8 T cells (olive), and mature peripheral CD8 T cells pre-treated with neuraminidase (aqua). (E) Time course of DxS $[Ca^{2+}]_i$ rises in cells from a WT (blue) and LFA-1$^{-/-}$ mouse (grey). (F) Same as in (E) but for $[Na^+]_i$.

The respective time courses depicted in Figure 3.12E & F (grey), show a large reduction of the rises, comparable to the findings for CD8β$^{-/-}$ thymocytes (A & B, red). The peak amplitude of DxS $[Ca^{2+}]_i$ and $[Na^+]_i$ rises from CD11a-deficient mice were reduced by 69.6 ± 6.5 and 76.9 ± 7.2%, respectively (Figure 3.12C, grey boxes; n = 5, p_t <0.0001). Interestingly, this reduction was not different to the one seen with CD8β$^{-/-}$ thymocytes (p_t = 0.7 and 0.53, respectively).

However, there is an interesting difference between the CD8β$^{-/-}$ and LFA-1$^{-/-}$ thymocytes. With LFA-1 deficiency (grey), *i.e.* when CD8 including CD8β signalling remains intact, there is a slow linear rise to the same peak amplitudes for both Ca^{2+} and Na^+. This may indicate that this linear rise is caused by the DxS-CD8β interaction. In contrast, with CD8β deficiency (red), *i.e.* with LFA-1 intact, the rise is supralinear and occurs with a delay, suggesting that LFA-1 may provide a supralinear amplification upon the signalling provided by CD8β.

Both lines of experiment indicate that CD8β and LFA-1 are critical receptor components in the signalling leading up to the two rises. They may suggest that for a full rise, DxS likely interacts with both surface proteins. These observations point to the co-activation of signalling steps downstream of CD8 and LFA-1 binding.

3.5.5 **Involvement of Src kinase**

It is hypothesised that the signal transduction initiated by DxS binding to the CD8β coreceptor results in the activation of Lck, which belongs to the family of Src kinases. It is highly expressed in DP thymocytes (Figure 3.13A) and importantly, in these cells it is associated with the cytosolic C-terminal of the CD4 and to a lesser extent CD8 coreceptors (Wiest *et al.* 1993). This sequestration of Lck to the coreceptors ensures that during the selection process, TCR signal activation remains specific to MHC interactions (Van Laethem *et al.* 2007). However independent of MHC interaction, antibody cross-linking of surface CD8 receptors has been shown to increase tyrosine phosphorylation of Lck (Irie *et al.* 1998, Veillette *et al.* 1989). Furthermore, as stabilisation of the CD8–MHC-I interaction is enhanced by Lck-dependent activation of LFA-1 (Lepesant *et al.* 1990, Morgan *et al.* 2001), I checked if this Src kinase was involved downstream of DxS binding using the pan-Src kinase inhibitor PP2.

To inhibit Src kinase activity, the thymocytes were incubated at 37°C for 15 min with 100 nM PP2 (IC_{50} = 4 & 5 nM for Lck and Fyn, respectively; Hanke *et al.* 1996). To control for the longer incubation, the control sample was equally pre-warmed. Such an experiment is illustrated in Figure 3.13B & C (black). Notably, when Src kinase activity was blocked, both the Ca^{2+} and Na^{+} rises were completely abolished (n = 5, p_t <0.0001 in both cases). This indicates that Src kinase (most likely Lck) activation is critical in the signalling downstream of DxS binding. It suggests that tyrosine phosphorylation is essential step.

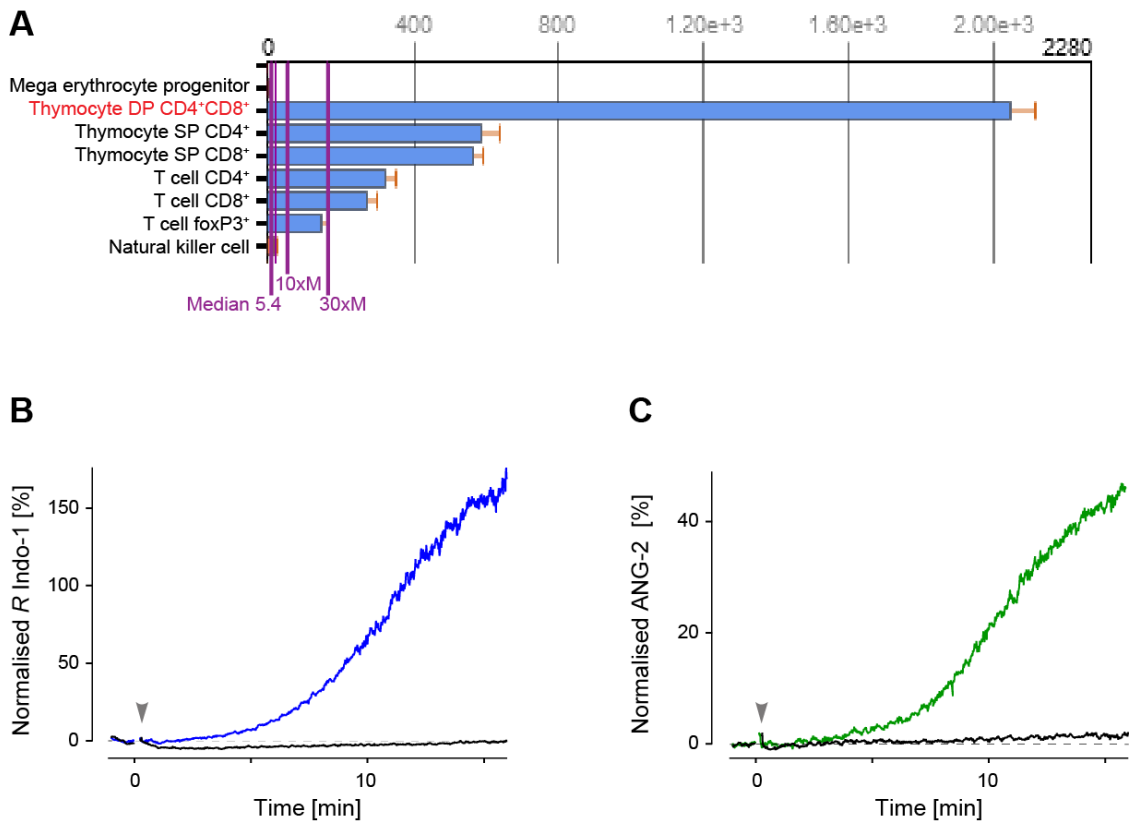

Figure 3.13 Involvement of Src kinase.

(A) *Lck* mRNA expression in T lymphocytes (probe set 1439146_s_at). (B) Time course of DxS $[Ca^{2+}]_i$ rise in control (blue) and after pre-incubation in PP2 (black). (C) Same as in (B), but for $[Na^+]_i$.

3.5.6 Channel activity may be modulated by PKC and PKA

In addition to Src kinases, in thymocytes, PKC and PKA both play important roles in thymocyte selection and apoptosis (Moen *et al.* 2017, Ohoka *et al.* 1996, Zambon *et al.* 2011). These two important effector kinases are activated by DAG (PKCα, -β -δ, -ε, -γ, η and θ isoforms) and cyclic adenosine monophosphate (cAMP), respectively. They target a broad repertoire of proteins, and notably the activity of a number of ion channels and the PMCA pump has been shown to be enhanced by PKC and/or PKA phosphorylation (reviewed by Balasubramanyam & Gardner 1995, Mandadi *et al.* 2011, Venkatachalam *et al.* 2003).

3.5.6.1 **PKC activation likely enhances the signalling cascade**

In DP thymocytes, the Ca^{2+}dependent isoforms PKCα, and PKCβ, and the Ca^{2+} independent isoforms, PKCδ, -η, and -θ, are well-expressed and, have roles in modulating signalling pathways that determine selection, apoptosis and differentiation (reviewed by Morley *et al.* 2008, Ohoka *et al.* 1996, Pfeifhofer-Obermair *et al.* 2012, Simon *et al.* 2000). Therefore, I used the broad-spectrum PKC inhibitor Gö6983 (3-[1-[3-(dimethylamino)propyl]-5-methoxy-1*H*-indol-3-yl]-4-(1*H*-indol-3-yl)-1*H*-pyrrole-2,5-dione) to check if PKC might crucially modulate the DxS $[Ca^{2+}]_i$ rise.

Gö6983 is a potent inhibitor of PKCα, -β, -γ, -δ isoforms with IC_{50} values of 7, 7, 6, 10, and 60, respectively (Gschwendt *et al.* 1996). I found that the addition of 0.1 μM Gö6983 prior to DxS, reduced the peak amplitude of the DxS $[Ca^{2+}]_i$ and $[Na^+]_i$ rises by 35.8 ± 2.8% and 34.8 ± 5.2%, respectively, compared to the normalised DxS rise value, represented by the dashed line in Figure 3.14A (n = 3, p_t = 0.015 and n = 3, p_t = 0.02, respectively). These results indicate likely enhancement of the signalling cascade by PKC phosphorylation of target molecules.

3.5.6.2 **PKA also enhances the cation influx**

I next checked the involvement of PKA in the signalling cascade. In DP thymocytes, the cAMP/PKA pathway is reported to mediate apoptosis (Zambon *et al.* 2011) and in T cells, it has been shown to promote negative regulation of Lck signalling, by way of phosphorylation of C-terminal Src kinase (Csk) which in turn phosphorylates and inhibits Lck (reviewed by Linden & Cekic 2012, Wehbi & Taskén 2016). Having found that activation of Src kinase (most likely Lck) is important in the transduction of the DxS induced signalling cascade, I investigated the role of PKA.

Specifically, I used 500 nM H-89 (*N*-2-[3-(4-bromophenyl)prop-2-enylamino] ethyl isoquinoline-5-sulfonamide) to inhibit PKA activation (IC_{50} = 135 nM; Davies *et al.* 2000). Importantly, as shown in (Figure 3.14B, red boxes), this concentration did not affect resting $[Ca^{2+}]_i$ ($n = 4$, $p_t = 0.24$) or $[Na^+]_i$ ($n = 5$, $p_t = 0.53$). Shown in Figure 3.14B (grey boxes) and C & D (grey traces), preincubating cells for 15 min with H-89 significantly reduced the amplitude of the DxS $[Ca^{2+}]_i$ rise ($n = 4$, $p_t = 0.001$) and $[Na^+]_i$ rise ($n = 4$, $p_t = 0.006$). These data suggest that PKA has a role in promoting the DxS cation influx mechanism.

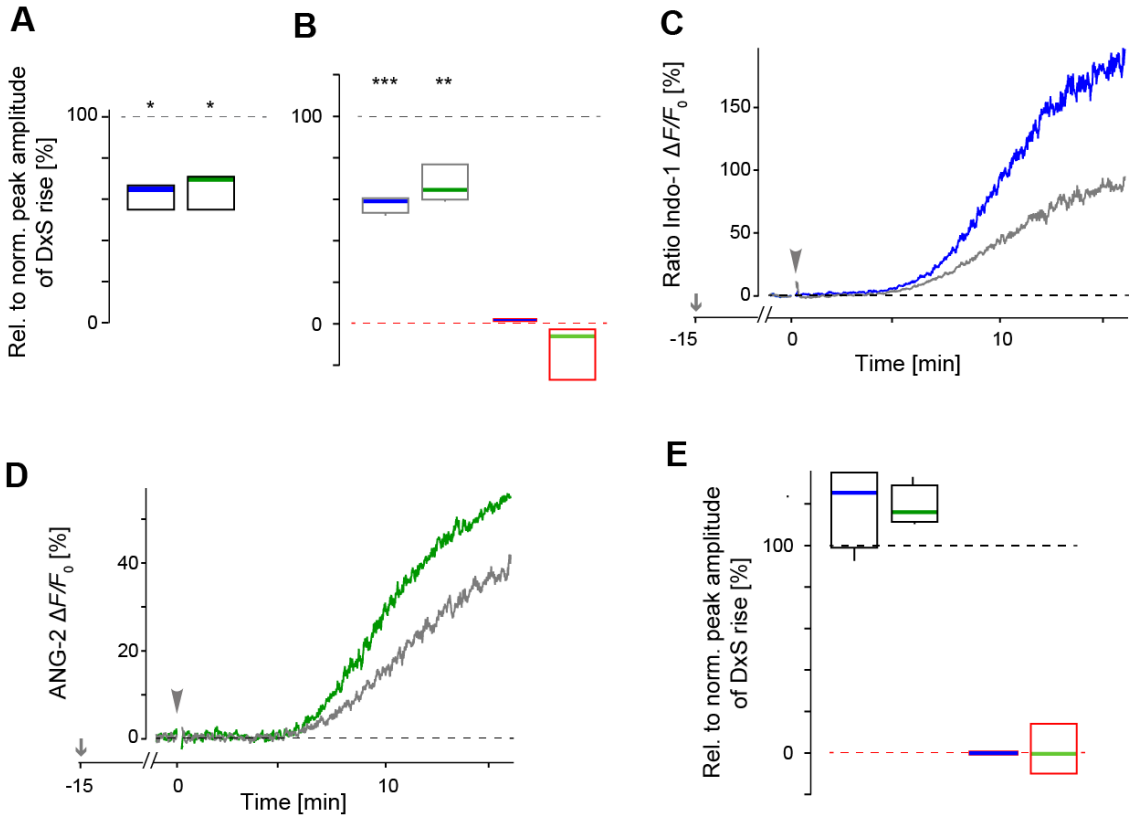

Figure 3.14 PKC and PKA activity likely enhance the Ca^{2+} and Na^+ influx

(A) Box-and-whisker plots of relative peak amplitudes of $[Ca^{2+}]_i$ (blue) and $[Na^+]_i$ (green) in the presence of Gö6983 with the control value indicated by the grey dash, * for $p < 0.05$. (B) As in (A) but in the presence of H-89 (grey boxes), *** for $p < 0.001$ ** for $p < 0.01$. The red boxes show H-89 on its own did not significantly alter resting $[Ca^{2+}]_i$ and $[Na^+]_i$ compared to untreated cells, indicated by the red dash. (C) Time course of DxS $[Ca^{2+}]_i$ rise in control (blue) and after pre-incubation in H-89 (grey). (D) Same as in (C), but for $[Na^+]_i$. (E) Box-and-whisker plots of relative peak amplitudes of $[Ca^{2+}]_i$ (blue) and $[Na^+]_i$ (green) in the presence of caffeine (black boxes) which are not significantly different from the control value indicated by the grey dash. Red boxes show

the addition of caffeine did not significantly change resting $[Ca^{2+}]_i$ and $[Na^+]_i$ compared to untreated cells, indicated by the red dash

To further explore the effect of PKA on the DxS induced cation influx, I used 400 μM caffeine to inhibit phosphodiesterase degradation of cAMP and hence augment the concentration of PKA. Shown in Figure 3.14E (red boxes), 500 μM caffeine did not significantly change resting $[Ca^{2+}]_i$ (n = 3, p_t = 0.12) or $[Na^+]_i$ (n = 3, p_t = 0.94). Also shown in this box-and-whisker plot, the addition of caffeine 5 min prior to DxS (black boxes) caused no significant increase in the peak amplitude of the cation rises (Ca^{2+}: p_t = 0.1; Na^+: p_t = 0.15). Notably, there was moderate variation in the data recorded from four experiments

Finding that PKA and PKC reduced, but did not abolish the DxS rises, I next investigated the role of PI_3K. This kinase has a crucial role in thymocyte transition from the immediate single positive to the preselection DP stage (Xue *et al.* 2008).

3.5.7 The cation influx requires PI_3K activation

Recruited to the TCR by CD3ζ and Lck, $PI_3K\delta$ activation downstream of Lck signalling increases the production of phosphatidylinositol (3,4,5)-tris-phosphate (PIP_3; Okkenhaug & Vanhaesebroeck 2003, Sánchez-Martín *et al.* 2004). In response to the PIP_3 increase, the interleukin-2 tyrosine kinase (Itk) is recruited to the PM where it interacts with the adaptor proteins LAT, SLP-76 and the enzyme PLC-γ1 (Min *et al.* 2009), the latter of which is critical for the cation influx.

To test if PI_3K activation was involved, LY294002 was used to inhibit its activation (IC_{50} = 10 μM; Davies *et al.* 2000). Specifically, the cell suspensions were pre-incubated with 50 μM LY294002 for 15 min at 37°C. Titration experiments found that at this concentration the DxS rises were optimally inhibited whilst having negligible effect on the resting $[Ca^{2+}]_i$ and $[Na^+]_i$. As shown in Figure 3.15A & B, when exposed to DxS and compared to control (blue and green), there was a large

reduction in both cation influxes (black), on average by 72 ± 4% for $[Ca^{2+}]_i$ (n = 6; p_t <0.0001) and 46 ± 4% for $[Na^+]_i$ (n = 8, p_t <0.001). Notably, the effect of inhibiting PI_3K resulted in time courses comparable to those observed in the $CD8\beta^{-/-}$ thymocytes (Figure 3.12A & B). Furthermore, as the reduction of the $[Ca^{2+}]_i$ (n = 5, p_t = 0.9) and $[Na^+]_i$ rise (n = 3, p_t = 0.09) was comparable, it suggests the LY294002 inhibition of PI_3K activation was potent.

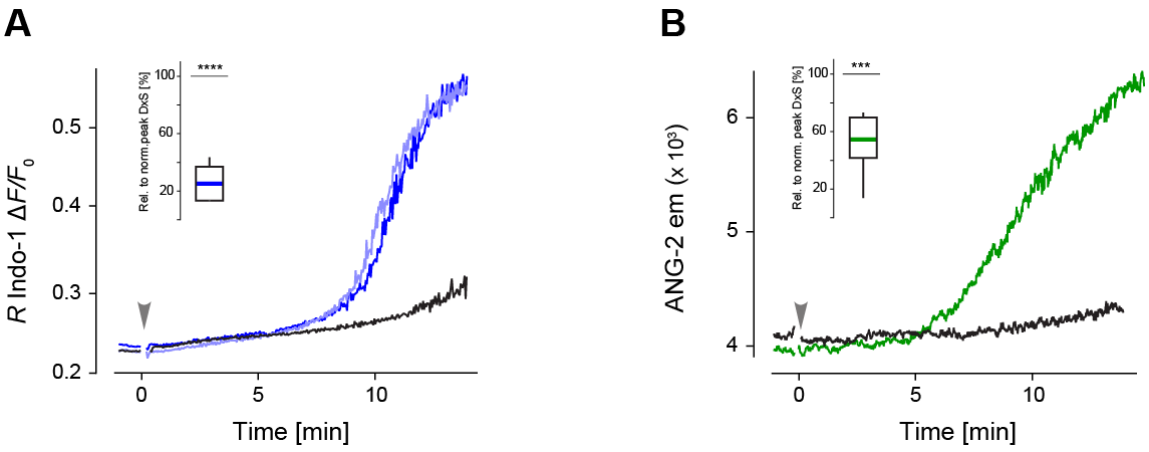

Figure 3.15 Inhibition of PI_3K reduces the cation influx

(A) Time courses for DxS $[Ca^{2+}]_i$ under control conditions (blue), or when prewarmed for 15 min (mauve), and when incubated with LY294002 for 15 min (black) prior to addition of DxS (t =0, grey arrowhead). Inset: Whisker plot showing the effect of 15 min pre-incubation with 1 μM LY294002 on DxS $[Ca^{2+}]_i$ rise amplitude. (B) Same as in (A) but for $[Na^+]_i$, the 15 min prewarmed control (green) and when preincubated with LY294002 (black). Inset: Whisker plot showing the effect of 15 min pre-incubation with 1 μM LY294002 on DxS $[Na^+]_i$ rise amplitude. **** for p <0.0001.

These data suggest a critical role of PI_3K in activation of both rises. As PI_3K catalyses PIP_3 synthesis by PIP_2 phosphorylation, it is either the PIP_3 availability or the local depletion of PIP_2 that activates the influxes. However, since block of PLC-γ1 also lead to a similar block (see above), it is likely that PIP_2 depletion underpins the two rises.

PI_3K activation may lead to increased surface expression of proteins (reviewed by Cayouette & Boulay 2007). Given that it takes ~5 min until the start of the rises,

both membrane insertion and cytoskeletal re-arrangements could be consistent with such a delay. Therefore, the effect of disrupting the actin cytoskeleton on the DxS rises was investigated next.

3.5.8 Cytoskeletal disruption prevents the influx

Inhibition of Lck likely prevents signal transduction via the CD8 coreceptor and indirectly inhibits LFA-1. It appears that LFA-1 activation is dependent upon cytoskeletal rearrangement (Cairo *et al.* 2006, Morgan *et al.* 2001, Perez *et al.* 2003). This involvement with the cytoskeleton downstream of Lck and PI_3K raises the hypothesis that F-actin polymerization also plays an essential role in promoting the DxS rises.

In this set of experiments, F-actin polymerization was inhibited using latrunculin B (LatB). In mouse fibroblasts, incubation for 1 h with LatB (~1 μM) has been shown to disrupt microfilaments (Spector *et al.* 1989). To interfere with actin filaments, thymocytes were incubated with 1 μM LatB for 55 min at RT and then pre-warmed to 37°C for 5 min. The control sample was subjected to the same sequence. Such an experiment is depicted in Figure 3.16A & B. A marked inhibition of the DxS $[Ca^{2+}]_i$ (aqua; $n = 3$, $p_t < 0.001$) and $[Na^+]_i$ rise (light green; $p_t < 0.001$) was observed (Figure 3.16C). The results of these experiments are consistent with the hypothesis that inhibition of F-actin polymerization with LatB 1 μM impedes the rises.

To rule out if LatB pre-incubation alone markedly increased background $[Ca^{2+}]_i$ and $[Na^+]_i$, control samples were pre-warmed for 5 min and recording started. 1 μM LatB was added at $t = 0$ min and data acquisition continued for a further 5 min (Figure 3.16A & B insets). LatB on its own caused a transient $[Na^+]_i$ rise only, which returned to the resting level within 5 min. To check if LatB after 1 hour, changed the background concentrations, the same sample was removed from

recording and left at RT incubation for another 45 min. It was pre-warmed again and acquired on the cytometer for another 5 min (insets). Data was appended to the original recording for comparison of the background $[Ca^{2+}]_i$ and $[Na^+]_i$. After 1h, on its own, LatB may have caused a small decrease in resting $[Ca^{2+}]_i$. However, when compared to a control sample with no LatB added, the change in resting $[Ca^{2+}]_i$ and $[Na^+]_i$ after 60 min was not significantly different (n = 3, p_t >0.05 for both). These results rule out the possibility that a change in resting $[Ca^{2+}]_i$ and $[Na^+]_i$ by LatB caused the disruption of the rises.

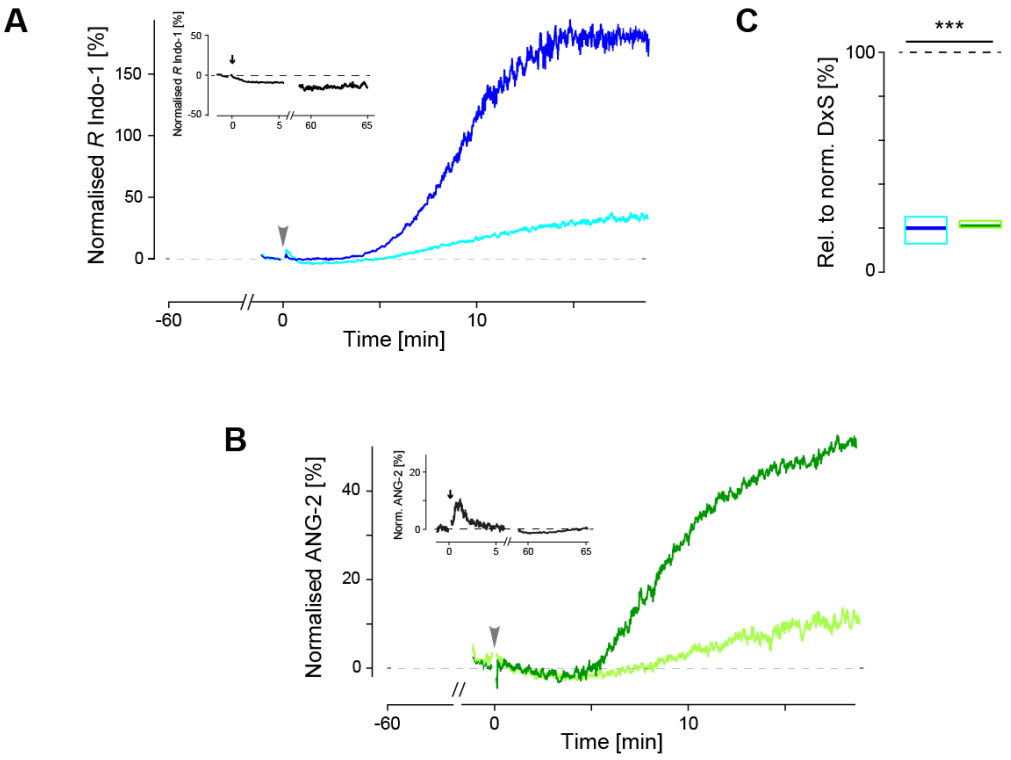

Figure 3.16 Disruption of the cytoskeleton inhibits DxS rises

(A) DxS $[Ca^{2+}]_i$ rise in control conditions (blue) and when the sample was incubated with LatB for 60 min prior to the addition of DxS (t =0 min; aqua). Inset shows $[Ca^{2+}]_i$ when LatB was added (t = 0 min). The effect on $[Ca^{2+}]_i$ after 1 h was also recorded (black). (B) Same as in (A) but for $[Na^+]_i$ (control green; LatB light green). (C) Box-and-whisker plot showing the reduction in peak amplitude when incubated with LatB prior to DxS. The control DxS rise amplitude is indicated by the black dashed line.

This set of experiments demonstrates that blocking F-actin polymerization resulted in a large reduction of both the $[Ca^{2+}]_i$ and $[Na^+]_i$ rises. This suggests that downstream of DxS binding, cell signalling includes F-actin polymerization and cytoskeletal changes.

Since the cytoskeleton can shield mechanosensitive elements in the PM from exposure to shear forces, it may be that the cation influxes occur as a consequence of mechanical stimulation. To test this idea, stretch activated cation (SAC) channels were blocked with the tarantula peptide toxin M-thepaphotoxin-Gr1a (GsMTx4).

Exposure to low micromolar concentrations of GsMTx4 has been shown to specifically inhibit SAC channels (K_c ~600 nM in adult rat astrocytes; Suchyna *et al.* 2000) by impeding the propagation of tensile forces in the local PM region (Gnanasambandam *et al.* 2017, Gottlieb *et al.* 2007, Suchyna *et al.* 2004). Where the lipid tension is altered in the region of SAC channels, it modifies their gating.

3.5.9 DxS rises are fully blocked after preincubation with GsMTx4

To investigate if the addition of DxS leads to altered PM tension, I used 3 μM GsMTx4. It was added to the sample at t = -5 min to check its effect on the background $[Na^+]_i$ or $[Ca^{2+}]_i$ (Figure 3.17A & B; black). Having found it did not increase the resting $[Ca^{2+}]_i$ DxS was added at t = 0 min. Significantly, both rises were fully blocked. This experiment was repeated 4 times and compared to the respective control rises. In all instances, these were completely blocked (p_t <0.001). This finding indicates that the DxS rises are potently sensitive to GsMTx4 and suggests that mechanically transduced force is involved. This may indicate that, a SAC channel is likely involved.

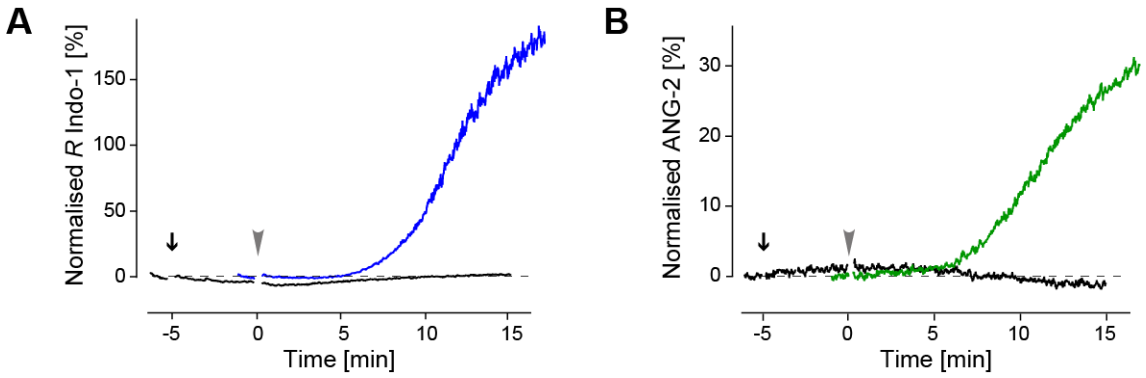

Figure 3.17 Signal transduction is mechanosensitive

(A) Time courses of DxS $[Ca^{2+}]_i$ control (blue) and when pre-incubated with GsTMx4 (black arrow, trace) for 5 min and DxS added at t = 0 min (black). (B) As in (A) but monitoring $[Na^+]_i$.

3.6 Discussion

3.6.1 Summary

In this chapter, I have been able to confirm using indo-1 Ca^{2+} imaging with FACS that there is indeed a Ca^{2+} rise in DP thymocytes after the addition of 1 μg/mL DxS. This rise has most of the hallmarks of that described by Tellam & Parish and was not caused by SOCE via STIM/Orai channel activation. However, using simultaneous Na^+ imaging I discovered that there is also a concomitant large $[Na^+]_i$ rise, which notably, is independent of $[Ca^{2+}]_o$. Furthermore, I found that Mg^{2+} blocked both rises in a concentration-dependent manner such that it was fully blocked with 30 mM $[Mg^{2+}]_o$. I also observed that if background Ca^{2+} in these thymocytes was elevated by about 60 nM, both the Na^+ and Ca^{2+} rises were blocked. Notably, I found the DxS rises were sensitive to lowering the temperature <30°C. These data suggest that the rises may be due to the activation of a non-selective cation-channel.

I also evaluated if blocking signalling elements abolished the rises seen. I have shown that blocking Src kinase abolished the DxS induced rises. Also, I show that blocking PLC and PI_3K activation significantly inhibited both rises. Furthermore, the rises were decidedly diminished in mice deficient in either CD8β or LFA-1. In addition, block of cytoskeletal re-arrangement prevented the rises as did GsMTx4, suggestive of an involvement of a mechanosensitive element. Blocking PKC and PKA reduced both rises indicative of channel modulation by both kinases, consistent with TRP channels being the target.

3.6.2 Simultaneous Ca^{2+} and Na^+ imaging using FACS

Ion imaging with FACS has advantages and at least one drawback. The advantages are that it is simple to implement and provides data from a very large number of cells (at least 10^6 cells over 15 min). Due to the manual handling of the

container, there is a gap in acquisition of about 10–40 s after the addition of DxS. If a rise and decay had occurred during this time, it would have escaped detection. Single-cell imaging might be the technique to circumvent this limitation.

Imaging of $[Ca^{2+}]_i$ in thymocytes has been done since the early days of Ca^{2+} imaging (Davey *et al.* 1998, Hesketh *et al.* 1983, Mahaut-Smith & Mason 1991, Tsien *et al.* 1982). Using ionomycin, I was able to show that the rise observed was well within the linear range of indo-1 and far from dye saturation.

Novel in this chapter is the extension of FACS imaging to include the simultaneous tracking of $[Na^+]_i$. When using ANG-2, there is moderate spill from the free indo-1 emission into the Na^+ fluorescence that required compensation. In contrast to Ca^{2+} imaging and estimating the relevant concentrations, I was only partially successful in precisely quantifying the change in $[Na^+]_i$. The reasons are that thymocytes responded poorly to AmpB. I suspect that exposure to AmpB would have caused a prolonged and considerable depolarisation to close to 0 mV with all its consequences that likely lead to apoptosis. Chelation of $[Ca^{2+}]_o$, using EGTA, may reduce this issue. However, despite this, I am quite confident that the estimate for $[Na^+]_i$ is in the ballpark, as when bracketed against the rise caused by ConA (Segel *et al.* 1979), largely the same value was obtained.

3.6.3 **Characteristics of the rises**

In agreement with Tellam and Parish (1987), I found the $[Ca^{2+}]_i$ rise resulted from influx across the PM as it was abolished when $[Ca^{2+}]_o$ was nominally <50 nM (1 mM EGTA, as estimated by MaxChelator). Under these conditions, the Na^+ influx remained unchanged.

In contrast to the time course in Tellam and Parish (1987), I did not observe a biphasic rise. Specifically, ~1 min following the addition of DxS, a small rise was

detected when monitoring $[Ca^{2+}]_i$ with a spectrometer. However, this rise was not apparent in my data. This discrepancy might be explained by the condition under which the data was acquired.

Firstly, in flow cytometry experiments, the cells are in suspension when imaged. In contrast, during spectrometry, cell adhesion to the glass cuvette is possible and, perhaps as observed in T cells, adhesion to the glass may have primed the cells. Stimulation of adhesion–primed T cells is associated with larger Ca^{2+} rises, thought to be a consequence of increased store filling (Randriamampita *et al.* 2003). Secondly, distinct from flow cytometry which detects fluorescence emission from cells as they rapidly pass by the detector (~800/s), the signal detected during spectrometry recording is acquired from the total cell sample and corresponds to a spatial mean.

I could not detect any difference in time courses between either the Ca^{2+} or Na^+ rise as the values for half-activation were indistinguishable (~11 min). However, this does not exclude the possibility that one of the rises may have preceded the other as the variability in time course may have prevented its detection. In fact, in the next Chapter, I observe that when recorded at 30°C, the rise in Na^+ precedes that of Ca^{2+}.

Both rises also reached a plateau, with the rate of rise marginally faster for that of Na^+ than Ca^{2+}. This difference is likely due to the sensitivity and property of the dye rather than the underlying influx as both time courses when superimposed were indistinguishable (see Figure 3.4A).

3.6.3.1 **Ca^{2+} rise**

There is little disagreement about the background concentration of Ca^{2+} in thymocytes with values between 90–120 nM reported. For my estimation, I used

a value of 110 nM and calculated that the change in $[Ca^{2+}]_i$ was 165 ± 11 nM, consistent with earlier reports (Tellam & Parish 1987, Weston *et al.* 1991).

3.6.3.2 **Na^+ rise**

I found that $[Na^+]_i$ rose by ~20 mM as determined by the fluorescence change from ANG-2. This value was bracketed against the known rise caused by ConA (Segel *et al.* 1979). I note that in contrast to Ca^{2+}, Na^+ is not buffered intracellularly, but some of it can be sequestered into endosomal compartments (Nass *et al.* 1997, Xiang *et al.* 2007). I am unable to estimate how much Na^+ enters the cell but given this large $[Na^+]_i$ change, a considerable depolarisation must be associated with it. Resulting from the depolarisation and the concomitant $[Ca^{2+}]_i$ rise, activation of known $K_V1.3$ and $K_{Ca}3.1$ would provide the "counter currents" to the Na^+ influx. These counter currents act to hyperpolarise membrane, with the aim of restoring the resting V_m. This likely explains why these cells, despite being electrically "silent", express such K^+ channels at a considerable density (Lewis & Cahalan 1988, Mahaut-Smith & Mason 1991). It is expected that some of the counter currents may also stem from homeostatically active transporters like the NCX (see next), Na/H exchanger and Na/K-ATPase. The observation of a large conductance change is consistent with my observation made during my Honours project (Feakes 2012) that when cells were patched and exposed to DxS, there was a large inward current after ~5 min which ultimately exceeded the range of the voltage-clamp amplifier.

These considerations imply that the permeation of Na^+ is very likely much larger than that of Ca^{2+} by several orders of magnitude. It requires the consideration of a channel not only with large partial permeability for Na^+ but also of large conductance.

3.6.3.3 **Involvement of NCX**

I found that the amplitude of the Ca^{2+} rise was partially dependent upon the Na^+ entry from NCX transport in reverse mode, as it was reduced by ~40% when $[Na^+]_o$ was replaced with NMDG and when NCX was inhibited by 3 μM SN-6 or 0.5 μM YM244769. The incomplete block may have at least two explanations. Firstly, the rises are likely the result of permeation via a non-specific cation channel which may even be co-localised with NCX as reported for TRPC6 (Syyong *et al.* 2007). It is worth pointing out that the block of NCX did not affect the $[Na^+]_i$, consistent with the statement above that Na^+ imaging tracks much higher concentrations than those associated with Ca^{2+} as a consequence of NCX activity. Secondly, since I did not concomitantly block NCKX, the possibility exists that the remainder was due to exchange via NCKX. While I think that this is unlikely, I note that relatively high expression of *NCKX4* mRNA was detected in rat thymic tissue (Li *et al.* 2002b).

3.6.3.4 **Plateau phase**

A plateau of $[Ca^{2+}]_i$ and $[Na^+]_i$ elevation is reached if the driving force for the current approaches the reversal potential or if the influx of Na^+ is matched by an outflow of ions (counter currents). Since the reversal potential for non-specific cation channels is around 0 mV, it is possible that V_m may depolarise close to this value. Whilst I cannot exclude this consideration due to the inability to keep these cells in voltage-clamp, I think that the second possibility is more likely due to the fact that upon a large and slow depolarisation, homeostatic mechanisms would kick in quickly. Consequently, the plateau of Na^+ is likely the "driver" for that of Ca^{2+}. The small influx of Ca^{2+} is then the result of limited expression of NCX/NCKX in the PM.

3.6.4 **Lack of store involvement**

The experiment in which the extracellular Ca^{2+} was lowered with EGTA does not rule out the possibility that a small transmembrane Ca^{2+} influx is amplified by intracellular release akin to what is observed for cardiac myocytes (Franzini-Armstrong *et al.* 1998). Two lines of evidence rule this possibility out. Firstly, my results confirm the observation made by Tellam and Parish (1987), in that intracellular release caused by ConA when added during the plateau phase remained additive and had a fast onset (Figure 3.2A). Furthermore, store depletion using SERCA inhibition in cells with a considerable ER leak together with Orai block, did not significantly reduce the DxS-induced cation influx either (Figure 3.10D). It is therefore highly unlikely that elements of SOCE are involved. Secondly, I used norgestimate to activate a large intracellular Ca^{2+} release and was able to dissect the contribution of IP_3R to the rise using XestC. The IP_3R-mediated component had an intermediate onset, much faster than the DxS rise. Even with IP_3R largely blocked, the rises remained ruling out the possibility of IP_3R-modulation of channels like TRPC6 (Patterson *et al.* 2004). Likewise, the idea that IP_3R in the PM could underpin the rises is very unlikely (Khan *et al.* 1992a, Khan *et al.* 1992b).

These results also show that thymocytes contain the elements for SOCE and ROCE, but neither of them seems to be employed for the DxS rises.

3.6.5 **Mg^{2+} sensitivity**

I found that the cation rise was blocked Mg^{2+} in a concentration dependent way at >10 mM, with a full block around 25 mM. The target(s) of this block remain unclear but could involve a TRP channel and perhaps elements in the signalling cascade.

In the first case, the mechanism of block at a high divalent concentration may likely be unspecific and not physiologically relevant (Hille 2001). Channel activation may shift to more depolarised potentials (Kostyuk *et al.* 1982) caused by gating modification by the surface charge effect (Frankenhaeuser & Hodgkin 1957) or actual binding or competitive unbinding in the channel pore (Armstrong & Bezanilla 1973, Obukhov & Nowycky 2005). The latter mechanism is likely in the inhibition of TRPV3 by $[Mg^{2+}]_o$. Specifically, Luo *et al.* (2012) show that inhibition of TRPV3 in the presence of 10 mM $[Mg^{2+}]_o$ was dependent upon Mg^{2+} interaction with an aspartic acid residue in the outer pore region.

Alternatively, at high concentrations, Mg^{2+} may cross the membrane via TRPM6 or TRPM7 and cause a block from the inside as described for TRPV3, -C5, -M1, -M3, -M6 and -M7 channels (reviewed by Bouron *et al.* 2015, Luo *et al.* 2012, Obukhov & Nowycky 2005, Rampino & Nawy 2011). In this second case, Mg^{2+} would have to pass across the membrane for example as indicated above and affect the signalling cascade as a cofactor. ATP binding to kinases and some serine/threonine phosphatases (PP2C) are known to be Mg^{2+}-dependent (Kanellopoulou *et al.* 2019, Wera & Hemmings 1995). Given that increased $[Mg^{2+}]_i$ generally leads to improved enzymatic activity, elements of the signalling cascade may be modulated.

3.6.6 Elevated background $[Ca^{2+}]_i$ associated with block

I have been able to show that if background $[Ca^{2+}]_i$ was elevated by ~60 nM (see Figure 3.2B—D), the addition of DxS did not cause any further rise. Several drugs used during this project (*eg*. ConA, Pyr3, FFA, CPZ and NS8593) "blocked" the rises, due to this mechanism. In some cases, it was possible to lower the respective concentration to still allow for either partial or full rises (shown in Figure 4.10A & B and later in Figure 4.14A).

The mechanism behind this block remains unclear. Potential explanations could include, negative regulation of the protein tyrosine phosphatase CD45 (a crucial regulator of Lck activation; Ostergaard & Trowbridge 1991, Wang *et al.* 2000) or activation of the serine/threonine phosphatase calcineurin (phosphatase 2A; Zheng *et al.* 2019). In this instance, the modulated phosphatase activity would "counter" the kinase activity required for the signalling pathway(s) discussed below. The fact that with store emptying (Figure 3.10E), "blocking" concentrations of intracellular Ca^{2+} were apparent at the time of DxS addition, yet the rises could still be evoked, may point to spatial and temporal Ca^{2+} modulated signalling requirements downstream of Lck activation, perhaps even Ca^{2+}–CAM modulation of channel gating. Notably, most TRP channels are modulated by $[Ca^{2+}]$.

In addition to the $[Ca^{2+}]_i$ elevation, other limiting factors could be involved. A common proximal signalling step might not only lead to the Ca^{2+} rise by 60 nM but may also cause a concurrent change in lipid composition (such as PIP_2 depletion) blocking channel gating (Borbiro *et al.* 2015, Tsuchiya *et al.* 2018).

3.6.7 **Temperature sensitivity**

Unexpectedly, I found that lowering the temperature to <30°C abolished both rises (see Figure 3.2F and Figure 3.4D). The abolition of both rises may be caused by an elevation in background $[Ca^{2+}]_i$ dependent upon the thermally sensitive STIM1 molecule (Xiao *et al.* 2011). This perhaps involves temperature dependent conformational change of the STIM1, its clustering in ER-PM junctions and consequent activation of Orai1 channels independent of store Ca^{2+} release (Nwokonko *et al.* 2019, Xiao *et al.* 2011). Notably in preselection DP thymocytes, the expression of Orai1 is low, however a 3-fold increase in its expression has been reported in DP that have commenced positive selection (Appendix 6.6). In Jurkat cells, heat (41°C) induced STIM1 activation was shown by Xiao *et al.* (2011)

to enable progressive gating of Orai1 channels notably as the applied heat was reduced back to 25°C. The onset of the Ca^{2+} influx occurred at ~ 37°C. This store independent STIM1/Orai1 activation mechanism and subsequent sustained Ca^{2+} entry may also provide a mechanism for negative regulation of the non-selective cation entry channel. Such an increase in background Ca^{2+} might explain the loss of the DxS induced cation influx when the temperature is <30°C.

Furthermore, it is possible that during the fluorescent dye loading procedure, the incubation at 37°C for 1 h may have been sufficient to thermally activate a conformational change of STIM1 and puncta formation at the PM that is independent of store Ca^{2+} depletion. Subsequent lowering of the temperature could perhaps then result in Orai1 channel activation and a sustained rise in basal $[Ca^{2+}]_i$ in mature thymocytes. However, based on the findings presented by (Xiao *et al.* 2011) it is hypothesised that this Ca^{2+} rise would decay over time when thymocytes are maintained at RT as depicted in Figure 3.2F (inset).

It is noted that in thymocytes kept on ice, background $[Ca^{2+}]_i$ is indeed elevated; reminiscent of a similar temperature-sensitivity found in platelets (Oliver *et al.* 1999). This rise cannot be explained by a change in indo-1 fluorescence intensity. The fluorescence intensity of many fluorescent probes increases at lower temperatures. However, as the bound and free states of indo-1 respond differently, the *R* indo-1 (F_b/F_f) reportedly reduces as the temperature is decreased (Oliver *et al.* 2000).

While the mechanism of thermal sensitivity of the DxS induced cation influx may indicate that there is a critical step in the signalling leading up to gating that is highly temperature-sensitive it may also point to a temperature-sensitive non-specific cation channel like TRPV1–4, TRPM3 or TRPA1 (see next chapter).

3.6.8 Mechanosensitivity

I have been able to fully block both rises using 3 μM GsMTx4. As this tarantula toxin is inserted into the lipid bilayers and alters lipid packing, it is postulated that it may prevent a mechanosensitive element from being exposed to membrane tension stress (Gnanasambandam *et al.* 2017, reviewed by Gottlieb *et al.* 2007, Suchyna *et al.* 2004). This block suggests an involvement of a mechanosensitive element, the molecular nature of which remains unclear. However, candidates include Piezo1 and several TRP channels (TRPV1, TRPV2, TRPV4, TRPC1, TRPC6 TRPM2 TRPM4 and TRPM7). The activation and inactivation properties of Piezo1 described earlier (1.7.2, p. 82) would suggest that this channel, if involved, is upstream of activation of a second non-selective cation channel.

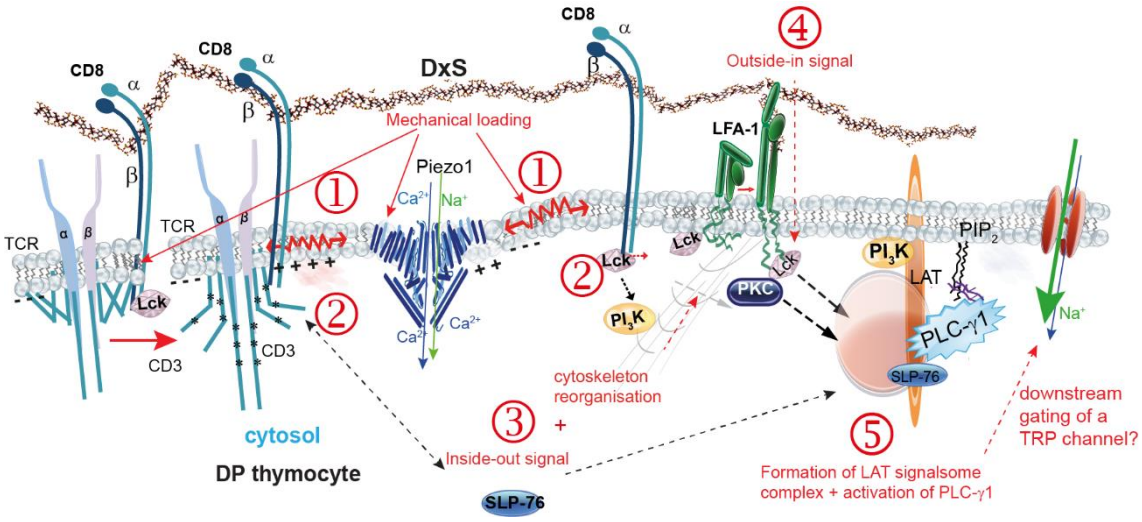

Figure 3.18 Proposed mechanosensitive involvement

Without TCR engagement DxS binding to HS binding sites on CD8β results in both (1) transmission of mechanical load directly to the CD3 tails and to the local PM which promotes both gating of local Piezo1 channels and (2) both activation of Lck. A transient local Ca^{2+} influx within the region of the CD3 membrane bound tails enhances CD3 conformational change exposing Lck phosphorylation sites. (3) activation of an inside out signal and cytoskeleton reorganisation leads to LFA-1 conformational change (4) Synergistic outside in signalling enable formation of the LAT signalosome and PLC-γ1 activation.

Whether this toxin has alternate inhibitory targets such as mechanosensitive G-proteins, such as the highly expressed angiotensin II type 1 receptor (Storch *et al.* 2012), is unknown. How the addition of GsMTx4 might alter activation of mechanosensitive transduction proteins, apart from ion channels, in thymocytes remains to be elucidated.

3.6.9 **Signalling steps upstream of the rises**

Results presented in this chapter indicate that the DxS $[Ca^{2+}]_i$ rise occurs downstream of signalling pathways likely triggered by DxS cross-linking of CD8β and LFA-1 as both rises were significantly reduced in thymocytes from both CD8β$^{-/-}$ and LFA-1$^{-/-}$ mice. This step is likely the most proximal in the steps required to gate the channel. In addition, in peripheral CD8$^+$ lymphocytes that normally do not respond to DxS, when sialylation was cleaved, using neuraminidase, the rises were re-established (Figure 3.12D). This indicates that this post-translational modification is a critical molecular regulator and it impedes the signalling cascade leading to the activation of the non-specific cation channel(s).

Since DxS does not stimulate the TCR directly but elements of the coreceptor complex, the signalling that leads to the rises, may likely involve synergistic amplification of concurrent signalling pathways. This idea is consistent with the observation that in thymocytes from these KO animals, both rises were significantly diminished (Figure 3.12A-B & E-F).

An additional pathway that might augment local signalling is likely dependent upon Lck tyrosine phosphorylation (Src kinase) as it was potently blocked by 0.1 μM PP2, a pan Src-family kinase blocker that potently blocks Lck and Fyn (Hanke *et al.* 1996).

The finding that both fluxes were blocked in conditions where resting Ca^{2+} was stably elevated by ~60 nM, prior to the addition of DxS, may suggest altered phosphatase and/or kinase activity. Signal transduction can be modulated by PKC or PKA phosphorylation of effector molecules. In addition, PKC and PKA phosphorylation of some ion channels, including some TRP channels, can enhance their open probability. Using Gö9683 or H-89 to broadly inhibit PKC or PKA, respectively, I found the DxS rises were only reduced by ~35%. This finding suggests PKC and PKA activation likely modulates the signalling mechanism, in contrast to the critical role of Src kinase(s) in enabling it.

The rise was largely blocked when PLC, most likely the γ1 isoform, was blocked with 1 μM edelfosine. At this concentration, this drug is not toxic to thymocytes and does not stimulate a mitogenic response (Cardile *et al.* 1997). In addition, it is below the concentration used to inhibit PI_3K in mouse fibroblasts (IC_{50} = 35 μM; Berggren *et al.* 1993). Furthermore, unlike U73122, a structurally different PLC inhibitor, edelfosine does not have the side effect of partial PLC activation if left in the suspension (Thyagarajan *et al.* 2009). However, given that in mouse fibroblasts, the reported the IC_{50} of edelfosine for PLC inhibition was 9.6 μM (Powis *et al.* 1992), the much smaller concentration used here may have resulted in an incomplete block with small rises remaining. However, concentrations >1.5 μM have been shown to decrease thymocyte viability (Cardile *et al.* 1997) and massively increased $[Ca^{2+}]_i$ in thymocytes (Figure 3.10A inset, red). This finding therefore is consistent with a view that PLC-γ is downstream of CD8β, LFA-1, Lck and PI_3K, the knock-out or block of which also fully abolishes the cation rise.

Since PIP_2 hydrolysis by PLC-γ1 results in the production of DAG, channel activation may be caused by either PIP_2 depletion or DAG increase. Examples of such channels for the former are TRPM1, -V3 and -V4 and for the latter some members of the TRPC subgroup, TRPA1 and -V2. However, I have been able to

rule out that the other signalling molecule, namely IP_3, is not involved in the cation rise since the block of IP_3R by XestC did not show any effect even when accounting for its slow on-rate.

3.6.10 Candidate channels activated downstream of DxS

Altogether, the results from this chapter, do not point to a specific channel underlying the DxS rises. Rather, many of the characteristics, such as enhanced channel activity following Src kinase phosphorylation and/or PIP_2 depletion, mechanosensitivity and coupling to NCX activity can be found spread across a number of non-selective channels from the TRPC, TRPV and TRPM subgroups and Piezo1. To help narrow the scope of the next step, a list of potential candidates was compiled and is presented below in Table 3.2. Included are channels which have properties that are modulated by mechanisms that affect the cation influx. TRP channels listed on the left side contain more of the positive (green shading) characteristics required for the DxS induced cation rise and so were considered as the primary candidates for investigation. TRP channels listed toward the right of the table have fewer positive characteristics, however they cannot be discounted at this point. Other members of these subfamilies that do not share at least four of the properties listed were omitted from Table 3.2. It needs to be pointed out that some of these properties were obtained in heterologous expression systems and therefore should be considered with caution.

Table 3.2 Candidate channels

Characteristics	TRPV1	TRPV3	TRPV4	TRPC6	TRPA1	TRPV2	TRPM1	TRPC2	TRPM2	TRPM6	TRPM3	TRPM7	TRPC7	TRPC1	Piezo1
mRNA >3x median (BioGPS)		◊	◊			●		●		◊		●			◊
Src kinase modulation	↑	↑	↑	↑					↑	↑					
STIM1 interaction				#	●			●						#	
IP_3R interaction			●	●				●					●	●	
Coupled to NCX	●		●	●	●	●									
PLC-γ1 dependent		●	●	●			●	●					●	●	
PIP_2 binding	#	∨	#	∧	#	∧	∨			∧	∧	#	∧		∧
Activated by DAG	●			●	●		□	●					●		
Activated by AA		●	□	●	●										
PKC modulation	↑	↑	↑	↓			↑		↑					↑	
PKA modulation	↑	↑	↑		↑		↑								
PI_3K modulation	●	●				●				●	●				
Mechanosensitivity	●		●	●	#	●					●	●		●	●
Thermal sensitivity	●	●	●		#	●			●		●				
Ca^{2+} sensitivity	↓	↓	↓		↑				↓				↑		↓
Mg^{2+} sensitivity		↓			↓		↓			↓		↓			
	[1–9]	[10–12]	[13–21]	[22–30]	[31–39]	[40–44]	[45]	[46–48]	[49–54]	[55–57]	[58–60]	[61–64]	[29,65,66]	[67–71]	[72,73]

● Positive evidence. ◊ Spike in DP population (ImmGen database). **#** Contrary evidence: dependent on cell type and expression system. □ Indirect activation. ∧ Rise enables activation. ∨ Depletion enables activation. ↑ Potentiation and ↓ inhibition. References can be found at the end the reference section.

I have considered the exquisitely mechanosensitive Piezo1 in this selection of channels for the following reason. Recently reported evidence shows that a discrete transient Ca^{2+} influx enabled by Piezo1 activation facilitates the TCR/CD3 signal transduction in mature T lymphocytes (Liu *et al.* 2018). While DxS is not thought to stimulate the αβTCR, its binding to the CD8β coreceptor is perhaps sufficient to initiate a mechano-sensitive (*i.e.* Piezo1) and biochemical (*i.e.* Lck activation) signal transduction. However, the rapid, transient activation and sustained inactivation properties of Piezo1 do not match with the delayed onset of the Ca^{2+} and Na^{+} rises. For this reason, Piezo1 would likely require activation of a second channel to account for the plateau phase of both rises.

In the following chapter, I will present results that focus on the non-specific cation channels listed in Table 3.2, with the aim of identifying if any of these channels could underpin the DxS rises. Notably, as shown in Table 3.2, TRPV1, TRPC6, TRPA1, TRPC2 and TRPC7 can be directly activated by DAG. Having this characteristic will provide the starting point for channel investigation.

4 Evaluation of candidate channels

4.1 Introduction

Identification of ion channels and transporters that have functional roles in enabling discrete and global changes in $[Ca^{2+}]_i$ during DP thymocyte selection and differentiation is far from complete. While it appears SOCE channels are activated in response to highly avid TCR–pMHC engagement during thymocyte–stromal cell interaction, this mechanism of Ca^{2+} entry is not required for signalling leading to positive selection. Furthermore, channels that might enable synergistic Ca^{2+} entry and so modify signal transduction where TCR–pMHC engagement is suboptimal, while predicted, are yet to be identified.

In peripheral T lymphocytes, Ca^{2+} entry via TRP channels (*e.g.* TRPC3 and TRPV1) and Piezo1 have been shown to synergistically enhance TCR signal transduction (Bertin *et al.* 2014, Liu *et al.* 2018, Philipp *et al.* 2003, Wenning *et al.* 2011), while TRPA1 linked inhibition of TRPV1 activity reduces TCR induced Ca^{2+} entry in CD4 T-cells (Bertin *et al.* 2017). Hypothesised to mimic an endogenous heparin sulfate evoked signalling cascade, the addition of DxS results in a sustained $[Ca^{2+}]_i$ increase of ~170 nM and a concomitant $[Na^+]_i$ increase of ~20 mM. This Ca^{2+} and Na^+ entry occurs in preselection DP thymocytes, and while dependent upon CD8β and LFA-1 co-stimulation, it is independent of αβTCR stimulation by pMHC-I engagement (Simon Davis 2015). Notably the cation influx appears to be positively modulated by warming to 37°C, membrane tension, AA, phosphorylation and the chemical 2-APB. Multimodal stimuli variably sensitise TRPV, TRPM, TRPA1 and TRPC channel gating, however, no single channel appears to be sensitised by all these gating modulators. Rather, the results of pharmacological testing presented in this chapter suggest that while

TRPV3 is the likely channel, the involvement of Piezo1 and TRPM1 remains to be clarified.

In recent years, evidence of Ca^{2+} permeable TRP channels and Piezo1 expression in T lymphocytes has emerged (reviewed by Bertin & Raz 2016, Khalil *et al.* 2018, Liu *et al.* 2018, Majhi *et al.* 2015). However, the interplay of signalling pathways and multiple gating mechanisms that lead to TRP channel activation, together with significant functional redundancy, heteromeric channel formation, functional differences between cell type, and a dearth of selective activating and inhibitory drugs, often means the functional role of many of these channels remains obscure. Furthermore, the patterning and duration of Ca^{2+} rises likely involve multiple mechanisms regulating $[Ca^{2+}]_i$ (reviewed by Christo *et al.* 2015, Feske 2007, Feske *et al.* 2015, Nohara *et al.* 2015, Robert *et al.* 2011, Winslow *et al.* 2003).

Considering these challenges, this chapter explores the potential involvement of a number of TRP and Piezo channels in contributing to the sustained $[Ca^{2+}]_i$ and $[Na^+]_i$ increases in DP thymocytes following the addition of DxS.

Results presented in the previous chapter indicate that following the addition of DxS, activation of one or more signalling pathways precedes activation of the cation influx. Initiation of the rises was strictly dependent upon CD8β and LFA-1, most likely as they are cross-linked by DxS. Subsequent Src kinase activation and tyrosine phosphorylation of adaptor molecules such as SLP-76 (Simon Davis 2015) facilitate recruitment and activation of PLC-γ1 and PI_3K (Shim *et al.* 2011). Enzymatic activity of both PLC-γ1 and PI_3K can locally alter the membrane lipid composition, in particular PIP_2, a significant modulator of TRP and Piezo1 channel activity.

The hydrolysis of PIP_2 by PLC-γ1 increases the availability IP_3 and DAG. As presented in 3.6.2, IP_3 activation of IP_3R and ER store Ca^{2+} release do not appear to be a necessary component of the DxS rises. Rather channel activation is proposed to involve PIP_2, DAG or a downstream metabolite such as AA. As with PIP_2, DAG and AA have also been found to modulate channel gating of some TRPC, TRPA and TRPV members. The finding that the rise is potently blocked by prior addition of GsMTx4, suggests that a mechanosensitive element is likely involved. These characteristics provide the starting point for evaluating potential candidate channels.

4.2 Materials

Details of the solutions and chemicals commonly used in cell preparation and flow cytometry experiments can be found in Chapter 2. Table 4.1 provides details of the concentrations and different protocols of the various inhibitory or activating chemicals used to assess the role of channels in the DxS rises. In most instances, the chemical was added at t = -1 min followed by DxS at t = 0 min. When checking the effect of the chemical on its own, it was added at t = 0 min.

Table 4.1 List of chemicals

Time and details of when the relevant chemical was added to the cell suspension in flow cytometry experiments where DxS was also added at $t = 0$.

Chemical	Putative Target	Action	Protocol	Conc. (μM)
2-APB	* TRPs		t = -1 min	16
A967079	TRPA1	inhibitor	t = -5 min	1
AMG9810	TRPV1	inhibitor	t = -1 min	0.5
Arachidonic acid	TRPV3 TRPM7	activator inhibitor	t = 0 min	10
Capsazepine	TRPV1	inhibitor	t = -1 min	0.5
Gadolinium	TRPs	inhibitor	DxS not added	10
GSK2193874	TRPV4	inhibitor	t = 1 min	0.04
HC030031	TRPA1	inhibitor	t = -1 min	20
Hyperforin	TTRPC6	activator	t = 0 min	5
Na–ATP	TRPV3	activator	t = 0 min	100
NDGA	TRPM7	inhibitor	t = -1 min	4
Norgestimate	∞TRPC6	inhibitor	t = -1 or t = 1 min	10–15
OAG	TRPC2,6,7 TRPA1,V1	activator	DxS not added	100
SKF96365	#TRPC6	inhibitor	t = -1 or t = 12 min	5–15
NS8593	TRPM7	inhibitor	t = -5 or t = 14 min	10–15
Ruthenium red	* TRPVs		t = -1 or t = 12 min	2.5 or 10
Tranilast	TRPV2	inhibitor	t = -1 min	75

* See Table 1.3 Pharmacological effects of 2-APB and ruthenium red; # pan TRPC channel inhibitor and Orai channel inhibitor; ∞ TRPC3, 6 antagonist and progesterone receptor agonist

4.3 Results

4.3.1 *In silico* data base screening of mRNA expression

To investigate the likely expression of channels in DP thymocytes considered as potential candidates, searches of genes in the Immunological Genome Project database (ImmGen; http://www.immgen.org/databrowser/index.html) were undertaken for probe sets for mice. The data available were derived by profiling gene expression on Affymetrix microarrays in cells from 5-week-old C57/Bl6J mice. The DP thymocyte populations of interest are described in the abT cell data group (*i.e.* cells expressing the α and β chains of the TCR).

Adapted from the ImmGen site, Figure 4.1 shows the mRNA expression for genes coding for non-selective cation channels that reportedly have mechanosensitive properties: *Trpc1, Trpc6, Trpv1, Trpv2, Trpv4, Trpa1, Trpm3, Trpm7 and Piezo1 (Fam38a) and Piezo 2 (Fam38b)* (Dietrich *et al.* 2007, Gottlieb *et al.* 2008, Grimm *et al.* 2003, Haselwandter & MacKinnon 2018, Maroto *et al.* 2005, Rocio Servin-Vences *et al.* 2017, Spassova *et al.* 2006). These panels indicate high expression of *Trpv2*, *Trpm7* and *Fam38a* (top row) across the $\alpha\beta$T cell group and specifically in the different DP populations bounded by the red and black dashed lines. The remaining genes, in contrast, appear to be minimally expressed. High expression refers to the arbitrary numbers of transcripts given along the abscissa, where typically >120 indicates true expression (more than 95% probability), while <47 suggests the gene expression is unlikely or silent (Ericson *et al.* 2019). In addition, I have included the expression profiles of two indirectly mechanosensitive channels *Trpc7* and *Trpm4* (Gonzales *et al.* 2014, Liu & Montell 2015). The expression of *Tprc7* is also low, and notably Inada *et al.* (2006) did not detect *Trpc7* in thymocytes (Figure 1.13). Importantly, high mRNA expression of a gene in DP thymocytes does not necessarily indicate a similarly high level of protein expression in these cells (Schwanhausser *et al.* 2011, Tian *et al.* 2004).

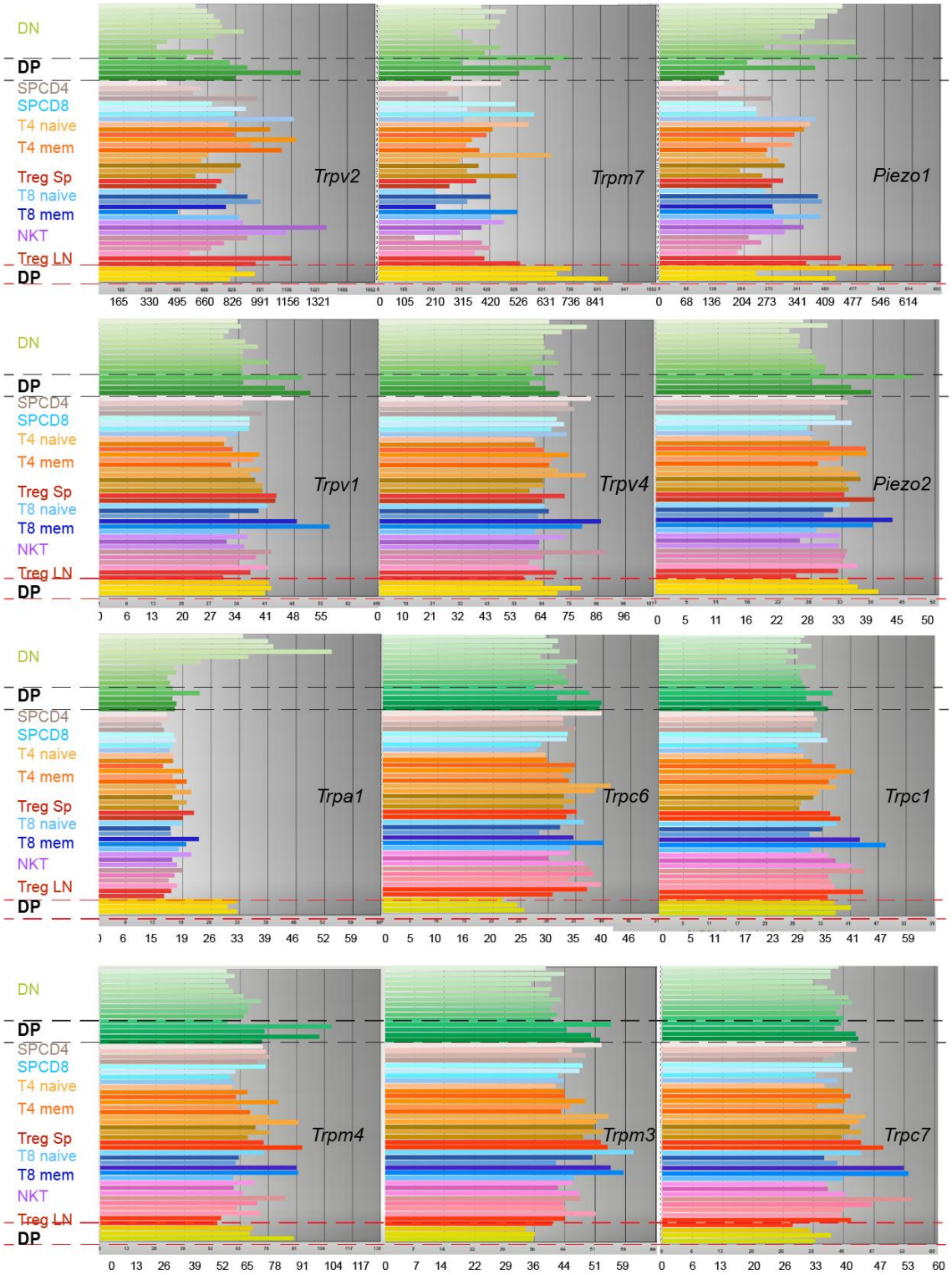

Figure 4.1 Gene expression of proposed mechanosensitive channels

Relative mRNA expression of *Trpv1*, *Trpv2*,*Trpv4*, *Trpc1*, *Trpc6*, *Trpc7*, *Trpa1*, *Trpm3*, *Trpm4*,*Trpm7*, *Piezo1 and Piezo2* transcripts. transcripts in αβT cell populations (ImmGen database). The

expression is predicted by the arbitrary numbers of transcripts given along the abscissa, where typically >120 indicates true expression (more than 95% probability), while <47 suggests the gene expression is unlikely or silent (Ericson *et al.* 2019). In descending order, the four DP subpopulations framed by the dashed black lines are: all, blasts, small resting, and DP early positive selection 69^+ thymocytes. The three DP subpopulations framed by the dashed red lines are DP 69^- preselection, DP 69^+ early positive selection, and DP early positive selection.

Considering the arbitrary values given in Figure 4.1, it appears that gene expression of *Trpv1*, *Trpa1*, *Trpc6* and perhaps also *Trpv4* in 'preselection DP $CD69^-$ thymocytes' may be silenced. Referring to Table 3.2, these four channels were predicted to be 'good' potential candidate channels. Therefore, I checked if the protein might nevertheless be present in the PM of DP thymocytes.

4.3.2 Protein detection indicates mechanosensitive channels on the PM

As the amount of gene expression does not necessarily indicate the presence of the protein in the PM, and, conversely, protein may be present despite negligible gene expression, ICC experiments were undertaken to check if channels thought to show mechanosensitive properties might be present. The cells were prepared following the protocol described in section 2.3.5, and the data was acquired on a BD LSRII flow cytometer. Commercially available extra-cellular Ab_1 against TRPC6, -C7, -V2, -V4 and -A1 (described in Table 2.4) were applied and detected by secondary staining with an Ab raised against the host species IgG and conjugated to the fluorochrome FITC (Ab_2). Owing to the lack of commercially available Ab_1 against an extracellular epitope on Piezo1, TRPV1, -M3, or -M7 the expression of these channels was not investigated.

The contour plots of CD8α against TRP channel expression are shown in Figure 4.2. From left to right, the four plots show the relative density and frequency of i) unstained cells, ii) anti-CD8α–AF647 plus Ab_2 (without Ab_1) stained cells, iii) anti-CD8α–AF647 plus Ab_1 (anti-TRP) preincubated with antigen (blocking) peptide (BP) plus Ab_2 stained cells, and iv) anti-CD8α–AF647 plus Ab_1 (anti-TRP)

plus Ab_2 stained cells which detect binding of the primary anti-TRP channel antibody. The threshold for detection of Ab_1 binding in $CD8^{hi}$ cells was set as illustrated in (iii) by positioning the vertex of a quadrant gate (red) immediately to the right and beneath the main population density. The same quadrant gating was also copied into plots i, ii and iv. The relative frequency in these sample plots is indicated by the percentage value in each quadrant.

Examining the plots in which Ab_1 cell staining was included (iv), there were significant shifts of the respective population densities into the top right quadrant in all cases ($p_{KS} \ll 10^{-30}$). This indicates that several target channel proteins are likely present in the PM surface in $CD8^{hi}$ thymocytes. Notably, the anti-TRPV4 Ab_1 binding was not specific to its immunogen. This is shown by the increased fluorescence detected in the TRPV4 Ab_1–BP control (bottom row; iii) compared to the anti-CD8–Ab_2 only control (ii).

I note that immunocytochemical detection of TRP channel protein doesn't imply that the channels are in a conductive state, however, their possible presence needs to be considered when interpreting subsequent data.

As indicated in Table 3.2, TRPC6 has been described as mechanosensitive channel that is positively modulated by Src kinase, directly activated by DAG, inhibited by GsMTx4 and may couple to NCX. These properties combined with the presumed expression of TRPC6 on the PM led to this channel being considered as the conduit to the cation rise.

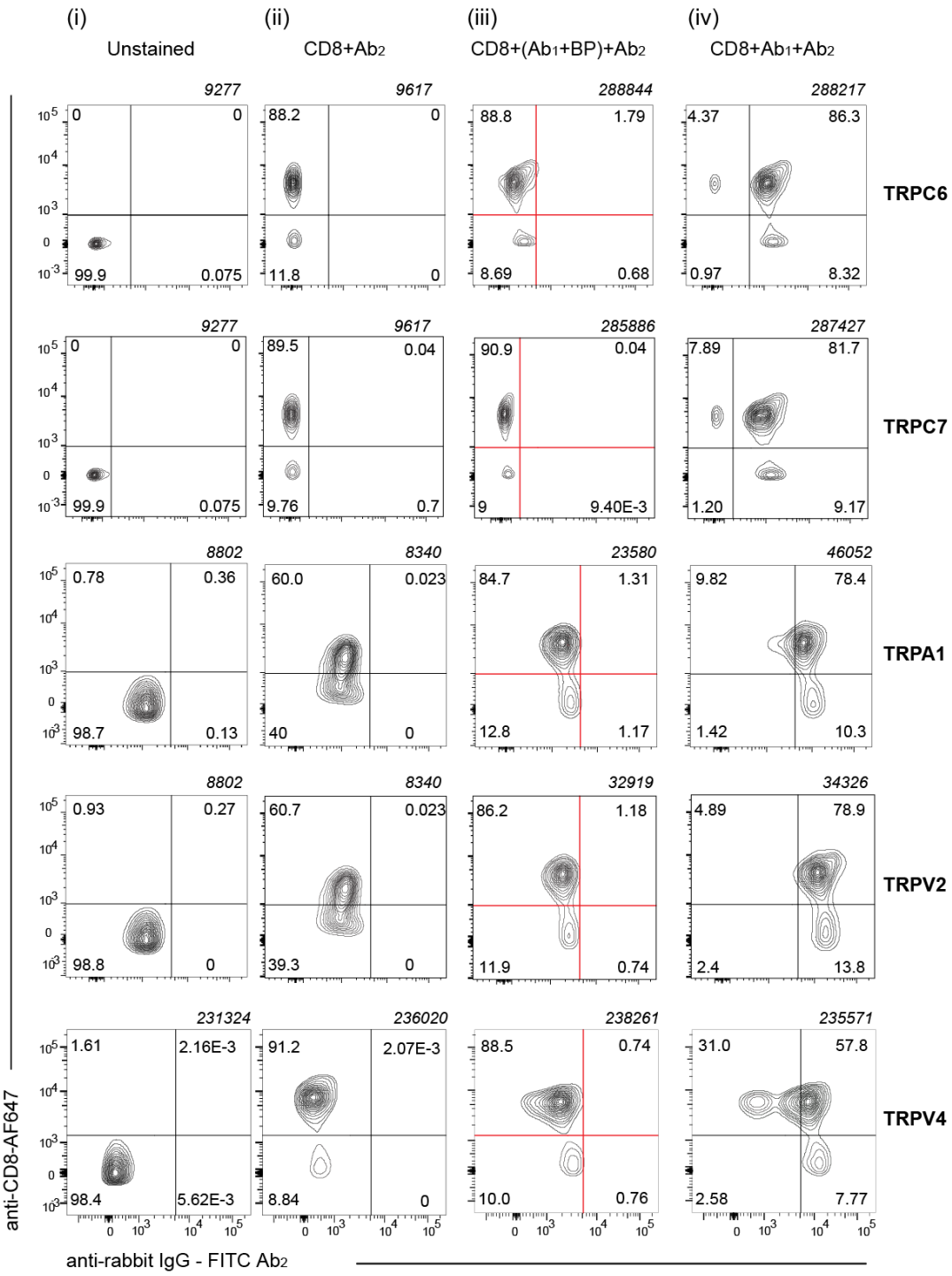

Figure 4.2 Detection of mechanosensitive channels on the PM

Typical contour plots representative of ICC experiments investigating the possible presence of TRPC6,TRPC7, TRPA1, TRPV2 and TRPV4 channel protein on the surface of $CD8^{hi}$ thymocytes. The fluorescence intensities of the five Ab_1 against TRP channels (rows) are shown in (iv) and the respective controls in columns (i–iii). Red lines indicate the quadrant gates set on the control Ab intensities in (iii) and copied (black) into the others. The relative percentages are given in each quadrant and the total number of cells top right outside the box.

4.3.3 OAG activated TRP channels are in the PM

Based on my ICC results, several DAG sensitive TRP channels may be present in the PM. These include TRPC2, -C3, -C6, -C7, -A1 and -V1. To check if some of these channels could be activated independently of DxS, I used the DAG analogue OAG (1-oleoyl-2-acetyl-*sn*-glycerol). As shown in Figure 4.3A, the addition of 50 μM OAG induced a transient rise in both $[Ca^{2+}]_i$ and $[Na^+]_i$ (black and grey, respectively). Notably, the onset and rate rise were faster than that caused by DxS and, compared to the DxS control, these rises had a smaller amplitude for both Ca^{2+} (23 ± 6%, n = 6) and Na^+ (38 ± 2%, n = 3). In addition, the $[Na^+]_i$ rise was delayed and dissociated from the time course of Ca^{2+}. This dissociation suggests that the addition of OAG may have activated more than one channel/transporter, either directly, or by changing membrane tension (Spassova *et al.* 2006), or may be the result of NCX activity.

Since many TRP channels are blocked by Gd^{3+}, I checked if it blocked the OAG induced rises. For this purpose, I added 10 μM Gd^{3+} immediately prior to OAG at t = 0 min. This concentration should potently inhibit TRPC6, TRPC3 and TRPA1, but not TRPC7 nor TRPV1 (summarised below in Table 4.2).

Table 4.2 Modulation of TRP channels by Gd^{3+}

Gd^{3+} (μM)	Inhibits	Activates
1	TRPA1 (Nagata *et al.* 2005)	
10	TRPC6, C3 (Chen *et al.* 2017b, Inoue *et al.* 2001)	
100	TRPC7 (Okada *et al.* 1999)	TRPV1 TRPC4, C5 (Plant & Schaefer 2005, Tousova *et al.* 2005)
300	TRPV1 (Tousova *et al.* 2005)	

Shown in Figure 4.3, the addition of Gd^{3+} only partially inhibited the OAG evoked $[Ca^{2+}]_i$ (B, ochre; $n = 3$, $p_t < 0.001$) and $[Na^+]_i$ rises (C, ochre; $n = 3$, $p_t < 0.01$). This data suggests that OAG activates rises that are partially sensitive to Gd^{3+}, consistent with TRP channels.

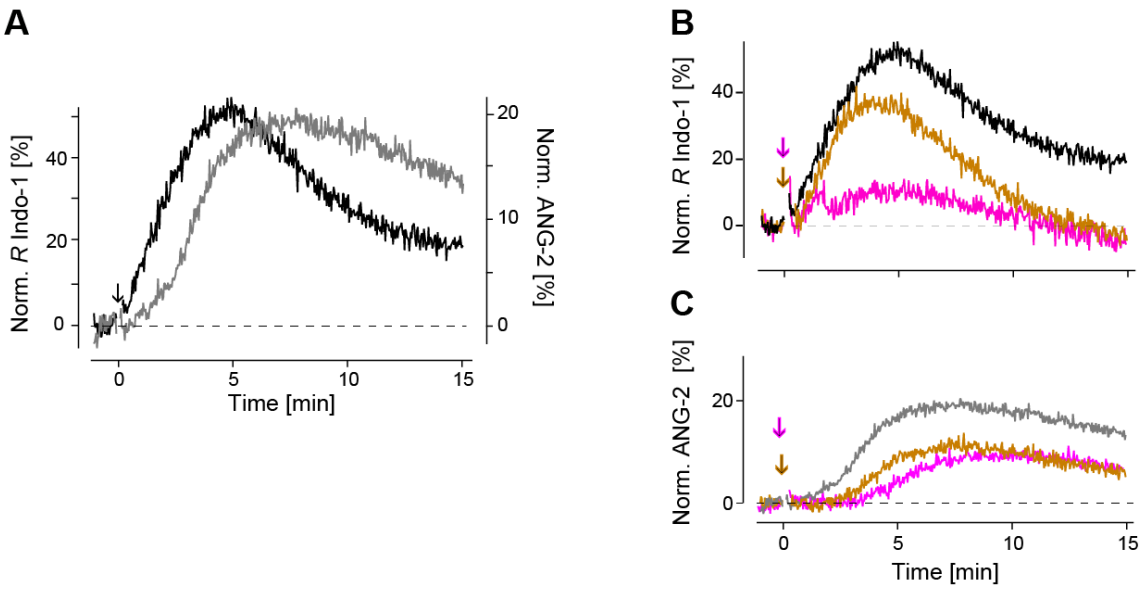

Figure 4.3 OAG activates a Ca^{2+} and Na^+ rise

(A) Appended time courses for $[Ca^{2+}]_i$ (black) and $[Na^+]_i$ (grey) when OAG added at $t = 0$ min. (B) Time course plots of the $[Ca^{2+}]_i$ response when at $t = 0$ min, either OAG (black); OAG plus Gd^{3+} (ochre) was added, or OAG plus 80 μM 2-APB was added (pink). (C) shows the time course plots for $[Na^+]_i$ time in these same experiments.

I also checked the effect of 80 μM 2-APB on the OAG rise. 2-APB should inhibit TRPC channels and potentiate TRPA1 and TRPV1 (see Table 1.3, p. 108). The addition of 80 μM 2-APB also reduced the OAG evoked rises (Figure 4.3B & C, pink) indicating the presence of at least one TRPC channel. Together the Gd^{3+} and 2-APB data indicate that multiple TRP channels are likely expressed in the PM. Their presence may well confound some of the results presented later in this chapter.

4.3.4 Hyperforin activates a cation rise

I next checked if a non-selective cation rise could be elicited by 5 μM hyperforin, a proposed TRPC6 activator (Leuner *et al.* 2007). Shown in Figure 4.4A, the addition of hyperforin at t = 0 min (red arrow) caused a $[Ca^{2+}]_i$ rise that was notably faster and 39.6 ± 2.9% smaller than the DxS $[Ca^{2+}]_i$ rise (red; n = 10, p_t <0.0001). Additionally, a small concomitant $[Na^+]_i$ rise that was 16.8 ± 0.6% of the DxS peak amplitude was also observed (Figure 4.4B; red, n = 3, p_t <0.001). This data is consistent with the idea that TRPC6 channels in the PM can be activated.

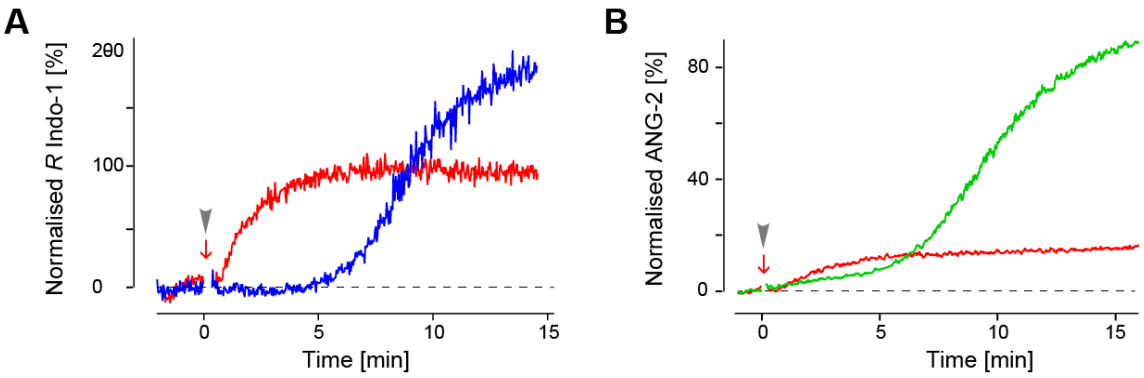

Figure 4.4 Hyperforin evokes a cation influx

(A) Time course of $[Ca^{2+}]_i$ when hyperforin was added at t = 0 min (red arrow/ trace) compared with the control DxS rise (blue). (B). As in (A) but monitoring $[Na^+]_i$.

4.3.4.1 TRPC6 inhibition does not abolish DxS cation rise

To determine if TRPC6 played a role in the DxS $[Ca^{2+}]_i$ rise I checked if the DxS cation rise could be inhibited either by norgestimate or SKF96365 (1-(β[3-(4-methoxyphenyl)propoxy]-4-methoxyphenethyl)-1*H*-imidazolehydrochloride), both non-selective blockers of TRPC6. In mouse smooth muscle cells, 10 μM norgestimate (IC_{50} ~5 μM; Miehe *et al.* 2012) and 5 μM SKF96365 (IC_{50} = 4.25 μM; Inoue *et al.* 2009, Inoue *et al.* 2001) have been shown to markedly inhibit TRPC6

channel activation. Notably both these drugs act on other targets . In Figure 3.10F (grey), I have shown that 15 μM norgestimate on its own caused a large and sustained $[Ca^{2+}]_i$ rise in these cells, indicative of SOCE. With such a rise, the DxS rise is not apparent and likely inhibited.

To circumvent this problem, I investigated the effect of lowering the hyperforin concentration. Shown in Figure 4.5A, the addition of 12 μM norgestimate on its own caused a small $[Ca^{2+}]_i$ rise (grey). When added at t = 7 min after DxS (aqua), the $[Ca^{2+}]_i$ rise was not inhibited (n = 3, p_t = 0.92). Reducing the norgestimate concentration further, to <10 μM, I found that resting $[Ca^{2+}]_i$ (n =6, p_t = 0.52) remained stable. Notably, when added 1 min prior to DxS, <10 μM norgestimate did not significantly block the DxS induced $[Ca^{2+}]_i$ rise (Figure 4.5B). This data indicates that a putative block of TRPC6 does not reduce the Ca^{2+} rise. To eliminate the notion that 12 μM norgestimate might not have been sufficient to block TRPC6 and the confounding issue of background Ca^{2+} elevation, I checked if SKF96365 could block the rise.

Similarly, the addition of 10 μM SKF96365 did neither inhibit the $[Ca^{2+}]_i$ nor the $[Na^+]_i$ rise (Figure 4.5C & D, black; n = 3, p_t = 0.84; p_t = 0.82, respectively). Significantly, higher concentrations of SKF96365 have been shown to inhibit the SERCA pump in thymocytes (Mason *et al.* 1993). This is apparent in Figure 4.5E & F (black traces), where, following preincubation with 3 μM YM58483 to block SOCE and DxS addition at t = 0 min, 20 μM SKF96365 added at 12 min (black arrow) caused a transient $[Ca^{2+}]_i$ rise but did not markedly affect the $[Na^+]_i$ rise suggestive of a tonic Ca^{2+} leak from either stores and/or mitochondria.

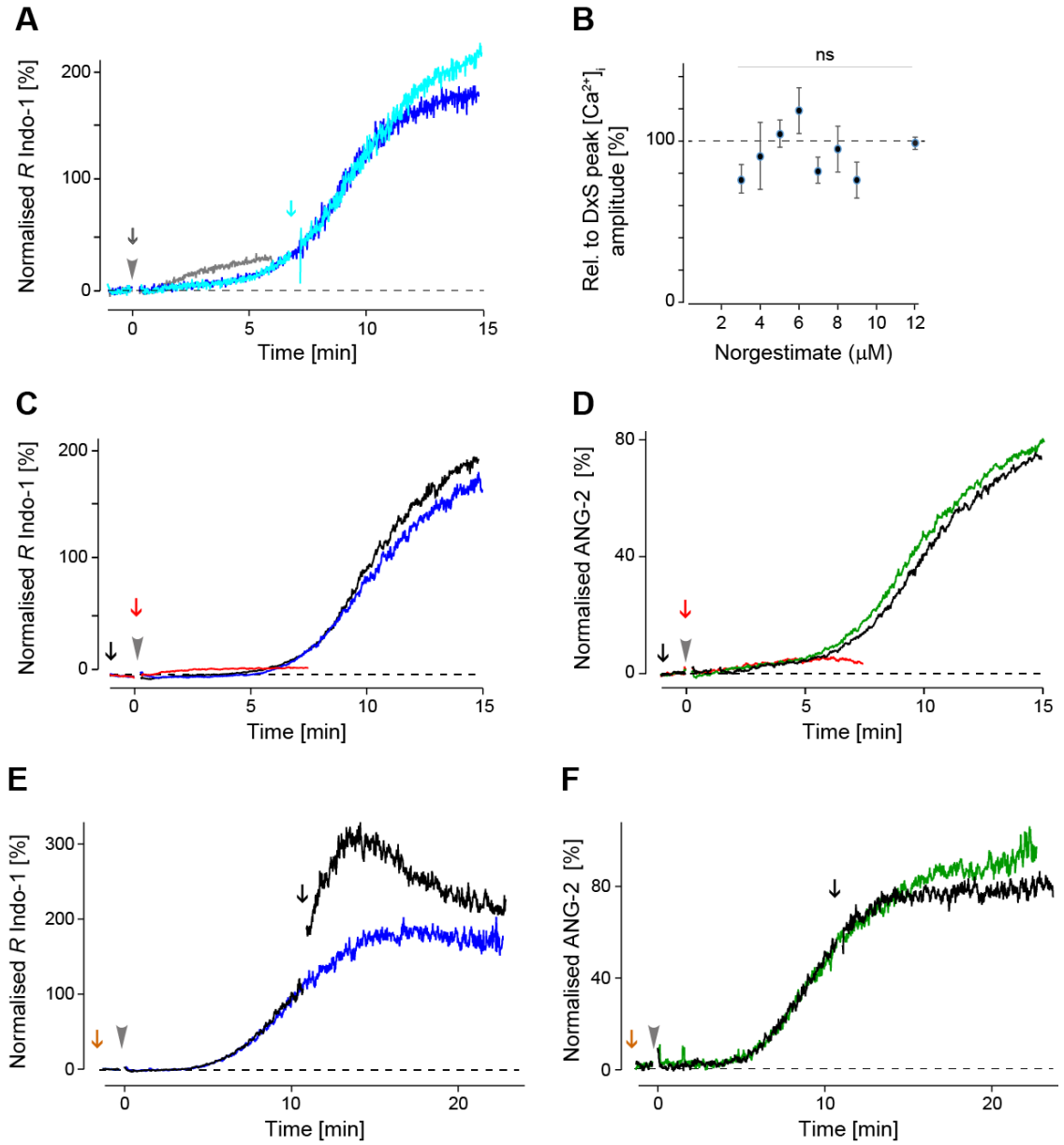

Figure 4.5 TRPC6 channels can be activated with hyperforin

(A) Time courses of $[Ca^{2+}]_i$ when 12 μM norgestimate only was added at $t = 0$ min (grey) and when added at t = 12 min (aqua) (B) Normalised peak DxS $[Ca^{2+}]_i$ amplitudes following 5 min preincubation with 3, 4, 5, 6, 7, 8 ,9 and 12 μM norgestimate (dashed line indicates control peak amplitude). (C) Time courses of $[Ca^{2+}]_i$ when 10 μM SKF96365 was added at $t = 0$ min (red arrow/ trace), the control DxS rise (blue) and when SKF96365 (black arrow/trace) was added prior to adding DxS at t = 0 min. (D). As in (C) but monitoring $[Na^+]_i$. (E) Time course of $[Ca^{2+}]_i$ when preincubated with 3 μM YM58463 (orange arrow), before adding DxS at t = 0 min (grey arrowhead) and 20 μM SKF96365 at $t = 12$ min (black). (F) As in (E) but for $[Na^+]_i$.

Both data sets are not consistent with TRPC6 involvement in the DxS rise. However, it is noted that the analysis of the results is confounded by the $[Ca^{2+}]_i$ rise from of intracellular stores. Therefore, to add more evidence that TRPC6 is not involved, I checked if 2-APB, another non-specific inhibitor of TRPC channels (Lievremont *et al.* 2005, Viitanen *et al.* 2013, Xu *et al.* 2005) could block the rises.

As detailed in Table 1.3, 2-APB has many targets. Concentrations of 30—300 μM progressively inhibit TRPC3, -C6 and -C7 channels and activate TRPV1, -V2 and -V3 channels (Chung *et al.* 2004, Hu *et al.* 2004, Lievremont *et al.* 2005). Having previously found that a stable rise in background $[Ca^{2+}]_i$ has an inhibitory effect on the DxS rise, I checked the effect of 30–100 μM 2-APB alone. Shown in Figure 4.6A (aqua), the addition of up to 100 μM 2-APB did not markedly elevate background $[Ca^{2+}]_i$. Consequently, I used 70 μM 2-APB (Figure 4.6B, aqua; $n = 5$, $p_t = 0.62$), a concentration below the block of PMCA (Peppiatt *et al.* 2003). In Figure 4.6C & D, the DxS rises are presented with the respective control (blue and green). In contrast to the expected block by 70 μM 2-APB, there was a large potentiation of both the $[Ca^{2+}]_i$ and $[Na^+]_i$ rises (black, 186 ± 29%; $n = 4$, $p_t > 0.001$ and 145 ± 14%; $n = 3$, $p_t > 0.05$, respectively). I found no difference between the two extents of potentiation ($n = 5$; $p_t = 0.36$) and the rate of rise of either cation ($n = 5$, $p_t = 0.48$). Consistent with the data presented above, these results do not suggest TRPC6 underlies the cation influxes.

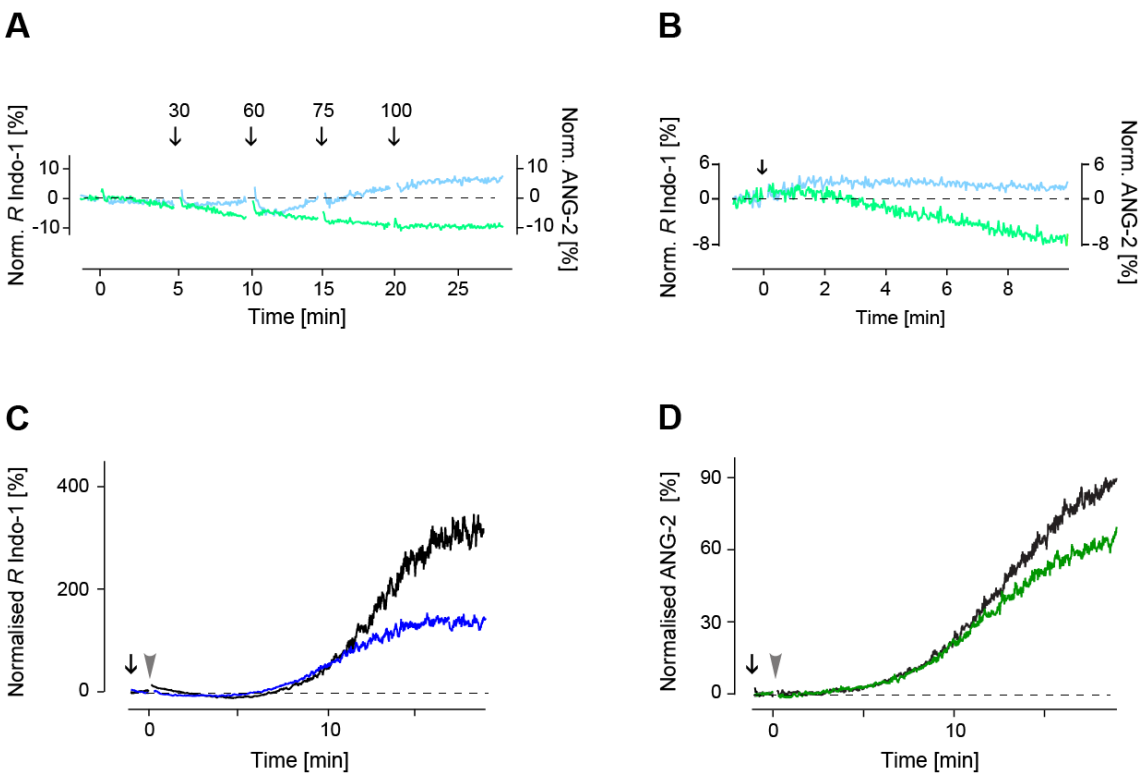

Figure 4.6 2-APB potentiates both rises

(A) Time course of background $[Ca^{2+}]_i$ (light blue) and $[Na^+]_i$ (light green) in response to 30, 60, 75 and 100 μM 2-APB (arrows). (B) Time courses of $[Ca^{2+}]_i$ (light blue) and $[Na^+]_i$ (light green) after exposure to 70 μM 2-APB added at t = 0 min. (C) Time course of DxS $[Ca^{2+}]_i$ control (blue) and when 70 μM 2-APB was added 1 min prior to DxS (black). (D) Same as in (C) but for $[Na^+]_i$.

However, because unspecific effects of 2-APB could have possibly confounded these results, additional experiments were undertaken using TRPC1,3,6,7$^{-/-}$ mice, with the aim of obtaining the best evidence regarding TRPC6, and coincidently TRPC1, 3 and 7.

4.3.4.2 The DxS $[Ca^{2+}]_i$ rise occurs in TRPC1,3,6,7$^{-/-}$ thymocytes

If TRPC6 channels were involved in the DxS rises, then the rises should be abolished in TRPC1,3,6,7$^{-/-}$ mice. It is important to note that, in contrast to the commonly used C57BL/6J mice, in these experiments the TRPC1,3,6,7$^{-/-}$ mice contained mixed C57BL/6J–129SvEv strains (refer to 2.1) rederived into 129SvEv mice. Since 4 genes on different chromosomes were altered in these functional

knock-out (KO) mice, litter mates could not be considered as appropriate controls. Rather, in this case, both age- and sex-matched C57BL/6J or 129SvEv WT mice were used.

A set of typical experiments using thymocytes from such mice are shown in Figure 4.7. Here, the time course of the DxS induced rises in thymocytes from the TRPC1,3,6,7$^{-/-}$ mice (aqua and light green for Ca^{2+} and Na^{+}, respectively) typically lay between the time courses from C57BL/6J (Figure 4.7A & B, blue or green) and 129SvEv WT "controls" (mauve or olive). Specifically, in mice with a SvEv background, the rises were diminished and appeared delayed (Figure 4.7C; t_{half} for both Ca^{2+} and Na^{+}; $n = 6$, $p_t < 0.01$). However, the amplitudes of the DxS $[Ca^{2+}]_i$ rise was not significantly different between the TRPC1,3,6,7$^{-/-}$ and WT 129SvEv thymocytes (Figure 4.7D; $n = 14$, $p_t \sim 0.3$). Likewise, between the 129SvEv WT mice and the TRPC1,3,6,7$^{-/-}$ mice, the $[Na^{+}]_i$ rise was not significantly different either (Figure 4.7E; $n = 14$, $p_t \sim 0.6$). These experiments not only rule out TRPC6 as a candidate, consistent with the observations above, but also TRPC1, -C3 and -C7. The difference in both the Ca^{2+} and Na^{+} rises in mice with a 129SvEv background could indicate that the signalling leading to channel gating requires extended time for amplification and may suggest strain differences in the signalling strength.

Whilst TRPC1,3,6,7$^{-/-}$ mice allowed the exclusion of the respective TRPC channels, it does not rule out TRPC2 channels which are also activated by DAG. Therefore, I turned my attention to this channel.

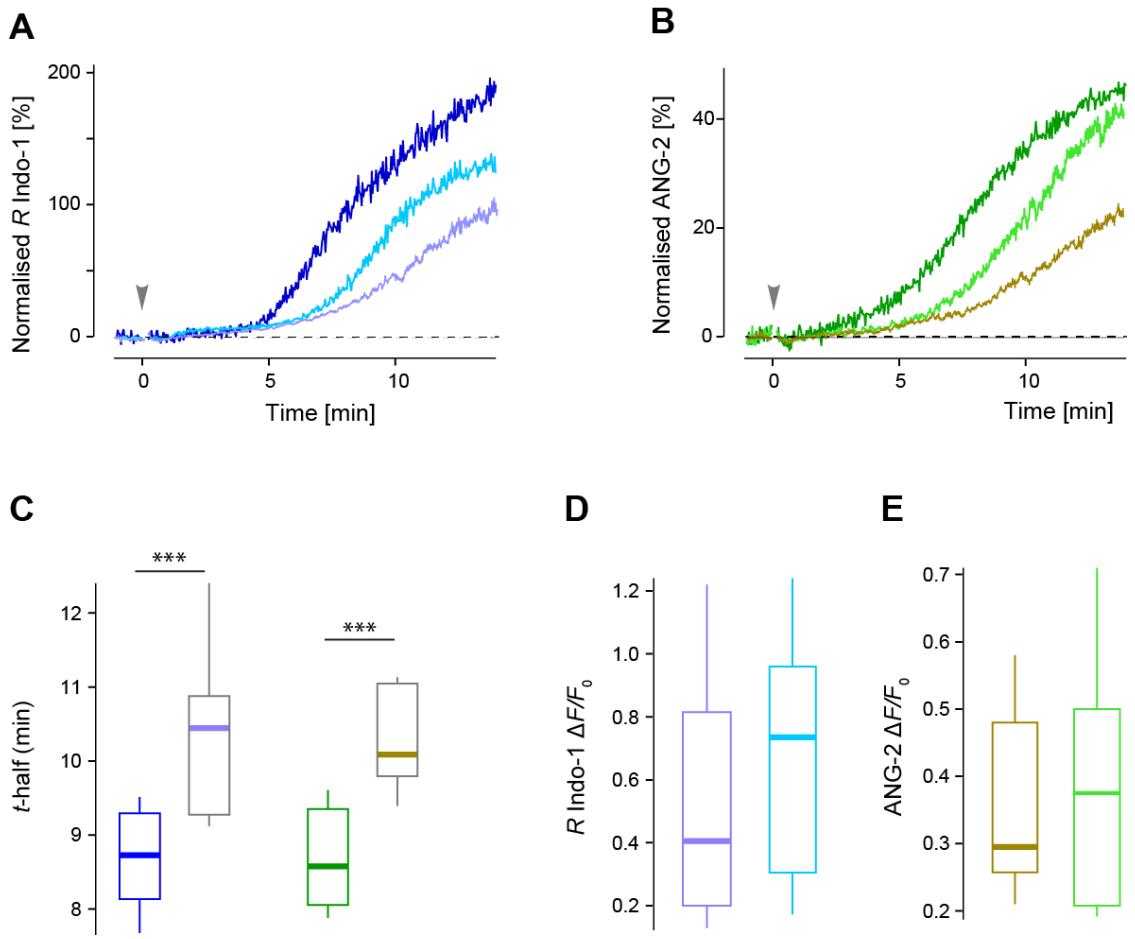

Figure 4.7 DxS rises remain in TRPC1,3,6,7$^{-/-}$ thymocytes

(A) Time courses of DxS $[Ca^{2+}]_i$ rises from a WT C57BL/6J (blue), a SvEv129TRPC1,3,6,7$^{-/-}$ (aqua) and a 129SvEv (mauve) mouse. DxS is added at t = 0 min. (B) Same as in (A) but for $[Na^+]_i$. KO (light green), WT SvEv (olive) (C) Box-and-whisker plot showing the t_{half} in C57BL/6J (blue and green, controls) and 129SvEv strain mice (grey boxes, Ca^{2+} purple median bar, Na^+ olive median bar) (D) Box-and-whisker plot of peak amplitudes of the $[Ca^{2+}]_i$ rises was not significantly different between the 129SvEv (mauve) and 129SvEvTRPC1,3,6,7$^{-/-}$ (aqua, n = 14). (E) Same as in (D) but for $[Na^+]_i$, 129SvEv (olive) and 129SvEvTRPC1,3,6,7$^{-/-}$ (light green, n = 14).

4.3.4.3 TRPC2 is unlikely involved either

Trpc2 has been shown to be highly expressed in mouse thymocytes (Figure 1.13; Inada *et al.* 2006). However, there is no evidence either for or against TRPC2 protein expression in these cells. To address this, I used ICC to check for it, using an Ab_1 against an extracellular TRPC2 epitope (Table 2.4). Results from ICC flow cytometry experiments (n = 4) consistently showed low levels of anti-TRPC2 Ab

binding (Figure 4.8). The small shift in the population density toward to right upper quadrant in Figure 4.8(iv) perhaps indicates very low expression of TRPC2 protein on the PM. This data neither supports nor refutes a likely role for TRPC2.

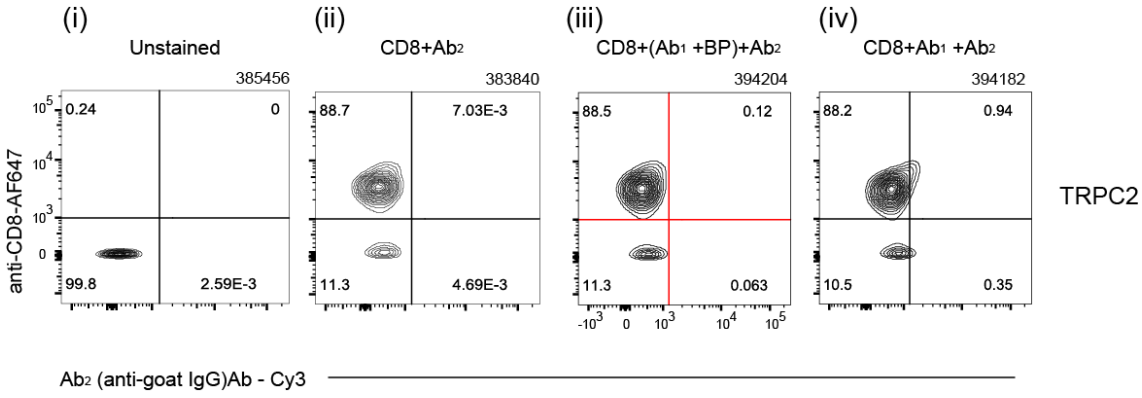

Figure 4.8 TRPC2 is poorly detected

Typical contour plots showing expression of TRPC2 channel protein on the surface of $CD8^{hi}$ thymocytes. This figure panel corresponds with those in Fig. 4.2. The legend for Fig 4.2 applies here as well.

Unfortunately, there is a current lack of specific TRPC2 antagonists. However, like for TRPC3, -C6 and -C7, the TRPC2 channel can also be blocked by 2-APB (50 μM; Lucas *et al.* 2003, Viitanen *et al.* 2013). Given that 2-APB actually caused a potentiation of the DxS rises (see above), this data is inconsistent with TRPC2 playing a significant role in the DxS rises.

4.3.5 TRPA1 does not underlie the DxS rises

Since TRPA1 is predicted to be present in the PM (see Figure 4.2), I checked if the OAG-induced rise could be blocked by the selective TRPA1 antagonist HC030031 (2-(1,3-dimethyl-2,6-dioxo-2,3,6,7-tetrahydro-1*H*-purin-7-yl)-*N*-[4-(propan-2-yl)phenyl]acetamide). This is illustrated in Figure 4.9A & B. Compared with the OAG controls (Ca^{2+}, black; Na^{+}, grey), the addition of 20 μM HC030031 (IC_{50} ~6 μM; McNamara *et al.* 2007) with OAG at t = 0 min (arrow) reduced both cation rises (aqua; n = 2). This finding confirms that TRPA1 channels are present in the

PM, but their activation does not account for all the OAG-induced cation influx. This suggests that other OAG-sensitive channels contribute to the rises.

Having evidence that TRPA1 channels can be activated in thymocytes, I investigated if it was involved in the DxS rises using 20 μM HC030031 or the more potent TRPA1 blocker A967079 (IC_{50} rat ~0.29 μM; Chen & Hackos 2015). I note that the efficacy of these chemicals varies depending upon species, cell type and channel activation mechanisms (reviewed by Chen & Hackos 2015) and that their inhibitory effect has not been reported specifically for thymocytes.

Investigating the role of TRPA1, either 20 μM HC030031 or 1 μM A967079 ((NE)-*N*-[(E)-1-(4-fluoro phenyl)-2 methyl pent-1-en-3-ylidene] hydroxylamine) were added at 1 or 5 min prior to DxS, respectively. As shown in Figure 4.9C–E, preincubation with A967079 did not alter the DxS induced $[Ca^{2+}]_i$ and $[Na^+]_i$ rises (black trace and boxes; Ca^{2+}: n = 4, p_t = 0.9; Na^+: n = 4, p_t = 0.7). Similarly, in the presence of HC030031 (Figure 4.9E, orange boxes), the peak amplitudes of the $[Ca^{2+}]_i$ (n = 4, p_t = 0.7) and $[Na^+]_i$ rises (n = 4, p_t = 0.2) were not significantly changed. These findings suggest that TRPA1 is unlikely to be involved in the DxS rises.

To strengthen this argument even more, I checked if the DxS rise was absent in thymocytes from a $TRPA1^{-/-}$ mouse. In such thymocytes, the *Trpa1* mutation (Kwan *et al.* 2006) is presumed to cause the same loss of function as confirmed in neocortical pyramidal cells (Kheradpezhouh *et al.* 2017). Shown in Figure 4.9F, the DxS induced cation rise was still present in $TRPA1^{-/-}$ thymocytes. This result strengthens the argument that TRPA1 channels are not involved. It leaves TRPV1 as the remaining DAG sensitive channel to be explored. While the OAG with added 2-APB results do not support the presence of this channel, it may be that the 50 μM OAG concentration was insufficient to activate TRPV1.

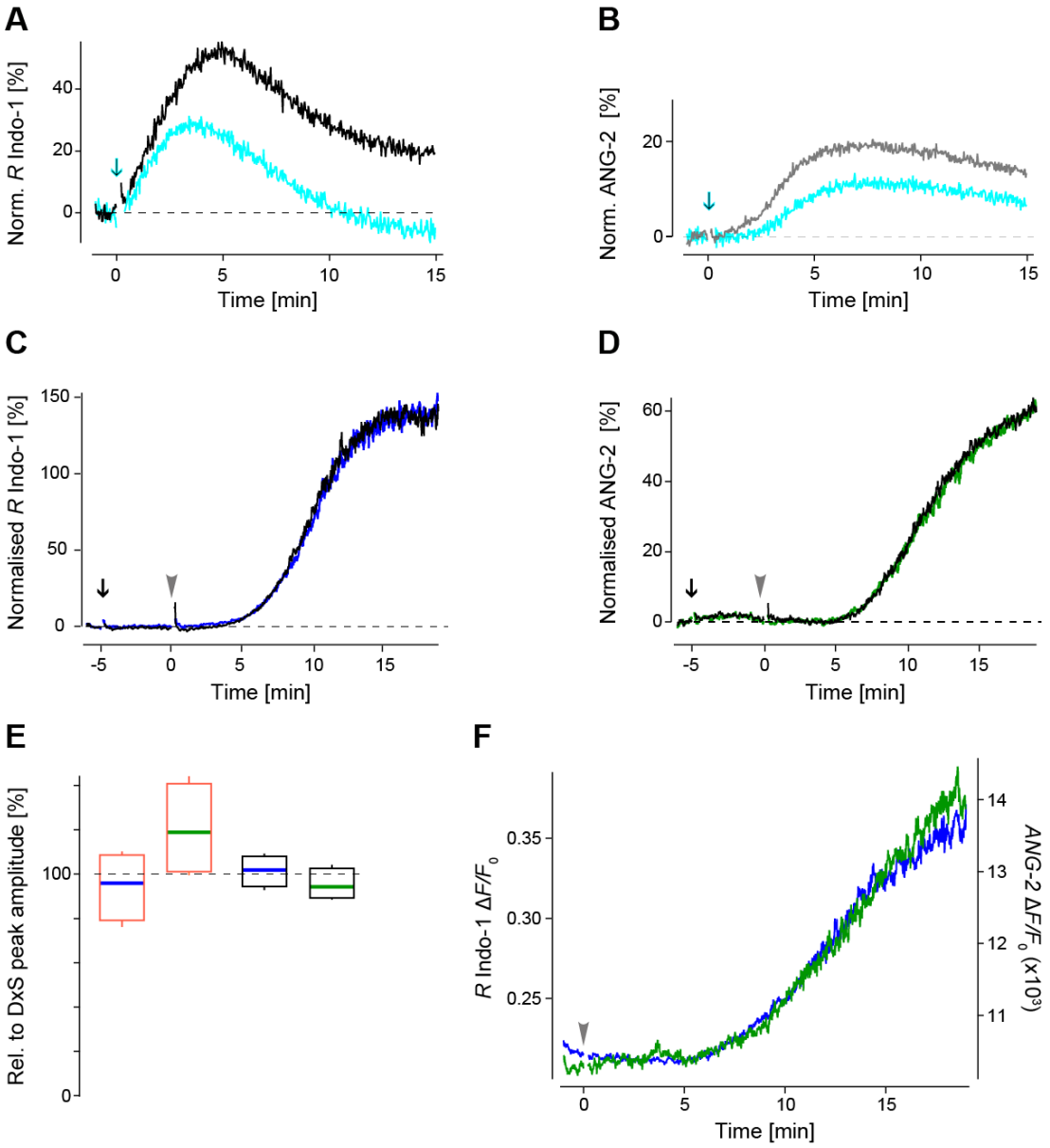

Figure 4.9 OAG activates more than one channel

(A) Time course plots of the $[Ca^{2+}]_i$ response when at t = 0 min either OAG (black); or OAG plus HC030031(aqua) were added. (B) Same as in (A) but for $[Na^+]_i$.(C) Time course of DxS $[Ca^{2+}]_i$ in control (blue) and when A967079 is added (black arrow) 5 min prior to DxS (black trace). (E) As in (D) but for $[Na^+]_i$ control (green). (E) Box-and-whisker plots summarising the effect of HC030031 (orange) and A967079 (black) on DxS Ca^{2+} and Na^+ peak amplitude relative to the DxS control peak amplitude indicated by grey dashed line. (F) Time courses of Ca^{2+} and Na^+ rises in TRPA1$^{-/-}$ thymocytes.

4.3.6 TRPV1 antagonists do not block the rises

Hence, I investigated if selective blockers of TRPV1 abolished the DxS cation rises. Both, capsazepine (CPZ; *N*-[2-(4-chlorophenyl)ethyl]-7,8-dihydroxy-1,3, 4,5-tetrahydro-2-benzazepine-2-carbothioamide) and AMG9810 (3-(4-tert butyl phenyl)-*N*-(2,3-dihydro-1,4-benxodioxin-7-yl)prop-2-enamide) are blockers of TRPV1 (Amantini *et al.* 2017, Gavva *et al.* 2005). AMG9810 reportedly inhibits rat TRPV1 with an IC_{50} of ~85 nM and here, I used it at 500 nM. The potency of CPZ as a TRPV1 blocker varies between species. In HEK-293 cells transfected with mTRPV1, Correll *et al.* (2004) reported that the IC_{50} was ~1.4 μM. In thymocytes, Amantini *et al.* (2017) showed incubation with 1 μM CPZ was sufficient to inhibit TRPV1 function. Here, I initially chose 1.2 μM.

An experiment in which 1.2 μM CPZ was used is illustrated in Figure 4.10A (inset). Compared to the control for Ca^{2+} (blue), the peak amplitude with 1.2 μM CPZ added 1 min before DxS shows an apparent inhibition (red). Notably the red trace starts from an elevated baseline, indicating that this concentration of CPZ likely caused a rise in $[Ca^{2+}]_i$. The control for CPZ alone added at t = 0 min (inset: black arrow/trace) confirms this suspicion. As a consequence, I reduced the CPZ concentration to 0.5 μM and checked if this prevented the rise in background $[Ca^{2+}]_i$. The results are presented in Figure 4.10A & B. Exposure to this concentration alone (black) did not elevate the background $[Ca^{2+}]_i$ or $[Na^+]_i$. Additionally, when then exposed to DxS after pre-incubation for 1 min (red arrow), neither the DxS $[Ca^{2+}]_i$ nor $[Na^+]_i$ rises were inhibited (red, n = 5, p_t = 0.45 and 0.65, respectively). While this result could indicate that TRPV1 channels are not involved, the apparent lack of block may simply be explained by having chosen an insufficient CPZ concentration.

To rule this possibility out, the more potent antagonist AMG9810 was used. Its addition to the suspension did not notably elevate background $[Ca^{2+}]_i$ (Figure

4.10C, black) and, when added 1 min prior to DxS, it did not significantly block either the $[Ca^{2+}]_i$ (Figure 4.10C, grey, n = 7, p_t = 0.6) or $[Na^+]_i$ rise (Figure 4.10D, grey, n = 7, p_t = 0.9). These findings indicate that AMG9810 was also unable to block both rises and suggests that TRPV1 does not underlie the DxS induced cation rises. This now means that all the DAG activated candidates TRPC6, TRPA1 and TRPV1 have been ruled out. Summarised in Figure 4.11, this finding, however, may point to the involvement of a channel activated by a metabolite of DAG such as arachidonic acid (AA).

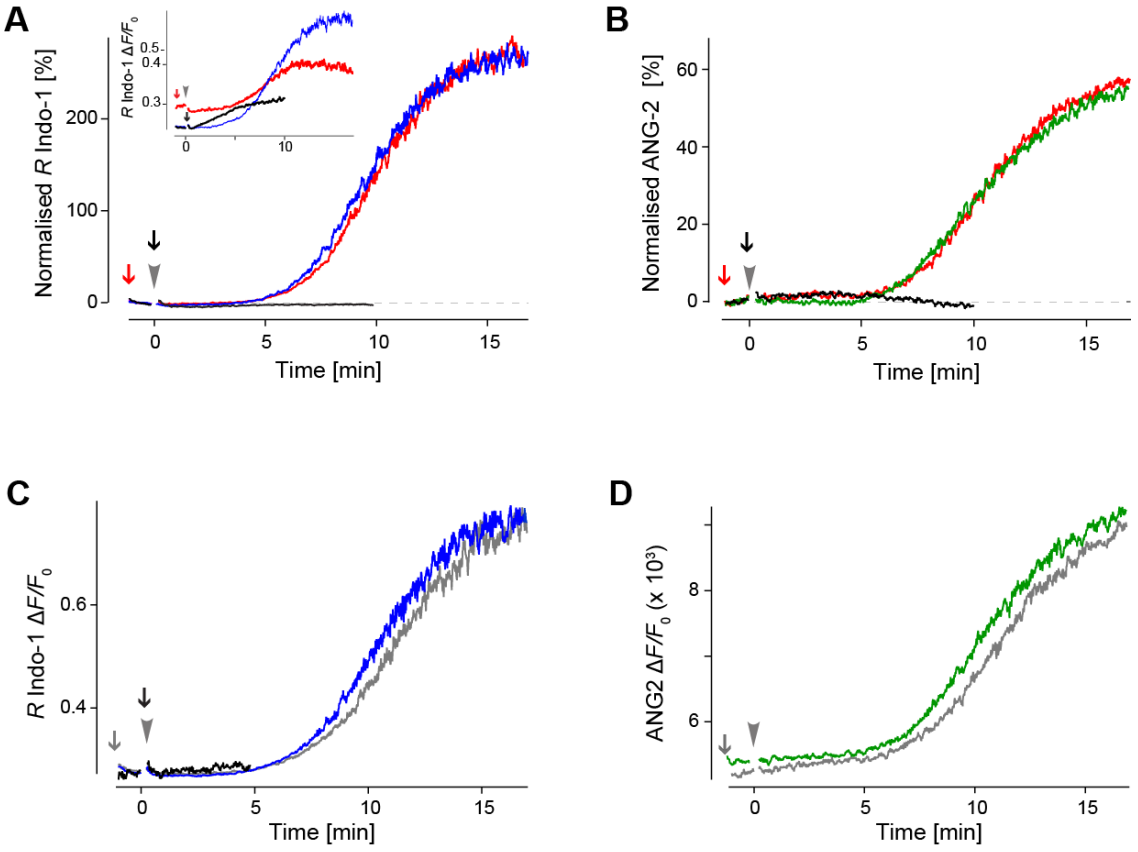

Figure 4.10 DxS rises not due to TRPV1

(A) Time courses of $[Ca^{2+}]_i$ when 0.5 µM CPZ was added at t = 0 min (black), or at t = -1 min (red) with DxS added at 0 min (red trace) and control (blue). Inset: Same traces but plotted as R indo-1 $\Delta F/F_0$ when 1.2 µM CPZ was added. (B) As in A, but monitoring $[Na^+]_i$. (C) Time courses of R indo-1 $\Delta F/F_0$ in control (blue) with DxS added at t = 0 min (grey arrowhead) and when incubated with AMG (grey), and AMG on its own (black). (D) Same as in (C) for$[Na^+]_i$ but without the AMG on its own.

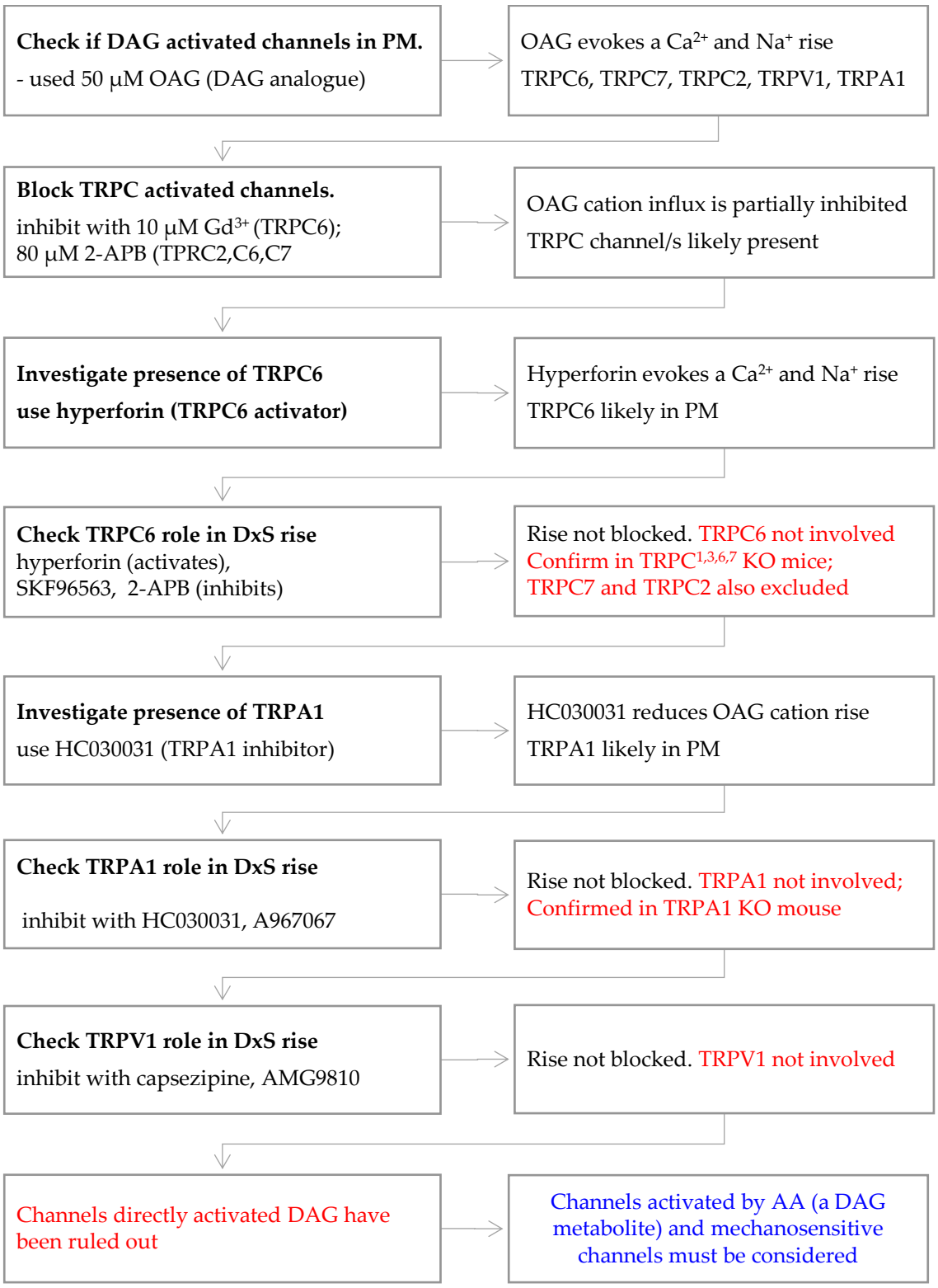

Figure 4.11 Channels directly activated by DAG are excluded

Summary of the pharmacological screening steps used to exclude DAG activated channels from the DxS induced cation rise and direct the research toward the examination of channels that are activated by AA and/or are directly gated by mechanical stress.

4.3.7 **Arachidonic acid and 5-LOX inhibition potentiate the rises**

Turning my attention to the DAG metabolite, AA, I checked if the cation rise was sensitive to this PUFA. In thymocytes the response to exogenously applied AA is varied. Khodorova and Astashkin (1994) showed that, the addition of 6 μM AA caused a rapid increase in $[Ca^{2+}]_i$ by ~100 nM, and Astashkin *et al.* (1993) found that 3 μM AA led to rapid intracellular acidification by ~0.2 pH units. Considering this, I used AA at 10 μM.

Such a set of experiments is illustrated in Figure 4.12A & B (black). The addition of 10 μM AA 1 min prior to DxS significantly potentiated the increase in $[Ca^{2+}]_i$ but not $[Na^+]_i$ ($n = 3$, $p_t < 0.01$ and $p_t = 0.76$, respectively). However, when I tested if there was a difference between the two extents of potentiation, I found there was none ($n = 3$, $p_t = 0.54$). This outcome is likely due to the small sample size and large variability seen within the data for Na^+. Using the principle of parsimony, these two answers are best reconciled if there was an increase in both. Interestingly, following the addition of 10 μM AA and DxS at $t = 0$ min (Figure 4.12A, black), there was a rapid increase in $[Ca^{2+}]_i$, albeit small. While this early rise might reflect a direct activation of an AA- or pH-sensitive channel extraneous to the DxS $[Ca^{2+}]_i$ rise, the fact that both rises maintain a similar time course suggests AA potentiated the channel causing both rises.

In support of this idea, I found that the rises were also potentiated by the addition of 4 μM nordihydroguaiaretic acid (NDGA; 4-[4-(3,4-dihydroxy phenyl)-2,3-dimethylbutyl]benzene-1,2-diol). This chemical is reported to potently inhibit TRPM7 (IC_{50} = 6.5 μM in HEK293 cells; Chen *et al.* 2010). However, it is also an inhibitor of 5-lipoxygenase (5-LOX; Papadogiannakis & Barbieri 1997) which, in T-lymphocytes, plays an important role in the metabolism of AA and formation of immunomodulatory leukotrienes (Cook-Moreau *et al.* 2007). Inhibition of 5-LOX is predicted to drive up endogenous AA levels and thus could provide a

mechanism for potentiating activation of an AA-sensitive channel involved in the DxS rises.

As shown in Figure 4.12D & E (grey), the addition of 4 μM NDGA at t = 0 min on its own did not elevate background $[Ca^{2+}]_i$. Rather, it slowly rose over 10 min, while $[Na^+]_i$ remained unchanged. It is therefore unlikely that this small elevation would have had an inhibitory effect on the cation rises. After pre-treatment with NDGA and compared to control, the Ca^{2+} rise was significantly potentiated, but not the one for Na^+ (Figure 4.12F, orange box-and-whisker plots; Ca^{2+}: n = 5,p_t <0.01; Na^+: n = 5, p_t = 0.69). However, as found with AA, there was no difference between the two extents of potentiation (n = 4, p_t = 0.33). I note that in contrast to the case with AA, there was no immediate rise in Ca^{2+} suggestive of the idea that it takes time for AA to build up when the 5-LOX pathway is blocked, in contrast to when exogenous AA is added to the suspension. Both sets of data strongly suggest that the channel activated by the signalling cascade is modulated by the lipid contents in the membrane.

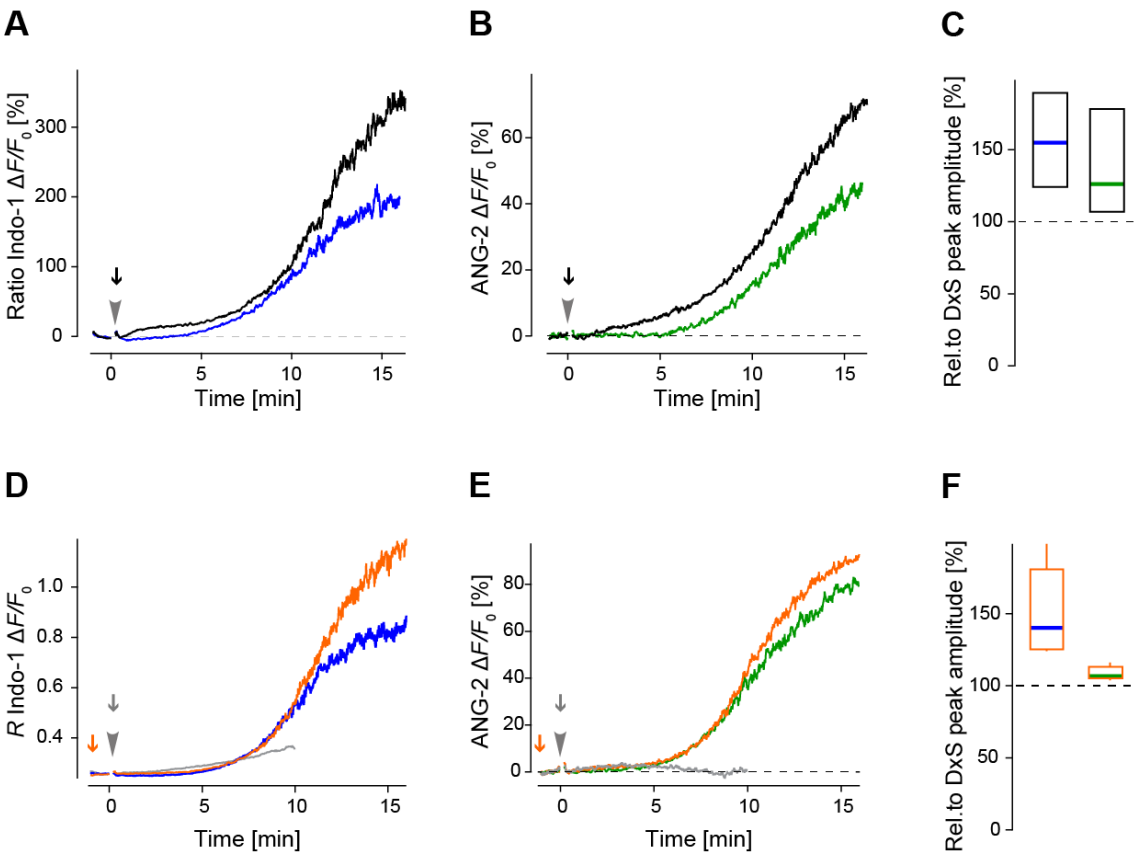

Figure 4.12 Arachidonic acid and NDGA both potentiate both rises

(A) Time courses of $[Ca^{2+}]_i$ under control conditions (blue) and when AA is added (black arrow) with DxS at $t = 0$ (grey arrowhead). (B) Same as in (A) but for $[Na^+]_i$. (C) Box-and-whisker plots summarising the potentiation by AA of both rises (black) relative to the respective control (dashed line). (D) Time courses for DxS $[Ca^{2+}]_i$ under control conditions (blue) and when 4 μM NDGA is added (orange) 1 min prior to DxS at $t = 0$ (grey arrowhead) and when 4 μM NDGA only is added at $t = 0$ (grey). (E) As in (D) but for $[Na^+]_i$. (F) Same as in (C) but for NDGA.

Table 4.3 Pharmacological properties of remaining candidate channels

Reported properties with references and where relevant concentrations.

Chemical	Activated	Inhibited	Insensitive	Unknown
AA	TRPV3 (Hu *et al.* 2006), TRPM2 (Hara *et al.* 2002) TRPV4 (indirectly; Watanabe *et al.* 2003b)	TRPM7 (Chen *et al.* 2010); Enhances Piezo1 inactivation (Romero *et al.* 2019)	TRPM3 (Rampino & Nawy 2011)	TRPM6, TRPM6/7, TRPV2
2-APB	TRPV2, TRPV3, TRPM6, TRPM6/7 TRPM1 (? potentiates; Shen *et al.* 2009)	TRPM7 (50 μM) TRPM3 (100 μM; Xu *et al.* 2005)TRPM2 (30 μM; Togashi *et al.* 2008)	TRPV4	Piezo1
GsMTx4		Piezo1, TRPV2 (Zanou *et al.* 2015)a	TRPV4 (Miyamoto *et al.* 2014)	TRPM7

Given these observations, I refocussed my investigation towards remaining channels that are modulated by AA (or its metabolites) and 2-APB and blocked by GsMTx4. These channels are presented in Table 4.3. It is evident that none of these candidates has all the "right" properties. Only TRPV3 is known to be sensitive to both AA and 2-APB. While there is no evidence to suggest TRPV3 is directly mechanically gated, it could be indirectly mechanosensitive. For example, via loss of coupling to the cytoskeleton and/or a change in membrane curvature caused by alteration of the composition of lipids. Alternatively, it may be that the sequential activation of two channels is required. In this amended list of candidate channels, TRPV2, -M7, -V4 and Piezo1 are reportedly mechanosensitive, but of these, only TRPV2 is known to be both activated by 2-APB and inhibited by GsMTx4 (Zanou *et al.* 2015). Therefore, I examined if TRPV2 could be involved in the rises.

4.3.8 TRPV2 is unlikely involved either

Trpv2 is highly expressed in thymocytes (Fig. 1.13; Inada *et al.* 2006). In addition, my ICC results in Figure 4.2 support the idea that the protein is expressed on the PM. To explore the involvement of TRPV2, I used the antagonist tranilast (2-[3-(3,4-dimethoxy phenyl)prop-2-enoyl-amino] benzoic acid) at 75 μM (Aoyagi *et al.* 2010, Sugio *et al.* 2017) and such an experiment in illustrated in Figure 4.13A & B. Specifically, I found the addition of 75 μM tranilast 1 min before that of DxS had no effect on both the Ca^{2+} (n = 4, p_t >0.9) and the Na^+ rises (n = 4, p_t >0.9). This data does not support involvement of TRPV2 channels.

Since TRPV2 is unlikely, the other mechanosensitive channels that need evaluating are TRPV4 and TRPM7. While the effect of GsMTx4 on TRPM7 is unknown, TRPV4 is reportedly insensitive to this blocker, which makes it an unlikely candidate.

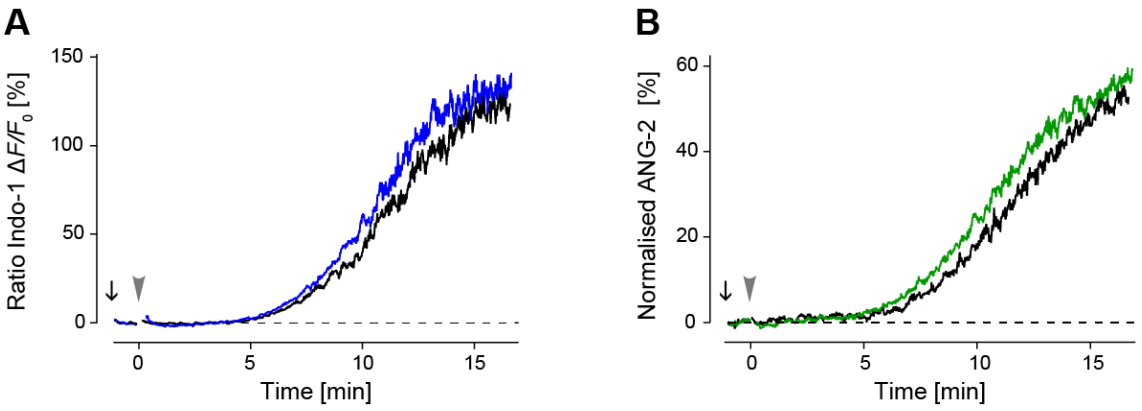

Figure 4.13 TRPV2 in unlikely involved

(A) Time courses of $[Ca^{2+}]_i$ with DxS added at t = 0 min in control (blue) and when pre-incubated with tranilast for 1 min prior to adding DxS (black). (B) Same as in (A) but for $[Na^+]_i$.

4.3.9 **TRPV4 is not involved either**

Nevertheless I checked for its involvement using the antagonist GSK2193874 (3-([1,4'-Bipiperidin]-1'-ylmethyl)-7-bromo-*N*-(1-phenylcyclopropyl)-2-[3-(trifluoro methyl)phenyl]-4-quinolinecarboxamide, IC_{50} = 5 nM; Thorneloe *et al.* 2012). I found that when 40 nM GSK2193874 was added 1 min after DxS (data not shown), neither the Ca^{2+} (n = 3, p_t = 0.34) nor the Na^+ rise (n = 4, p_t = 0.83) were affected. This finding is consistent with the idea mentioned in the lead-in and suggests that TRPV4 does not appear to be involved.

The next channel to consider was therefore TRPM7.

4.3.10 **TRPM7 is also an unlikely candidate**

Trpm7 is very highly expressed in thymocytes, but distinct from TRPV2, it can be inhibited by 2-APB. In Jurkat cells, 50 μM 2-APB has been shown to partially inhibit TRPM7 (Prakriya & Lewis 2002), although the mechanism of inhibition may be indirect (Chokshi *et al.* 2012a, Pang *et al.* 2012). While the potentiation by 2-APB presented above (Figure 4.6C & D) is inconsistent with the properties reported for TRPM7, it cannot be ruled out that a heteromeric TRPM6/7 channel could be potentiated. Therefore, I evaluated if TRPM7 or TRPM6/7 when blocked with 10 μM NS8593 (IC_{50} ~1.6 μM; Chubanov *et al.* 2012, Luongo *et al.* 2018) was involved in the rises.

I found that the addition of NS8593 at t = 1 min did not significantly reduce the amplitude of the $[Ca^{2+}]_i$ and $[Na^+]_i$ rises (Figure 4.14A & B, red; n = 5, p_t = 0.42 and n = 5, p_t = 0.34, respectively). To rule out the possibility that a block could only be achieved when the channel is open, NS8593 was added at t = 14 min. Still, the DxS rise was not reduced (n = 2). Notably, when added at t = 1 min, 10 μM NS8593 caused an early small Ca^{2+} increase, that interestingly did not inhibit the rises. However, preincubation with 15 μM NS8593 did abolish the rises (Figure 4.14C

& D, grey), but notably with this higher concentration there was an increased elevation of background $[Ca^{2+}]_i$ (Figure 4.14C, black). Therefore, this "block" of the DxS rise is unlikely attributable to TRPM7 channel block but rather to elevated background $[Ca^{2+}]_i$, similar to the block shown in 3.3.3 and 3.4.5.

This set of experiments also rules TRPM7 out and confirms the observation that a block of the rises can be caused by prior elevation of background Ca^{2+}. It also rules out TRPM6, which is potently inhibited by 10 μM NS8593 (Ferioli *et al.* 2017).

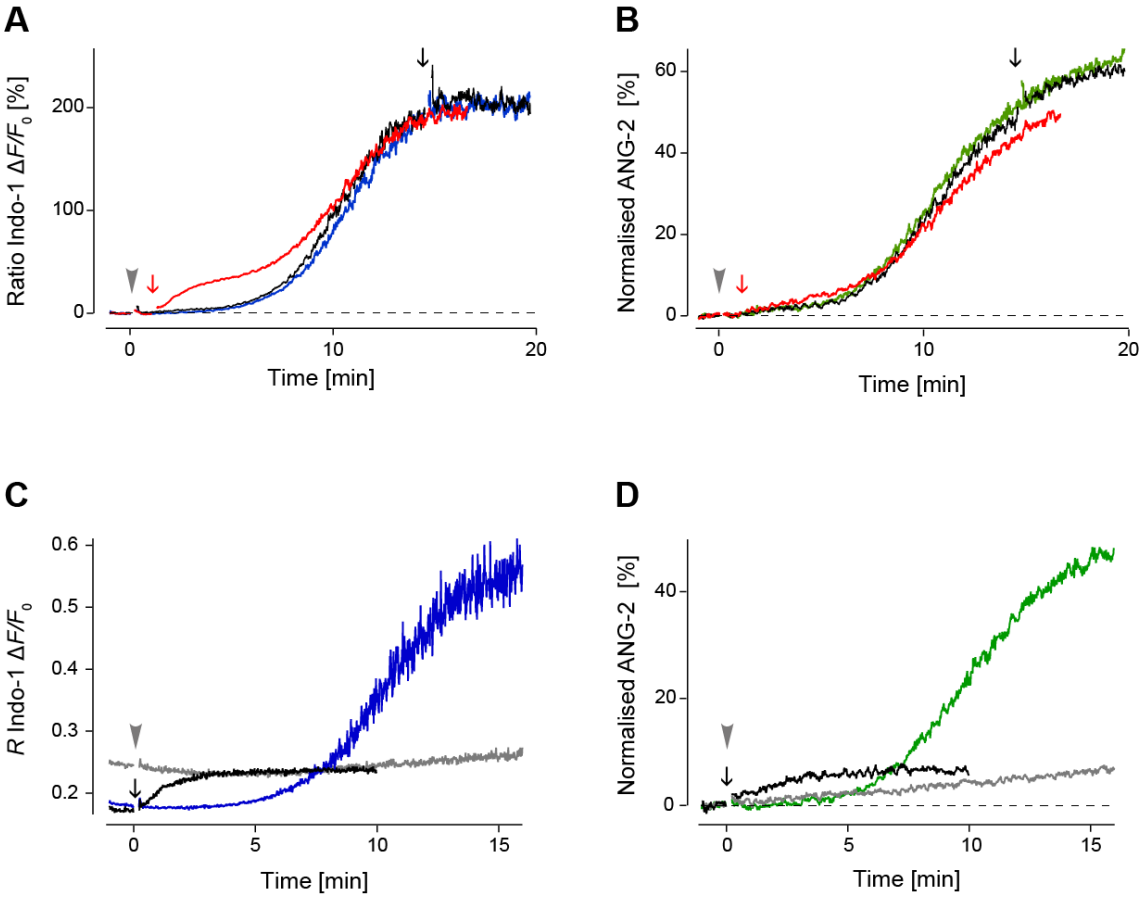

Figure 4.14 Unlikely involvement of TRPM7 or TRPM6/7

(A) Time courses of $[Ca^{2+}]_i$ with DxS added at t = 0 min in control (blue), with 10 μM NS8593 added 1 min (red) or 14 min after DxS (black).(B) Same as in (A) but for $[Na^+]_i$. (C) Time courses of $[Ca^{2+}]_i$ given as R indo-1 $\Delta F/F_0$ with DxS added at t = 0 min for control (blue), when added at t = 0 min on its own (black) and after pre-incubation 5 min with 15 μM NS8593 (grey). (D) Same as in (C) but for $[Na^+]_i$ and after normalising for the baseline.

The next step was to evaluate if TRPV3, TRPM1 or Piezo1 channels are involved. Common to all TRPV, some TRPM and Piezo1 channels is that they are sensitive to the hexacationic dye ruthenium red (RuR). I, therefore, considered if RuR could block the DxS rises.

4.3.11 **Ruthenium red blocks both rises**

RuR has a reported IC_{50} of 0.12 μM for TRPV3 in mouse (Grubisha *et al.* 2014). While the IC_{50} value for TRPM1 has not been determined, it can be blocked with 10 μM (Shen *et al.* 2009). Recalling from the Introduction (see Table 1.3), RuR has many molecular targets, including the mechanosensitive Piezo1 channel (IC_{50} = 5.4 μM; Coste *et al.* 2012). Nevertheless, it is frequently used to investigate TRPV channel activity (Ahluwalia *et al.* 2002, Grubisha *et al.* 2014, Güler *et al.* 2002, Li *et al.* 2006, Peier *et al.* 2002, Watanabe *et al.* 2003a) and has, on one occasion, been used to block TRPM1 (Shen *et al.* 2009). I, therefore, checked if the DxS rises were sensitive to RuR and used it at 2.5 or 10 μM.

RuR causes an open channel block (Cibulsky & Sather 1999). Therefore, I added it after reaching the plateau phase of the cationic rise, when a maximum number of channels is open. Such an experiment is shown in Figure 4.15A & B. Compared to the control DxS rises, when 10 μM RuR (n = 9) was added at t = 12 min (red), both $[Ca^{2+}]_i$ and $[Na^+]_i$ started to decay, the former exponentially, the latter delayed. In both cases the block was incomplete. Since DxS is a polyanionic chemical binding to sites on the PM, it may be that in the presence of DxS the hexavalent cation RuR may not easily get access to the outside of the channel pore. To address this, I added it much earlier, specifically at t = 1 min after DxS. As shown in Figure 4.15A & B (grey), when added early, the rises were completely blocked. As seen several times before, this could have been the result of RuR elevating background $[Ca^{2+}]_i$. I therefore provide evidence that this was

not the case (Figure 4.15A, inset, pink). After adding 10 μM RuR on its own, the background $[Ca^{2+}]_i$ did not rise ruling this possibility out.

I wondered if a much lower concentration of RuR could also block the cationic rise. For this I chose 2.5 μM RuR. When it was added at t = 12 min (Figure 4.15C & D, black), only $[Ca^{2+}]_i$ was significantly affected and the decay became linear. Figure 4.15E provides a box plot which compares the reduction of both $[Ca^{2+}]_i$ and $[Na^+]_i$ associated with 10 and 2.5 μM RuR added at t = 1 and t = 12 min. In such experiments, the reductions in $[Ca^{2+}]_i$ were highly significant, regardless of time and concentration. The $[Na^+]_i$ reduction at 10 μM was also significant (n = 7, p_t <0.0001), but not for 2.5 μM added at t = 12 min (black/green box, n = 9).

This set of experiments shows that the DxS rise is caused by (an) element(s) that is/are sensitive to RuR as both 2.5 and 10 μM were able to block it. Notably, the 2.5 μM concentration is below the IC_{50} reported for Piezo1 channels, but not for TRPV3.

Having already presented evidence in the Introduction, for high expression of *Piezo1* (Figure 1.9) and *Trpm1* (Figure 1.13 and Figure 1.15), I decided to check the expression of *Trpv3* and *Trpm1* in the ImmGen database for the αβT cell group.

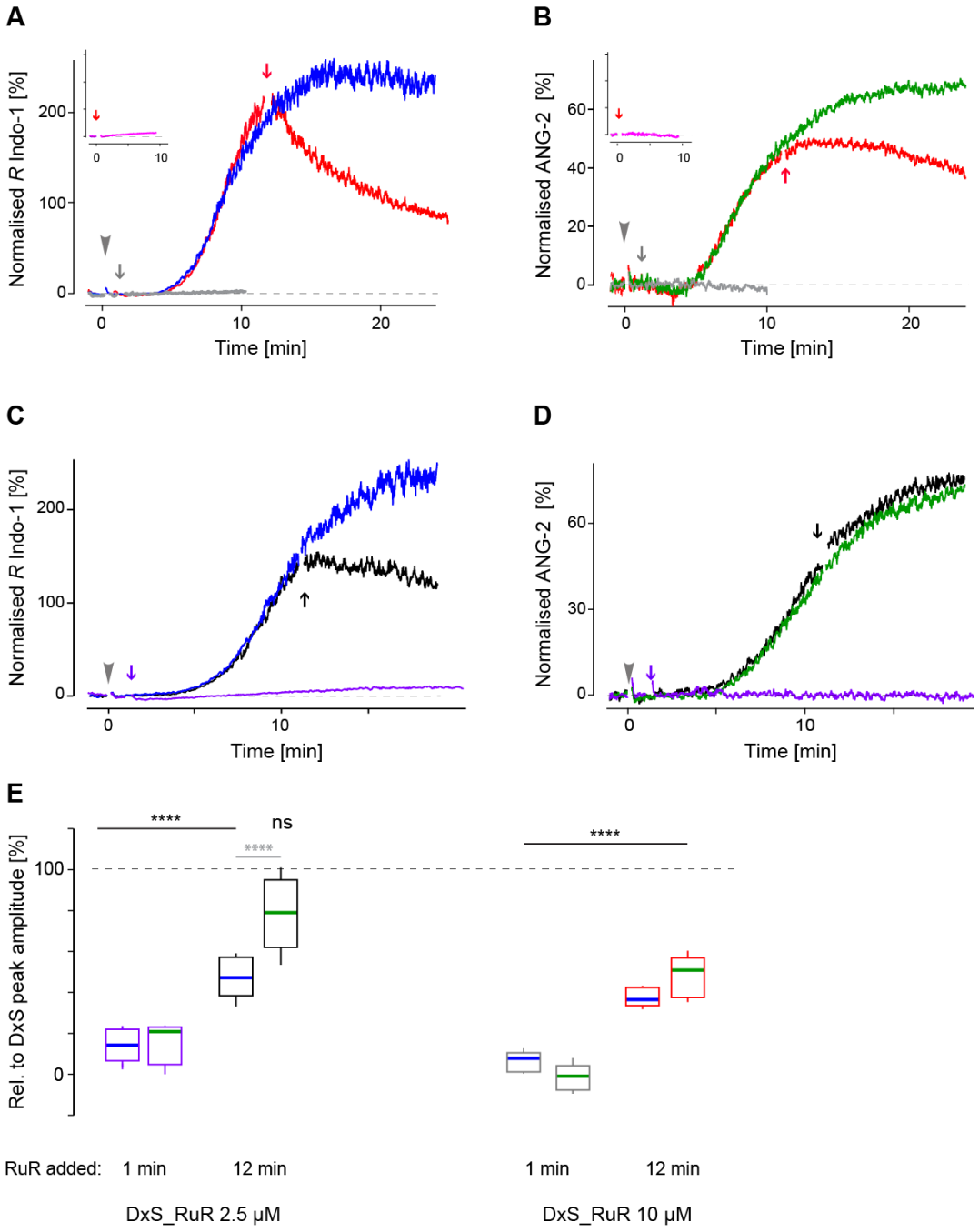

Figure 4.15 Ruthenium red blocks both rises

(A) Time courses of the DxS $[Ca^{2+}]_i$ rise in control (blue) and after 10 µM RuR added at t = 12 min (red) or at t = 1 min (grey). Inset: Time course of $[Ca^{2+}]_i$ when 10 µM RuR was added on its own at t = 0 min (pink).(B) Same as in (A) but monitoring $[Na^+]_i$. (C) Time courses of $[Ca^{2+}]_i$ in control (blue) and after 2.5 µM RuR added at t = 12 min (black) or at t = 1 min (purple). (D) Same as in (C) but for $[Na^+]_i$. (E) Box-and-whisker plots summarising blocks for 2.5 (purple n = 5; black n = 9) and 10 µM (grey n = 5; red, n = 9) for Ca^+ and Na^+ relative to the DxS peak amplitude (dashed line, grey).

4.3.12 TRPV3 and TRPM1 expression in thymocytes

The relative expression level of *Trpv3* was examined by searching the αβT cell group in the ImmGen database. Shown in Figure 4.16A & B, there is an ~2-fold increase in the expression of *Trpv3* and *Trpm1* within the DP thymocyte subset. These data concur with the findings reported by Inada *et al.* (2006).

As there is no extracellular anti-TRPM1 Ab_1 available, I only investigated the expression of TRPV3 protein in the PM using ICC. As shown in Figure 4.16C, a distinct shift in fluorescence intensity occurred when detecting the anti-TRPV3 Ab_1 by staining with a FITC conjugated Ab_2 (iv). This result is suggestive of the presence of TRPV3 protein. Additionally, the Ab_1 was found to be sensitive to immunogen, as indicated by the low detection when preincubated with the blocking peptide (iii).

I next explored if TRPV3 was involved in the cation rise. TRPV3 is an unusual thermosensitive channel in that it does not open readily. Rather its activation can be sensitised with repeated thermal stimuli or by co-stimulation by dissimilar agonists acting at different sites (Liu *et al.* 2011, Zhang *et al.* 2019). Such sensitisation has been shown to produce a biphasic time course (Chung *et al.* 2005). Specifically, channel activation is possible at subthreshold temperatures (<33°C) if synergistically exposed to 2-APB (Chung *et al.* 2004). Distinct from TRPV3, TRPM1 is not known to be temperature-sensitive.

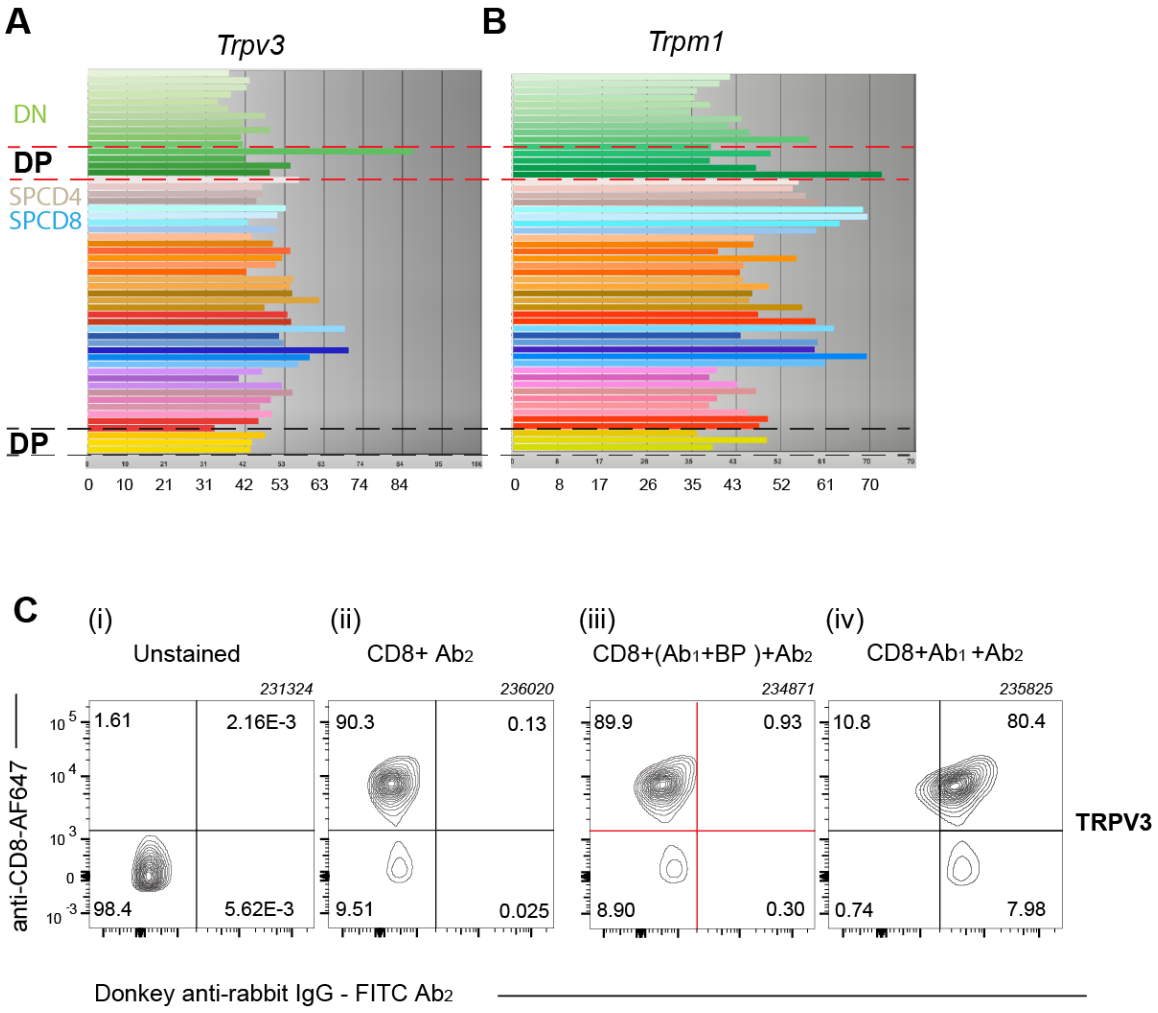

Figure 4.16 Expression of TRPV3 and TRPM1

(A) mRNA expression of *Trpv3* as provided for the ImmGen database abT cell group; Probe set:10378367. In descending order, the four DP populations enclosed by the red dashed lines are: all; blasts; small resting; and CD69^{+} early positive selection. The subpopulations framed by the dashed black lines are DP 69^{-} preselection, DP 69^{+} early positive selection and DP early positive selection. (B) Same as in (A) but for *Trpm1*. Probe set:10553861. (C) Typical contour plots from ICC experiments used to detect TRPV3 protein in the PM of CD8^{hi} thymocytes.

4.3.13 2-APB at 30°C restores the DxS $[Ca^{2+}]_i$ rise

To check for the functional involvement of TRPV3, I investigated if the DxS cation rise could be activated at subthreshold temperature (30°C) in the presence of 70 μM 2-APB. The failure of DP thymocytes to respond to the addition of DxS when the cell suspension was maintained at 30 rather than 37°C is shown in Figure

4.17A & B (aqua). However, the addition of 70 μM 2-APB prior to the DxS at this temperature indeed brought the rises back (pink, as compared to blue/green recorded at 37°C). Consistent with sensitisation at 30°C, there was a longer delay to t_{half}. Overlaying the two time courses, I found that under these conditions, the Na^+ rise slightly preceded that of Ca^{2+} suggestive of a channel letting predominantly Na^+ in (Figure 4.17C and inset). This did not show up in the pooled data as there was no difference between t_{half} and rate of Ca^{2+} and Na^+ (n = 3, p_t = 0.85 and 0.93, respectively) suggestive of the fact that the variability between samples hid this subtle difference. Even though it looks as if the rise in A was potentiated compared to the control at 37°C, but that in B was not, this observation is made with caution, as the relevant comparator would be a rise at 30°C, which unfortunately could not be obtained. Most likely, this reflects that the regulation of the Ca^{2+} homeostasis at the two temperatures is likely very different. In accordance with the finding reported by Xu *et al.* (2002), the mechanism of 2-APB sensitisation at 30°C could also be blocked by the addition of 10 μM RuR at t = 1 min (Figure 4.17A & B, black). The amount of potentiation against three different 2-APB concentrations at 37°C is given in Figure 4.17D. Additionally, the case for sensitisation at 30°C is given (pink), which is the justification for using 70 μM in these experiments. These data strongly suggest that TRPV3 activation could very likely contribute to DxS induced cation rises. It may suggest that in this case, this channel predominantly lets Na^+ through and a significant amount of the concomitant Ca^{2+} rise is likely due to NCX in reverse mode.

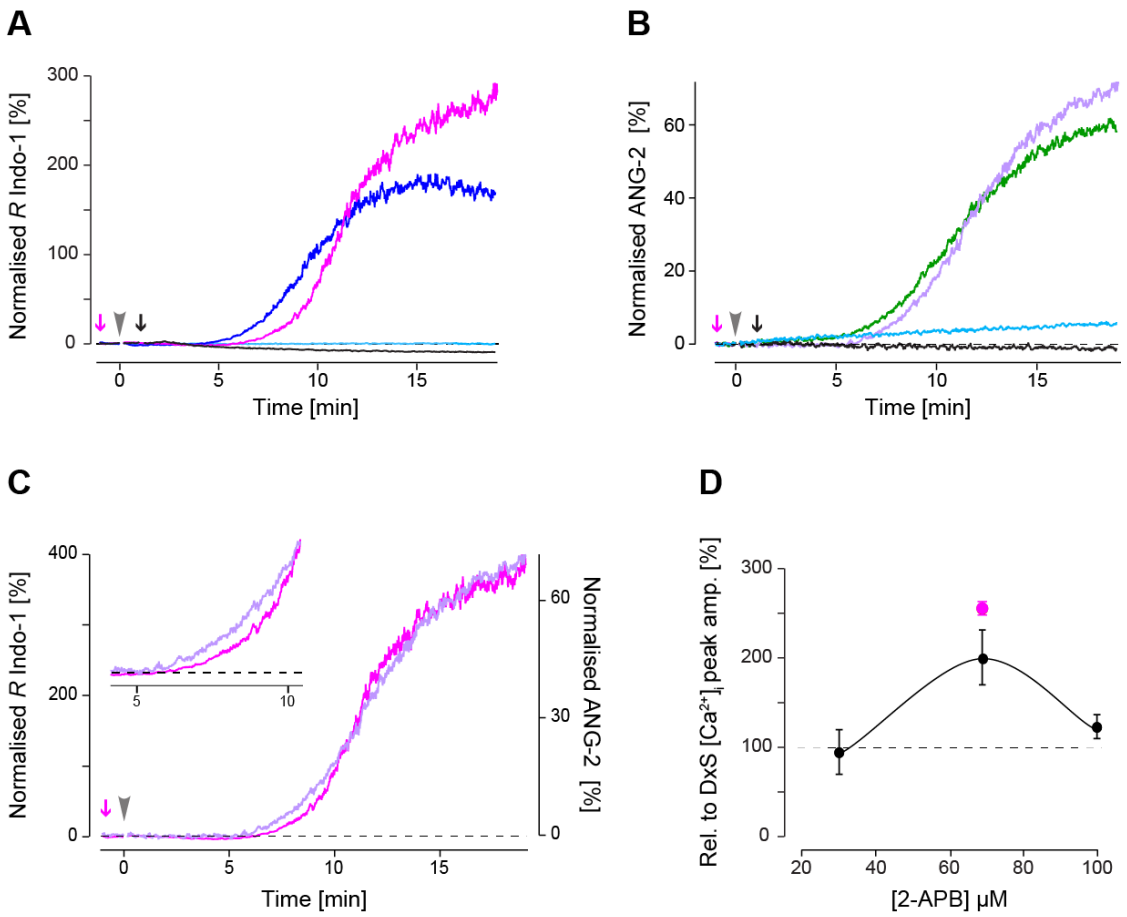

Figure 4.17 2-APB sensitisation at 30°C rescues both cation rises

(A) Time courses of $[Ca^{2+}]_i$ under control conditions at 37°C (blue), at 30°C (aqua), when 2-APB was added at 30°C at t = -1 min (pink) and in the presence of RuR (black) added at t = 1 min. (B) Same as in (A) but for $[Na^+]_i$. (C) Overlay of both cation rises with the same colour code as in (A) and (B). Inset: blow-up to reveal that the early Na^+ rise precedes that of Ca^{2+}. (D) Dose-response relationship between $[Ca^{2+}]_i$ rise and 2-APB concentration at 37°C (black). The values are joined by a polynomial spline with the dashed line indicating the normalised $[Ca^{2+}]_i$ rise. The pink dot at 70 µM outside the joined dots was obtained for the case of sensitisation at 30°C.

4.3.14 Extracellular ATP potentiates the cation rises

Having previously found that 100 μM ATP on its own did not reproduce the Ca^{2+} rise (Feakes 2012), I quickly checked if the DxS rises might be sensitive to ATP as described by Doerner *et al.* (2011) for TRPV3. Shown in Figure 4.18A & B, the addition of 100 μM ATP potentiated both the Ca^{2+} and Na^{+} rise. This finding further supports the argument that TRPV3 likely underlies the DxS rises.

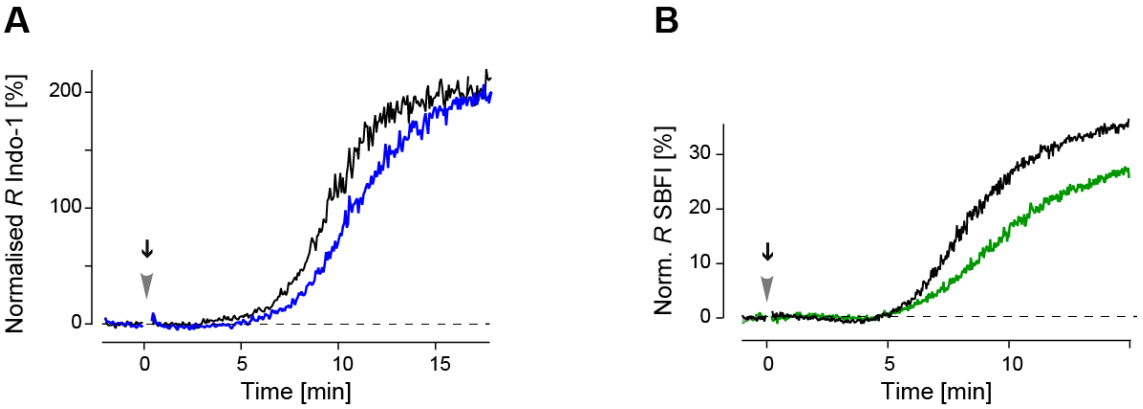

Figure 4.18 Extracellular ATP potentiates the DxS rise

(A) Time course plot of $[Ca^{2+}]_i$ under control conditions (blue) and when 100 μM ATP was added with DxS at t = 0 min (black). (B) As for (A) but for $[Na^{+}]_i$.

Having previously concluded that the channel involved while not directly activated by DAG, was likely gated by its metabolite, Figure 4.19 provides a flow chart of the pharmacological investigations that lead to TRPV3 being decided as the most likely candidate underlying the DxS induced cation rise.

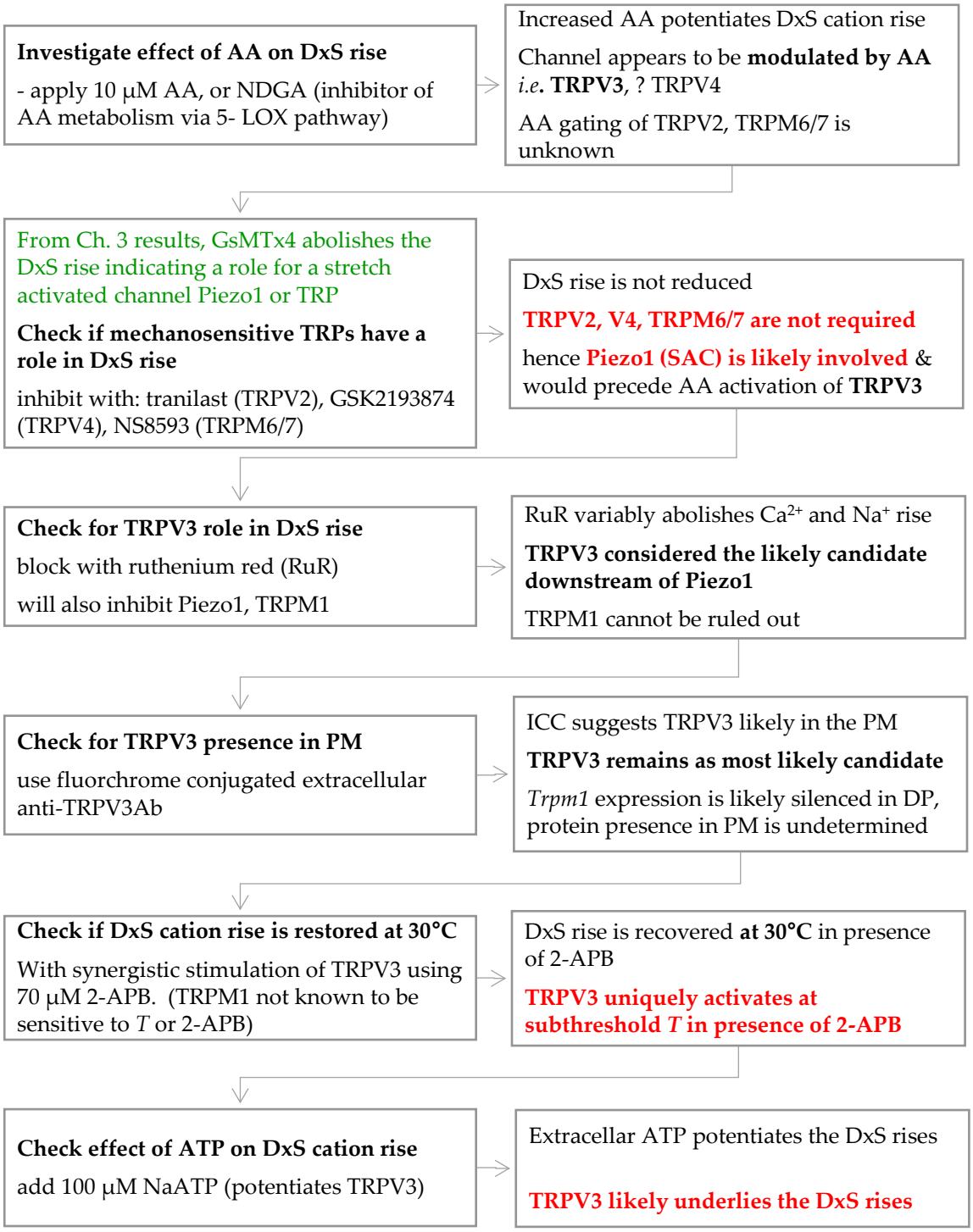

Figure 4.19 Pharmacology indicates TRPV3 likely underlies the DxS rises

Summary of the flow of pharmacological experiments which lead to the conclusion that TRPV3 activation underlies the DxS rises. Notably, mechanosensitive TRP channels are shown not to play a role in the DxS cation rise. Rather activation of the mechanosensitive Piezo1 channels is predicted to occur at the initiation of the signal transduction.

4.4 Discussion

4.4.1 Summary

The results presented in this chapter indicate that several TRP channels show a high level of mRNA expression and, using ICC, are likely co-expressed in the PM of thymocytes. In addition, I show that some of them can be activated and blocked by agonists and antagonists, a fact which likely confounded the pharmacological exploration presented. In addition to what was presented in Chapter 3, I found that the channel(s) underlying the DxS rises is/are 1) unlikely activated by DAG, but rather by a downstream signalling molecule, most likely a lipid like AA or its metabolite as the latter potentiated the rises. 2) In addition, I found that the rises were also potentiated by 70 μM 2-APB, a property that excludes a number of TRP channels listed in Table 3.2. 3) The cation rises are blocked by ≥2.5 μM RuR , 4) 100 μM ATP potentiated the rises and 5) 2-APB at 30°C rescues the rises, a temperature at which normally no rise can be elicited. These features are known characteristics of the channel TRPV3 and suggest that this channel likely underlies the DxS rises.

4.4.2 mRNA expression as a guide to channel expression

With scarce evidence of TRP channels in thymocytes, the level of gene expression in the various thymocyte populations was reviewed. In this thesis, I have referred to the BioGPS and ImmGen databases. The former provides information on the expression level in broad DP and SP thymocyte populations relative to a wide range of other tissue and cell types, while the later more specifically compares expression levels between multiple distinct subpopulations of immature and mature αβT cells. Understanding that the correlation between mRNA and protein expression is loose (Schwanhausser *et al.* 2011, Tian *et al.* 2004), it is nevertheless assumed that where a marked increase in mRNA transcription

occurs, the level of protein expression is also high. However, several times, this assumption led the research toward wrong candidate channels.

4.4.3 **ICC detection in the PM**

The ICC results indicated the anti-TRPC6, -C7, -A1, -V2, and -V3 antibodies were, in general, sensitive and specific to their respective immunogen which corresponded to an epitope in an extracellular domain of the protein. Moderate off-target binding was apparent with the anti-TRPV4 Ab_1 (Figure 4.2iii, bottom row). Also, despite its high mRNA expression, TRPC2 was poorly detected by ICC (Figure 4.8). These results suggest that either the antibody was insufficiently sensitive to the immunogen, the epitope was hidden, or as found in primary erythroid cells (Chu *et al.* 2004), detection of TRPC2 in the PM is negligible. In mice, expression of the TRPC2 protein appears predominantly in the vomeronasal organ and testis. Its trafficking to the PM may be impaired dependent upon splice variation (Hofmann *et al.* 2000).

Considering the negligible level of *Trpc7* mRNA reported by Inada *et al.* (2006, Fig. 1.13), the detection of the anti-TRPC7 Ab_1 was not anticipated (Figure 4.2iv, row 2). This could be explained by delayed protein degradation, or alternatively could indicate "off-target" Ab_1 binding to surface protein(s) that contain a similar epitope. If indeed TRPC7 is present, this highlights the issue of using mRNA data to extrapolate to channel protein presence in these cells. While not conclusive, the incomplete block by 10 μM Gd^{3+} and 80 μM 2-APB of the OAG rises could suggest the presence of the Gd^{3+}-insensitive TRPC7 channel, which is inhibited at considerably higher concentration (100 μM; Okada *et al.* 1999).

Acknowledging that variation between batches occurs, I note that the anti-TRPC6 and -TRPA1 antibodies have been validated by others (anti-TRPC6; Diez-Bello *et al.* 2019, anti-TRPA1; Sullivan *et al.* 2015). In this study the TRPC1,3,6,$7^{-/-}$ and

TRPA1$^{-/-}$ mice used were functional KOs with a mutation within the channel pore. Not unexpectedly, I found the proteins were still detected, albeit with a lesser intensity (data not shown).

4.4.4 Activation of TRP channels in the PM

Besides ICC, I was able to use "specific" activators of some TRP channels as a means to detect if they were functionally expressed in the PM and if they were involved in the DxS rises.

4.4.4.1 TRPA1

I confirmed the presence of DAG sensitive channels, specifically TRPA1 and likely TRPC7 using the activator OAG, a DAG analogue, together with specific channel blockers. The partial block of the OAG-induced cation rises by HC030031 and A967076 (as well as by 10 μM Gd^{3+}) is consistent with TRPA1 channels in the PM. However, TRPA1 does not underlie the DxS rise. I showed that the DxS rise was still present in thymocytes from a TRPA1$^{-/-}$ mouse.

Also present in the OAG rise is a Gd^{3+} insensitive channel which, based on the 2-APB block, is more likely TRPC7 than TRPV1 (see below).

4.4.4.2 TRPC6

TRPC6 can be activated by 5 μM hyperforin (Leuner *et al.* 2007). This chemical also caused a non-selective cation rise, consistent with the presence of TRPC6 channels in the PM. However, I found no evidence that supported involvement of TRPC6 in the DxS rises. Neither adding the TRPC6 antagonists norgestimate (Miehe *et al.* 2012) nor SKF96365 (He *et al.* 2017, Inoue *et al.* 2001), at 9 μM and 10 μM, respectively, blocked the DxS rises. Furthermore, instead of blocking TRPC6 channels, 70 μM 2-APB (Lievremont *et al.* 2005) potentiated the rises.

Strengthening this argument, and also providing evidence against involvement of TRPC7, -C3, and -C1, I showed that the DxS rises persisted in thymocytes from TRPC1,3,6,7$^{-/-}$ mice.

4.4.5 Exclusion of other candidate channels

I have also tested for other candidate channels proposed in Table 3.2. However, for most of these, it was not possible to find suitable agonists. Consequently, I used mostly "specific antagonists" to see if they affected the DxS rises. It is important to note that during the time of this research, I learnt that a lot of specific antagonists were rather "unspecific". As a consequence, in some instances and where possible, I used more than one blocker and based my deductions on the internal consistency between the two. Lacking expression systems for the various TRP channels, unfortunately, in many instances, it was not possible to provide positive controls. I do not think that this is a major issue as overall, the final conclusion is not based on the result of a single antagonist but rather on the consideration of a combined set of features.

4.4.5.1 **TRPC2**

Unfortunately, there are no selective blockers for this channel since in humans, *TRPC2* is a pseudogene. This channel was ruled out on the basis that it should have been inhibited by 2-APB (Zhang *et al.* 2010).

4.4.5.2 **TRPM2**

As with TRPC2, the 2-APB potentiation of the DxS rises does not support involvement of TRPM2. This channel is potently inhibited by 30 μM 2-APB (Togashi *et al.* 2008), however using this concentration I found the DxS rises were not notably changed (Figure 4.17D). Additionally, both PIP_2 (Tóth & Csanády 2012) and intracellular Ca^{2+} (Csanády & Törőcsik 2009) are obligate co-activators

of TRPM2. Therefore, my results that showed the DxS induced cation rises were significantly reduced when PLC activation was blocked (Figure 3.10A & B) and when background $[Ca^{2+}]_i$ was elevated do not favour TRPM2 involvement.

4.4.5.3 **TRPM3**

Having no specific TRPM3 channel blocker, it was ruled out as a likely candidate based on my 2-APB and edelfosine results (Figure 4.6A & B and Figure 3.10C & D). Specifically, Xu *et al.* (2005) have shown 100 μM 2-APB potently blocks TRPM3, which is contrary to the potentiation I observed with 70 μM 2-APB. Furthermore, like TRPM2, TRPM3 activation is dependent upon PIP_2 as a cofactor (Badheka *et al.* 2015) and hydrolysis of PIP_2 by PLC activity acts to negatively regulate TRPM3 (Tóth *et al.* 2015). Therefore, my finding that PLC inhibition significantly reduced the DxS rise, also suggests TRPM3 involvement is not likely.

4.4.5.4 **TRPM6/7**

These channels were excluded as the inhibition with 10 μM NS8593 (Chubanov *et al.* 2012, Ferioli *et al.* 2017) did not block the cation rises either. In addition, although most likely present in thymocytes (Jin *et al.* 2008a), the involvement of TRPM7 was not supported by the 2-APB potentiation nor by addition of the 5-LOX inhibitor NDGA, a reported potent inhibitor of TRPM7 (Chen *et al.* 2010).

4.4.5.5 **TRPV1**

The evidence for TRPV1 expression in the PM of DP thymocytes is not strong (Amantini *et al.* 2017, Amantini *et al.* 2004, Farfariello *et al.* 2012). But, since this channel is commonly co-expressed with TRPA1 (Schwartz *et al.* 2011, Staruschenko *et al.* 2010, Zhou *et al.* 2013), it seemed prudent to clarify that TRPV1

was indeed not involved in DxS rises. I found the addition of AMG9810, a potent selective TRPV1 blocker, did not reduce the rises.

4.4.5.6 **TRPV2**

Similarly, exposure to 75 μM tranilast (Aoyagi *et al.* 2010) did not notably reduce the DxS rises. Additionally, while not definitive, inhibition of the DxS $[Ca^{2+}]_i$ and $[Na^+]_i$ rises by edelfosine (a PLC inhibitor, Figure 3.10A & B) and by LY294002 (a PI_3K inhibitor, Figure 3.15A & B) does not support involvement of TRPV2. As depletion of PIP_2 reportedly has a crucial role in TRPV2 desensitisation (Mercado *et al.* 2010), I would expect the DxS rises to remain unchanged or perhaps potentiated when PIP_2 hydrolysis was impeded. This was not the case.

4.4.5.7 **TRPV4**

The involvement of TRPV4 was tested using 40 nM GSK2193874 (Thorneloe *et al.* 2012) and again, the DxS rises persisted. I note that the Ca^{2+} influx detected in ConA stimulated T cells was shown by Majhi *et al.* (2015) to require TRPV4 and TRPV1 activation. In agreement with Tellam and Parish (1987) I found in DP thymocytes stimulated with DxS, the addition of ConA at t = 20 min (Figure 3.2Figure 3.1A) caused an additive $[Ca^{2+}]_i$ rise that was indicative of activation of another Ca^{2+} permeable channel. Whilst I did not further investigate the channel(s) associated with this additive $[Ca^{2+}]_i$ rise, it perhaps indirectly provides evidence against TRPV4 and TRPV1 involvement in the DxS $[Ca^{2+}]_i$ rise.

Based on Table 3.2, Piezo1 was the remaining channel that is directly activated by mechanical force.

4.4.6 **RuR abolishes the rises**

Interestingly, concentrations >2.5 μM abolished the DxS rises when added at t = 1 min. However, when added at t = 12 min after DxS, the block was incomplete.

This observation may be explained by steric hindrance between the polyanionic DxS and the polycationic RuR . Nevertheless, the RuR block is highly suggestive of an involvement of a member of the TRPV family (Ahluwalia *et al.* 2002, Grubisha *et al.* 2014, Güler *et al.* 2002, Peier *et al.* 2002, Watanabe *et al.* 2003a), but does not rule out that other channels may also be blocked by it. Notably, TRPM1 (Shen *et al.* 2009) and Piezo1 are also sensitive to RuR (Coste *et al.* 2012).

4.4.7 2-APB at 30°C rescues the DxS rises

Having provided evidence in Chapter 3 that the DxS rises were abolished at temperatures ≤30°C, I have shown here that 70 μM 2-APB can rescue the rise at this subthreshold temperature. This sensitisation by 2-APB is a known and unique feature of TRPV3 (Chung *et al.* 2005, Chung *et al.* 2004) strongly suggesting that this channel underlies both cation rises.

In 3.6.7 (p. 207), I proposed that a thermally activated *STIM1*/*Orai1* sustained Ca^{2+} influx might act to negatively regulate TRPV3 activation. Supporting this proposal, it is notable that, in *STIM1*/*Orai1* transfected HEK293 cells, 50 μM 2-APB inhibits the thermally activated Ca^{2+} influx (Liu *et al.* 2019). Perhaps concurrent inhibition of STIM1/Orai channels and subthreshold activation of TRPV3 channels by 2-APB explains why the DxS cation rises not only recovered at subthreshold *T* but were also potentiated.

4.4.8 TRPV3 as most likely candidate

By process of elimination, I have arrived at TRPV3 as the most likely candidate based largely on two characteristics, namely its subthreshold sensitisation at 30°C by 2-APB plus its block by RuR, which in the presence of Ca^{2+} remains incomplete. The fact that elevated background $[Ca^{2+}]_i$ can inhibit cation permeation also supports this argument as raised Ca^{2+} increases Ca/CaM-binding to TRPV3 leading to channel inhibition (Phelps *et al.* 2010). In addition, this

channel also activates upon PIP_2 depletion and is potentiated with 100 μM ATP (Doerner *et al.* 2011)

Despite these considerations, I cannot fully exclude the possibility that TRPM1 or Piezo1 may be involved (see below). I note that both TRPV3 and TRPM1 are both "neglected" entities in their respective families (Irie & Furukawa 2014, Nilius *et al.* 2014). Additionally, Piezo1 has been known for about 15 years, but only recently has received much attention.

4.4.8.1 **Conductance and ion selectivity**

Among all TRPV channels, TRPV3 apparently has by far the largest single channel conductance (Yang & Zhu 2014). The question is if its partial conductance is sufficiently large to bring about the observed Na^+ rise. This may indeed be the case as the channel may undergo pore dilation to allow even $NMDG^+$ to permeate (Chung *et al.* 2005, Xiao *et al.* 2008), with some uncertainty remaining about how pore-dilation affects ion selectivity (Chung *et al.* 2005). Furthermore, there are reports in the literature that at 25 and 39°C, the conductances are 201 and 337 pS (Chung *et al.* 2004), respectively.

In addition to the Ca^{2+} entry, the large Na^+ conductance of this channel is well suited to maintain a high $[Na^+]_i$ for a considerable time as the extrusion/sequestration of Na^+ using pumps is very much smaller (Hille 2001). This $[Na^+]_i$ then drives a rise in $[Ca^+]_i$ for an equally long time, by bringing in additional Ca^{2+} via transport activation. As well, activation of counter currents facilitates restoration of the resting membrane potential and, in doing so, increases the electrical driving force for Ca^{2+} entry through TRPV3.

Originally, TRPV3 was described as a channel with considerable Ca^{2+} permeability (Peier *et al.* 2002, Smith *et al.* 2002, Xu *et al.* 2002). However, more recent data indicates that this may not be the case. In fact, bovine TRPV3 show a

large single channel conductance for Na^+ at physiological potentials (~73 pS; Schrapers *et al.* 2018). There are several known splice variants in mice (Smith *et al.* 2002, Wang 2006, Yang & Zhu 2014), but unfortunately, most of them have not been investigated in regard to ion-selectivity or conductance remains to be investigated in the most variants. However, it has been found that colocalization of a short variant, which cannot form a functional channel, with functional TRPV3 channels significantly increases the channel activity (Wang 2006).

Whether or not TRPV3 has an additional permeation pathway, that activates following channel hysteresis, remains to be investigated. However, I note that at least for TRPM3, two ion permeation pathways have been described. The canonical pore had a partial conductance for both Na^+ and Ca^{2+} with strong rectification in the physiological range (Vriens *et al.* 2014). The non-canonical pathway had a much larger conductance and loss of rectification.

4.4.8.2 **Ca^{2+} and Mg^{2+} sensitivity**

High-affinity channel inhibition has been described for Ca^{2+}-binding to an area around Asp-641 in the pore loop area (Luo *et al.* 2012). In addition, this site is also important for RuR binding. Once Ca^{2+} is bound, RuR is in competition for channel block. This is consistent with my observation that once the Ca^{2+} had reached a plateau, the block by RuR was incomplete.

However, Ca^{2+} together with CaM can also affect the channel from the intracellular side by forming a Ca^{2+}–CaM complex. Since this complex maintains the channel in a low activity state (Xiao *et al.* 2008), this could be the explanation for the observation that elevated background Ca^{2+} blocked the channel. This also occurs in a realistic concentration as the first Ca^{2+} binding to CaM is in the range of ~100 nM; *i.e.* just around the resting background $[Ca^{2+}]_i$ (Persechini & Cronk 1999). Notably, the Ca^{2+}–CAM inhibition of TRPV3 is attenuated in response to

repeated stimulation leading to channel sensitisation (Phelps *et al.* 2010, Xiao *et al.* 2008).

It is known that Mg^{2+} can inhibit TRPV3 also both from the intra- and extracellular sides. It apparently does this by reducing the unitary conductance with little influence on the open probability, again with Asp-641 (see above) identified as the site of action on the extracellular side. With 10 mM Mg^{2+}, a channel block of ~60% was seen (Luo *et al.* 2012), largely consistent what I saw in my data. Unfortunately, no data for higher concentrations was given. The intracellular binding site is in the C-terminus of the channel (Luo *et al.* 2012).

4.4.8.3 **Thermosensitivity**

TRPV3 is a channel sensitive within the warm range (~31 – 39°C, Peier *et al.* 2002), but there are reports using fast temperature changes that on its own, temperature activates this channel >54°C (Yao *et al.* 2011). However, its sensitivity is increased at depolarised voltages (Xu *et al.* 2002), with increased Ca^{2+} influx at a high rate of temperature change, if repeatedly stimulated (Liu & Qin 2017, Xiao *et al.* 2008) and if exposed to plant alkaloids like camphor and citral (Stotz *et al.* 2008) or the chemical 2-APB (Chung *et al.* 2004). This suggests that in contrast to other thermo-sensitive channels, its activation may reflect some "coincidence detection", whereby within the warm range, at least two factors may have to cooperate to lead to channel opening. This "sensitisation", consistent with what I have found, seems to be a unique feature of TRPV3.

4.4.8.4 **Mechanosensitivity**

Results in Chapter 3 indicated that the DxS induced $[Ca^{2+}]_i$ and rises $[Na^+]_i$ were sensitive to GsTMx4. To the best of my knowledge, mechanosensation is not an explicit property of TRPV3. However, I would like to point out that in a recent review Liu and Montell (2015) suggested that "most TRPs are actually

mechanosensitive channels, which undergo conformational changes in response to tension imposed on the lipid bilayer, resulting in channel gating." Consequently, mechanosensation may not be a distinctive feature as first assumed.

4.4.8.5 **Presence in the membrane**

Upon Ca^{2+} influx, a number of channels can be inserted into the membrane quite quickly (reviewed by Montell 2004). For example, during neurite growth, in response to epidermal growth factor stimulation, TRPC5 channels are rapidly inserted in the PM ($t_{½}$ = 49 ± 2.4 s, Bezzerides *et al.* 2004). Furthermore, these authors showed the PI_3K dependent insertion was inhibited by LY294002. The delay in the onset of the DxS rises is consistent with the idea that TRPV3 channels may not be in the membrane and require insertion first. However, based on the data showing that elevated background $[Ca^{2+}]_i$ blocks the rises, such a scenario is unlikely. In addition, insertion from the endosome would preclude mechano-sensation. Consequently, TRPV3 channels are very likely already present in the PM. This idea, however, does not rule out that its rate of insertion or removal may not be affected by the signalling cascade and/or the Ca^{2+} rise.

4.4.8.6 **PIP_2 depletion**

Even though PIP_2 is a universal channel modulator (reviewed by Hilgemann *et al.* 2001, Ramsey *et al.* 2006), in the case of TRPV3, its hydrolysis potentiates the channel (Doerner *et al.* 2011) via an interaction in the C-terminus. In this light, the experiment with DAG might have increased PIP_2 availability, but at the same time, its activation of PKC may have occluded the expected inhibition of the channel.

4.4.8.7 **Potentiation by extracellular ATP**

Another feature consistent with TRPV3 is that the influx was potentiated using 100 μM ATP. This has also been seen Doerner *et al.* (2011). This feature further adds to the growing body of evidence that TRPV3 is the most likely channel.

4.4.8.8 **Lipid modulation**

It has been reported that polyunsaturated acids like AA are capable of potentiating TRPV3 (Hu *et al.* 2006) consistent with what I saw. In addition, 5-LOX inhibition also showed a potentiation. This is most likely due to the fact that when 5-LOX is blocked, the concentration of AA in the PM increases.

4.4.8.9 **Homo- vs. heteromeric channels**

It has been reported that TRPV3 and TRPV1 channels may form heteromeric channels (Smith *et al.* 2002). In HEK293 cells, these channels exhibit unique activation properties that derive from both proteins and are influenced by subunit stoichiometry (Cheng *et al.* 2012). While these proteins are co-expressed in neural cells (Brown *et al.* 2013), there is no evidence confirming that such a heteromeric configuration exists in thymocytes or related lymphocytes.

4.4.9 **Alternative 1: TRPM1**

The attractiveness of TRPM1 lies with the fact that it is associated with a multimolecular signalling complex containing GRP179, which has a binding site for HS (Orlandi *et al.* 2013, Orlandi *et al.* 2018). TRPM1 sensitivity to 2-APB has so far not been reported, however it shares the block by RuR (Shen *et al.* 2009). Notably, this channel has a large partial conductance for Na^+, which also makes it very attractive in this instance (Oancea *et al.* 2009). While activation by PIP_2 depletion remains to be clarified, PIP_2 hydrolysis and DAG generation indirectly modulate the channel. Specifically, DAG-dependent activation of PKC removes

an inhibitory Mg^{2+} block of TRPM1 (Rampino & Nawy 2011). While TRPM8 and more recently TRPM2, -M3, -M4 and -M5 are reportedly thermosensitive (Held *et al.* 2015, Tan & McNaughton 2016, Tominaga 2007), to my knowledge this feature has not been reported for TRPM1. Consequently, despite several attractive features, TRPM1 involvement in the cation rises is not very likely.

4.4.10 **Alternative 2: Piezo1**

This channel shares a number of properties with TRPV3, among them mechano-sensation and block by RuR (Coste *et al.* 2012). The block by 2.5 μM RuR is half of the IC_{50} for this channel suggesting that it is unlikely that this channel is involved as the conduit to cation permeation. Piezo1 channels are potently inhibited by GsMTx4, however it is important to note that the inhibition is not direct. Rather the gating of the channel is modified by GsMTx4 insertion into the lipid bilayer altering lipid composition and tension transduction to the channel (Suchyna *et al.* 2004). The reason to keep this channel in consideration is because it quickly activates and inactivates (Gottlieb & Sachs 2012, Wu *et al.* 2017b, Zhao *et al.* 2016). Because of this, there is a possibility that this channel could have activated immediately upon DxS addition and escaped detection. Because it can pass a significant amount of Ca^{2+}, it then could have kick-started the signalling cascade by priming LFA-1. Without data during the gap, it is futile to speculate about Piezo1 involvement any further.

4.4.11 **Conclusion**

After excluding a considerable number of channel candidates from several families and based on the pharmacological properties uncovered, I am concluding that the most likely candidate gating the cation rises observed in DP thymocytes upon stimulation with DxS is TRPV3. However, I have not been able to test this idea in KO mice. In contrast to the outset of this project thinking that

DxS caused a Ca^{2+} rise, I have also come to the conclusion that there is a much larger concurrent Na^{+} rise present in these cells. Without further quantification of the size of the Na^{+} rise and involving realistic simulations, I may be tempted to speculate that a significant component of the Ca^{2+} rise may in fact be driven by the accumulation of Na^{+}.

In the next chapter, possible physiological and immunological implications will be explored

5 Physiological and immunological implications

Ca^{2+} is without doubt a pivotal messenger in a myriad of cellular functions. In T cell development it plays a decisive role in regulating the migration, proliferation, differentiation, apoptotic death by instruction or neglect, and selection of thymocytes. Discreet Ca^{2+} flickers, increased oscillations and large global rises have been shown to effect thymocyte migration, arrest and sustained stromal cell–thymocyte interaction, respectively (Bhakta & Lewis 2005, Bhakta *et al.* 2005, Bunnell *et al.* 2011, Melichar *et al.* 2013, Ross *et al.* 2014, Wei *et al.* 2009). Furthermore, it appears that the amplitude of the $[Ca^{2+}]_i$ rise associated with positive selection events may reflect the "strength" of TCR–pMHC engagement, and with recurring TCR–pMHC interactions there is an associated elevation in $[Ca^{2+}]_i$ (Fu *et al.* 2013, Ross *et al.* 2014). I propose that in some DP thymocytes undergoing early positive selection, the $[Ca^{2+}]_i$ rise induced by TCR signalling may be elevated by Ca^{2+} entering synergistically through TRPV3 channels. Dependent upon repeated stimulation, this non-selective cation channel is activated by a signalling cascade triggered by the CD8β coreceptors interacting with HS on stromal cells. Notably, this mechanism is restricted to thymocytes in which the CD8 coreceptor is minimally sialylated.

For this thesis, I examined a DxS induced signalling pathway that leads to a sustained $[Ca^{2+}]_i$ rise of ~160 nM. This pathway is specific to a subpopulation of DP thymocytes. Even though this $[Ca^{2+}]_i$ rise has been known for over 30 years, the molecular elements that underpin this rise remained unknown. As it is hypothesised that the DxS $[Ca^{2+}]_i$ rise may mimic a similar rise recorded in preselection DP thymocytes during rosette formation with $cTEC^{hi}$, I am interested in understanding the mechanisms that lead to this Ca^{2+} influx. Furthermore, I am particularly intrigued by the signalling pathway activated following CD8β

binding DxS, this interaction inducing the $[Ca^{2+}]_i$ flux that normally occurs in preselection αβTCR DP thymocytes during their adhesion to $cTEC^{hi}$ (Simon Davis 2015).

Notably, the $[Ca^{2+}]_i$ rise is dependent upon either DxS or HS binding to CD8β on preselection DP thymocytes (Simon Davis 2015). The addition of DxS is proposed to cross-link and stimulate multiple surface receptors, including at least both CD8β and LFA-1. However, adding an equivalent amount of heparin to a thymocyte suspension does not reproduce the rise, this discrepancy probably being due to heparin having a much lower mol. wt. than DxS (*i.e.*, 10–15 kDa *vs*. 500 kDa) and thus unable to cross-link CD8 molecules as effectively as DxS (Simon Davis 2015). Also, unlike DxS, heparin has not been shown to bind LFA-1 (Vermot-Desroches *et al.* 1991) however, during cell–cell interactions, LFA-1 would likely be activated by its endogenous ligand ICAM-1.

Altogether, my results from Chapters 3 and 4 indicate that the channel underlying the DxS induced $[Ca^{2+}]_i$ rise is 1) a non-selective cation channel with a large partial conductance for Na^+, 2) thermosensitive and sensitised by 2-APB at subthreshold temperatures, 3) mechanosensitive, 4) blocked by increased background $[Ca^{2+}]_i$, 5) activated downstream of PLC-γ1 or -β2, 6) not gated by either IP_3 or DAG, 7) potentiated by AA, 2-APB and ATP, 8) enhanced by PKC and/or PKA phosphorylation, and 9) blocked by RuR.

Perhaps excluding direct mechanical gating, TRPV3 is a channel that has all these properties. The functional and immunological implications of this conclusion will be discussed below.

5.1 Functional implications

The process of selection is rigorous and markedly costly, with only 3–5% of DP thymocytes maturing to the SP phase of development (Merkenschlager *et al.* 1997). Within the large pool of preselection DP thymocytes ($88.39 \pm 60 \cdot 10^6$) ~66% will die by neglect because they express nascent αβTCRs that do not sufficiently engage with pMHC molecules (Sawicka *et al.* 2014). Of the remaining DP thymocytes, ~91% will express αβTCRs that strongly bind pMHC complexes. To prevent maturation of likely autoreactive T cells, excessively avid αβTCR–pMHC interaction activates negative selection signalling that triggers SOCE mechanisms to cause apoptosis and clonal deletion.

In contrast, preselection DP thymocytes expressing αβTCR that bind pMHC molecules, with the bond duration and strength reaching an optimal range, receive positive selection signals. These activated DP thymocytes continue to undergo further interactions with stromal cells as they make their way back to the medulla. Increasingly stringent testing of the TCR–pMHC bond strength ensures tolerance to self-peptides as they mature to become SP thymocytes. The outcome of rigorous selection is the generation of a pool of peripheral T cells; with an average of 2×10^6 (Casrouge *et al.* 2000) and 2×10^7 (Naylor *et al.* 2005) clones in mice and humans, respectively.

5.2 A proposed role for TRPV3

A synergistic Ca^{2+} influx via TRPV3 activation may provide a mechanism that 1) enhances positive selection of thymocyte clones that risk death by neglect due to unsatisfactory MHC engagements and 2) fine tune selection of clones that border on self-reactivity. Specifically, activated downstream of MHC-I–CD8–HS binding, this Ca^{2+} rise could synergistically augment TCR/CD3 dependent Ca^{2+} signalling and influence selection outcome, thus refining the repertoire of T cells.

Figure 5.1 & 5.2 illustrate the proposed role of TRPV3 when TCR–pMHC-I binding is absent, suboptimal or super-optimal.

5.3 Without TCR–pMHC-I interaction

In preselection thymocytes, MHC-I–CD8 binding without TCR engagement has been suggested to promote death by neglect (Grebe *et al.* 2004). Where the TCR fails to engage with the MHC (Figure 5.1A), I suggest CD8 signalling activated by binding to both MHC-I and HS (augmented during rosette formation on $cTEC^{hi}$) may hasten the deletion of such T cell clones. In fact, I propose that without TCR engagement, TRPV3 channel activation and the resultant sustained rise in Na^+ (green) and Ca^{2+} (blue) triggers "death by instruction" signalling.

5.4 With sub-optimal TCR–pMHC-I interaction

In contrast, when thymocyte clones express TCRs that sub-optimally engage pMHCs, activation of TRPV3 may play an important role in prolonging their survival by adding to a basal $[Ca^{2+}]_i$ rise of ~250–550 nM (Figure 5.1C). Depicted in Figure 5.1D, initial CD8β–MHC–HS binding (black dashes) stabilises suboptimal TCR–pMHC binding (red dashes) and initiates signalling that enables ongoing survival of clones that otherwise will die by neglect. Repeated transient TCR–pMHC evoked Ca^{2+} entry (red) summates with the TRPV3 dependent Ca^{2+} influx (blue). While the concomitant Na^+ influx likely helps to maintain the Ca^{2+} rise. Positively selecting cells have been shown to increase their background $[Ca^{2+}]_i$ overtime (Nakayama *et al.* 1992, Ross *et al.* 2014). Therefore, despite suboptimal TCR/CD3 signalling, this synergistic Ca^{2+} entry may eventually lead positive selection of these clones. Notably, the identity of this other Ca^{2+} channel remains unclear.

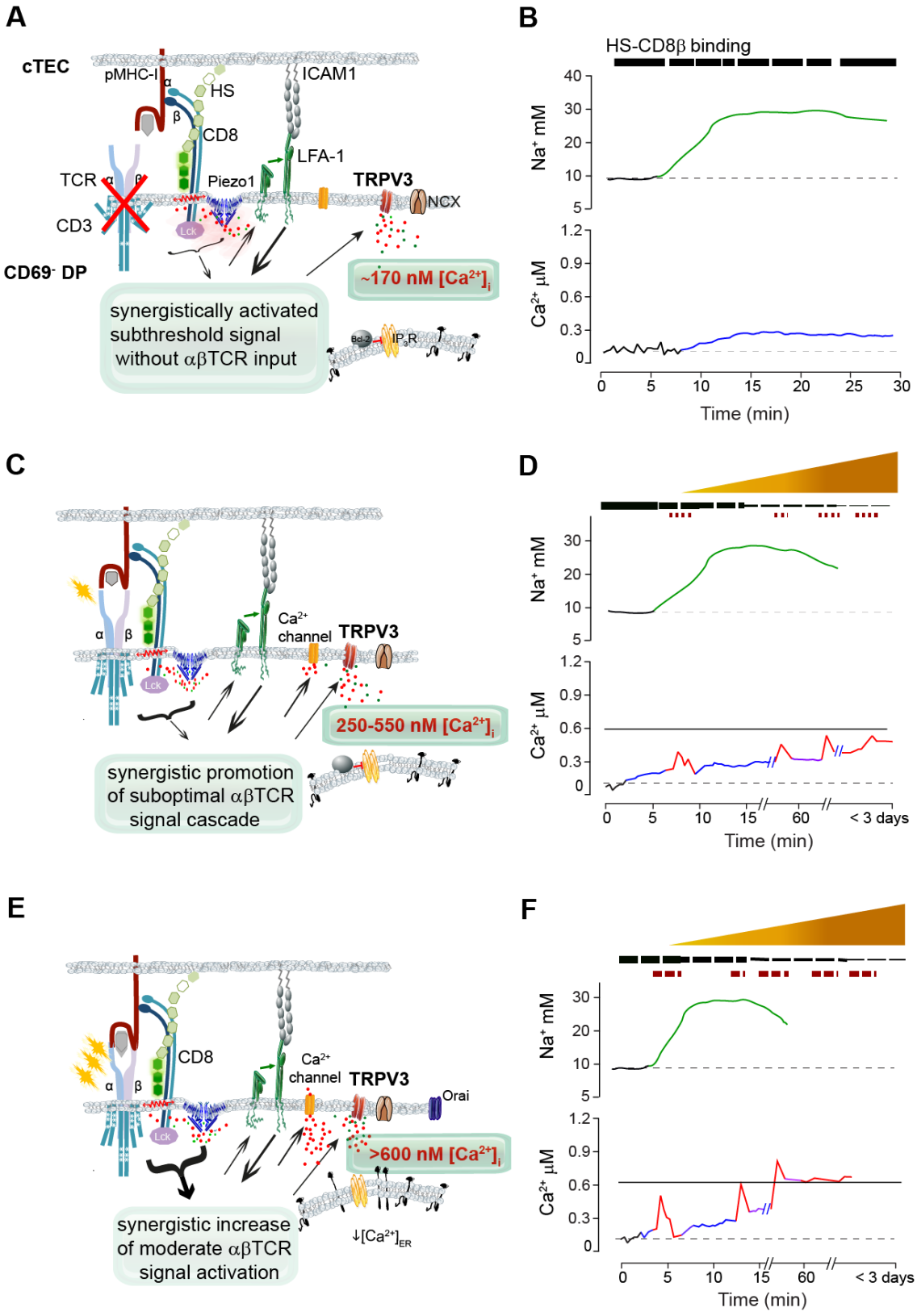

Figure 5.1 TRPV3 enhances the $[Ca^{2+}]_i$ rise evoked by TCR/CD3 signalling

(A) Without TCR–pMHC engagement synergistic signalling downstream of HS–CD8β and ICAM1–LFA-1 interaction results in TRPV3 activation. (B) Dependent upon the strength and duration of HS–CD8β interaction (black dash), activation of TRPV3 channels leads to sustained concomitant $[Na^+]_i$ and $[Ca^{2+}]_i$ rises sufficient to promote 'death by instruction' signalling pathways. (C) In suboptimal TCR–pMHC–CD8 engagement, HS–CD8β binding synergistically enhances the signalling cascade. The $[Ca^{2+}]_i$ rise is within the range for promotion of positive selection. (D) Concurrent CD8β–HS induced TRPV3 Ca^{2+} entry (blue) adds to a $[Ca^{2+}]_i$ rise (red) evoked by suboptimal TCR–pMHC interaction and avidity (dark red dash). Increasing CD8β sialylation (orange triangle) progressively impedes the strength and duration of HS–CD8β interaction (black dash). TRPV3 concomitant supporting Na^+ rise (green). (E) Concurrent with overly moderate TCR–pMHC–CD8 engagement, HS–CD8β binding synergistically enhances the signalling cascade. The $[Ca^{2+}]_i$ rise exceeds the range for positive selection. (F) The amplitude of Ca^{2+} transients evoked by TCR–pMHC interaction and avidity (dark red dash) is increased by the elevated basal $[Ca^{2+}]_i$ due to TRPV3 activation, to exceed the positive selection limit (black line).

Crucially, the TRPV3 activation mechanism is curtailed as the thymocyte matures. Progressively sialylation of CD8β in response to thymocyte activation, sterically hinders MHC-I–CD8–HS binding and beneficially decreases the sensitivity of the TCR–pMHC allowing the clone to undergo more stringent testing as it returns to the medulla. Activation of this mechanism in this population is predicted to expand the repertoire of the peripheral T cell pool at the lower (weakly binding) end as illustrated in Figure 5.2.

5.5 With moderate TCR–pMHC-I interaction

Finally, shown in Figure 5.1E & F is a proposed mechanism for redirecting selection in a population of preselection thymocytes when the TCR–pMHC-I bond strength is near the self-reactive/negative selection threshold. Notably, this population is thought to be small as activation of TRPV3 mechanism will only occur if CD8β sialylation is low and where background $[Ca^{2+}]_i$ is not already elevated in response to prior activation of the TCR/CD3 signalling complex. In these preselection thymocyte clones, concomitant activation of TRPV3 (down-stream of MHC-I–CD8–HS stimulation) and the unknown Ca^{2+} permeable channel (activated by TCR/CD3 signalling) could rapidly raise background $[Ca^{2+}]_i$

so that it exceeds the upper limit for positive selection signalling which is reportedly >600nM (F. black line). Whether the signalling pathways activated by such a $[Ca^{2+}]_i$ increase now direct differentiation pathways leading to "specialised" T cells development or instead promote a negative selection outcome remains to be investigated. Inhibition of the TRPV3 mechanism in this population of thymocytes may result in the unwanted export of T cells, that verge on being self-reactive, to the peripheral pool.

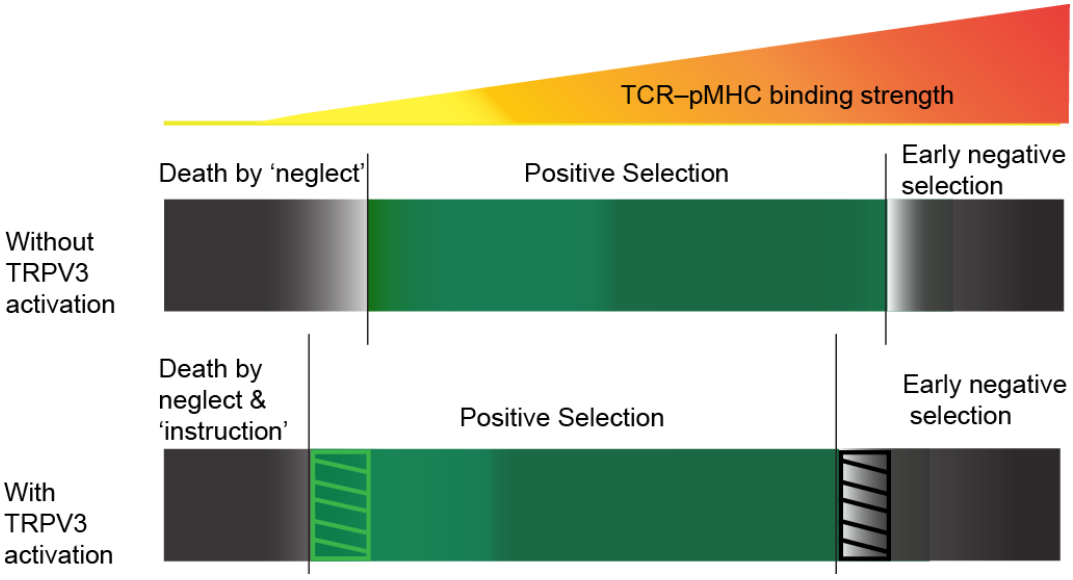

Figure 5.2 Proposed selection tuning with TRPV3 activity

Activation of TRPV3 in preselection thymocytes alters the range of thymocyte survival. In suboptimal TCR–pMHC binding, TRPV3 activity will promote positive selection (green striped). TRPV3 activity in cells which bind with moderate/strong force will fail positive selection (black striped).

5.6 Possible implications to disease

TRPV3$^{-/-}$ mice do not have an overt T cell phenotype (Bertin & Raz 2016). However, this observation does not rule out possible subtle changes to the range of the T cell repertoire. This remains to be investigated.

I have shown that the activation of TRPV3 was inhibited in conditions where background $[Ca^{2+}]_i$ was already raised by at least 60 nM. Interestingly, thermally activated STIM/Orai1 has been shown to raise background $[Ca^{2+}]_i$ and therefore could potentially inhibit TRPV3 activation during preselection thymocytes—cTEC^{hi} interactions. As activation of the inhibitory Orai1 evoked Ca^{2+} influx occurs as temperatures fall from 39 to 37°C, perhaps fever spikes in this range during childhood results in adverse changes in the peripheral T lymphocyte repertoire.

As indicated in Figure 5.2, I proposed inhibition of TRPV3 during thymopoiesis results in a shift in positive selection, increasing the likelihood of maturation of thymocytes that verge on being self-reactive. Having these clones in the peripheral T cell pool, would potentially increase the chance of developing an autoimmune disorder if TRPV3 channels were to reactivate as a consequence of reduced surface sialylation.

Furthermore, inhibition of TPRV3 during thymopoiesis would narrow the range of survival of clones found at the lower end of TCR avidity scale (Figure 5.2). Preselection thymocytes with poor TCR–pMHC binding capability may not sufficiently increase $[Ca^{2+}]_i$ and so fail to be positively selected. Loss of these potentially beneficial T cells clones from the peripheral pool may result in a weaker immune system where activation of the immune system response may be poorer.

A reduced TCR repertoire may result in less effective recognition when rare harmful endogenous or exogenous antigens are presented. In humans, this might be associated with an increased susceptibility to infection, particularly with ageing (Naylor et al 2005), and perhaps a poorer prognosis in some cancers (Cui.et al 2018). While it is interesting to note that inflammatory skin disorders are linked to TRPV3 dysfunction (Wang et al 2017), to my knowledge, association of these disorders with an altered T cell repertoire has not been studied.

Sialylation of CD8 in mature inactive mouse T cells impedes the mechanism I believe leads to TRPV3 activation. Notably, following mitogenic activation of Jurkat and mouse splenic T cells, Majhi *et al.* (2015) showed at least a 2-fold increase in TRPV1 >TRPV4 >TRPV3 >TRPV2 in the PM. However, while these authors detected activation of TRPV1 and TRPV4 they did not detect activation of TRPV3 downstream of either ConA or anti-CD3/anti-CD28 Ab activation. Perhaps because the stimuli provided did not lead to sensitisation of TRPV3, or as I have shown, a prior increase in $[Ca^{2+}]_i$ would have an inhibitory effect on TRPV3. Nevertheless, following T cell activation, I propose CD8 de-sialylation could re-enable the mechanism that leads to TRPV3 activation.

Sensitisation of TRPV3 by repeated multiple stimuli, including AA, inflammatory mediators and fever, would enable a sustained Na^+ and Ca^{2+} influx. Whether such an increase in background $[Ca^{2+}]_i$ enhances Ca^{2+} cellular functions such as proliferation of activated T cells or cytotoxic activity, remains to be explored. Importantly, activation of such a mechanism would be curtailed by sialylation of CD8 with inactivation of the inflammatory response.

This raises the question as to what would happen if CD8 sialylation levels were pathologically impaired. Significantly, in mature T cells, TCR/CD3 expression level is higher (Guidos *et al.* 1990) and their aggregation is thought to enable amplification of TCR/CD3 signal strength. If combined with unimpeded HS–

CD8β–MHC-I binding and subsequent TRPV3 activation, I propose the resultant Na^+ and Ca^{2+} influx could prime the TCR sensitivity, in doing so, increase the response in some clones to self-antigen–MHC complex ligation. In conditions of acquired idiopathic autoimmune disorders, perhaps triggered by viral infection, investigation of T cell sialylation state could perhaps prove interesting. As TRPV3 protein has been reported in human peripheral T cells (Majhi *et al.* 2015) perhaps this channel might present a novel therapeutic target in the future management of autoimmune disorders linked with abnormal sialylation.

5.7 Concluding remark

Throughout the course of this project, my thinking about selection shifted from involving Ca^{2+} rises to concomitant rises of both Na^+ and Ca^{2+} and finally to a large Na^+ influx together with a small Ca^{2+} rise. Given that Na^+ rises have not received much attention in immunology and since in several systems Na^+-dependent signalling has been described (Rishal *et al.* 2003, reviewed by Rose & Verkhratsky 2016, Verkhratsky *et al.* 2017), I would not be surprised if in the near future, such signalling outcomes may be uncovered.

References

Adebiyi A, Narayanan D, Jaggar JH. 2011. Caveolin-1 assembles type 1 inositol 1,4,5-trisphosphate receptors and canonical transient receptor potential 3 channels into a functional signaling complex in arterial smooth muscle cells. *J Biol Chem* **286**: 4341-4348

Affaticati P, Mignen O, Jambou F, Potier MC, Klingel-Schmitt I, Degrouard J, . . . Cohen-Kaminsky S. 2010. Sustained calcium signalling and caspase-3 activation involve NMDA receptors in thymocytes in contact with dendritic cells. *Cell Death Differ* **18**: 99-108

Ahluwalia J, Rang H, Nagy I. 2002. The putative role of vanilloid receptor-like protein-1 in mediating high threshold noxious heat-sensitivity in rat cultured primary sensory neurons. *Eur J Neurosci* **16**: 1483-1489

Albarran L, Dionisio N, Lopez E, Salido GM, Redondo PC, Rosado JA. 2014. STIM1 regulates TRPC6 heteromultimerization and subcellular location. *Biochem J* **463**: 373-381

Albarrán L, Lopez JJ, Dionisio N, Smani T, Salido GM, Rosado JA. 2013. Transient receptor potential ankyrin-1 (TRPA1) modulates store-operated Ca^{2+} entry by regulation of STIM1-Orai1 association. *Biochimica et Biophysica Acta (BBA) - Mol Cell Res* **1833**: 3025-3034

Alexander SP, Mathie A, Peters JA. 2011. Guide to receptors and channels (grac), 5th edition. *Br J Pharmacol* **164** S166 - S174

Alpizar YA, Gees M, Sanchez A, Apetrei A, Voets T, Nilius B, Talavera K. 2013. Bimodal effects of cinnamaldehyde and camphor on mouse TRPA1. *Pflug Arch Eur J Phy* **465**: 853-864

Altimimi HF, Schnetkamp PP. 2007. Na^+/Ca^{2+}-K^+ exchangers (NCKX): Functional properties and physiological roles. *Channels* **1**: 62-69

Altin JG, Pagler EB, Parish CR. 1994. Evidence for cell surface association of CD2 and LFA-1 (CD11a/CD18) on T lymphocytes. *Eur J Immunol* **24**: 450-457

Altschul SF, Wootton JC, Gertz EM, Agarwala R, Morgulis A, Schaffer AA, Yu YK. 2005. Protein database searches using compositionally adjusted substitution matrices. *FEBS J* **272**: 5101-5109

Alvarez-Collazo J, Alonso-Carbajo L, Lopez-Medina AI, Alpizar YA, Tajada S, Nilius B, . . . Alvarez JL. 2014. Cinnamaldehyde inhibits L-type calcium channels in mouse ventricular cardiomyocytes and vascular smooth muscle cells. *Pflugers Arch* **466**: 2089-2099

Alves LA, Coutinho-Silva R, Savino W. 1999. Extracellular ATP: Further modulator in neuroendocrine control of the thymus. *NeuroImmuno Modulation* **6**: 81-89

Amantini C, Farfariello V, Cardinali C, Morelli MB, Marinelli O, Nabissi M, . . . Santoni G. 2017. The TRPV1 ion channel regulates thymocyte

differentiation by modulating autophagy and proteasome activity. *Oncotarget* **8**: 90766-90780

Amantini C, Mosca M, Lucciarini R, Perfumi M, Morrone S, Piccoli M, Santoni G. 2004. Distinct thymocyte subsets express the vanilloid receptor VR1 that mediates capsaicin-induced apoptotic cell death. *Cell Death Differ* **11**: 1342-1356

Amarouch MY, Syam N, Abriel H. 2013. Biochemical, single-channel, whole-cell patch clamp, and pharmacological analyses of endogenous TRPM4 channels in HEK293 cells. *Neurosci Lett* **541**: 105-110

Ambudkar IS, Ong HL. 2007. Organization and function of TRPC channelosomes. *Pflug Arch Eur J Phy* **455**: 187-200

Amcheslavsky A, Wood ML, Yeromin AV, Parker I, Freites JA, Tobias DJ, Cahalan MD. 2015. Molecular biophysics of Orai store-operated Ca^{2+} channels. *Biophys J* **108**: 237-246

Anderson M, Kim EY, Hagmann H, Benzing T, Dryer SE. 2013. Opposing effects of podocin on the gating of podocyte TRPC6 channels evoked by membrane stretch or diacylglycerol. *Am J Physiol Cell Physiol* **305**: C276-289

Andersson DA, Gentry C, Moss S, Bevan S. 2008. Transient receptor potential A1 is a sensory receptor for multiple products of oxidative stress. *J Neurosci* **28**: 2485-2494

Antigny F, Sabourin J, Saüc S, Bernheim L, Koenig S, Frieden M. 2017. TRPC1 and TRPC4 channels functionally interact with STIM1L to promote myogenesis and maintain fast repetitive Ca^{2+} release in human myotubes. *Biochimica et Biophysica Acta (BBA) - Mol Cell Res* **1864**: 806-813

Aoyagi K, Ohara-Imaizumi M, Nishiwaki C, Nakamichi Y, Nagamatsu S. 2010. Insulin/phosphoinositide 3-kinase pathway accelerates the glucose-induced first-phase insulin secretion through TRPV2 recruitment in pancreatic β-cells. *Biochem J* **432**: 375

Appay V, Sauce D. 2014. Naive T cells: The crux of cellular immune aging? *Exp Gerontol* **54**: 90-93

Armstrong CM, Bezanilla F. 1973. Currents related to movement of the gating particles of the sodium channels. *Nature* **242**: 459-461

Artyomov MN, Lis M, Devadas S, Davis MM, Chakraborty AK. 2010. CD4 and CD8 binding to MHC molecules primarily acts to enhance Lck delivery. *Proc Natl Acad Sci USA* **107**: 16916-16921

Astashkin EI, Khodorova AB, Surin AM. 1993. Arachidonic acid abolishes the mitogen-induced increase in cytosolic free Ca^{2+} and intracellular pH_i in rat thymocytes. *FEBS Lett* **329**: 72-74

Bachmann MF, Barner M, Kopf M. 1999. CD2 sets quantitative thresholds in T cell activation. *J Exp Med* **190**: 1383-1392

Badheka D, Borbiro I, Rohacs T. 2015. Transient receptor potential melastatin 3 is a phosphoinositide-dependent ion channel. *J Gen Physiol* **146**: 65-77

Badou A, Jha MK, Matza D, Flavell RA. 2013. Emerging roles of L-type voltage-gated and other calcium channels in T lymphocytes. *Front Immunol* **4**: 243-243

Badou A, Jha MK, Matza D, Mehal WZ, Freichel M, Flockerzi V, Flavell RA. 2006. Critical role for the β regulatory subunits of Ca_V channels in T lymphocyte function. *Proc Natl Acad Sci USA* **103**: 15529-15534

Baez D, Raddatz N, Ferreira G, Gonzalez C, Latorre R. 2014. Gating of thermally activated channels. *Curr Top Membr* **74**: 51-87

Bai CX, Giamarchi A, Rodat-Despoix L, Padilla F, Downs T, Tsiokas L, Delmas P. 2008. Formation of a new receptor-operated channel by heteromeric assembly of TRPP2 and TRPC1 subunits. *EMBO Rep* **9**: 472-479

Baker K, Raemdonck K, Dekkak B, Snelgrove RJ, Ford J, Shala F, . . . Birrell MA. 2016. Role of the ion channel, transient receptor potential cation channel subfamily V member 1 (TRPV1), in allergic asthma. *Resp Res* **17**: 67

Baker RG, Hsu CJ, Lee D, Jordan MS, Maltzman JS, Hammer DA, . . . Koretzky GA. 2009. The adapter protein SLP-76 mediates "outside-in" integrin signaling and function in T cells. *Mol Cell Biol* **29**: 5578

Balasubramanyam M, Gardner JP. 1995. Protein kinase C modulates cytosolic free calcium by stimulating calcium pump activity in Jurkat T cells. *Cell calcium* **18**: 526-541

Balla T. 2009. Regulation of Ca^{2+} entry by inositol lipids in mammalian cells by multiple mechanisms. *Cell calcium* **45**: 527-534

Bandell M, Story GM, Hwang SW, Viswanath V, Eid SR, Petrus MJ. 2004. Noxious cold ion channel TRPA1 is activated by pungent compounds and bradykinin. *Neuron* **41**:

Bandyopadhyay BC, Ong HL, Lockwich TP, Liu X, Paria BC, Singh BB, Ambudkar IS. 2008. TRPC3 controls agonist-stimulated intracellular Ca^{2+} release by mediating the interaction between inositol 1,4,5-trisphosphate receptor and RACK1. *J Biol Chem* **283**: 32821-32830

Bang S, Hwang SW. 2009. Polymodal ligand sensitivity of TRPA1 and its modes of interactions. *J Gen Physiol* **133**: 257-262

Bang S, Yoo S, Yang TJ, Cho H, Hwang SW. 2012. 17(R)-Resolvin D1 specifically inhibits transient receptor potential ion channel vanilloid 3 leading to peripheral antinociception. *Br J Pharmacol* **165**: 683-692

Banke TG, Chaplan SR, Wickenden AD. 2010. Dynamic changes in the TRPA1 selectivity filter lead to progressive but reversible pore dilation. *Am J Physiol Cell Physiol* **298**: C1457-1468

Barbat C, Trucy M, Sorice M, Garofalo T, Manganelli V, Fischer A, Mazerolles F. 2007. $P56^{lck}$, LFA-1 and PI_3K but not SHP-2 interact with G_{M1}- or G_{M3}-enriched microdomains in a CD4–$p56^{lck}$ association-dependent manner. *Biochem J* **402**: 471

Barbet G, Demion M, Moura IC, Serafini N, Leger T, Vrtovsnik F, . . . Launay P. 2008. The calcium-activated nonselective cation channel TRPM4 is essential for the migration but not the maturation of dendritic cells. *Nat Immunol* **9**: 1148-1156

Barda-Saad M, Braiman A, Titerence R, Bunnell SC, Barr VA, Samelson LE. 2004. Dynamic molecular interactions linking the T cell antigen receptor to the actin cytoskeleton. *Nat Immunol* **6**: 80

Barrett T, Wilhite SE, Ledoux P, Evangelista C, Kim IF, Tomashevsky M, . . . Soboleva A. 2013. NCBI geo: Archive for functional genomics data sets--update. *Nucleic acids research* **41**: D991-995

Beck A, Kolisek M, Bagley LA, Fleig A, Penner R. 2006. Nicotinic acid adenine dinucleotide phosphate and cyclic ADP-ribose regulate TRPM2 channels in T lymphocytes. *FASEB J* **20**: 962-964

Beesetty P, Wieczerzak KB, Gibson JN, Kaitsuka T, Luu CT, Matsushita M, Kozak JA. 2018. Inactivation of TRPM7 kinase in mice results in enlarged spleens, reduced T-cell proliferation and diminished store-operated calcium entry. *Sci Rep-UK* **8**: 3023

Belmonte C, Viana F. 2008. Molecular and cellular limits to somatosensory specificity. *Mol Pain* **4**: 14-14

Berggren MI, Gallegos A, Dressler LA, Modest EJ, Powis G. 1993. Inhibition of the signalling enzyme phosphatidylinositol-3-kinase by antitumor ether lipid analogues. *Cancer Res* **53**: 4297-4302

Berjukow S, Doring F, Froschmayr M, Grabner M, Glossmann H, Hering S. 1996. Endogenous calcium channels in human embryonic kidney (HEK293) cells. *Br J Pharmacol* **118**: 748-754

Berridge MJ, Bootman MD, Lipp P. 1998. Calcium - a life and death signal. *Nature* **395**: 645

Berridge MJ, Bootman MD, Roderick HL. 2003. Calcium signalling: Dynamics, homeostasis and remodelling. *Nat Rev Mol Cell Biol* **4**: 517-529

Berridge MJ, Lipp P, Bootman MD. 2000. The versatility and universality of calcium signalling. *Nat Rev Mol Cell Biol* **1**: 11-21

Bertin S, Aoki-Nonaka Y, de Jong PR, Nohara LL, Xu H, Stanwood SR, . . . Raz E. 2014. The ion channel TRPV1 regulates the activation and proinflammatory properties of $CD4^+$ T cells. *Nat Immunol* **15**: 1055-1063

Bertin S, Aoki-Nonaka Y, Lee J, de Jong PR, Kim P, Han T, . . . Raz E. 2017. The TRPA1 ion channel is expressed in $CD4^+$ T cells and restrains T-cell-mediated colitis through inhibition of TRPV1. *Gut* **66**: 1584-1596

Bertin S, Raz E. 2016. Transient receptor potential (TRP) channels in T cells. *Semin Immunopathol* **38**: 309-319

Bessac BF, Sivula M, von Hehn CA, Escalera J, Cohn L, Jordt SE. 2008. TRPA1 is a major oxidant sensor in murine airway sensory neurons. *J Clin Invest* **118**: 1899-1910

Bettini ML, Guy C, Dash P, Vignali KM, Hamm DE, Dobbins J, . . . Vignali DA. 2014. Membrane association of the CD3ε signaling domain is required for optimal T cell development and function. *J Immunol* **193**: 258-267

Bezzerides VJ, Ramsey IS, Kotecha S, Greka A, Clapham DE. 2004. Rapid vesicular translocation and insertion of TRP channels. *Nat Cell Biol* **6**: 709-720

Bhakta NR, Lewis RS. 2005. Real-time measurement of signaling and motility during T cell development in the thymus. *Semin Immunopathol* **17**: 411-420

Bhakta NR, Oh DY, Lewis RS. 2005. Calcium oscillations regulate thymocyte motility during positive selection in the three-dimensional thymic environment. *Nat Immunol* **6**: 143-151

Bhandoola A, Cibotti R, Punt JA, Granger L, Adams AJ, Sharrow SO, Singer A. 1999. Positive selection as a developmental progression initiated by αβTCR signals that fix TCR specificity prior to lineage commitment. *Immunity* **10**: 301-311

Bierer BE, Peterson A, Gorga JC, Herrmann SH, Burakoff SJ. 1988. Synergistic T cell activation via the physiological ligands for CD2 and the T cell receptor. *J Exp Med* **168**: 1145-1156

Bishop JR, Schuksz M, Esko JD. 2007. Heparan sulphate proteoglycans fine-tune mammalian physiology. *Nature* **446**: 1030-1037

Blaustein MP, Lederer WJ. 1999. Sodium/calcium exchange: Its physiological implications. *Physiol Rev* **79**: 763-854

Bonilla FA, Oettgen HC. 2010. Adaptive immunity. *J Allergy Clin Immunol* **125**: S33-40

Boonyaratanakornkit V, Scott MP, Ribon V, Sherman L, Anderson SM, Maller JL, . . . Edwards DP. 2001. Progesterone receptor contains a proline-rich motif that directly interacts with SH3 domains and activates c-Src family tyrosine kinases. *Mol Cell* **8**: 269-280

Borbiro I, Badheka D, Rohacs T. 2015. Activation of TRPV1 channels inhibits mechanosensitive piezo channel activity by depleting membrane phosphoinositides. *Sci Signal* **8**: ra15

Borger JG, Zamoyska R, Gakamsky DM. 2014. Proximity of TCR and its CD8 coreceptor controls sensitivity of T cells. *Immunol Lett* **157**: 16-22

Borin M, Siffert W. 1990. Stimulation by thrombin increases the cytosolic free Na^+ concentration in human platelets. Studies with the novel fluorescent cytosolic Na^+ indicator sodium-binding benzofuran isophthalate. *J Biol Chem* **265**: 19543-19550

Bouron A, Kiselyov K, Oberwinkler J. 2015. Permeation, regulation and control of expression of TRP channels by trace metal ions. *Pflugers Archiv* **467**: 1143-1164

Bousova K, Jirku M, Bumba L, Bednarova L, Sulc M, Franek M, . . . Teisinger J. 2015. PIP_2 and PIP_3 interact with N-terminus region of TRPM4 channel. *Biophys Chem* **205**: 24-32

Brandao K, Deason-Towne F, Perraud A-L, Schmitz C. 2013. The role of Mg^{2+} in immune cells. *Immunol Res* **55**: 261-269

Brauchi S, Orta G, Mascayano C, Salazar M, Raddatz N, Urbina H, . . . Latorre R. 2007. Dissection of the components for PIP_2 activation and thermosensation in TRP channels. *Proc Natl Acad Sci USA* **104**: 10246

Brauchi S, Orta G, Salazar M, Rosenmann E, Latorre R. 2006. A hot-sensing cold receptor: C-terminal domain determines thermosensation in transient receptor potential channels. *J Neurosci* **26**: 4835-4840

Brown TE, Chirila AM, Schrank BR, Kauer JA. 2013. Loss of interneuron LTD and attenuated pyramidal cell LTP in *Trpv1* and *Trpv3* KO mice. *Hippocampus* **23**: 662-671

Bugaj V, Alexeenko V, Zubov A, Glushankova L, Nikolaev A, Wang Z, . . . Mozhayeva GN. 2005. Functional properties of endogenous receptor- and store-operated calcium influx channels in HEK293 cells. *J Biol Chem* **280**: 16790-16797

Bunnell TM, Burbach BJ, Shimizu Y, Ervasti JM. 2011. B-actin specifically controls cell growth, migration, and the G-actin pool. *Mol Biol Cell* **22**: 4047-4058

Burnstock G, Boeynaems J-M. 2014. Purinergic signalling and immune cells. *Purinerg Signal* **10**: 529-564

Buttgereit F, Brand MD, Muller M. 1993. Effects of methylprednisolone on the energy metabolism of quiescent and ConA-stimulated thymocytes of the rat. *Biosci Rep* **13**: 41-52

Buttgereit F, Krauss S, Brand MD. 1997. Methylprednisolone inhibits uptake of Ca^{2+} and Na^{+} ions into concanavalin a-stimulated thymocytes. *Biochem J* **326 (Pt 2)**: 329-332

Cahalan MD, Chandy KG. 2009. The functional network of ion channels in T lymphocytes. *Immunol Rev* **231**: 59-87

Cahalan MD, Wulff H, Chandy KG. 2001. Molecular properties and physiological roles of ion channels in the immune system. *J Clin Immunol* **21**: 235-252

Cai N, Bai Z, Nanda V, Runnels LW. 2017. Mass spectrometric analysis of TRPM6 and TRPM7 phosphorylation reveals regulatory mechanisms of the channel-kinases. *Sci Rep-UK* **7**: 42739

Cai N, Lou L, Al-Saadi N, Tetteh S, Runnels LW. 2018. The kinase activity of the channel-kinase protein TRPM7 regulates stability and localization of the TRPM7 channel in polarized epithelial cells. *J Biol Chem*:

Caires R, Sierra-Valdez FJ, Millet JRM, Herwig JD, Roan E, Vasquez V, Cordero-Morales JF. 2017. Omega-3 fatty acids modulate TRPV4 function through plasma membrane remodeling. *Cell Rep* **21**: 246-258

Cairo CW, Mirchev R, Golan David E. 2006. Cytoskeletal regulation couples LFA-1 conformational changes to receptor lateral mobility and clustering. *Immunity* **25**: 297-308

Camello C, Lomax R, Petersen OH, Tepikin AV. 2002. Calcium leak from intracellular stores-the enigma of calcium signalling. *Cell calcium* **32**: 355-361

Cao E, Liao M, Cheng Y, Julius D. 2013. TRPV1 structures in distinct conformations reveal activation mechanisms. *Nature* **504**: 113-118

Cao G, van der Wijst J, van der Kemp A, van Zeeland F, Bindels RJ, Hoenderop JG. 2009. Regulation of the epithelial Mg^{2+} channel TRPM6 by estrogen and the associated repressor protein of estrogen receptor activity (rea). *J Biol Chem* **284**: 14788-14795

Cao X, Yang F, Zheng J, Wang K. 2012. Intracellular proton-mediated activation of TRPV3 channels accounts for the exfoliation effect of α-hydroxyl acids on keratinocytes. *J Biol Chem* **287**: 25905-25916

Carafoli E, Krebs J. 2016. Why calcium? How calcium became the best communicator. *J Biol Chem* **291**: 20849-20857

Cardile V, Mudò G, Jiang X, Casella F, Bindoni M, Belluardo N. 1997. Thymotrophic effect of ether lipid 1-*O*-octadecyl-2-*O*-methoxy-rac-glicero-3-phosphocholine in the mouse. *Immunopharmacology* **37**: 199-207

Carpenter AC, Bosselut R. 2010. Decision checkpoints in the thymus. *Nat Immunol* **11**: 666-673

Carrillo C, Hichami A, Andreoletti P, Cherkaoui-Malki M, del Mar Cavia M, Abdoul-Azize S, . . . Khan NA. 2012. Diacylglycerol-containing oleic acid induces increases in $[Ca^{2+}]_i$ via TRPC3/6 channels in human t-cells. *Biochimica et Biophysica Acta (BBA) - Mol Cell Biol Lipid* **1821**: 618-626

Casabó LG, Mamalaki C, Kioussis D, Zamoyska R. 1994. T cell activation results in physical modification of the mouse CD8β chain. *J Immunol* **152**: 397

Casey Crooks ME, Littman DR. 1994. Disruption of T lymphocyte positive and negative selection in mice lacking the CD8β chain. *Immunity* **1**: 277-285

Casrouge A, Beaudoing E, Dalle S, Pannetier C, Kanellopoulos J, Kourilsky P. 2000. Size estimate of the αβ TCR repertoire of naive mouse splenocytes. *J Immunol* **164**: 5782-5787

Castillo K, Diaz-Franulic I, Canan J, Gonzalez-Nilo F, Latorre R. 2018. Thermally activated TRP channels: Molecular sensors for temperature detection. *Phys Biol* **15**: 021001

Castonguay A, Robitaille R. 2002. Xestospongin C is a potent inhibitor of SERCA at a vertebrate synapse. *Cell calcium* **32**: 39-47

Cataldi M, Perez-Reyes E, Tsien RW. 2002. Differences in apparent pore sizes of low and high voltage-activated Ca^{2+} channels. *J Biol Chem* **277**: 45969-45976

Caterina MJ, Rosen TA, Tominaga M, Brake AJ, Julius D. 1999. A capsaicin-receptor homologue with a high threshold for noxious heat. *Nature* **398**: 436-441

Caterina MJ, Schumacher MA, Tominaga M, Rosen TA, Levine JD, Julius D. 1997. The capsaicin receptor: A heat-activated ion channel in the pain pathway. *Nature* **389**: 816-824

Cayouette S, Boulay G. 2007. Intracellular trafficking of TRP channels. *Cell calcium* **42**: 225-232

Cerny AC, Huber A. 2011. Regulation of TRP signalling by ion channel translocation between cell compartments In *Transient receptor potential channels*, ed. MS Islam, pp. 545-572: Springer Science

Chandy KG, Wulff H, Beeton C, Pennington M, Gutman GA, Cahalan MD. 2004. K^+ channels as targets for specific immunomodulation. *Trends Pharmacol Sci* **25**: 280-289

Chao DT, Linette GP, Boise LH, White L, Thompson CB, Korsmeyer SJ. 1995. Bcl-X_L and Bcl-2 repress a common pathway of cell death. *J Exp Med* **182**: 821-828

Chen H-C, Xie J, Zhang Z, Su L-T, Yue L, Runnels LW. 2010. Blockade of TRPM7 channel activity and cell death by inhibitors of 5-lipoxygenase. *PLOS One* **5**: e11161

Chen J, Hackos DH. 2015. TRPA1 as a drug target—promise and challenges. *N-S Arch Pharmacol* **388**: 451-463

Chen J, Kang D, Xu J, Lake M, Hogan JO, Sun C, . . . Kim D. 2013. Species differences and molecular determinant of TRPA1 cold sensitivity. *Nat Commun* **4**: 2501

Chen J, Kim D, Bianchi BR, Cavanaugh EJ, Faltynek CR, Kym PR, Reilly RM. 2009. Pore dilation occurs in TRPA1 but not in TRPM8 channels. *Mol Pain* **5**: 3-3

Chen L, Xu A, Yin N, Zhao M, Wang Z, Chen T, . . . Chen Z. 2017a. Enhancement of immune cytokines and splenic $CD4^+$ T cells by electroacupuncture at ST36 acupoint of SD rats. *PLOS One* **12**: e0175568

Chen R, Valencia I, Zhong F, McColl KS, Roderick HL, Bootman MD, . . . Distelhorst CW. 2004. Bcl-2 functionally interacts with inositol 1,4,5-trisphosphate receptors to regulate calcium release from the ER in response to inositol 1,4,5-trisphosphate. *J Cell Biol* **166**: 193-203

Chen XX, Zhang JH, Pan BH, Ren HL, Feng XL, Wang JL, Xiao JH. 2017b. Role of canonical transient receptor potential channel-3 in acetylcholine-induced mouse airway smooth muscle cell proliferation. *Life Sci* **187**: 64-73

Cheng W, Yang F, Liu S, Colton CK, Wang C, Cui Y, . . . Zheng J. 2012. Heteromeric heat-sensitive transient receptor potential channels exhibit distinct temperature and chemical response. *J Biol Chem* **287**: 7279-7288

Chicoine LM, Bahr BA. 2007. Excitotoxic protection by polyanionic polysaccharide: Evidence of a cell survival pathway involving AMPA receptor–MAPK interactions. *J Neurosci Res* **85**: 294-302

Chicoine LM, Suppiramaniam V, Vaithianathan T, Gianutsos G, Bahr BA. 2004. Sulfate- and size-dependent polysaccharide modulation of AMPA receptor properties. *J Neurosci Res* **75**: 408-416

Chokshi R, Fruasaha P, Kozak JA. 2012a. 2-aminoethyl diphenyl borinate (2-APB) inhibits TRPM7 channels through an intracellular acidification mechanism. *Channels* **6**: 362-369

Chokshi R, Matsushita M, Kozak JA. 2012b. Sensitivity of TRPM7 channels to Mg^{2+} characterized in cell-free patches of Jurkat T lymphocytes. *Am J Physiol-Cell Ph* **302**: C1642-C1651

Chow J, Norng M, Zhang J, Chai J. 2007. TRPV6 mediates capsaicin-induced apoptosis in gastric cancer cells—mechanisms behind a possible new "hot" cancer treatment. *Biochimica et Biophysica Acta (BBA) - Mol Cell Res* **1773**: 565-576

Christo SN, Diener KR, Hayball JD. 2015. The functional contribution of calcium ion flux heterogeneity in T cells. *Immunol Cell Biol* **93**: 694-704

Chu X, Tong Q, Cheung JY, Wozney J, Conrad K, Mazack V, . . . Miller BA. 2004. Interaction of TRPC2 and TRPC6 in erythropoietin modulation of calcium influx. *J Biol Chem* **279**: 10514-10522

Chubanov V, Ferioli S, Wisnowsky A, Simmons DG, Leitzinger C, Einer C, . . . Gudermann T. 2016. Epithelial magnesium transport by TRPM6 is essential for prenatal development and adult survival. *eLife* **5**: e20914

Chubanov V, Mederos y Schnitzler M, Meißner M, Schäfer S, Abstiens K, Hofmann T, Gudermann T. 2012. Natural and synthetic modulators of SK ($k_{ca}2$) potassium channels inhibit magnesium-dependent activity of the kinase-coupled cation channel TRPM7. *Brit J Pharmacol* **166**: 1357-1376

Chubanov V, Waldegger S, Mederos y Schnitzler M, Vitzthum H, Sassen MC, Seyberth HW, . . . Gudermann T. 2004. Disruption of TRPM6/TRPM7 complex formation by a mutation in the *TRPM6* gene causes hypomagnesemia with secondary hypocalcemia. *Proc Natl Acad Sci USA* **101**: 2894-2899

Chubinskiy-Nadezhdin VI, Efremova TN, Khaitlina SY, Morachevskaya EA. 2013. Functional impact of cholesterol sequestration on actin cytoskeleton in normal and transformed fibroblasts. *Cell Biol Int* **37**: 617-623

Chun JN, Lim JM, Kang Y, Kim EH, Shin Y-C, Kim H-G, . . . Jeon J-H. 2014. A network perspective on unraveling the role of TRP channels in biology and disease. *Pflüg Arch Eur J Phy* **466**: 173-182

Chung M-K, Güler AD, Caterina MJ. 2005. Biphasic currents evoked bychemical or thermal activation of the heat-gated ion channel, TRPV3. *J Biol Chem* **280**: 15928-15941

Chung M-K, Lee H, Mizuno A, Suzuki M, Caterina MJ. 2004. 2-aminoethoxydiphenyl borate activates and sensitizes the heat-gated ion channel TRPV3. *J Neurosci* **24**: 5177

Chung MK, Guler AD, Caterina MJ. 2008. TRPV1 shows dynamic ionic selectivity during agonist stimulation. *Nat Neurosci* **11**: 555-564

Chvatchko Y, Valera S, Aubry J-P, Renno T, Buell G, Bonnefoy J-Y. 1996. The involvement of an ATP-gated ion channel, P2X1, in thymocyte apoptosis. *Immunity* **5**: 275-283

Ciardo MG, Ferrer-Montiel A. 2017. Lipids as central modulators of sensory TRP channels. *BBA-Biomembranes* **1859**: 1615-1628

Cibulsky SM, Sather WA. 1999. Block by ruthenium red of cloned neuronal voltage-gated calcium channels. *J Pharrmacol Exp Ther* **289**: 1447

Clapham DE. 2003. TRP channels as cellular sensors. *Nature* **426**: 517-524

Clapham DE. 2007a. Calcium signaling. *Cell* **131**: 1047-1058

Clapham DE. 2007b. Snapshot: Mammalian TRP channels. *Cell* **129**: 220

Clark K, Langeslag M, van Leeuwen B, Ran L, Ryazanov AG, Figdor CG, . . . van Leeuwen FN. 2006. TRPM7, a novel regulator of actomyosin contractility and cell adhesion. *EMBO J* **25**: 290-301

Cook-Moreau JM, El-Makhour Hojeij Y, Barrière G, Rabinovitch-Chable HC, Faucher KS, Sturtz FG, Rigaud MA. 2007. Expression of 5-lipoxygenase (5-lox) in T lymphocytes. *Immunology* **122**: 157-166

Corbett EF, Michalak M. 2000. Calcium, a signaling molecule in the endoplasmic reticulum? *Trends Biochem Sci* **25**: 307-311

Cordero-Morales JF, Vásquez V. 2018. How lipids contribute to ion channel function, a fat perspective on direct and indirect interactions. *Curr Opin Struc Biol* **51**: 92-98

Correll CC, Phelps PT, Anthes JC, Umland S, Greenfeder S. 2004. Cloning and pharmacological characterization of mouse TRPV1. *Neurosci Lett* **370**: 55-60

Cosens DJ, Manning A. 1969. Abnormal electroretinogram from a *drosophila* mutant. *Nature* **224**: 285

Coste B, Mathur J, Schmidt M, Earley TJ, Ranade S, Petrus MJ, . . . Patapoutian A. 2010. Piezo1 and piezo2 are essential components of distinct mechanically activated cation channels. *Science* **330**: 55

Coste B, Xiao B, Santos JS, Syeda R, Grandl J, Spencer KS, . . . Patapoutian A. 2012. Piezo proteins are pore-forming subunits of mechanically activated channels. *Nature* **483**: 176

Courageot M-P, Lépine S, Hours M, Giraud F, Sulpice J-C. 2004. Involvement of sodium in early phosphatidylserine exposure and phospholipid scrambling induced by P2X7 purinoceptor activation in thymocytes. *J Biol Chem* **279**: 21815-21823

Cowan AI, Martin RL. 1995. Simultaneous measurement of pH and membrane potential in rat dorsal vagal motoneurons during normoxia and hypoxia: A comparison in bicarbonate and HEPES buffers. *J Neurophysiol* **74**: 2713-2721

Cox CD, Bae C, Ziegler L, Hartley S, Nikolova-Krstevski V, Rohde PR, . . . Martinac B. 2016. Removal of the mechanoprotective influence of the cytoskeleton reveals piezo1 is gated by bilayer tension. *Nat Commun* **7**: 10366

Cribbs LL, Satin J, Fozzard HA, Rogart RB. 1990. Functional expression of the rat heart I Na^+ channel isoform. Demonstration of properties characteristic of native cardiac Na^+ channels. *FEBS Lett* **275**: 195-200

Csanády L, Törőcsik B. 2009. Four Ca^{2+} ions activate TRPM2 channels by binding in deep crevices near thepore but intracellularly of the gate. *J Gen Physiol* **133**: 189-203

Cui J, Matkovich SJ, deSouza N, Li S, Rosemblit N, Marks AR. 2004. Regulation of the type 1 inositol 1,4,5-trisphosphate receptor by phosphorylation at tyrosine 353. *J Biol Chem* **279**: 16311-16316

Cui Y, Yang F, Cao X, Yarov-Yarovoy V, Wang KW, Zheng J. 2012. Selective disruption of high sensitivity heat activation but not capsaicin activation of TRPV1 channels by pore turret mutations. *J Gen Physiol* **139**: 273

Danielian S, Alcover A, Polissard L, Stefanescu M, Acuto O, Fischer S, Fagard R. 1992. Both T cell receptor (tcr)-CD3 complex and CD2 increase the tyrosine kinase activity of $p56^{lck}$. CD2 can mediate TcR-CD3-independent and CD45-dependent activation of $p56^{lck}$. *Eur J Immunol* **22**: 2915-2921

Daniels MA, Devine L, Miller JD, Moser JM, Lukacher AE, Altman JD, . . . Jameson SC. 2001. CD8 binding to MHC class I molecules is influenced by T cell maturation and glycosylation. *Immunity* **15**: 1051-1061

Daniels MA, Teixeiro E, Gill J, Hausmann B, Roubaty D, Holmberg K, . . . Palmer E. 2006. Thymic selection threshold defined by compartmentalization of ras/MAPK signalling. *Nature* **444**: 724

Davenport B, Li Y, Heizer JW, Schmitz C, Perraud A-L. 2015. Signature channels of excitability no more: L-type channels in immune cells. *Front Immunol* **6**:

Davey GM, Schober SL, Endrizzi BT, Dutcher AK, Jameson SC, Hogquist KA. 1998. Preselection thymocytes are more sensitive to T cell receptor stimulation than mature T cells. *J Exp Med* **188**: 1867-1874

Davies SP, Reddy H, Caivano M, Cohen P. 2000. Specificity and mechanism of action of some commonly used protein kinase inhibitors. *Biochem J* **351**: 95-105

Davis MM, Bjorkman PJ. 1988. T-cell antigen receptor genes and T-cell recognition. *Nature* **334**: 395-402

de la Cruz J, Kruger T, Parks CA, Silge RL, van Oers NSC, Luescher IF, . . . Gil D. 2011. Basal and antigen-induced exposure of the proline-rich sequence in cd3ε. *J Immunol* **186**: 2282

De Smet P, Parys JB, Callewaert G, Weidema AF, Hill E, De Smedt H, . . . Missiaen L. 1999. Xestospongin C is an equally potent inhibitor of the inositol 1,4,5-trisphosphate receptor and the endoplasmic-reticulum Ca^{2+} pumps. *Cell calcium* **26**: 9-13

DeHaven WI, Jones BF, Petranka JG, Smyth JT, Tomita T, Bird GS, Putney JW, Jr. 2009. TRPC channels function independently of STIM1 and Orai1. *J Physiol* **587**: 2275-2298

Deinum J, Wallin M, Jensen PW. 1985. The binding of ruthenium red to tubulin. *Biochimica et Biophysica Acta (BBA) - Gen Subjects* **838**: 197-205

Delfino DV, Pozzesi N, Pierangeli S, Ayroldi E, Fierabracci A. 2011. Manipulating thymic apoptosis for future therapy of autoimmune diseases. *Curr Pharm Design* **17**: 3108-3119

Delon J, Gregoire C, Malissen B, Darche S, Lemaitre F, Kourilsky P, . . . Trautmann A. 1998. CD8 expression allows T cell signaling by monomeric peptide-MHC complexes. *Immunity* **9**: 467-473

Demeuse P, Penner R, Fleig A. 2006. TRPM7 channel is regulated by magnesium nucleotides via its kinase domain. *J Gen Physiol* **127**: 421-434

den Braber I, Mugwagwa T, Vrisekoop N, Westera L, Mögling R, Bregje de Boer A, . . . Tesselaar K. 2012. Maintenance of peripheral naive T cells is sustained by thymus output in mice but not humans. *Immunity* **36**: 288-297

Dhaka A, Uzzell V, Dubin A, Mathur J, Petrus M, Bandell M, Patapoutian A. 2009. TRPV1 senses both acidic and basic pH. *J Neurosci* **29**: 153-158

Diarra A, Sheldon C, Church J. 2001. *In situ* calibration and $[h^+]$ sensitivity of the fluorescent Na^+ indicator SBFI. *Am J Physiol-Cell Ph* **280**: C1623

Diaz-Franulic I, Poblete H, Mino-Galaz G, Gonzalez C, Latorre R. 2016. Allosterism and structure in thermally activated transient receptor potential channels. *Annu Rev Biophys* **45**: 371-398

Diercks B-P, Fliegert R, Guse A. 2017. Mag-fluo4 in T cells: Imaging of intra-organelle free Ca^{2+} concentrations. *Biochem Biophys Acta* **1864**: 977 -986

Dietrich A, Kalwa H, Storch U, Mederos y Schnitzler M, Salanova B, Pinkenburg O, . . . Gudermann T. 2007. Pressure-induced and store-operated cation influx in vascular smooth muscle cells is independent of TRPC1. *Pflugers Arch* **455**: 465-477

Dietrich A, Mederos y Schnitzler M, Emmel J, Kalwa H, Hofmann T, Gudermann T. 2003. *N*-linked protein glycosylation is a major determinant for basal TRPC3 and TRPC6 channel activity. *J Biol Chem* **278**: 47842-47852

Dietrich A, Mederos YSM, Gollasch M, Gross V, Storch U, Dubrovska G, . . . Birnbaumer L. 2005. Increased vascular smooth muscle contractility in $TRPC6^{-/-}$ mice. *Mol Cell Biol* **25**: 6980-6989

Dietsch MT, Chan PY, Kanner SB, Gilliland LK, Ledbetter JA, Linsley PS, Aruffo A. 1994. Coengagement of CD2 with LFA-1 or VLA-4 by bispecific ligand fusion proteins primes T cells to respond more effectively to T cell receptor-dependent signals. *J Leukocyte Biol* **56**: 444-452

Diez-Bello R, Jardin I, Lopez JJ, El Haouari M, Ortega-Vidal J, Altarejos J, . . . Rosado JA. 2019. (-)oleocanthal inhibits proliferation and migration by modulating Ca^{2+} entry through TRPC6 in breast cancer cells. *Biochim Biophys Acta Mol Cell Res* **1866**: 474-485

Dobrovinskaya O, Delgado-Enciso I, Quintero-Castro LJ, Best-Aguilera C, Rojas-Sotelo RM, Pottosin I. 2015. Placing ion channels into a signaling network of T cells: From maturing thymocytes to healthy T lymphocytes or leukemic T lymphoblasts. *BioMed Res Internat* **2015**:

Doerner JF, Gisselmann G, Hatt H, Wetzel CH. 2007. Transient receptor potential channel A1 is directly gated by calcium ions. *J Biol Chem* **282**:

Doerner JF, Hatt H, Ramsey IS. 2011. Voltage- and temperature-dependent activation of TRPV3 channels is potentiated by receptor-mediated $PI(4,5)P_2$ hydrolysis. *J Gen Physiol* **137**: 271

Dong H-W, Davis JC, Ding S, Nai Q, Zhou F-M, Ennis M. 2012. Expression of transient receptor potential (TRP) channel mRNAs in the mouse olfactory bulb. *Neurosci Lett* **524**: 49-54

Donnadieu E, Trautmann A. 1993. Is there a Na^+/Ca^{2+} exchanger in macrophages and in lymphocytes? *Pflügers Archiv* **424**: 448-455

Doucey M-A, Goffin L, Naeher D, Michielin O, Baumgärtner P, Guillaume P, . . . Luescher IF. 2003. Cd3δ establishes a functional link between the T cell receptor and CD8. *J Biol Chem* **278**: 3257-3264

Dubin AE, Murthy S, Lewis AH, Brosse L, Cahalan SM, Grandl J, . . . Patapoutian A. 2017. Endogenous piezo1 can confound mechanically activated channel identification and characterization. *Neuron* **94**: 266-270.e263

Dubin AE, Schmidt M, Mathur J, Petrus MJ, Xiao B, Coste B, Patapoutian A. 2012. Inflammatory signals enhance piezo2-mediated mechanosensitive currents. *Cell Rep* **2**: 511-517

Duplay P, Lancki D, Allison JP. 1989. Distribution and ontogeny of CD2 expression by murine T cells. *J Immunol* **142**: 2998- 3005

Dzhagalov I, Phee H. 2012. How to find your way through the thymus: A practical guide for aspiring T cells. *Cell Mol Life Sci* **69**: 663-682

Echevarria-Lima J, de Araújo EG, de Meis L, Rumjanek VM. 2003. Ca^{2+} mobilization induced by ouabain in thymocytes involves intracellular and extracellular Ca^{2+} pools. *Hypertension* **41**: 1386-1392

Echevarria-Lima J, Kyle-Cezar F, P. Leite DF, Capella L, Capella MAM, Rumjanek VM. 2005. Expression and activity of multidrug resistance protein 1 in a murine thymoma cell line. *Immunology* **114**: 468-475

Eder P, Schindl R, Romanin C, Groschner K. 2007. *Protein–protein interactions in TRPC channel complexes.* pp. 331- 348. Boca Raton (FL) CRC Press/Taylor & Francis.

Edgar R, Domrachev M, Lash AE. 2002. Gene expression omnibus: NCBI gene expression and hybridization array data repository. *Nucleic acids research* **30**: 207-210

Egan TJ, Acuna MA, Zenobi-Wong M, Zeilhofer HU, Urech D. 2016. Effects of *N*-glycosylation of the human cation channel TRPA1 on agonist-sensitivity. *Biosci Rep*:

Egerton M, Scollay R, Shortman K. 1990. Kinetics of mature T-cell development in the thymus. *Proc Natl Acad Sci USA* **87**: 2579-2582

Eijkelkamp N, Quick K, Wood JN. 2013. Transient receptor potential channels and mechanosensation. *Annu Rev Neurosci* **36**: 519-546

El-Moatassim C, Bernad N, Mani J-C, Dornand J. 1989. Extracellular ATP induces a nonspecific permeability of thymocyte plasma membranes. *Biochem Cell Biol* **67**: 495-502

Engelke M, Friedrich O, Budde P, Schafer C, Niemann U, Zitt C, . . . Frey J. 2002. Structural domains required for channel function of the mouse transient receptor potential protein homologue trp1β. *FEBS Lett* **523**: 193-199

Ericson J, Davis S, Lesh J, Howard M, Mathis D, Benoist C. 2019. *Immgen microarray gene expression data: Data generation and quality control pipeline*.

Erler I, Hirnet D, Wissenbach U, Flockerzi V, Niemeyer BA. 2004. Ca^{2+}-selective transient receptor potential V channel architecture and function require a specific ankyrin repeat. *J Biol Chem* **279**: 34456-34463

Ermakov YA, Averbakh AZ, Yusipovich AI, Sukharev S. 2001. Dipole potentials indicate restructuring of the membrane interface induced by gadolinium and beryllium ions. *Biophys J* **80**: 1851-1862

Espagnolle N, Depoil D, Zaru R, Demeur C, Champagne E, Guiraud M, Valitutti S. 2007. CD2 and TCR synergize for the activation of phospholipase Cγ1/calcium pathway at the immunological synapse. *Int Immunol* **19**: 239-248

Fagerholm S, Hilden TJ, Gahmberg CG. 2002. Lck tyrosine kinase is important for activation of the CD11a/CD18-integrins in human T lymphocytes. *Eur J Immunol* **32**: 1670-1678

Fang D, Setaluri V. 2000. Expression and up-regulation of alternatively spliced transcripts of melastatin, a melanoma metastasis-related gene, in human melanoma cells. *Biochem Biophys Res Commun* **279**: 53-61

Faouzi M, Kilch T, Horgen FD, Fleig A, Penner R. 2017. The TRPM7 channel kinase regulates store-operated calcium entry. *J Physiol* **595**: 3165-3180

Farfariello V, Amantini C, Santoni G. 2012. Transient receptor potential vanilloid 1 activation induces autophagy in thymocytes through ROS-regulated AMPK and Atg4C pathways. *J Leukocyte Biol* **92**: 421-431

Feakes DA. 2012. *Mechanisms responsible for the intracellular calcium rise in $CD4^+CD8^+$ (double positive) thymocytes*. thesis. Australian National University. pp.

Fedorenko OA, Popugaeva E, Enomoto M, Stathopulos PB, Ikura M, Bezprozvanny I. 2014. Intracellular calcium channels: Inositol-1,4,5-trisphosphate receptors. *Eur J Pharmacol* **739**: 39-48

Ferioli S, Zierler S, Zaißerer J, Schredelseker J, Gudermann T, Chubanov V. 2017. TRPM6 and TRPM7 differentially contribute to the relief of heteromeric TRPM6/7 channels from inhibition by cytosolic Mg^{2+} and Mg·ATP. *Sci Rep-UK* **7**: 8806

Fernandes ES, Fernandes MA, Keeble JE. 2012. The functions of TRPA1 and TRPV1: Moving away from sensory nerves. *Br J Pharmacol* **166**:

Ferreira LG, Faria RX. 2016. Trping on the pore phenomenon: What do we know about transient receptor potential ion channel-related pore dilation up to now? *J Bioenerg Biomembr* **48**: 1-12

Feske S. 2007. Calcium signalling in lymphocyte activation and disease. *Nat Rev Immunol* **7**: 690

Feske S. 2013. Ca^{2+} influx in T cells: How many Ca^{2+} channels? *Front Immunol* **4**: 99

Feske S, Prakriya M, Rao A, Lewis RS. 2005. A severe defect in CRAC Ca^{2+} channel activation and altered K^+ channel gating in T cells from immunodeficient patients. *J Exp Med* **202**: 651-662

Feske S, Wulff H, Skolnik EY. 2015. Ion channels in innate and adaptive immunity. *Annu Rev Immunol* **33**: 291-353

Fine JS, Kruisbeek AM. 1991. The role of LFA-1/ICAM-1 interactions during murine T lymphocyte development. *J Immunol* **147**: 2852

Fischer MJ, Balasuriya D, Jeggle P, Goetze TA, McNaughton PA, Reeh PW, Edwardson JM. 2014. Direct evidence for functional TRPV1/TRPA1 heteromers. *Pflugers Arch* **466**: 2229-2241

Fonfria E, Marshall ICB, Boyfield I, Skaper SD, Hughes JP, Owen DE, . . . McNulty S. 2005. Amyloid β-peptide(1–42) and hydrogen peroxide-induced toxicity are mediated by TRPM2 in rat primary striatal cultures. *J Neurochem* **95**: 715-723

Formigli L, Sassoli C, Squecco R, Bini F, Martinesi M, Chellini F, . . . Meacci E. 2009. Regulation of transient receptor potential canonical channel 1 (TRPC1) by sphingosine 1-phosphate in C2C12 myoblasts and its relevance for a role of mechanotransduction in skeletal muscle differentiation. *J Cell Sci* **122**: 1322

Foyouzi-Youssefi R, Arnaudeau S, Borner C, Kelley WL, Tschopp J, Lew DP, . . . Krause K-H. 2000. Bcl-2 decreases the free Ca^{2+} concentration within the endoplasmic reticulum. *Proc Natl Acad Sci USA* **97**: 5723

Frankenhaeuser B, Hodgkin AL. 1957. The action of calcium on the electrical properties of squid axons. *J Physiol* **137**: 218-244

Franzini-Armstrong C, Protasi F, Ramesh V. 1998. Comparative ultrastructure of Ca^{2+} release units in skeletal and cardiac muscle. *Ann N Y Acad Sci* **853**: 20-30

Fraser SP, Diss JKJ, Lloyd LJ, Pani F, Chioni A-M, George AJT, Djamgoz MBA. 2004. T-lymphocyte invasiveness: Control by voltage-gated Na^+ channel activity. *FEBS Lett* **569**: 191-194

Freedman BD, Fleischmann BK, Punt JA, Gaulton G, Hashimoto Y, Kotlikoff MI. 1995. Identification of Kv1.1 expression by murine $CD4^-CD8^-$ thymocytes. *J Biol Chem* **270**: 22406-22411

Freedman BD, Liu Q H, Gaulton G, Kotlikoff MI, Hescheler J, Fleischmann BK. 1999. ATP-evoked Ca^{2+} transients and currents in murine thymocytes: Possible role for P2X receptors in death by neglect. *Eur J Immunol* **29**: 1635-1646

Fruhwald J, Camacho Londono J, Dembla S, Mannebach S, Lis A, Drews A, . . . Philipp SE. 2012. Alternative splicing of a protein domain indispensable for function of transient receptor potential melastatin 3 (TRPM3) ion channels. *J Biol Chem* **287**: 36663-36672

Fu G, Casas J, Rigaud S, Rybakin V, Lambolez F, Brzostek J, . . . Gascoigne NRJ. 2013. Themis sets the signal threshold for positive and negative selection in T-cell development. *Nature* **504**: 441-445

Fu G, Vallée S, Rybakin V, McGuire MV, Ampudia J, Brockmeyer C, . . . Gascoigne NRJ. 2009. Themis controls thymocyte selection through regulation of T cell antigen receptor–mediated signaling. *Nat Immunol* **10**: 848

Fu G, Yu M, Chen Y, Zheng Y, Zhu W, Newman DK, . . . Wen R. 2017. Phospholipase Cγ1 is required for pre-TCR signal transduction and pre-T cell development. *Eur J Immunol* **47**: 74-83

Fujii T, Mashimo M, Moriwaki Y, Misawa H, Ono S, Horiguchi K, Kawashima K. 2017. Expression and function of the cholinergic system in immune cells. *Front Immunol* **8**:

Fujimori T, Jencks WP. 1990. Lanthanum inhibits steady-state turnover of the sarcoplasmic reticulum calcium ATPase by replacing magnesium as the catalytic ion. *J Biol Chem* **265**: 16262-16270

Gafni J, Munsch JA, Lam TH, Catlin MC, Costa LG, Molinski TF, Pessah IN. 1997. Xestospongins: Potent membrane permeable blockers of the inositol 1,4,5-trisphosphate receptor. *Neuron* **19**: 723-733

Gagnon E, Schubert DA, Gordo S, Chu HH, Wucherpfennig KW. 2012. Local changes in lipid environment of TCR microclusters regulate membrane binding by the CD3ε cytoplasmic domain. *J Exp Med* **209**: 2423-2439

Gandhi NS, Mancera RL. 2008. The structure of glycosaminoglycans and their interactions with proteins. *Chem Biol Drug Des* **72**: 455-482

Ganor Y, Besser M, Ben-Zakay N, Unger T, Levite M. 2003. Human T cells express a functional ionotropic glutamate receptor GluR3, and glutamate by itself triggers integrin-mediated adhesion to laminin and fibronectin and chemotactic migration. *J Immunol* **170**: 4362

Garcia-Elias A, Berna-Erro A, Rubio-Moscardo F, Pardo-Pastor C, Mrkonjić S, Sepúlveda RV, . . . Valverde MA. 2015. Interaction between the linker, Pre-S1, and TRP domains determines folding, assembly, and trafficking of TRPV channels. *Structure (London, England : 1993)* **23**: 1404-1413

Garcia-Elias A, Lorenzo IM, Vicente R, Valverde MA. 2008. IP_3 receptor binds to and sensitizes TRPV4 channel to osmotic stimuli via a calmodulin-binding site. *J Biol Chem* **283**: 31284-31288

Gasser A, Glassmeier G, Fliegert R, Langhorst MF, Meinke S, Hein D, . . . Guse AH. 2006. Activation of T cell calcium influx by the second messenger ADP-ribose. *J Biol Chem* **281**: 2489-2496

Gasser A, Guse AH. 2005. Determination of intracellular concentrations of the TRPM2 agonist ADP-ribose by reversed-phase hplc. *J Chromatogr B* **821**: 181-187

Gaudet R. 2008. TRP channels entering the structural era. *J Physiol* **586**: 3565-3575

Gavva NR, Tamir R, Qu Y, Klionsky L, Zhang TJ, Immke D, . . . Treanor JJ. 2005. AMG 9810 [(*E*)-3-(4-*t*-Butylphenyl)-*N*-(2,3-dihydrobenzo[*b*][1,4] dioxin-6-yl)acrylamide], a novel vanilloid receptor 1 (TRPV1) antagonist with antihyperalgesic properties. *J Pharmacol Exp Ther* **313**: 474-484

Gavva NR, Treanor JJ, Garami A, Fang L, Surapaneni S, Akrami A, . . . Davar G. 2008. Pharmacological blockade of the vanilloid receptor TRPV1 elicits marked hyperthermia in humans. *Pain* **136**: 202-210

Ge J, Li W, Zhao Q, Li N, Chen M, Zhi P, . . . Yang M. 2015. Architecture of the mammalian mechanosensitive piezo1 channel. *Nature* **527**: 64-69

Gees M, Colsoul B, Nilius B. 2010. The role of transient receptor potential cation channels in Ca^{2+} signaling. *Cold Spring Harb Perspect Biol* **2**:

Gees M, Owsianik G, Nilius B, Voets T. 2011. TRP channels In *Comprehensive physiology*, pp. 563 -596: John Wiley & Sons, Inc.

Gerasimenko JV, Petersen OH, Gerasimenko OV. 2014. Monitoring of intra-ER free Ca^{2+}. *WIRES Membrane Transport and Signaling* **3**: 63-71

Ghosh A, Khandelwal N, Kumar A, Bera AK. 2017. Leucine-rich repeat-containing 8B (LRRC8B) protein is associated with the endoplasmic reticulum calcium leak in HEK293 cells. *J Cell Sci*: jcs.203646

Gil D, Schamel WW, Montoya M, Sanchez-Madrid F, Alarcon B. 2002. Recruitment of Nck by CD3ε reveals a ligand-induced conformational change essential for T cell receptor signaling and synapse formation. *Cell* **109**: 901-912

Gil D, Schrum AG, Alarcón B, Palmer E. 2005. T cell receptor engagement by peptide-MHC ligands induces a conformational change in the CD3 complex of thymocytes. *J Exp Med* **201**: 517-522

Gil D, Schrum AG, Daniels MA, Palmer E. 2008. A role for CD8 in the developmental tuning of antigen recognition and CD3 conformational change. *J Immunol* **180**: 3900

Gillis S, Smith KA. 1977. Long term culture of tumour-specific cytotoxic T cells. *Nature* **268**: 154

Gnanasambandam R, Bae C, Gottlieb PA, Sachs F. 2015. Ionic selectivity and permeation properties of human piezo1 channels. *PLOS One* **10**: e0125503

Gnanasambandam R, Ghatak C, Yasmann A, Nishizawa K, Sachs F, Ladokhin AS, . . . Suchyna TM. 2017. GsMTx4: Mechanism of inhibiting mechanosensitive ion channels. *Biophys J* **112**: 31-45

Gonzales AL, Yang Y, Sullivan MN, Sanders L, Dabertrand F, Hill-Eubanks DC, . . . Earley S. 2014. A PLCγ1-dependent, force-sensitive signaling network in the myogenic constriction of cerebral arteries. *Sci Signal* **7**: ra49

Gordon-Shaag A, Zagotta WN, Gordon SE. 2008. Mechanism of Ca^{2+}-dependent desensitization in TRP channels. *Channels* **2**: 125-129

Goswami C, Hucho T. 2008. Submembraneous microtubule cytoskeleton: Biochemical and functional interplay of TRP channels with the cytoskeleton. *FEBS J* **275**: 4684-4699

Gothard LQ, Ruffner ME, Woodward JG, Park-Sarge O-K, Sarge KD. 2003. Lowered temperature set point for activation of the cellular stress response in T-lymphocytes. *J Biol Chem* **278**: 9322-9326

Gottlieb P, Folgering J, Maroto R, Raso A, Wood T, Kurosky A, . . . Honoré E. 2008. Revisiting TRPC1 and TRPC6 mechanosensitivity. *Pflüg Arch Eur J Phy* **455**: 1097-1103

Gottlieb PA, Bae C, Sachs F. 2012. Gating the mechanical channel piezo1: A comparison between whole-cell and patch recording. *Channels* **6**: 282-289

Gottlieb PA, Sachs F. 2012. Piezo1: Properties of a cation selective mechanical channel. *Channels* **6**: 214-219

Gottlieb PA, Suchyna TM, Sachs F. 2007. Properties and mechanism of the mechanosensitive ion channel inhibitor gsmtx4, a therapeutic peptide derived from tarantula venom In *Curr top membr*, ed. OP Hamill, pp. 81-109: Academic Press

Grandl J, Hu H, Bandell M, Bursulaya B, Schmidt M, Petrus M, Patapoutian A. 2008. Pore region of TRPV3 ion channel is specifically required for heat activation. *Nat Neurosci* **11**: 1007-1013

Gratiot-Deans J, Ding L, Turka LA, Nuñez G. 1993. Bcl-2 proto-oncogene expression during human T cell development. Evidence for biphasic regulation. *J Immunol* **151**: 83

Grebe KM, Clarke RL, Potter TA. 2004. Ligation of CD8 leads to apoptosis of thymocytes that have not undergone positive selection. *Proc Natl Acad Sci USA* **101**: 10410-10415

Grimm C, Kraft R, Sauerbruch S, Schultz G, Harteneck C. 2003. Molecular and functional characterization of the melastatin-related cation channel TRPM3. *J Biol Chem* **278**: 21493-21501

Gross SA, Guzman GA, Wissenbach U, Philipp SE, Zhu MX, Bruns D, Cavalie A. 2009. TRPC5 is a Ca^{2+}-activated channel functionally coupled to Ca^{2+}-selective ion channels. *J Biol Chem* **284**: 34423-34432

Grubisha O, Mogg AJ, Sorge JL, Ball L-J, Sanger H, Ruble CLA, . . . Broad LM. 2014. Pharmacological profiling of the TRPV3 channel in recombinant and native assays. *Brit J Pharmacol* **171**: 2631-2644

Grundler W, Dirscherl P, Beisker W, Marx K, Stampfl A, Maier K, . . . Nüsse M. 2001. Early functional apoptotic responses of thymocytes induced by tri-n-butyltin. *Cytometry* **44**: 45-56

Grynkiewicz G, Poenie M, Tsien RY. 1985. A new generation of Ca^{2+} indicators with greatly improved fluorescence properties. *J Biol Chem* **260**: 3440-3450

Gschwendt M, Dieterich S, Rennecke J, Kittstein W, Mueller HJ, Johannes FJ. 1996. Inhibition of protein kinase Cμ by various inhibitors. Differentiation from protein kinase C isoenzymes. *FEBS Lett* **392**: 77-80

Guidos CJ, Danska JS, Fathman CG, Weissman IL. 1990. T cell receptor-mediated negative selection of autoreactive T lymphocyte precursors occurs after commitment to the CD4 or CD8 lineages. *J Exp Med* **172**: 835-845

Guinamard R, Simard C, Del Negro C. 2013. Flufenamic acid as an ion channel modulator. *Pharmacol Ther* **138**: 272-284

Güler AD, Lee H, Iida T, Shimizu I, Tominaga M, Caterina M. 2002. Heat-evoked activation of the ion channel, TRPV4. *J Neurosci* **22**: 6408

Gunther T, Vormann J. 1992. Activation of Na^{+}/Mg^{2+} antiport in thymocytes by cAMP. *FEBS Lett* **297**: 132-134

Gunther T, Vormann J, Merker HJ, Averdunk R, Peter HW, Wonigeit K. 1984. Membrane alterations in magnesium-deficiency-induced malignant T cell lymphoma. *Magnesium* **3**: 29-37

Guo J, Zhang Y, Li H, Chu H, Wang Q, Jiang S, . . . Xu C. 2018. Intramembrane ionic protein–lipid interaction regulates integrin structure and function. *PLOS Biol* **16**: e2006525

Guo YR, MacKinnon R. 2017. Structure-based membrane dome mechanism for piezo mechanosensitivity. *eLife* **6**:

Gwack Y, Srikanth S, Oh-hora M, Hogan PG, Lamperti ED, Yamashita M, . . . Rao A. 2008. Hair loss and defective T- and B-cell function in mice lacking orai1. *Mol Cell Biol* **28**: 5209-5222

Gwanyanya A, Sipido KR, Vereecke J, Mubagwa K. 2006. ATP and PIP_2 dependence of the magnesium-inhibited, TRPM7-like cation channel in cardiac myocytes. *Am J Physiol Cell Physiol* **291**: C627-635

Hajdu P, Varga Z, Pieri C, Panyi G, Gaspar RJ. 2003. Cholesterol modifies the gating of Kv1.3 in human T lymphocytes. *Pflugers Arch* **445**: 674-682

Hajnóczky G, Csordás G, Das S, Garcia-Perez C, Saotome M, Sinha Roy S, Yi M. 2006. Mitochondrial calcium signalling and cell death: Approaches for assessing the role of mitochondrial Ca^{2+} uptake in apoptosis. *Cell calcium* **40**: 553-560

Halaszovich CR, Zitt C, Jüngling E, Lückhoff A. 2000. Inhibition of trp3 channels by lanthanides. *J Biol Chem* **275**: 37423-37428

Han Q, Liu D, Convertino M, Wang Z, Jiang C, Kim YH, . . . Ji R-R. 2018. miRNA-711 binds and activates TRPA1 extracellularly to evoke acute and chronic pruritus. *Neuron* **99**: 449-463.e446

Hanke JH, Gardner JP, Dow RL, Changelian PS, Brissette WH, Weringer EJ, . . . Connelly PA. 1996. Discovery of a novel, potent, and Src family-selective tyrosine kinase inhibitor. *J Biol Chem* **271**: 695-701

Hansen SB. 2015. Lipid agonism: The PIP_2 paradigm of ligand-gated ion channels. *Biochimica et Biophysica Acta (BBA) - Mol Cell Biol Lipid* **1851**: 620-628

Hara Y, Wakamori M, Ishii M, Maeno E, Nishida M, Yoshida T, . . . Mori Y. 2002. LTRPC2 Ca^{2+}-permeable channel activated by changes in redox status confers susceptibility to cell death. *Mol Cell* **9**: 163-173

Hardie RC, Minke B. 1992. The *trp* gene is essential for a light-activated Ca^{2+} channel in *drosophila* photoreceptors. *Neuron* **8**: 643-651

Hardie RC, Minke B. 1993. Novel Ca^{2+} channels underlying transduction in drosophilaphotoreceptors: Implications for phosphoinositide-mediated Ca^{2+} mobilization. *Trends Neurosci* **16**: 371-376

Hare KJ, Pongracz J, Jenkinson EJ, Anderson G. 2003. Modeling TCR signaling complex formation in positive selection. *J Immunol* **171**: 2825-2831

Harootunian AT, Kao JP, Eckert BK, Tsien RY. 1989. Fluorescence ratio imaging of cytosolic free Na^+ in individual fibroblasts and lymphocytes. *J Biol Chem* **264**: 19458-19467

Harteneck C. 2003. Proteins modulating TRP channel function. *Cell calcium* **33**: 303-310

Harteneck C. 2013. Pregnenolone sulfate: From steroid metabolite to TRP channel ligand. *Molecules* **18**: 12012-12028

Hartmann J, Dragicevic E, Adelsberger H, Henning HA, Sumser M, Abramowitz J, . . . Konnerth A. 2008. TRPC3 channels are required for synaptic transmission and motor coordination. *Neuron* **59**: 392-398

Hasan R, Leeson-Payne ATS, Jaggar JH, Zhang X. 2017. Calmodulin is responsible for Ca^{2+}-dependent regulation of TRPA1 channels. *Sci Rep-UK* **7**: 45098

Hasan R, Zhang X. 2018. Ca^{2+} regulation of TRP ion channels. *Int J Mol Sci* **19**:

Haselwandter CA, MacKinnon R. 2018. Piezo's membrane footprint and its contribution to mechanosensitivity. *eLife* **7**: e41968

He B, Soderlund DM. 2010. Human embryonic kidney (HEK293) cells express endogenous voltage-gated sodium currents and Nav1.7 sodium channels. *Neurosci Lett* **469**: 268-272

He X, Li S, Liu B, Susperreguy S, Formoso K, Yao J, . . . Liao Y. 2017. Major contribution of the 3/6/7 class of TRPC channels to myocardial ischemia/reperfusion and cellular hypoxia/reoxygenation injuries. *Proc Natl Acad Sci USA* **114**: E4582

Held K, Voets T, Vriens J. 2015. TRPM3 in temperature sensing and beyond. *Temperature* **2**: 201-213

Heng TS, Painter MW. 2008. The immunological genome project: Networks of gene expression in immune cells. *Nat Immunol* **9**: 1091-1094

Hesketh TR, Smith GA, Moore JP, Taylor MV, Metcalfe JC. 1983. Free cytoplasmic calcium concentration and the mitogenic stimulation of lymphocytes. *J Biol Chem* **258**: 4876-4882

Hess SD, Oortgiesen M, Cahalan MD. 1993. Calcium oscillations in human t and natural killer cells depend upon membrane potential and calcium influx. *J Immunol* **150**: 2620-2633

Hilgemann DW. 2007. Local PIP_2 signals: When, where, and how? *Pflüg Arch Eur J Phy* **455**: 55-67

Hilgemann DW, Feng S, Nasuhoglu C. 2001. The complex and intriguing lives of PIP_2 with ion channels and transporters. *Sci Signal* **2001**: re19-re19

Hill K, Schaefer M. 2007. TRPA1 is differentially modulated by the amphipathic molecules trinitrophenol and chlorpromazine. *J Biol Chem* **282**: 7145-7153

Hille B. 2001. *Ion channels of excitable membranes*. pp. 647-662. Oxford University Press UK.

Hille B, Dickson EJ, Kruse M, Vivas O, Suh BC. 2015. Phosphoinositides regulate ion channels. *Biochim Biophys Acta* **1851**: 844-856

Hisatsune C, Kuroda Y, Nakamura K, Inoue T, Nakamura T, Michikawa T, . . . Mikoshiba K. 2004. Regulation of TRPC6 channel activity by tyrosine phosphorylation. *J Biol Chem* **279**: 18887-18894

Hofmann T, Obukhov AG, Schaefer M, Harteneck C, Gudermann T, Schultz G. 1999. Direct activation of human TRPC6 and TRPC3 channels by diacylglycerol. *Nature* **397**: 259-263

Hofmann T, Schaefer M, Schultz G, Gudermann T. 2000. Cloning, expression and subcellular localization of two novel splice variants of mouse transient receptor potential channel 2. *Biochem J* **351**: 115-122

Hogg N, Patzak I, Willenbrock F. 2011. The insider's guide to leukocyte integrin signalling and function. *Nat Rev Immunol* **11**: 416

Holakovska B, Grycova L, Bily J, Teisinger J. 2011. Characterization of calmodulin binding domains in TRPV2 and TRPV5 c-tails. *Amino acids* **40**: 741-748

Holendova B, Grycova L, Jirku M, Teisinger J. 2012. Ptdins(4,5)p_2 interacts with cam binding domains on TRPM3 N-terminus. *Channels* **6**: 479-482

Holzer P, Izzo AA. 2014. The pharmacology of TRP channels. *Br J Pharmacol* **171**: 2469-2473

Hong J, Ge C, Jothikumar P, Yuan Z, Liu B, Bai K, . . . Zhu C. 2018. A TCR mechanotransduction signaling loop induces negative selection in the thymus. *Nat Immunol* **19**: 1379-1390

Horejsi V, Otahal P, Brdicka T. 2010. LAT--an important raft-associated transmembrane adaptor protein. . *FEBS J* **277**: 4383-4397

Horinouchi T, Higashi T, Higa T, Terada K, Mai Y, Aoyagi H, . . . Miwa S. 2012. Different binding property of STIM1 and its novel splice variant STIM1L to Orai1, TRPC3, and TRPC6 channels. *Biochem Biophys Res Commun* **428**: 252-258

Horn J, Wang X, Reichardt P, Stradal TE, Warnecke N, Simeoni L, . . . Kliche S. 2009. Src homology 2-domain containing leukocyte-specific phosphoprotein of 76 kDa is mandatory for TCR-mediated inside-out signaling, but dispensable for CXCR4-mediated LFA-1 activation, adhesion, and migration of T cells. *J Immunol* **183**: 5756-5767

Horowitz LF, Hirdes W, Suh B-C, Hilgemann DW, Mackie K, Hille B. 2005. Phospholipase c in living cells. *J Gen Physiol* **126**: 243

Horváth Á, Tékus V, Boros M, Pozsgai G, Botz B, Borbély É, . . . Helyes Z. 2016. Transient receptor potential ankyrin 1 (TRPA1) receptor is involved in chronic arthritis: *In vivo* study using TRPA1-deficient mice. *Arthritis Res Ther* **18**: 1-14

Hu H-Z, Gu Q, Wang C, Colton CK, Tang J, Kinoshita-Kawada M, . . . Zhu MX. 2004. 2-aminoethoxydiphenyl borate is a common activator of TRPV1, TRPV2, and TRPV3. *J Biol Chem* **279**: 35741-35748

Hu H-Z, Xiao R, Wang C, Gao N, Colton CK, Wood JD, Zhu MX. 2006. Potentiation of TRPV3 channel function by unsaturated fatty acids. *J Cell Physiol* **208**: 201-212

Hu H, Grandl J, Bandell M, Petrus M, Patapoutian A. 2009. Two amino acid residues determine 2-APB sensitivity of the ion channels TRPV3 and TRPV4. *Proc Natl Acad Sci USA* **106**: 1626

Hu KH, Butte MJ. 2016. T cell activation requires force generation. *J Cell Biol* **213**: 535

Huang SM, Li X, Yu Y, Wang J, Caterina MJ. 2011. TRPV3 and TRPV4 ion channels are not major contributors to mouse heat sensation. *Mol Pain* **7**: 37

Huber A, Sander P, Gobert A, Bahner M, Hermann R, Paulsen R. 1996. The transient receptor potential protein (TRP), a putative store-operated Ca^{2+} channel essential for phosphoinositide-mediated photoreception, forms a signaling complex with norpa, inac and inad. *EMBO J* **15**: 7036-7045

Huber TB, Schermer B, Muller RU, Hohne M, Bartram M, Calixto A, . . . Benzing T. 2006. Podocin and mec-2 bind cholesterol to regulate the activity of associated ion channels. *Proc Natl Acad Sci USA* **103**: 17079-17086

Hurne AM, Chai CLL, Moerman K, Waring P. 2002. Influx of calcium through a redox-sensitive plasma membrane channel in thymocytes causes early necrotic cell death induced by the epipolythiodioxopiperazine toxins. *J Biol Chem* **277**: 31631-31638

Huster D, Paasche G, Dietrich U, Zschörnig O, Gutberlet T, Gawrisch K, Arnold K. 1999. Investigation of phospholipid area compression induced by calcium-mediated dextran sulfate interaction. *Biophys J* **77**: 879-887

Hwang SW, Cho H, Kwak J, Lee S-Y, Kang C-J, Jung J, . . . Oh U. 2000. Direct activation of capsaicin receptors by products of lipoxygenases: Endogenous capsaicin-like substances. *Proc Natl Acad Sci USA* **97**: 6155-6160

Iamshanova O, Mariot P, Lehen'kyi Vy, Prevarskaya N. 2016. Comparison of fluorescence probes for intracellular sodium imaging in prostate cancer cell lines. *Eur Biophys J* **45**: 765-777

Ignatowska-Jankowska B, Jankowski M, Glac W, Swiergel AH. 2009. Cannabidiol-induced lymphopenia does not involve nkt and nk cells. *J Physiol Pharmacol* **60 Suppl 3**: 99-103

Imai Y, Itsuki K, Okamura Y, Inoue R, Mori MX. 2012. A self-limiting regulation of vasoconstrictor-activated TRPC3/c6/c7 channels coupled to $PI(4,5)P_2$-diacylglycerol signalling. *J Physiol-London* **590**: 1101-1119

Inada H, Iida T, Tominaga M. 2006. Different expression patterns of TRP genes in murine b and T lymphocytes. *Biochem Biophys Res Commun* **350**: 762-767

Inoue R, Jensen LJ, Jian Z, Shi J, Hai L, Lurie AI, . . . Ito Y. 2009. Synergistic activation of vascular TRPC6 channel by receptor and mechanical stimulation via phospholipase C/diacylglycerol and phospholipase a2/ω-hydroxylase/20-hete pathways. *Circ Res* **104**: 1399-1409

Inoue R, Okada T, Onoue H, Hara Y, Shimizu S, Naitoh S, . . . Mori Y. 2001. The transient receptor potential protein homologue TRP6 is the essential component of vascular α_1-adrenoceptor-activated Ca^{2+}-permeable cation channel. *Circ Res* **88**: 325-332

Iordanov I, Mihalyi C, Toth B, Csanady L. 2016. The proposed channel-enzyme transient receptor potential melastatin 2 does not possess ADP ribose hydrolase activity. *eLife* **5**:

Irie HY, Mong MS, Itano A, Crooks MEC, Littman DR, Burakoff SJ, Robey E. 1998. The cytoplasmic domain of CD8β regulates Lck kinase activation and CD8 T cell development. *J Immunol* **161**: 183-191

Irie S, Furukawa T. 2014. TRPM1 In *Mammalian transient receptor potential (TRP) cation channels: Volume I*, ed. B Nilius, V Flockerzi, pp. 387-402. Berlin, Heidelberg: Springer Berlin Heidelberg

Ishida Y, Chused TM. 1988. Heterogeneity of lymphocyte calcium metabolism is caused by T cell-specific calcium-sensitive potassium channel and sensitivity of the calcium ATPase pump to membrane potential. *J Exp Med* **168**: 839-852

Ishida Y, Chused TM. 1993. Lack of voltage sensitive potassium channels and generation of membrane potential by sodium potassium ATPase in murine T lymphocytes. *J Immunol* **151**: 610-620

Ishikawa J, Ohga K, Yoshino T, Takezawa R, Ichikawa A, Kubota H, Yamada T. 2003. A pyrazole derivative, YM-58483, potently inhibits store-operated sustained Ca^{2+} influx and IL-2 production in T lymphocytes. *J Immunol* **170**: 4441

Israelson A, Zaid H, Abu-Hamad S, Nahon E, Shoshan-Barmatz V. 2008. Mapping the ruthenium red-binding site of the voltage-dependent anion channel-1. *Cell calcium* **43**: 196-204

Iwamoto T, Inoue Y, Ito K, Sakaue T, Kita S, Katsuragi T. 2004. The exchanger inhibitory peptide region-dependent inhibition of Na^+/Ca^{2+} exchange by SN-6 [2-[4-(4-Nitrobenzyloxy)benzyl] thiazolidine-4-carboxylic acid ethyl ester], a novel benzyloxyphenyl derivative. *Mol Pharmacol* **66**: 45-55

Iwamoto T, Watanabe Y, Kita S, Blaustein MP. 2007. Na^+/Ca^{2+} exchange inhibitors: A new class of calcium regulators. *Cardiovasc Hematol Disord Drug Targets* **7**: 188-198

Jabba S, Goyal R, Sosa-Pagán JO, Moldenhauer H, Wu J, Kalmeta B, . . . Grandl J. 2014. Directionality of temperature activation in mouse TRPA1 ion channel can be inverted by single-point mutations in ankyrin repeat six. *Neuron* **82**: 1017-1031

Jaquemar D, Schenker T, Trueb B. 1999. An ankyrin-like protein with transmembrane domains is specifically lost after oncogenic transformation of human fibroblasts. *J Biol Chem* **274**: 7325-7333

Jardín I, López JJ, Redondo PC, Salido GM, Rosado JA. 2009. Store-operated Ca^{2+} entry is sensitive to the extracellular Ca^{2+} concentration through plasma membrane STIM1. *Biochimica et Biophysica Acta (BBA) - Mol Cell Res* **1793**: 1614-1622

Jayaraman T, Ondrias K, Ondriasova E, Marks AR. 1996. Regulation of the inositol 1,4,5-trisphosphate receptor by tyrosine phosphorylation. *Science* **272**: 1492-1494

Jeon JP, Hong C, Park EJ, Jeon JH, Cho NH, Kim IG, . . . So I. 2012. Selective gαi subunits as novel direct activators of transient receptor potential canonical (TRPC)4 and TRPC5 channels. *J Biol Chem* **287**: 17029-17039

Jha A, Singh AK, Weissgerber P, Freichel M, Flockerzi V, Flavell RA, Jha MK. 2015. Essential roles for $ca_v\beta 2$ and Ca_v1 channels in thymocyte development and T cell homeostasis. *Sci Signal* **8**: ra103

Jha MK, Badou A, Meissner M, McRory JE, Freichel M, Flockerzi V, Flavell RA. 2009. Defective survival of naive $CD8^+$ T lymphocytes in the absence of the β3 regulatory subunit of voltage-gated calcium channels. *Nat Immunol* **10**: 1275-1282

Jiang N, Huang J, Edwards LJ, Liu B, Zhang Y, Beal CD, . . . Zhu C. 2011. Two-stage cooperative T cell receptor-peptide major histocompatibility complex-CD8 trimolecular interactions amplify antigen discrimination. *Immunity* **34**: 13-23

Jiang S, Kull B, Fredholm BB, Orrenius S. 1996. P2X purinoceptor is not important in thymocyte apoptosis. *Immunol Lett* **49**: 197-201

Jin J, Desai BN, Navarro B, Donovan A, Andrews NC, Clapham DE. 2008a. Deletion of *Trpm7* disrupts embryonic development and thymopoiesis without altering Mg^{2+} homeostasis. *Science* **322**: 756-760

Jin R, Wang W, Yao J-Y, Zhou Y-B, Qian X-P, Zhang J, . . . Chen W-F. 2008b. Characterization of the *in vivo* dynamics of medullary $CD4^+$ $CD8^-$ thymocyte development. *J Immunol* **180**: 2256

Jin X, Morsy N, Winston J, Pasricha PJ, Garrett K, Akbarali HI. 2004. Modulation of TRPV1 by nonreceptor tyrosine kinase, c-Src kinase. *Am J Physiol Cell Physiol* **287**: C558-563

Jirku M, Bumba L, Bednarova L, Kubala M, Sulc M, Franek M, . . . Bousova K. 2015. Characterization of the part of N-terminal PIP_2 binding site of the TRPM1 channel. *Biophys Chem* **207**: 135-142

Jirku M, Lansky Z, Bednarova L, Sulc M, Monincova L, Majer P, . . . Bousova K. 2016. The characterization of a novel S100A1 binding site in the N-terminus of TRPM1. *Int J Biochem Cell Biol* **78**: 186-193

Joseph N, Reicher B, Barda-Saad M. 2014. The calcium feedback loop and T cell activation: How cytoskeleton networks control intracellular calcium flux. *Biochimica et Biophysica Acta - Biomembranes* **1838**: 557-568

Jungnickel MK, Marrero H, Birnbaumer L, Lemos JR, Florman HM. 2001. Trp2 regulates entry of Ca^{2+} into mouse sperm triggered by egg ZP3. *Nat Cell Biol* **3**:

Juntilla MM, Koretzky GA. 2008. Critical roles of the PI_3K/akt signaling pathway in T cell development. *Immunol Lett* **116**: 104-110

Juvin V, Penna A, Chemin J, Lin Y-L, Rassendren F-A. 2007. Pharmacological characterization and molecular determinants of the activation of transient

receptor potential V2 channel orthologs by 2-aminoethoxydiphenyl borate. *Mol Pharmacol* **72**: 1258-1268

Juzan M, Hostein I, Gualde N. 1992. Role of thymus-eicosanoids in the immune response. *Prostag Leukotr Ess* **46**: 247-255

Kalia J, Swartz KJ. 2013. Exploring structure-function relationships between TRP and Kv channels. *Sci Rep-UK* **3**: 1523

Kane LP, Hedrick SM. 1996. A role for calcium influx in setting the threshold for $CD4^+$ $CD8^+$ thymocyte negative selection. *J Immunol* **156**: 4594-4601

Kanellopoulou C, George AB, Masutani E, Cannons JL, Ravell JC, Yamamoto TN, . . . Lenardo MJ. 2019. Mg^{2+} regulation of kinase signaling and immune function. *J Exp Med*: jem.20181970

Kanner SB, Grosmaire LS, Ledbetter JA, Damle NK. 1993. B_2-integrin LFA-1 signaling through phospholipase C-γ1 activation. *Proc Natl Acad Sci USA* **90**: 7099-7103

Karashima Y, Damann N, Prenen J, Talavera K, Segal A, Voets T, Nilius B. 2007. Bimodal action of menthol on the transient receptor potential channel TRPA1. *J Neurosci* **27**: 9874

Kazama I, Maruyama Y, Murata Y. 2012. Suppressive effects of nonsteroidal anti-inflammatory drugs diclofenac sodium, salicylate and indomethacin on delayed rectifier K^+-channel currents in murine thymocytes. *Immunopharm Immunot* **34**: 874-878

Khalil M, Alliger K, Weidinger C, Yerinde C, Wirtz S, Becker C, Engel MA. 2018. Functional role of transient receptor potential channels in immune cells and epithelia. *Front Immunol* **9**: 174

Khan A, Steiner J, Klein M, Schneider M, Snyder S. 1992a. IP_3 receptor: Localization to plasma membrane of T cells and cocapping with the T cell receptor. *Science* **257**: 815-818

Khan AA, Soloski MJ, Sharp AH, Schilling G, Sabatini DM, Li SH, . . . Snyder SH. 1996. Lymphocyte apoptosis: Mediation by increased type 3 inositol 1,4,5-trisphosphate receptor. *Science* **273**: 503-507

Khan AA, Steiner JP, Snyder SH. 1992b. Plasma membrane inositol 1,4,5-trisphosphate receptor of lymphocytes: Selective enrichment in sialic acid and unique binding specificity. *Proc Natl Acad Sci USA* **89**: 2849-2853

Kheradpezhouh E, Choy JMC, Daria V, Arabzadeh E. 2017. TRPA1 expression and its functional activation in rodent cortex. *Open Biol* **7**:

Khodorova AB, Astashkin EI. 1994. A dual effect of arachidonic acid on Ca^{2+} transport systems in lymphocytes. *FEBS Lett* **353**: 167-170

Kim JY, Saffen D. 2005. Activation of M1 muscarinic acetylcholine receptors stimulates the formation of a multiprotein complex centered on TRPC6 channels. *J Biol Chem* **280**: 32035-32047

Kim JY, Zeng W, Kiselyov K, Yuan JP, Dehoff MH, Mikoshiba K, . . . Muallem S. 2006. Homer 1 mediates store- and inositol 1,4,5-trisphosphate receptor-

dependent translocation and retrieval of TRPC3 to the plasma membrane. *J Biol Chem* **281**: 32540-32549

Kim K, Wang L, Hwang I. 2009a. LFA-1-dependent Ca^{2+} entry following suboptimal T cell receptor triggering proceeds without mobilization of intracellular Ca^{2+}. *J Biol Chem* **284**: 22149-22154

Kim M, Carman CV, Springer TA. 2003. Bidirectional transmembrane signaling by cytoplasmic domain separation in integrins. *Science* **301**: 1720

Kim ST, Takeuchi K, Sun Z-YJ, Touma M, Castro CE, Fahmy A, . . . Reinherz EL. 2009b. The $\alpha\beta$T cell receptor is an anisotropic mechanosensor. *J Biol Chem* **284**: 31028-31037

Kim Y, Wong AC, Power JM, Tadros SF, Klugmann M, Moorhouse AJ, . . . Housley GD. 2012. Alternative splicing of the TRPC3 ion channel calmodulin/IP_3 receptor-binding domain in the hindbrain enhances cation flux. *J Neurosci* **32**: 11414-11423

Kinoshita S, Seki T, Liu TF, Kushida T. 1988. Fluorescence of hematoporphyrin in living cells and in solution. *J Photochem Photobiol B* **2**: 195-208

Kiselyov K, Kim JY, Zeng W, Muallem S. 2005. Protein-protein interaction and functiontrpc channels. *Pflugers Arch* **451**: 116-124

Kiselyov K, Xu X, Mozhayeva G, Kuo T, Pessah I, Mignery G, . . . Muallem S. 1998. Functional interaction between $InsP_3$ receptors and store-operated htrp3 channels. *Nature* **396**: 478-482

Kittaka H, Yamanoi Y, Tominaga M. 2017. Transient receptor potential vanilloid 4 (TRPV4) channel as a target of crotamiton and its bimodal effects. *Pflugers Arch*:

Kivens WJ, Hunt SWr, Mobley JL, Zell T, Dell CL, Bierer BE, Shimizu Y. 1998. Identification of a proline-rich sequence in the CD2 cytoplasmic domain critical for regulation of integrin-mediated adhesion and activation of phosphoinositide 3-kinase. *Mol Cell Biol* **18**: 5291-5307

Klein AS, Tannert A, Schaefer M. 2014. Cholesterol sensitises the transient receptor potential channel TRPV3 to lower temperatures and activator concentrations. *Cell calcium* **55**: 59-68

Knaus HG, Moshammer T, Friedrich K, Kang HC, Haugland RP, Glossman H. 1992. *In vivo* labeling of L-type Ca^{2+} channels by fluorescent dihydropyridines: Evidence for a functional, extracellular heparin-binding site. *Proc Natl Acad Sci USA* **89**: 3586

Knaus HG, Scheffauer F, Romanin C, Schindler AG, Glossmann H. 1990. Heparin binds with high affinity to voltage dependent L-type Ca^{2+} channels. *J Biol Chem.* **266**: 11156 - 11166

Koh WS, Yoon SY, Kwon BM, Jeong TC, Nam KS, Han MY. 1998. Cinnamaldehyde inhibits lymphocyte proliferation and modulates T-cell differentiation. *Int J Immunopharmaco* **20**:

Koike C, Obara T, Uriu Y, Numata T, Sanuki R, Miyata K, . . . Furukawa T. 2010. TRPM1 is a component of the retinal on bipolar cell transduction channel in the mglur6 cascade. *Proc Natl Acad Sci USA* **107**: 332-337

Kong Y-Y, Fischer K-D, Bachmann MF, Mariathasan S, Kozieradzki I, Nghiem MP, . . . Penninger JM. 1998. Vav regulates peptide-specific apoptosis in thymocytes. *J Exp Med* **188**: 2099-2111

Koni PA, Khanna R, Chang MC, Tang MD, Kaczmarek LK, Schlichter LC, Flavell RA. 2003. Compensatory anion currents in k_v1.3 channel-deficient thymocytes. *J Biol Chem* **278**: 39443-39451

Koo GC, Blake JT, Talento A, Nguyen M, Lin S, Sirotina A, . . . Feeney W. 1997. Blockade of the voltage-gated potassium channel Kv1.3 inhibits immune responses *in vivo*. *J Immunol* **158**: 5120-5128

Kostyuk PG, Mironov SL, Doroshenko PA, Ponomarev VN. 1982. Surface charges on the outer side of mollusc neuron membrane. *J Membrane Biol* **70**: 171-179

Kotturi MF, Hunt S, Jefferies WA. 2006. Roles of CRAC and Ca_V-like channels in T cells: More than one gatekeeper? *Trends Pharmacol Sci* **27**: 360-367

Kotturi MF, Jefferies WA. 2005. Molecular characterization of L-type calcium channel splice variants expressed in human T lymphocytes. *Mol Immunol* **42**: 1461-1474

Kozak JA, Cahalan MD. 2003. MIC channels are inhibited by internal divalent cations but not ATP. *Biophys J* **84**: 922-927

Kramer I. 2016. *Signal transduction*. San Diego CA. USA.: Elsevier Academic Press.

Krapivinsky G, Krapivinsky L, Manasian Y, Clapham DE. 2014. The TRPM7 chanzyme is cleaved to release a chromatin-modifying kinase. *Cell* **157**: 1061-1072

Krapivinsky G, Krapivinsky L, Renthal NE, Santa-Cruz A, Manasian Y, Clapham DE. 2017. Histone phosphorylation by TRPM6's cleaved kinase attenuates adjacent arginine methylation to regulate gene expression. *Proc Natl Acad Sci USA*:

Kunert-Keil C, Bisping F, Kruger J, Brinkmeier H. 2006. Tissue-specific expression of TRP channel genes in the mouse and its variation in three different mouse strains. *BMC genomics* **7**: 159

Kuras Z, Yun Y-H, Chimote AA, Neumeier L, Conforti L. 2012. K_{Ca}3.1 and TRPM7 channels at the uropod regulate migration of activated human T cells. *PLOS One* **7**: e43859

Kurd N, Robey EA. 2016. T cell selection in the thymus: A spatial and temporal perspective. *Immunol Rev* **271**: 114-126

Kwan KY, Allchorne AJ, Vollrath MA, Christensen AP, Zhang DS, Woolf CJ. 2006. TRPA1 contributes to cold, mechanical, and chemical nociception but is not essential for hair-cell transduction. *Neuron* **50**:

Kwon Y, Hofmann T, Montell C. 2007. Integration of phosphoinositide- and calmodulin-mediated regulation of TRPC6. *Mol Cell* **25**: 491-503

Kyewski BA, Rouse RV, Kaplan HS. 1982. Thymocyte rosettes: Multicellular complexes of lymphocytes and bone marrow-derived stromal cells in the mouse thymus. *Proc Natl Acad Sci USA* **79**: 5646-5650

Lai JP, Douglas SD, Ho WZ. 1998. Human lymphocytes express substance P and its receptor. *J Neuroimmunol* **86**: 80-86

Lambert S, Drews A, Rizun O, Wagner TF, Lis A, Mannebach S, . . . Oberwinkler J. 2011. Transient receptor potential melastatin 1 (TRPM1) is an ion-conducting plasma membrane channel inhibited by zinc ions. *J Biol Chem* **286**: 12221-12233

Langeslag M, Clark K, Moolenaar WH, van Leeuwen FN, Jalink K. 2007. Activation of TRPM7 channels by phospholipase C-coupled receptor agonists. *J Biol Chem* **282**: 232-239

Launay P, Cheng H, Srivatsan S, Penner R, Fleig A, Kinet JP. 2004. TRPM4 regulates calcium oscillations after T cell activation. *Science* **306**: 1374-1377

Launay P, Fleig A, Perraud A-L, Scharenberg AM, Penner R, Kinet J-P. 2002. TRPM4 is a Ca^{2+}-activated nonselective cation channel mediating cell membrane depolarization. *Cell* **109**: 397-407

Laursen WJ, Anderson EO, Hoffstaetter LJ, Bagriantsev SN, Gracheva EO. 2015. Species-specific temperature sensitivity of TRPA1. *Temperature: Multidisciplinary Biomed J* **2**: 214-226

Le Stunff H, Auger R, Kanellopoulos J, Raymond MN. 2004. The Pro-451 to Leu polymorphism within the C-terminal tail of P2X7 receptor impairs cell death but not phospholipase d activation in murine thymocytes. *J Biol Chem* **279**: 16918-16926

Ledbetter JA, Rabinovitch PS, Hellstrom I, Hellstrom KE, Grosmaire LS, June CH. 1988. Role of CD2 cross-linking in cytoplasmic calcium responses and T cell activation. *Eur J Immunol* **18**: 1601-1608

Lederman S, Gulick R, Chess L. 1989. Dextran sulfate and heparin interact with CD4 molecules to inhibit the binding of coat protein (gp120) of HIV. *J Immunol* **143**: 1149-1154

Lee G, Abdi K, Jiang Y, Michaely P, Bennett V, Marszalek PE. 2006. Nanospring behaviour of ankyrin repeats. *Nature* **440**: 246

Lee MS, Glassman CR, Deshpande NR, Badgandi HB, Parrish HL, Uttamapinant C, . . . Kuhns MS. 2015. A mechanical switch couples T cell receptor triggering to the cytoplasmic juxtamembrane regions of CD3ζζ. *Immunity* **43**: 227-239

Lemonnier L, Trebak M, Putney JW. 2008. Complex regulation of the TRPC3, 6 and 7 channel subfamily by diacylglycerol and phosphatidylinositol-4,5-bisphosphate. *Cell calcium* **43**: 506-514

Leonard RJ, Garcia ML, Slaughter RS, Reuben JP. 1992. Selective blockers of voltage-gated K^+ channels depolarize human T lymphocytes: Mechanism of the antiproliferative effect of charybdotoxin. *Proc Natl Acad Sci USA* **89**: 10094-10098

Lepesant H, Reggio H, Pierres M, Naquet P. 1990. Mouse thymic epithelial cell lines interact with and select a cd3lowcd4$^+$CD8$^+$ thymocyte subset through an LFA-1-dependent adhesion-de-adhesion mechanism. *Int Immunol* **2**: 1021-1032

Lépine S, Le Stunff H, Lakatos B, Sulpice JC, Giraud F. 2006. ATP-induced apoptosis of thymocytes is mediated by activation of P2X7 receptor and involves *de novo* ceramide synthesis and mitochondria. *Biochimica et Biophysica Acta (BBA) - Mol Cell Biol Lipid* **1761**: 73-82

Lettau M, Kliche S, Kabelitz D, Janssen O. 2014. The adapter proteins ADAP and Nck cooperate in T cell adhesion. *Mol Immunol* **60**: 72-79

Leuner K, Kazanski V, Muller M, Essin K, Henke B, Gollasch M, . . . Muller WE. 2007. Hyperforin-a key constituent of St. John's wort specifically activates TRPC6 channels. *FASEB J* **21**: 4101-4111

Levitan I, Singh DK, Rosenhouse-Dantsker A. 2014. Cholesterol binding to ion channels. *Front Physiol* **5**: 65

Lewis AH, Grandl J. 2015. Mechanical sensitivity of piezo1 ion channels can be tuned by cellular membrane tension. *eLife* **4**:

Lewis RS. 2001. Calcium signaling mechanisms in T lymphocytes. *Annu Rev Immunol* **19**: 497-521

Lewis RS, Cahalan MD. 1988. Subset-specific expression of potassium channels in developing murine T lymphocytes. *Science* **239**: 771-775

Li C, Fox CJ, Master SR, Bindokas VP, Chodosh LA, Thompson CB. 2002a. Bcl-XL affects Ca^{2+} homeostasis by altering expression of inositol 1,4,5-trisphosphate receptors. *Proc Natl Acad Sci USA* **99**: 9830-9835

Li FY, Chaigne-Delalande B, Kanellopoulou C, Davis JC, Matthews HF, Douek DC, . . . Lenardo MJ. 2011. Second messenger role for Mg^{2+} revealed by human T-cell immunodeficiency. *Nature* **475**: 471-476

Li J, Hou B, Tumova S, Muraki K, Bruns A, Ludlow MJ, . . . Beech DJ. 2014. Piezo1 integration of vascular architecture with physiological force. *Nature* **515**: 279

Li M, Jiang J, Yue L. 2006. Functional characterization of homo- and heteromeric channel kinases TRPM6 and TRPM7. *J Gen Physiol* **127**: 525 - 537

Li M, Toombes GES, Silberberg SD, Swartz KJ. 2015. Physical basis of apparent pore dilation of ATP-activated P2X receptor channels. *Nat Neurosci* **18**: 1577

Li Q-J, Chau J, Ebert PJR, Sylvester G, Min H, Liu G, . . . Chen C-Z. 2007. miR-181a is an intrinsic modulator of T cell sensitivity and selection. *Cell* **129**: 147-161

Li XF, Kraev AS, Lytton J. 2002b. Molecular cloning of a fourth member of the potassium-dependent sodium-calcium exchanger gene family, NCKX4. *J Biol Chem* **277**: 48410-48417

Li Y, Mariuzza R. 2013. Structural and biophysical insights into the role of CD4 and CD8 in T cell activation. *Front Immunol* **4**:

Li YC, Chen BM, Wu PC, Cheng TL, Kao LS, Tao MH, . . . Roffler SR. 2010. Cutting edge: Mechanical forces acting on T cells immobilized via the TCR complex can trigger TCR signaling. *J Immunol* **184**: 5959-5963

Liang X, Howard J. 2018. Structural biology: Piezo senses tension through curvature. *Curr Biol* **28**: R357-R359

Lichtenegger M, Tiapko O, Svobodova B, Stockner T, Glasnov TN, Schreibmayer W, . . . Groschner K. 2018. An optically controlled probe identifies lipid-gating fenestrations within the TRPC3 channel. *Nat Chem Biol* **14**: 396-404

Lievremont J-P, Bird GS, Putney JW. 2005. Mechanism of inhibition of TRPC cation channels by 2-aminoethoxydiphenylborane. *Mol Pharmacol* **68**: 758-762

Lièvremont J-P, Bird GSJ, Putney JW. 2004. Canonical transient receptor potential TRPC7 can function as both a receptor- and store-operated channel in HEK-293 cells. *Am J Physiol-Cell Ph* **287**: C1709-C1716

Lin H, Hutchcroft JE, Andoniou CE, Kamoun M, Band H, Bierer BE. 1998. Association of p59 ^{fyn} with the T lymphocyte costimulatory receptor CD2: Binding of the Fyn Src homology (sh) 3 domain is regulated by the Fyn SH2 domain. *J Biol Chem* **273**: 19914-19921

Linden J, Cekic C. 2012. Regulation of lymphocyte function by adenosine. *Arterioscl Throm Vas* **32**: 2097-2103

Lipkind GM, Fozzard HA. 1994. A structural model of the tetrodotoxin and saxitoxin binding site of the Na^+ channel. *Biophys J* **66**: 1-13

Lis A, Wissenbach U, Philipp SE. 2005. Transcriptional regulation and processing increase the functional variability of TRPM channels. *N-S Arch Pharmacol* **371**: 315-324

Liu B, Chen W, Evavold BD, Zhu C. 2014. Accumulation of dynamic catch bonds between TCR and agonist peptide-MHC triggers T cell signaling. *Cell* **157**: 357-368

Liu B, Qin F. 2017. Single-residue molecular switch for high-temperature dependence of vanilloid receptor TRPV3. *Proc Natl Acad Sci USA* **114**: 1589-1594

Liu B, Yao J, Zhu MX, Qin F. 2011. Hysteresis of gating underlines sensitization of TRPV3 channels. *J Gen Physiol* **138**: 509

Liu C, Montell C. 2015. Forcing open TRP channels: Mechanical gating as a unifying activation mechanism. *Biochem Biophys Res Commun* **460**: 22-25

Liu C, Shiu, Chen, Raychaudhuri D, Paul B, Chakrabarty Y, Ghosh AR, Rahaman O, . . . Ganguly D. 2018. Cutting edge: Piezo1 mechanosensors optimize human T cell activation. *J Immunol*:

Liu D, Liman ER. 2003. Intracellular Ca^{2+} and the phospholipid PIP_2 regulate the taste transduction ion channel TRPM5. *Proc Natl Acad Sci USA* **100**: 15160-15165

Liu Q-H, Fleischmann BK, Hondowicz B, Maier CC, Turka LA, Yui K, . . . Freedman BD. 2002. Modulation of Kv channel expression and function by TCR and costimulatory signals during peripheral $CD4^+$ lymphocyte differentiation. *J Exp Med* **196**: 897-909

Liu X, Wang H, Jiang Y, Zheng Q, Petrus M, Zhang M, . . . Xiao B. 2019. STIM1 thermosensitivity defines the optimal preference temperature for warm sensation in mice. *Cell Res* **29**: 95-109

Lo W-L, Donermeyer DL, Allen PM. 2012. A voltage-gated sodium channel is essential for the positive selection of $CD4^+$ T cells. *Nat Immunol* **13**: 880-887

Locovei S, Scemes E, Qiu F, Spray DC, Dahl G. 2007. Pannexin1 is part of the pore forming unit of the P2X(7) receptor death complex. *FEBS Lett* **581**: 483-488

Loew LM. 2007. Where does all the PIP_2 come from? *J Physiol* **582**: 945-951

Lub M, van Kooyk Y, van Vliet SJ, Figdor CG. 1997. Dual role of the actin cytoskeleton in regulating cell adhesion mediated by the integrin lymphocyte function-associated molecule-1. *Mol Biol Cell* **8**: 341-351

Lucas B, Stefanová I, Yasutomo K, Dautigny N, Germain RN. 1999. Divergent changes in the sensitivity of maturing T cells to structurally related ligands underlies formation of a useful T cell repertoire. *Immunity* **10**: 367-376

Lucas P, Ukhanov K, Leinders-Zufall T, Zufall F. 2003. A diacylglycerol-gated cation channel in vomeronasal neuron dendrites is impaired in TRPC2 mutant mice: Mechanism of pheromone transduction. *Neuron* **40**: 551-561

Lückhoff A. 1986. Measuring cytosolic free calcium concentration in endothelial cells with indo-1: The pitfall of using the ratio of two fluorescence intensities recorded at different wavelengths. *Cell calcium* **7**: 233-248

Lukacs V, Thyagarajan B, Varnai P, Balla A, Balla T, Rohacs T. 2007. Dual regulation of TRPV1 by phosphoinositides. *J Neurosci* **27**: 7070-7080

Luo J, Stewart R, Berdeaux R, Hu H. 2012. Tonic inhibition of TRPV3 by Mg^{2+} in mouse epidermal keratinocytes. *J Invest Dermatol* **132**: 2158-2165

Luongo F, Pietropaolo G, Gautier M, Dhennin-Duthille I, Ouadid-Ahidouch H, Wolf FI, Trapani V. 2018. TRPM6 is essential for magnesium uptake and epithelial cell function in the colon. *Nutrients* **10**: 784

Ma J. 1993. Block by ruthenium red of the ryanodine-activated calcium release channel of skeletal muscle. *J Gen Physiol* **102**: 1031

Ma Q, Shimaoka M, Lu C, Jing H, Carman CV, Springer TA. 2002. Activation-induced conformational changes in the I domain region of lymphocyte function-associated antigen 1. *J Biol Chem* **277**: 10638-10641

Ma X, Cao J, Luo J, Nilius B, Huang Y, Ambudkar IS, Yao X. 2010. Depletion of intracellular Ca^{2+} stores stimulates the translocation of vanilloid transient receptor potential 4-C1 heteromeric channels to the plasma membrane. *Arterioscl Throm Vas* **30**: 2249-2255

Ma Y, Poole K, Goyette J, Gaus K. 2017. Introducing membrane charge and membrane potential to T cell signaling. *Front Immunol* **8**:

Mace TA, Zhong L, Kilpatrick C, Zynda E, Lee C-T, Capitano M, . . . Repasky EA. 2011. Differentiation of $CD8^+$ T cells into effector cells is enhanced by physiological range hyperthermia. *J Leukocyte Biol* **90**: 951-962

Mace TA, Zhong L, Kokolus KM, Repasky EA. 2012. Effector $CD8^+$ T cell ifn-γ production and cytotoxicity are enhanced by mild hyperthermia. *Int J Hyperthermia* **28**: 9-18

Macpherson LJ, Geierstanger BH, Viswanath V, Bandell M, Eid SR, Hwang S. 2005. The pungency of garlic: Activation of TRPA1 and TRPV1 in response to allicin. *Curr Biol* **15**:

Macpherson LJ, Hwang SW, Miyamoto T, Dubin AE, Patapoutian A, Story GM. 2006. More than cool: Promiscuous relationships of menthol and other sensory compounds. *Mol Cell Neurosci* **32**: 335-343

Mahaut-Smith MP, Mason MJ. 1991. Ca^{2+}-activated K^+ channels in rat thymic lymphocytes: Activation by concanavalin a. *J Physiol* **439**: 513-528

Majhi RK, Sahoo SS, Yadav M, Pratheek BM, Chattopadhyay S, Goswami C. 2015. Functional expression of TRPV channels in T cells and their implications in immune regulation. *FEBS J* **282**: 2661-2681

Malin S, Molliver D, Christianson J, S Schwartz E, Cornuet P, Albers K, M Davis B. 2011. *TRPV1 and TRPA1 function and modulation are target tissue dependent*. 10516-10528 pp.

Malpuech-Brugere C, Nowacki W, Gueux E, Kuryszko J, Rock E, Rayssiguier Y, Mazur A. 1999. Accelerated thymus involution in magnesium-deficient rats is related to enhanced apoptosis and sensitivity to oxidative stress. *Br J Nutr* **81**: 405-411

Mandadi S, Armati P, Roufogalis B. 2011. Protein kinase C modulation of thermo-sensitive transient receptor potential channels: Implications for pain signaling. *J Nat Sci Biol Med* **2**: 13-25

Mandt T, Song Y, Scharenberg AM, Sahni J. 2011. SLC41A1 Mg^{2+} transport is regulated via Mg^{2+}-dependent endosomal recycling through its N-terminal cytoplasmic domain. *Biochem J* **439**: 129-139

Mann CL, Bortner CD, Jewell CM, Cidlowski JA. 2001. Glucocorticoid-induced plasma membrane depolarization during thymocyte apoptosis: Association with cell shrinkage and degradation of the Na^+/K^+-adenosine triphosphatase. *Endocrinology* **142**: 5059-5068

Maroto R, Raso A, Wood TG, Kurosky A, Martinac B, Hamill OP. 2005. TRPC1 forms the stretch-activated cation channel in vertebrate cells. *Nat Cell Biol* **7**: 179-185

Maruyama T, Kanaji T, Nakade S, Kanno T, Mikoshiba K. 1997. 2apb, 2-aminoethoxydiphenyl borate, a membrane-penetrable modulator of Ins(1,4,5)P_3-induced Ca^{2+} release. *J Biochem* **122**: 498-505

Mason MJ, Mayer B, Hymel LJ. 1993. Inhibition of Ca^{2+} transport pathways in thymic lymphocytes by econazole, miconazole, and skf 96365. *Am J Physiol* **264**: C654-662

Matsushita M, Kozak JA, Shimizu Y, McLachlin DT, Yamaguchi H, Wei FY, . . . Nairn AC. 2005. Channel function is dissociated from the intrinsic kinase activity and autophosphorylation of TRPM7/chak1. *J Biol Chem* **280**: 20793-20803

Matza D, Badou A, Klemic KG, Stein J, Govindarajulu U, Nadler MJ, . . . Flavell RA. 2016. T cell receptor mediated calcium entry requires alternatively spliced $Ca_V1.1$ channels. *PLOS One* **11**: 1-17

Matzinger P, Zamoyska R, Waldmann H. 1984. Self tolerance is H-2-restricted. *Nature* **308**: 738-741

McHugh BJ, Buttery R, Lad Y, Banks S, Haslett C, Sethi T. 2010. Integrin activation by fam38a uses a novel mechanism of R-Ras targeting to the endoplasmic reticulum. *J Cell Sci* **123**: 51

McHugh D, Flemming R, Xu SZ, Perraud AL, Beech DJ. 2003. Critical intracellular Ca^{2+} dependence of transient receptor potential melastatin 2 (TRPM2) cation channel activation. *J Biol Chem* **278**: 11002-11006

McIntyre P, McLatchie LM, Chambers A, Phillips E, Clarke M, Savidge J, . . . James IF. 2001. Pharmacological differences between the human and rat vanilloid receptor 1 (VR1). *Brit J Pharmacol* **132**: 1084-1094

McKemy DD, Neuhausser WM, Julius D. 2002. Identification of a cold receptor reveals a general role for TRP channels in thermosensation. *Nature* **416**: 52-58

McKinnon D, Ceredig R. 1986. Changes in the expression of potassium channels during mouse T cell development. *J Exp Med* **164**: 1846

McNamara CR, Mandel-Brehm J, Bautista DM, Siemens J, Deranian KL, Zhao M. 2007. TRPA1 mediates formalin-induced pain. *Proc Natl Acad Sci USA* **104**:

McRory JE, Hamid J, Doering CJ, Garcia E, Parker R, Hamming K, . . . Snutch TP. 2004. The *CACNA1F* gene encodes an L-type calcium channel with unique biophysical properties and tissue distribution. *J Neurosci* **24**: 1707-1718

Melichar HJ, Ross JO, Herzmark P, Hogquist KA, Robey EA. 2013. Distinct temporal pattern of T cell receptor signals during positive versus negative selection in situ. *Sci Signal* **6**: ra92-ra92

Melichar HJ, Ross JO, Taylor KT, Robey EA. 2015. Stable interactions and sustained TCR signaling characterize thymocyte–thymocyte interactions that support negative selection. *J Immunol* **194**: 1057-1061

Melzer N, Hicking G, Göbel K, Wiendl H. 2012. TRPM2 cation channels modulate T cell effector functions and contribute to autoimmune CNS inflammation. *PLOS One* **7**: e47617

Mendu SK, Schappe MS, Moser EK, Krupa JK, Rogers JS, Stipes EJ, . . . Desai BN. 2018. Targeting ion channel TRPM7 promotes the thymic development of regulatory T cells by increasing IL-2-dependent STAT5 activation. *bioRxiv*: 330233

Mercado J, Gordon-Shaag A, Zagotta WN, Gordon SE. 2010. Ca^{2+}-dependent desensitization of TRPV2 channels is mediated by hydrolysis of phosphatidylinositol 4,5-bisphosphate. *J Neurosci* **30**: 13338

Mercer JC, Qi Q, Mottram LF, Law M, Bruce D, Iyer A, . . . August A. 2010. Chemico-genetic identification of drebrin as a regulator of calcium responses. *Int J Biochem Cell B* **42**: 337-345

Merkenschlager M, Graf D, Lovatt M, Bommhardt U, Zamoyska R, Fisher AG. 1997. How many thymocytes audition for selection? *J Exp Med* **186**: 1149-1158

Meuer SC, Hussey RE, Fabbi M, Fox D, Acuto D, Fitzgerald KA, . . . Reinherz EL. 1984. An alternative pathway of T-cell activation: A functional role for the 50 kd T11 sheep erythrocyte receptor protein. *Cell* **36**: 897-906

Meyers JR, MacDonald RB, Duggan A, Lenzi D, Standaert DG, Corwin JT, Corey DP. 2003. Lighting up the senses: Fm1-43 loading of sensory cells through nonselective ion channels. *J Neurosci* **23**: 4054-4065

Miehe S, Crause P, Schmidt T, Löhn M, Kleemann H-W, Licher T, . . . Strübing C. 2012. Inhibition of diacylglycerol–sensitive TRPC channels by synthetic and natural steroids. *PLOS One* **7**: e35393

Milner RE, Famulski KS, Michalak M. 1992. Calcium binding proteins in the sarcoplasmic/endoplasmic reticulum of muscle and nonmuscle cells. *Mol Cell Biochem* **112**: 1-13

Min L, Joseph RE, Fulton DB, Andreotti AH. 2009. Itk tyrosine kinase substrate docking is mediated by a nonclassical SH2 domain surface of PLCγ1. *Proc Natl Acad Sci USA* **106**: 21143-21148

Minard A, Bauer C, Wright D, Rubaiy H, Muraki K, Beech D, Bon R. 2018. Remarkable progress with small-molecule modulation of TRPC1/4/5 channels: Implications for understanding the channels in health and disease. *Cells* **7**:

Minke B. 2006. TRP channels and Ca^{2+} signaling. *Cell calcium* **40**: 261-275

Missiaen L, Callewaert G, De Smedt H, Parys JB. 2001. 2-aminoethoxydiphenyl borate affects the inositol 1,4,5-trisphosphate receptor, the intracellular

Ca^{2+} pump and the non-specific Ca^{2+} leak from the non-mitochondrial Ca^{2+} stores in permeabilized A7r5 cells. *Cell calcium* **29**: 111-116

Miyamoto T, Mochizuki T, Nakagomi H, Kira S, Watanabe M, Takayama Y, . . . Tominaga M. 2014. Functional role for piezo1 in stretch-evoked Ca^{2+} influx and ATP release in urothelial cell cultures. *J Biol Chem* **289**: 16565-16575

Moen LV, Sener Z, Volchenkov R, Svarstad AC, Eriksen AM, Holen HL, Skålhegg BS. 2017. Ablation of the Cβ2 subunit of PKA in immune cells leads to increased susceptibility to systemic inflammation in mice. *Eur J Immunol* **47**: 1880-1889

Moingeon PE, Lucich JL, Stebbins CC, Recny MA, Wallner BP, Koyasu S, Reinherz EL. 1991. Complementary roles for CD2 and LFA-1 adhesion pathways during T cell activation. *Eur J Immunol* **21**: 605-610

Monteilh-Zoller MK, Hermosura MC, Nadler MJS, Scharenberg AM, Penner R, Fleig A. 2003. TRPM7 provides an ion channel mechanism for cellular entry of trace metal ions. *J Gen Physiol* **121**: 49-60

Montell C. 2004. Exciting trips for trps. *Nat Cell Biol* **6**: 690-692

Montell C, Birnbaumer L, Flockerzi V, Bindels RJ, Bruford EA, Caterina MJ, . . . Zhu MX. 2002. A unified nomenclature for the superfamily of TRP cation channels. *Mol Cell* **9**: 229-231

Montell C, Rubin GM. 1989. Molecular characterization of the drosophila *trp* locus: A putative integral membrane protein required for phototransduction. *Neuron* **2**: 1313-1323

Moody AM, Chui D, Reche PA, Priatel JJ, Marth JD, Reinherz EL. 2001. Developmentally regulated glycosylation of the CD8αβ coreceptor stalk modulates ligand binding. *Cell* **107**: 501-512

Moody AM, North SJ, Reinhold B, Van Dyken SJ, Rogers ME, Panico M, . . . Reinherz EL. 2003. Sialic acid capping of CD8β core 1-*O*-glycans controls thymocyte-major histocompatibility complex class I interaction. *J Biol Chem* **278**: 7240-7246

Moogk D, Natarajan A, Krogsgaard M. 2018. T cell receptor signal transduction: Affinity, force and conformational change. *Curr Opin Chem Eng* **19**: 43-50

Moore CL. 1971. Specific inhibition of mitochondrial Ca^{2+} transport by ruthenium red. *Biochem Biophys Res Commun* **42**: 298-305

Morales-Lázaro SL, Rosenbaum T. 2017. Multiple mechanisms of regulation of transient receptor potential ion channels by cholesterol In *Curr top membr*, ed. I Levitan, pp. 139-161: Academic Press

Moran MM. 2018. TRP channels as potential drug targets. *Annu Rev Pharmacol* **58**: 309-330

Morgan MM, Labno CM, Van Seventer GA, Denny MF, Straus DB, Burkhardt JK. 2001. Superantigen-induced T cell :B cell conjugation is mediated by LFA-1 and requires signaling through Lck, but not ZAP-70. *J Immunol* **167**: 5708

Morihara H, Obana M, Tanaka S, Kawakatsu I, Tsuchiyama D, Mori S, . . . Nakayama H. 2017. 2-aminoethoxydiphenyl borate provides an anti-oxidative effect and mediates cardioprotection during ischemia reperfusion in mice. *PLOS One* **12**: e0189948

Morley SC, Weber KS, Kao H, Allen PM. 2008. Protein kinase C-theta is required for efficient positive selection. *J Immunol* **181**: 4696-4708

Moroni M, Servin-Vences MR, Fleischer R, Sánchez-Carranza O, Lewin GR. 2018. Voltage gating of mechanosensitive piezo channels. *Nat Commun* **9**:

Mortadza SS, Sim JA, Stacey M, Jiang L-H. 2017. Signalling mechanisms mediating Zn^{2+}-induced TRPM2 channel activation and cell death in microglial cells. *Sci Rep-UK* **7**: 45032

Mosavi LK, Minor DL, Jr, Peng ZY. 2002. Consensus-derived structural determinants of the ankyrin repeat motif. *Proc Natl Acad Sci USA* **99**: 16029-16034

Motter AL, Ahern GP. 2012. TRPA1 is a polyunsaturated fatty acid sensor in mammals. *PLOS One* **7**: e38439

Mueller KL, Daniels MA, Felthauser A, Kao C, Jameson SC, Shimizu Y. 2004. Cutting edge: LFA-1 integrin-dependent T cell adhesion is regulated by both Ag specificity and sensitivity. *J Immunol* **173**: 2222-2226

Munns CH, Chung MK, Sanchez YE, Amzel LM, Caterina MJ. 2015. Role of the outer pore domain in transient receptor potential vanilloid 1 dynamic permeability to large cations. *J Biol Chem* **290**: 5707-5724

Murphy KM, Heimberger AB, Loh DY. 1990. Induction by antigen of intrathymic apoptosis of $CD4^+$ $CD8^+$ TCR^{lo} thymocytes *in vivo*. *Science* **250**: 1720-1723

Nadler MJ, Hermosura MC, Inabe K, Perraud AL, Zhu Q, Stokes AJ, . . . Fleig A. 2001. LTRPC7 is a Mg.ATP-regulated divalent cation channel required for cell viability. *Nature* **411**: 590-595

Nadolni W, Zierler S. 2018. The channel-kinase TRPM7 as novel regulator of immune system homeostasis. *Cells* **7**:

Nagarajan Y, Rychkov GY, Peet DJ. 2017. Modulation of TRP channel activity by hydroxylation and its therapeutic potential. *Pharmaceuticals* **10**:

Nagata K, Duggan A, Kumar G, García-Anoveros J. 2005. Nociceptor and hair cell transducer properties of TRPA1, a channel for pain and hearing. *J Neurosci* **25**:

Nagy PV, Fehér T, Morga S, Matkó J. 2000. Apoptosis of murine thymocytes induced by extracellular ATP is dose- and cytosolic pH-dependent. *Immunol Lett* **72**: 23-30

Nakayama T, June CH, Munitz TI, Sheard M, McCarthy SA, Sharrow SO, . . . Singer A. 1990. Inhibition of T cell receptor expression and function in immature $CD4^+$ $CD8^+$ cells by CD4. *Science* **249**: 1558-1561

Nakayama T, Ueda Y, Yamada H, Shores E, Singer A, June C. 1992. *In vivo* calcium elevations in thymocytes with T cell receptors that are specific for self ligands. *Science* **257**: 96-99

Nass R, Cunningham KW, Rao R. 1997. Intracellular sequestration of sodium by a novel Na^+/h^+ exchanger in yeast is enhanced by mutations in the plasma membrane h+-ATPase: Insights into mechanisms of sodium tolerance. *J Biol Chem* **272**: 26145-26152

Naylor K, Li G, Vallelo AN, Lee WW, Koetz K, Bryl E, . . . Goronzy JJ. 2005. The influence of age on T cell generation and TCR diversity. *J Immunol* **174**: 7446-7452

Nicholls DG. 2005. Mitochondria and calcium signaling. *Cell calcium* **38**: 311-317

Nijenhuis T, Hoenderop JG, Bindels RJ. 2005. TRPV5 and TRPV6 in Ca^{2+} (re)absorption: Regulating Ca^{2+} entry at the gate. *Pflugers Arch* **451**: 181-192

Nilius B, Bíró T, Owsianik G. 2014. TRPV3: Time to decipher a poorly understood family member! *J Physiol* **592**: 295-304

Nilius B, Mahieu F, Prenen J, Janssens A, Owsianik G, Vennekens R, Voets T. 2006. The Ca^{2+}-activated cation channel TRPM4 is regulated by phosphatidylinositol 4,5-biphosphate. *EMBO J* **25**: 467-478

Nilius B, Owsianik G. 2011. The transient receptor potential family of ion channels. *Genome Biol* **12**: 218

Nilius B, Owsianik G, Voets T. 2008. Transient receptor potential channels meet phosphoinositides. *EMBO J* **27**: 2809-2816

Nilius B, Owsianik G, Voets T, Peters JA. 2007. Transient receptor potential cation channels in disease. *Physiol Rev* **87**: 165-217

Nilius B, Prenen J, Janssens A, Owsianik G, Wang C, Zhu MX, Voets T. 2005. The selectivity filter of the cation channel TRPM4. *J Biol Chem* **280**: 22899-22906

Nilius B, Szallasi A. 2014. Transient receptor potential channels as drug targets: From the science of basic research to the art of medicine. *Pharmacol Rev* **66**: 676-814

Nilius B, Vennekens R, Prenen J, Hoenderop JGJ, Bindels RJ, Droogmans G. 2000. Whole-cell and single channel monovalent cation currents through the novel rabbit epithelial Ca^{2+} channel ECaC. *J Physiol* **527**: 239-248

Nishizuka Y. 1992. Intracellular signaling by hydrolysis of phospholipids and activation of protein kinase C. *Science* **258**: 607-614

Nohara LL, Stanwood SR, Omilusik KD, Jefferies WA. 2015. Tweeters, woofers and horns: The complex orchestration of calcium currents in T lymphocytes. *Front Immunol* **6**: 234

Nonoyama S, Nakayama M, Shiohara T, Yata J. 1989. Only dull $CD3^+$ thymocytes bind to thymic epithelial cells. The binding is elicited by both CD2/LFA-3 and LFA-1/ICAM-1 interactions. *Eur J Immunol* **19**: 1631-1635

Numata T, Kiyonaka S, Kato K, Takahashi N, Mori Y. 2011. Activation of TRP channels in mammalian systems In *TRP channels*, ed. MX Zhu. Boca Raton (FL): CRC Press/Taylor & Francis Llc.

Numata T, Shimizu T, Okada Y. 2007. Direct mechano-stress sensitivity of TRPM7 channel. *Cell Physiol Biochem* **19**: 1-8

Numazaki M, Tominaga T, Takeuchi K, Murayama N, Toyooka H, Tominaga M. 2003. Structural determinant of TRPV1 desensitization interacts with calmodulin. *Proc Natl Acad Sci USA* **100**: 8002

Nwokonko RM, Zhou Y, Gill DL. 2019. Stim1 is a precise thermo-sensor in skin. *Cell Research* **29**: 259-260

Oancea E, Vriens J, Brauchi S, Jun J, Splawski I, Clapham DE. 2009. TRPM1 forms ion channels associated with melanin content in melanocytes. *Sci Signal* **2**: ra21

Oberwinkler J, Lis A, Giehl KM, Flockerzi V, Philipp SE. 2005. Alternative splicing switches the divalent cation selectivity of TRPM3 channels. *J Biol Chem* **280**: 22540-22548

Obukhov AG, Nowycky MC. 2005. A cytosolic residue mediates Mg^{2+} block and regulates inward current amplitude of a transient receptor potential channel. *J Neurosci* **25**: 1234

Oh-hora M, Komatsu N, Pishyareh M, Feske S, Hori S, Taniguchi M, . . . Takayanagi H. 2013. Agonist-selected T cell development requires strong T cell receptor signaling and store-operated calcium entry. *Immunity* **38**: 881-895

Ohno H, Ushiyama C, Taniguchi M, Germain RN, Saito T. 1991. CD2 can mediate TCR/CD3-independent T cell activation. *J Immunol* **146**: 3742-3746

Ohoka Y, Kuwata T, Tozawa Y, Zhao Y, Mukai M, Motegi Y, . . . Iwata M. 1996. *In vitro* differentiation and commitment of $CD4^+$ $CD8^+$ thymocytes to the CD4 lineage, without TCR engagement. *Int Immunol* **8**: 297-306

Okada T, Inoue R, Yamazaki K, Maeda A, Kurosaki T, Yamakuni T, . . . Mori Y. 1999. Molecular and functional characterization of a novel mouse transient receptor potential protein homologue TRP7. . *J Biol Chem* **274**: 27359-27370

Okkenhaug K, Vanhaesebroeck B. 2003. PI_3K in lymphocyte development, differentiation and activation. *Nat Rev Immunol* **3**: 317-330

Oliveira-dos-Santos AJ, Penninger JM, Rieker-Geley T, Matsumoto G, Mak TM, Wick G. 1998. Thymic heterotypic cellular complexes in gene-targeted mice with defined blocks in T cell development and adhesion molecule expression. *Eur J Immunol* **28**: 2882-2892

Oliver AE, Baker GA, Fugate RD, Tablin F, Crowe JH. 2000. Effects of temperature on calcium-sensitive fluorescent probes. *Biophys J* **78**: 2116-2126

Oliver AE, Tablin F, Walker NJ, Crowe JH. 1999. The internal calcium concentration of human platelets increases during chilling. *BBA-Biomembranes* **1416**: 349-360

Omilusik K, Priatel JJ, Chen X, Wang YT, Xu H, Choi KB, . . . Jefferies WA. 2011. The Cav1.4 calcium channel is a critical regulator of T cell receptor signaling and naive T cell homeostasis. *Immunity* **35**: 349-360

Ong HL, Cheng KT, Liu X, Bandyopadhyay BC, Paria BC, Soboloff J, . . . Ambudkar IS. 2007. Dynamic assembly of TRPC1-STIM1-Orai1 ternary complex is involved in store-operated calcium influx: Evidence for similarities in store-operated and calcium release-activated calcium channel components. *J Biol Chem* **282**: 9105-9116

Onkal R, Mattis JH, Fraser SP, Diss JKJ, Shao D, Okuse K, Djamgoz MBA. 2008. Alternative splicing of Nav1.5: An electrophysiological comparison of 'neonatal' and 'adult' isoforms and critical involvement of a lysine residue. *J Cell Physiol* **216**: 716-726

Ori A, Wilkinson MC, Fernig DG. 2011. A systems biology approach for the investigation of the heparin/heparan sulfate interactome. *J Biol Chem* **286**: 19892-19904

Orlandi C, Cao Y, Martemyanov KA. 2013. Orphan receptor GPR179 forms macromolecular complexes with components of metabotropic signaling cascade in retina on-bipolar neurons. *Invest Ophthalmol Vis Sci* **54**: 7153-7161

Orlandi C, Omori Y, Wang Y, Cao Y, Ueno A, Roux MJ, . . . Martemyanov KA. 2018. Transsynaptic binding of orphan receptor GPR179 to dystroglycan-pikachurin complex is essential for the synaptic organization of photoreceptors. *Cell Rep* **25**: 130-145.e135

Ostergaard HL, Trowbridge IS. 1991. Negative regulation of CD45 protein tyrosine phosphatase activity by ionomycin in T cells. *Science* **253**: 1423-1425

Outram SV, Crompton T, Merida I, Varas A, Martinez-A C. 2002. Diacylglycerol kinase α activity promotes survival of $CD4^+$ $CD8^+$ double positive cells during thymocyte development. *Immunology* **105**: 391-398

Ouyang K, Leandro Gomez-Amaro R, Stachura DL, Tang H, Peng X, Fang X, . . . Chen J. 2014. Loss of IP_3R-dependent Ca^{2+} signalling in thymocytes leads to aberrant development and acute lymphoblastic leukemia. *Nat Commun* **5**: 4814

Paessens LC, Singh SK, Fernandes RJ, van Kooyk Y. 2008. Vascular cell adhesion molecule-1 (VCAM-1) and intercellular adhesion molecule-1 (ICAM-1) provide co-stimulation in positive selection along with survival of selected thymocytes. *Mol Immunol* **45**: 42-48

Painter MW, Davis S, Hardy RR, Mathis D, Benoist C. 2011. Transcriptomes of the B and T lineages compared by multiplatform microarray profiling. *J Immunol* **186**: 3047-3057

Palacios EH, Weiss A. 2004. Function of the Src-family kinases, Lck and Fyn, in T-cell development and activation. *Oncogene* **23**: 7990-8000

Palacios R, Sugawara I, Fernandez C. 1982. Dextran-sulfate: A mitogen for human T lymphocytes. *J Immunol* **128**: 621-624

Palmer E, Naeher D. 2009. Affinity threshold for thymic selection through a T-cell receptor-co-receptor zipper. *Nat Rev Immunol* **9**: 207-213

Palovcak E, Delemotte L, Klein ML, Carnevale V. 2015. Comparative sequence analysis suggests a conserved gating mechanism for TRP channels. *J Gen Physiol* **146**: 37

Pang B, Shin D, Park K, Huh Y, Woo J, Zhang Y-H, . . . Kim S. 2012. Differential pathways for calcium influx activated by concanavalin A and CD3 stimulation in Jurkat T cells. *Pflüg Arch Eur J Phy* **463**: 309-318

Papadogiannakis N, Barbieri B. 1997. Lipoxygenase inhibitors counteract protein kinase C mediated events in human T lymphocyte proliferation. *Int J Immunopharmaco* **19**: 263-275

Parish CR, Low L, Warren HS, Cunningham AL. 1990. A polyanion binding site on the CD4 molecule. Proximity to the HIV-gp120 binding region. *J Immunol* **145**: 1188-1195

Parish CR, Rylatt DB, Snowden JM. 1984. Demonstration of lymphocyte surface lectins that recognize sulphated polysaccharides. *J Cell Sci* **67**: 145-158

Park CW, Kim HJ, Choi YW, Chung BY, Woo SY, Song DK, Kim HO. 2017. TRPV3 channel in keratinocytes in scars with post-burn pruritus. *Int J Mol Sci* **18**:

Park CY, Shcheglovitov A, Dolmetsch R. 2010. The CRAC channel activator STIM1 binds and inhibits L-type voltage-gated calcium channels. *Science* **330**: 101-105

Pathak MM, Nourse JL, Tran T, Hwe J, Arulmoli J, Le DT, . . . Tombola F. 2014. Stretch-activated ion channel piezo1 directs lineage choice in human neural stem cells. *Proc Natl Acad Sci USA* **111**: 16148-16153

Patil MJ, Jeske NA, Akopian AN. 2010. Transient receptor potential v1 regulates activation and modulation of transient receptor potential A1 by Ca^{2+}. *Neuroscience* **171**: 1109-1119

Patterson RL, Boehning D, Snyder SH. 2004. Inositol 1,4,5-trisphosphate receptors as signal integrators. *Annu Rev Biochem* **73**: 437-465

Peier AM, Reeve AJ, Andersson DA, Moqrich A, Earley TJ, Hergarden AC, . . . Patapoutian A. 2002. A heat-sensitive TRP channel expressed in keratinocytes. *Science* **296**: 2046

Peng JB, Chen XZ, Berger UV, Vassilev PM, Tsukaguchi H, Brown EM, Hediger MA. 1999. Molecular cloning and characterization of a channel-like

transporter mediating intestinal calcium absorption. *J Biol Chem* **274**: 22739-22746

Peppiatt CM, Collins TJ, Mackenzie L, Conway SJ, Holmes AB, Bootman MD, . . . Roderick HL. 2003. 2-aminoethoxydiphenyl borate (2-APB) antagonises inositol 1,4,5-trisphosphate-induced calcium release, inhibits calcium pumps and has a use-dependent and slowly reversible action on store-operated calcium entry channels. *Cell calcium* **34**: 97-108

Perez-Leighton CE, Schmidt TM, Abramowitz J, Birnbaumer L, Kofuji P. 2011. Intrinsic phototransduction persists in melanopsin-expressing ganglion cells lacking diacylglycerol-sensitive TRPC subunits. *Eur J Neurosci* **33**: 856-867

Perez OD, Mitchell D, Jager GC, South S, Murriel C, McBride J, . . . Nolan GP. 2003. Leukocyte functional antigen 1 lowers T cell activation thresholds and signaling through cytohesin-1 and Jun-activating binding protein 1. *Nat Immunol* **4**: 1083-1092

Perraud AL, Takanishi CL, Shen B, Kang S, Smith MK, Schmitz C, . . . Scharenberg AM. 2005. Accumulation of free ADP-ribose from mitochondria mediates oxidative stress-induced gating of TRPM2 cation channels. *J Biol Chem* **280**: 6138-6148

Persechini A, Cronk B. 1999. The relationship between the free concentrations of Ca^{2+} and Ca^{2+}-calmodulin in intact cells. *J Biol Chem* **274**: 6827-6830

Pfeifhofer-Obermair C, Thuille N, Baier G. 2012. Involvement of distinct PKC gene products in T cell functions. *Front Immunol* **3**: 220-220

Phelps CB, Wang RR, Choo SS, Gaudet R. 2010. Differential regulation of TRPV1, TRPV3, and TRPV4 sensitivity through a conserved binding site on the ankyrin repeat domain. *J Biol Chem* **285**: 731-740

Philipp S, Strauss B, Hirnet D, Wissenbach U, Méry L, Flockerzi V, Hoth M. 2003. TRPC3 mediates T-cell receptor-dependent calcium entry in human T-lymphocytes. *J Biol Chem* **278**: 26629-26638

Plant TD, Schaefer M. 2005. Receptor-operated cation channels formed by TRPC4 and TRPC5. *N-S Arch Pharmacol* **371**: 266-276

Powis G, Seewald MJ, Gratas C, Melder D, Riebow J, Modest EJ. 1992. Selective inhibition of phosphatidylinositol phospholipase c by cytotoxic ether lipid analogues. *Cancer Res* **52**: 2835-2840

Prakriya M, Lewis RS. 2001. Potentiation and inhibition of Ca^{2+} release-activated Ca^{2+} channels by 2-aminoethyldiphenyl borate (2-APB) occurs independently of IP_3 receptors. *J Physiol* **536**: 3-19

Prakriya M, Lewis RS. 2002. Separation and characterization of currents through store-operated CRAC channels and Mg^{2+}-inhibited cation (MIC) channels. *J Gen Physiol* **119**: 487-507

Prawitt D, Monteilh-Zoller MK, Brixel L, Spangenberg C, Zabel B, Fleig A, Penner R. 2003. TRPM5 is a transient Ca^{2+} activated cation channel responding to rapid changes in $[Ca^{2+}]_i$. *Proc Natl Acad Sci USA* **100**: 15166

Pryshchep S, Zarnitsyna VI, Hong J, Evavold BD, Zhu C. 2014. Accumulation of serial forces on TCR and CD8 frequently applied by agonist antigenic peptides embedded in MHC molecules triggers calcium in T cells. *J Immunol* **193**: 68-76

Punt JA, Stranford S, Jones P, Owen JA. 2018. *Kuby immunolgy*. New York, NY, U.S.A: W.H. Freeman & Co Ltd.

Putney JW. 1999. Chapter 23. Calcium In *Basic neurochemistry. Molecular, cellular and medical aspects*, ed. GJ Siegel, BW Agranoff, RW Albers, SK Fisher, MD Uhler. Philladelphia: Lippincott-Raven

Qi Y, Andolfi L, Frattini F, Mayer F, Lazzarino M, Hu J. 2015. Membrane stiffening by STOML3 facilitates mechanosensation in sensory neurons. *Nat Commun* **6**: 8512

Quallo T, Alkhatib O, Gentry C, Andersson DA, Bevan S. 2017. G protein βγ subunits inhibit TRPM3 ion channels in sensory neurons. *eLife* **6**: e26138

Raffaello A, Mammucari C, Gherardi G, Rizzuto R. 2016. Calcium at the center of cell signaling: Interplay between endoplasmic reticulum, mitochondria, and lysosomes. *Trends Biochem Sci* **41**: 1035-1049

Rameh LE, Rhee SG, Spokes K, Kazlauskas A, Cantley LC, Cantley LG. 1998. Phosphoinositide 3-kinase regulates phospholipase Cγ-mediated calcium signaling. *J Biol Chem* **273**: 23750-23757

Rampino MAF, Nawy SA. 2011. Relief of Mg^{2+}-dependent inhibition of TRPM1 by PKCα at the rod bipolar cell synapse. *J Neurosci* **31**: 13596-13603

Ramsey IS, Delling M, Clapham DE. 2006. An introduction to TRP channels. *Annu Rev Physiol* **68**: 619-647

Rana A, Yen M, Sadaghiani AM, Malmersjö S, Park CY, Dolmetsch RE, Lewis RS. 2015. Alternative splicing converts STIM2 from an activator to an inhibitor of store-operated calcium channels. *J Cell Biol* **209**: 653

Randriamampita C, Boulla G, Revy P, Lemaitre F, Trautmann A. 2003. T cell adhesion lowers the threshold for antigen detection. *Eur J Immunol* **33**: 1215-1223

Raucher D, Stauffer T, Chen W, Shen K, Guo S, York JD, . . . Meyer T. 2000. Phosphatidylinositol 4,5-bisphosphate functions as a second messenger that regulates cytoskeleton-plasma membrane adhesion. *Cell* **100**: 221-228

Reddy TS, Bazan NG. 1987. Arachidonic acid, stearic acid, and diacylglycerol accumulation correlates with the loss of phosphatidylinositol 4,5-bisphosphate in cerebrum 2 seconds after electroconvulsive shock: Complete reversion of changes 5 minutes after stimulation. *J Neurosci Res* **18**: 449-455

Revilla C, González AL, Conde C, López-Hoyos M, Merino J. 1997. Treatment with anti-lfa-1α monoclonal antibody selectively interferes with the maturation of $CD4^{-}8^{+}$ thymocytes. *Immunology* **90**: 550-556

Riazanski V, Gabdoulkhakova AG, Boynton LS, Eguchi RR, Deriy LV, Hogarth DK, . . . Nelson DJ. 2015. TRPC6 channel translocation into phagosomal membrane augments phagosomal function. *Proc Natl Acad Sci USA* **112**: E6486-6495

Riccio A, Medhurst AD, Mattei C, Kelsell RE, Calver AR, Randall AD, . . . Pangalos MN. 2002. mRNA distribution analysis of human TRPC family in CNS and peripheral tissues. *Mol Brain Res* **109**: 95-104

Rink TJ, Tsien RY, Pozzan T. 1982. Cytoplasmic pH and free Mg^{2+} in lymphocytes. *J Cell Biol* **95**: 189-196

Rishal I, Keren-Raifman T, Yakubovich D, Ivanina T, Dessauer CW, Slepak VZ, Dascal N. 2003. Na^{+} promotes the dissociation between $G\alpha_{GDP}$ and $G\beta\gamma$, activating g protein-gated K^{+} channels. *J Biol Chem* **278**: 3840-3845

Robert V, Triffaux E, Savignac M, Pelletier L. 2011. Calcium signalling in T-lymphocytes. *Biochimie* **93**: 2087-2094

Rocio Servin-Vences M, Moroni M, Lewin GR, Poole K. 2017. Direct measurement of TRPV4 and piezo1 activity reveals multiple mechanotransduction pathways in chondrocytes. *eLife* **6**: e21074

Roder P, Hille C. 2014. ANG-2 for quantitative Na^{+} determination in living cells by time-resolved fluorescence microscopy. *Photoch Photobio Sci* **13**: 1699-1710

Rodrigues-Mascarenhas S, De Oliveira ADS, Amoedo ND, Affonso-Mitidieri OR, Rumjanek FD, Rumjanek VM. 2009. Modulation of the immune system by ouabain. *Ann NY Acad Sci* **1153**: 153-163

Rodriguez-Fernandez JL, Gomez M, Luque A, Hogg N, Sanchez-Madrid F, Cabanas C. 1999. The interaction of activated integrin lymphocyte function-associated antigen 1 with ligand intercellular adhesion molecule 1 induces activation and redistribution of focal adhesion kinase and proline-rich tyrosine kinase 2 in T lymphocytes. *Mol Biol Cell* **10**: 1891-1907

Rogers J, Robin Hesketh T, Smith GA, Beaven MA, Metcalfe JC, Johnson P, Garland PB. 1983. Intracellular pH and free calcium changes in single cells using quene 1 and quin 2 probes and fluorescence microscopy. *FEBS Lett* **161**: 21-27

Rohacs T. 2014. Phosphoinositide regulation of TRP channels. *Handb Exp Pharmacol* **223**: 1143-1176

Rohacs T, Lopes CM, Michailidis I, Logothetis DE. 2005. $PI(4,5)P_2$ regulates the activation and desensitization of TRPM8 channels through the TRP domain. *Nat Neurosci* **8**: 626-634

Romagnani A, Vettore V, Rezzonico-Jost T, Hampe S, Rottoli E, Nadolni W, . . . Zierler S. 2017. TRPM7 kinase activity is essential for T cell colonization and alloreactivity in the gut. *Nat Commun* **8**: 1917

Romero LO, Massey AE, Mata-Daboin AD, Sierra-Valdez FJ, Chauhan SC, Cordero-Morales JF, Vásquez V. 2019. Dietary fatty acids fine-tune piezo1 mechanical response. *Nat Commun* **10**: 1200

Rong Y-P, Aromolaran AS, Bultynck G, Zhong F, Li X, McColl K, . . . Distelhorst CW. 2008. Targeting Bcl-2-IP_3 receptor interaction to reverse bcl-2's inhibition of apoptotic calcium signals. *Mol Cell* **31**: 255-265

Rong Y-P, Bultynck G, Aromolaran AS, Zhong F, Parys JB, De Smedt H, . . . Distelhorst CW. 2009. The BH4 domain of Bcl-2 inhibits ER calcium release and apoptosis by binding the regulatory and coupling domain of the IP_3 receptor. *Proc Natl Acad Sci USA* **106**: 14397-14402

Rose CR, Verkhratsky A. 2016. Principles of sodium homeostasis and sodium signalling in astroglia. *Glia* **64**: 1611-1627

Ross JO, Melichar HJ, Au-Yeung BB, Herzmark P, Weiss A, Robey EA. 2014. Distinct phases in the positive selection of $CD8^+$ T cells distinguished by intrathymic migration and T-cell receptor signaling patterns. *Proc Natl Acad Sci USA* **111**: E2550-E2558

Ross PE, Cahalan MD. 1995. Ca^{2+} influx pathways mediated by swelling or stores depletion in mouse thymocytes. *J Gen Physiol* **106**: 415

Ross PE, Ehring GR, Cahalan MD. 1997. Dynamics of ATP-induced calcium signaling in single mouse thymocytes. *J Cell Biol* **138**: 987-998

Rossy J, Williamson DJ, Gaus K. 2012. How does the kinase Lck phosphorylate the T cell receptor? Spatial organization as a regulatory mechanism. *Front Immunol* **3**: 167-167

Rothberg BS, Wang Y, Gill DL. 2013. Orai channel pore properties and gating by STIM: Implications from the Orai crystal structure. *Sci Signal* **6**: pe9-pe9

Rousseau M, Naika GS, Perron J, Jacques F, Gelb MH, Boilard E. 2015. Study of the role of cytosolic phospholipase A2α in eicosanoid generation and thymocyte maturation in the thymus. *PLOS One* **10**: e0126204

Roy NH, MacKay JL, Robertson TF, Hammer DA, Burkhardt JK. 2018. Crk adaptor proteins mediate actin-dependent T cell migration and mechanosensing induced by the integrin LFA-1. *Sci Signal* **11**: eaat3178

Runnels LW, Yue L, Clapham DE. 2001. TRP-plik, a bifunctional protein with kinase and ion channel activities. *Science* **291**: 1043-1047

Runnels LW, Yue L, Clapham DE. 2002. The TRPM7 channel is inactivated by PIP_2 hydrolysis. *Nat Cell Biol* **4**: 329-336

Ryazanova LV, Dorovkov MV, Ansari A, Ryazanov AG. 2004. Characterization of the protein kinase activity of TRPM7/chak1 a protein kinase fused to the transient receptor potential ion channel. *J Biol Chem* **279**: 3708 - 3716

Ryazanova LV, Rondon LJ, Zierler S, Hu Z, Galli J, Yamaguchi TP, . . . Ryazanov AG. 2010. TRPM7 is essential for Mg^{2+} homeostasis in mammals. *Nat Commun* **1**: 109

Sahni J, Scharenberg A. 2008. TRPM7 ion channels are required for sustained phosphoinositide 3-kinase signaling in lymphocytes. *Cell Metab* **8**: 84 -93.

Sahoo H, Schwille P. 2013. Influence of glycosaminoglycans on lipid dynamics in supported phospholipid bilayers. *Soft Matter* **9**: 3859-3865

Saito S, Tominaga M. 2017. Evolutionary tuning of TRPA1 and TRPV1 thermal and chemical sensitivity in vertebrates. *Temperature* **4**: 141-152

Samanta K, Parekh AB. 2017. Spatial Ca^{2+} profiling: Decrypting the universal cytosolic Ca^{2+} oscillation. *J Physiol* **595**: 3053-3062

Sanaki T, Kasai-Yamamoto E, Yoshioka T, Sakai S, Yuyama K, Fujiwara T, . . . Igarashi Y. 2017. Direct involvement of arachidonic acid in the development of ear edema via TRPV3. *J Oleo Sci* **66**: 591-599

Sánchez-Martín L, Sánchez-Sánchez N, Gutiérrez-López MD, Rojo AI, Vicente-Manzanares M, Pérez-Alvarez MJ, . . . Cabañas C. 2004. Signaling through the leukocyte integrin LFA-1 in T cells induces a transient activation of Rac-1 that is regulated by Vav and PI_3K/akt-1. *J Biol Chem* **279**: 16194-16205

Sano Y, Inamura K, Miyake A, Mochizuki S, Yokoi H, Matsushime H, Furuichi K. 2001. Immunocyte Ca^{2+} influx system mediated by LTRPC2. *Science* **293**: 1327-1330

Santo-Domingo J, Demaurex N. 2010. Calcium uptake mechanisms of mitochondria. *BBA-Bioenergetics* **1797**: 907-912

Sasada T, Reinherz EL. 2001. A critical role for CD2 in both thymic selection events and mature T cell function. *J Immunol* **166**: 2394

Sasaki S, Suchi T. 1967. Mobilization of lymphocytes from lymph nodes and spleen by polysaccharide polysulphate. *Nature* **216**: 1013-1014

Sasaki T, Naka M, Nakamura F, Tanaka T. 1992. Ruthenium red inhibits the binding of calcium to calmodulin required for enzyme activation. *J Biol Chem* **267**: 21518-21523

Sato M, Sobhan DU, Tsumura M, Kuroda H, Soya M, Masamura A, . . . Shibukawa Y. 2013. Hypotonic-induced stretching of plasma membrane activates transient receptor potential vanilloid channels and sodium–calcium exchangers in mouse odontoblasts. *Journal of Endodontics* **39**: 779–787

Sauer K, Jegla TJ. 2006.

Saunders CI, Kunde DA, Crawford A, Geraghty DP. 2007. Expression of transient receptor potential vanilloid 1 (TRPV1) and 2 (TRPV2) in human peripheral blood. *Mol Immunol* **44**: 1429-1435

Savino W, Dalmau SR, Dealmeida VC. 2000. Role of extracellular matrix-mediated interactions in thymocyte migration. *Dev Immunol* **7**: 279-291

Sawicka M, Stritesky G, Reynolds J, Abourashchi N, Lythe G, Molina-Paris C, Hogquist K. 2014. From pre-DP, post-DP, SP4, and SP8 thymocyte cell counts to a dynamical model of cortical and medullary selection. *Front Immunol* **5**:

Schindl R, Romanin C. 2007. *Assembly domains in TRP channels*. 84-85 pp.

Schlingmann KP, Weber S, Peters M, Niemann Nejsum L, Vitzthum H, Klingel K, . . . Konrad M. 2002. Hypomagnesemia with secondary hypocalcemia is caused by mutations in TRPM6, a new member of the TRPM gene family. *Nat Genet* **31**: 166-170

Schmitz C, Brandao K, Perraud AL. 2014. The channel-kinase TRPM7, revealing the untold story of Mg^{2+} in cellular signaling. *Magnes Res* **27**: 9-15

Schmitz C, Dorovkov MV, Zhao X, Davenport BJ, Ryazanov AG, Perraud AL. 2005. The channel kinases TRPM6 and TRPM7 are functionally nonredundant. *J Biol Chem* **280**: 37763-37771

Schrapers KT, Sponder G, Liebe F, Liebe H, Stumpff F. 2018. The bovine TRPV3 as a pathway for the uptake of Na^{+}, Ca^{2+}, and $nh4^{+}$. *PLOS One* **13**: e0193519

Schrek R, Elrod LM, Batra KV. 1967. Cytocidal effect of dimethyl sulfoxide on normal and leukemic lymphocytes. *Ann NY Acad Sci* **141**: 202-213

Schrum AG, Turka LA, Palmer E. 2003. Surface T-cell antigen receptor expression and availability for long-term antigenic signaling. *Immunol Rev* **196**: 7-24

Schwanhausser B, Busse D, Li N, Dittmar G, Schuchhardt J, Wolf J, . . . Selbach M. 2011. Global quantification of mammalian gene expression control. *Nature* **473**: 337-342

Schwartz ES, Christianson JA, Chen X, La JH, Davis BM, Albers KM, Gebhart GF. 2011. Synergistic role of TRPV1 and TRPA1 in pancreatic pain and inflammation. *Gastroenterology* **140**: 1283-1291.e1281-1282

Segel GB, Simon W, Lichtman MA. 1979. Regulation of sodium and potassium transport in phytohemagglutinin-stimulated human blood lymphocytes. *J Clin Invest* **64**: 834-841

Sempowski GD, Gooding ME, Liao HX, Le PT, Haynes BF. 2002. T cell receptor excision circle assessment of thymopoiesis in aging mice. *Mol Immunol* **38**: 841-848

Shah DK, Zúñiga-Pflücker JC. 2014. An overview of the intrathymic intricacies of T cell development. *J Immunol* **192**: 4017

Shanley DP, Aw D, Manley NR, Palmer DB. 2009. An evolutionary perspective on the mechanisms of immunosenescence. *Trends Immunol* **30**: 374-381

Shen B, Wong CO, Lau OC, Woo T, Bai S, Huang Y, Yao X. 2015. Plasma membrane mechanical stress activates TRPC5 channels. *PLOS One* **10**: e0122227

Shen Y, Heimel JA, Kamermans M, Peachey NS, Gregg RG, Nawy S. 2009. A transient receptor potential-like channel mediates synaptic transmission in rod bipolar cells. *J Neurosci* **29**: 6088-6093

Shen Y, Rampino MA, Carroll RC, Nawy S. 2012. G-protein-mediated inhibition of the trp channel TRPM1 requires the Gβγ dimer. *Proc Natl Acad Sci USA* **109**: 8752-8757

Shi J, Mori E, Mori Y, Mori M, Li J, Ito Y, Inoue R. 2004. Multiple regulation by calcium of murine homologues of transient receptor potential proteins TRPC6 and TRPC7 expressed in HEK293 cells. *J Physiol* **561**: 415-432

Shi X, Bi Y, Yang W, Guo X, Jiang Y, Wan C, . . . Xu C. 2013. Ca^{2+} regulates T-cell receptor activation by modulating the charge property of lipids. *Nature* **493**: 111-115

Shim EK, Jung SH, Lee JR. 2011. Role of two adaptor molecules SLP-76 and LAT in the PI_3K signaling pathway in activated T cells. *J Immunol* **186**: 2926-2935

Shimizu Y, Mobley JL, Finkelstein LD, Chan AS. 1995. A role for phosphatidylinositol 3-kinase in the regulation of β1 integrin activity by the CD2 antigen. *J Cell Biol* **131**: 1867-1880

Shintaku K, Uchida K, Suzuki Y, Zhou Y, Fushiki T, Watanabe T, . . . Tominaga M. 2012. Activation of transient receptor potential A1 by a non-pungent capsaicin-like compound, capsiate. *Br J Pharmacol* **165**: 1476-1486

Shiroo M, Goff L, Biffen M, Shivnan E, Alexander D. 1992. CD45 tyrosine phosphatase-activated $p59^{fyn}$ couples the T cell antigen receptor to pathways of diacylglycerol production, protein kinase C activation and calcium influx. *EMBO J* **11**: 4887-4897

Shoji KF, Sáez PJ, Harcha PA, Aguila HL, Sáez JC. 2014. Pannexin1 channels act downstream of P2X7 receptors in ATP-induced murine T-cell death. *Channels* **8**: 142-156

Simkus CRL, Stricker C. 2002. The contribution of intracellular calcium stores to mEPSCs recorded in layer ii neurones of rat barrel cortex. *J Physiol* **545**: 521-535

Simon AK, Auphan N, Pophillat M, Boyer C, Ghosh S, Rincon M, . . . Schmitt-Verhulst AM. 2000. The lack of nf-κβ transactivation and PKCε expression in $CD4^+$ $CD8^+$ thymocytes correlates with negative selection. *Cell Death Differ* **7**: 1253-1262

Simon AK, Hollander GA, McMichael A. 2015. Evolution of the immune system in humans from infancy to old age. *Proceedings. Biological sciences* **282**: 20143085-20143085

Simon Davis DA. 2015. *Novel role for heparan sulfate in thymic development of $CD8^+$ T lymphocytes (doctoral dissertation).* thesis. Australian National University, Canberra ACT Australia, Retrieved from http://openresearch-repository.anu.edu.au (1885-107082.xml). 168 pp.

Simon Davis DA, Parish CR. 2013. Heparan sulfate: A ubiquitous glycosaminoglycan with multiple roles in immunity. *Front Immunol* **4**: 470

Simon F, Varela D, Cabello-Verrugio C. 2013. Oxidative stress-modulated TRPM ion channels in cell dysfunction and pathological conditions in humans. *Cell Signal* **25**: 1614-1624

Singer KH, Denning SM, Whichard LP, Haynes BF. 1990. Thymocyte LFA-1 and thymic epithelial cell ICAM-1 molecules mediate binding of activated human thymocytes to thymic epithelial cells. *J Immunol* **144**: 2931-2939

Singh AK, Saotome K, McGoldrick LL, Sobolevsky AI. 2018. Structural bases of TRP channel TRPV6 allosteric modulation by 2-APB. *Nat Commun* **9**: 2465

Sisignano M, Bennett DLH, Geisslinger G, Scholich K. 2014. TRP-channels as key integrators of lipid pathways in nociceptive neurons. *Prog Lipid Res* **53**: 93-107

Skou JC, Esmann M. 1992. The Na,k-ATPase. *J Bioenerg Biomembr* **24**: 249-261

Smith GD, Gunthorpe MJ, Kelsell RE, Hayes PD, Reilly P, Facer P, . . . Davis JB. 2002. TRPV3 is a temperature-sensitive vanilloid receptor-like protein. *Nature* **418**: 186-190

Smith JB, Knowlton RP, Agarwal SS. 1978. Human lymphocyte responses are enhanced by culture at 40°c. *J Immunol* **121**: 691-694

Solovyova N, Fernyhough P, Glazner G, Verkhratsky A. 2002. Xestospongin C empties the ER calcium store but does not inhibit $InsP_3$-induced Ca^{2+} release in cultured dorsal root ganglia neurones. *Cell calcium* **32**: 49-52

Sotomayor M, Corey DP, Schulten K. 2005. In search of the hair-cell gating spring elastic properties of ankyrin and cadherin repeats. *Structure (London, England : 1993)* **13**: 669-682

Spassova MA, Hewavitharana T, Xu W, Soboloff J, Gill DL. 2006. A common mechanism underlies stretch activation and receptor activation of TRPC6 channels. *Proc Natl Acad Sci USA* **103**: 16586-16591

Spector I, Shochet NR, Blasberger D, Kashman Y. 1989. Latrunculins-novel marine macrolides that disrupt microfilament organization and affect cell growth: I. Comparison with cytochalasin d. *Cell Motil Cytoskeleton* **13**: 127-144

Spinsanti G, Zannolli R, Panti C, Ceccarelli I, Marsili L, Bachiocco V, . . . Aloisi AM. 2008. Quantitative Real-Time PCR detection of TRPV1–4 gene expression in human leukocytes from healthy and hyposensitive subjects. *Mol Pain* **4**: 51-51

Starr TK, Daniels MA, Lucido MM, Jameson SC, Hogquist KA. 2003a. Thymocyte sensitivity and supramolecular activation cluster formation are developmentally regulated: A partial role for sialylation. *J Immunol* **171**: 4512

Starr TK, Jameson SC, Hogquist KA. 2003b. Positive and negative selection of T cells. *Annu Rev Immunol* **21**: 139-176

Startek JB, Talavera K, Voets T, Alpizar YA. 2018. Differential interactions of bacterial lipopolysaccharides with lipid membranes: Implications for TRPA1-mediated chemosensation. *Sci Rep-UK* **8**: 12010

Staruschenko A, Jeske NA, Akopian AN. 2010. Contribution of TRPV1-TRPA1 interaction to the single channel properties of the TRPA1 channel. *J Biol Chem* **285**: 15167-15177

Stepanek O, Prabhakar AS, Osswald C, King CG, Bulek A, Naeher D, . . . Palmer E. 2014. Coreceptor scanning by the T cell receptor provides a mechanism for T cell tolerance. *Cell* **159**: 333-345

Stewart MP, McDowall A, Hogg N. 1998. LFA-1-mediated adhesion is regulated by cytoskeletal restraint and by a Ca^{2+}-dependent protease, calpain. *J Cell Biol* **140**: 699-707

Storch U, Schnitzler MMy, Gudermann T. 2012. G protein-mediated stretch reception. *Am J Physiol-Heart C* **302**: H1241-H1249

Story GM, Peier AM, Reeve AJ, Eid SR, Mosbacher J, Hricik TR. 2003. Anktm1, a TRP-like channel expressed in nociceptive neurons, is activated by cold temperatures. *Cell* **112**:

Stotz SC, Vriens J, Martyn D, Clardy J, Clapham DE. 2008. Citral sensing by transient receptor potential channels in dorsal root ganglion neurons. *PLOS One* **3**: e2082

Streb H, Irvine RF, Berridge MJ, Schulz I. 1983. Release of Ca^{2+} from a nonmitochondrial intracellular store in pancreatic acinar cells by inositol-1,4,5-trisphosphate. *Nature* **306**: 67-69

Stritt S, Nurden P, Favier R, Favier M, Ferioli S, Gotru SK, . . . Braun A. 2016. Defects in TRPM7 channel function deregulate thrombopoiesis through altered cellular Mg^{2+} homeostasis and cytoskeletal architecture. *Nat Commun* **7**: 11097

Strotmann R, Schultz G, Plant TD. 2003. Ca^{2+}-dependent potentiation of the nonselective cation channel TRPV4 is mediated by a C-terminal calmodulin binding site. *J Biol Chem* **278**: 26541-26549

Suchyna TM, Johnson JH, Hamer K, Leykam JF, Gage DA, Clemo HF, . . . Sachs F. 2000. Identification of a peptide toxin from *grammostola spatulata* spider venom that blocks cation-selective stretch-activated channels. *J Gen Physiol* **115**: 583

Suchyna TM, Tape SE, Koeppe Ii RE, Andersen OS, Sachs F, Gottlieb PA. 2004. Bilayer-dependent inhibition of mechanosensitive channels by neuroactive peptide enantiomers. *Nature* **430**: 235

Sugawara I, Ishizaka S. 1982. Polysaccharides with sulfate groups are human T-cell mitogens and murine polyclonal B-cell activators (pbas): I. Fucoidan and heparin. *Cell Immunol* **74**: 162-171

Sugio S, Nagasawa M, Kojima I, Ishizaki Y, Shibasaki K. 2017. Transient receptor potential vanilloid 2 activation by focal mechanical stimulation requires

interaction with the actin cytoskeleton and enhances growth cone motility. *FASEB J* **31**: 1368-1381

Suh BC, Hille B. 2008. PIP_2 is a necessary cofactor for ion channel function: How and why? *Annu Rev Biophys* **37**: 175-195

Sullivan MN, Gonzales AL, Pires PW, Bruhl A, Leo MD, Li W, . . . Earley S. 2015. Localized TRPA1 channel Ca^{2+} signals stimulated by reactive oxygen species promote cerebral artery dilation. *Sci Signal* **8**: ra2

Sumoza-Toledo A, Penner R. 2011. TRPM2: A multifunctional ion channel for calcium signalling. *J Physiol* **589**: 1515-1525

Sunder-Plassmann R, Reinherz EL. 1998. A $p56^{lck}$-independent pathway of CD2 signaling involves jun kinase. *J Biol Chem* **273**: 24249-24257

Suppiramaniam V, Vaithianathan T, Manivannan K, Dhanasekaran M, Parameshwaran K, Bahr BA. 2006. Modulatory effects of dextran sulfate and fucoidan on binding and channel properties of AMPA receptors isolated from rat brain. *Synapse* **60**: 456-464

Surh CD, Sprent J. 1994. T-cell apoptosis detected in situ during positive and negative selection in the thymus. *Nature* **372**: 100-103

Suzuki J-i, Yamasaki S, Wu J, Koretzky GA, Saito T. 2007. The actin cloud induced by LFA-1–mediated outside-in signals lowers the threshold for T-cell activation. *Blood* **109**: 168

Suzuki S, Kupsch J, Eichmann K, Saizawa MK. 1992. Biochemical evidence of the physical association of the majority of CD3δ chains with the accessory/co-receptor molecules CD4 and CD8 on nonactivated T lymphocytes. *Eur J Immunol* **22**: 2475-2479

Suzuki S, Lis A, Schmitz C, Penner R, Fleig A. 2018. The TRPM7 kinase limits receptor-induced calcium release by regulating heterotrimeric g-proteins. *Cell Mol Life Sci* **75**: 3069-3078

Suzuki T, Suzuki J, Nagata S. 2014. Functional swapping between transmembrane proteins TMEM16A and TMEM16F. *J Biol Chem* **289**: 7438-7447

Suzuki Y, Watanabe M, Saito CT, Tominaga M. 2017. Expression of the TRPM6 in mouse placental trophoblasts; potential role in maternal-fetal calcium transport. *J Physiol Sci* **67**: 151-162

Swat W, Montgrain V, Doggett TA, Douangpanya J, Puri K, Vermi W, Diacovo TG. 2006. Essential role of $PI_3K\delta$ and $PI_3K\gamma$ in thymocyte survival. *Blood* **107**: 2415-2422

Syyong HT, Poburko D, Fameli N, van Breemen C. 2007. ATP promotes NCX-reversal in aortic smooth muscle cells by DAG-activated Na^+ entry. *Biochem Biophys Res Commun* **357**: 1177-1182

Szallasi A, Blumberg PM. 1996. Vanilloid receptors: New insights enhance potential as a therapeutic target. *Pain* **68**: 195-208

Szamel M, Rehermann B, Krebs B, Kurrle R, Resch K. 1989. Activation signals in human lymphocytes. Incorporation of polyunsaturated fatty acids into plasma membrane phospholipids regulates IL-2 synthesis via sustained activation of protein kinase C. *J Immunol* **143**: 2806

Szondy Z, Garabuczi E, Toth K, Kiss B, Koroskenyi K. 2012. Thymocyte death by neglect: Contribution of engulfing macrophages. *Eur J Immunol* **42**: 1662-1667

Ta TA, Feng W, Molinski TF, Pessah IN. 2006. Hydroxylated xestospongins block inositol-1,4,5-trisphosphate-induced Ca^{2+} release and sensitize Ca^{2+}-induced Ca^{2+} release mediated by ryanodine receptors. *Mol Pharmacol* **69**: 532-538

Taberner FJ, Fernandez-Ballester G, Fernandez-Carvajal A, Ferrer-Montiel A. 2015. TRP channels interaction with lipids and its implications in disease. *Biochim Biophys Acta* **1848**: 1818-1827

Takahama Y. 2006. Journey through the thymus: Stromal guides for T-cell development and selection. *Nat Rev Immunol* **6**: 127-135

Takezawa R, Cheng H, Beck A, Ishikawa J, Launay P, Kubota H, . . . Penner R. 2006. A pyrazole derivative potently inhibits lymphocyte Ca^{2+} influx and cytokine production by facilitating transient receptor potential melastatin 4 channel activity. *Mol Pharmacol* **69**: 1413-1420

Tan CH, McNaughton PA. 2016. The TRPM2 ion channel is required for sensitivity to warmth. *Nature* **536**: 460-463

Tang J, Lin Y, Zhang Z, Tikunova S, Birnbaumer L, Zhu MX. 2001. Identification of common binding sites for calmodulin and inositol 1,4,5-trisphosphate receptors on the carboxyl termini of TRP channels. *J Biol Chem* **276**: 21303-21310

Teh S-J, Killeen N, Tarakhovsky A, Littman DR, Teh H-S. 1997. CD2 regulates the positive selection and function of antigen-specific $CD4^{-}CD8^{+}$ T cells. *Blood* **89**: 1308-1318

Tellam RL, Parish CR. 1987. The effect of sulfated polysaccharides on the free intracellular calcium ion concentration of lymphocytes. *Biochim Biophys Acta* **930**: 55-64

Thakur DP, Tian JB, Jeon J, Xiong J, Huang Y, Flockerzi V, Zhu MX. 2016. Critical roles of gi/o proteins and phospholipase c-δ1 in the activation of receptor-operated TRPC4 channels. *Proc Natl Acad Sci USA* **113**: 1092-1097

Thebault S, Cao G, Venselaar H, Xi Q, Bindels RJ, Hoenderop JG. 2008. Role of the α-kinase domain in transient receptor potential melastatin 6 channel and regulation by intracellular ATP. *J Biol Chem* **283**: 19999-20007

Thome M, Germain V, DiSanto JP, Acuto O. 1996. The $p56^{lck}$ SH2 domain mediates recruitment of CD8/$p56^{lck}$ to the activated T cell receptor/CD3ζ complex. *Eur J Immunol* **26**: 2093-2100

Thorneloe KS, Cheung M, Bao W, Alsaid H, Lenhard S, Jian MY, . . . Willette RN. 2012. An orally active TRPV4 channel blocker prevents and resolves pulmonary edema induced by heart failure. *Sci Transl Med* **4**: 159ra148

Thyagarajan B, Benn B, Christakos S, Rohacs T. 2009. Phospholipase C-mediated regulation of transient receptor potential vanilloid 6 channels: Implications in active intestinal Ca^{2+} transport. *Mol Pharmacol* **75**: 608-616

Tian Q, Stepaniants SB, Mao M, Weng L, Feetham MC, Doyle MJ, . . . Hood LE. 2004. Integrated genomic and proteomic analyses of gene expression in mammalian cells. *Mol Cell Proteomics* **3**: 960-969

Togashi K, Inada H, Tominaga M. 2008. Inhibition of the transient receptor potential cation channel TRPM2 by 2-aminoethoxydiphenyl borate (2-APB). *Brit J Pharmacol* **153**: 1324-1330

Tolstykh GP, Thompson GL, Beier HT, Steelman ZA, Ibey BL. 2017. nsPEF-induced PIP_2 depletion, PLC activity and actin cytoskeletal cortex remodeling are responsible for post-exposure cellular swelling and blebbing. *Biochem Biophys Rep* **9**: 36-41

Tominaga M. 2007. The role of TRP channels in thermosensation In *TRP ion channel function in sensory transduction and cellular signaling cascades*, ed. B Liedtke W, S Heller. Boca Raton FL.: CRC Press/Taylor & Francis

Toth B, Csanady L. 2012. Pore collapse underlies irreversible inactivation of TRPM2 cation channel currents. *Proc Natl Acad Sci USA* **109**: 13440-13445

Tóth B, Csanády L. 2012. Pore collapse underlies irreversible inactivation of TRPM2 cation channel currents. *Proc Natl Acad Sci USA* **109**: 13440

Tóth BI, Konrad M, Ghosh D, Mohr F, Halaszovich CR, Leitner MG, . . . Voets T. 2015. Regulation of the transient receptor potential channel TRPM3 by phosphoinositides. *J Gen Physiol* **146**: 51-63

Tousova K, Vyklicky L, Susankova K, Benedikt J, Vlachova V. 2005. Gadolinium activates and sensitizes the vanilloid receptor TRPV1 through the external protonation sites. *Mol Cell Neurosci* **30**: 207-217

Toyabe S, Iiai T, Fukuda M, Kawamura T, Suzuki S, Uchiyama M, Abo T. 1997. Identification of nicotinic acetylcholine receptors on lymphocytes in the periphery as well as thymus in mice. *Immunology* **92**: 201-205

Trebak M, St. J. Bird G, McKay RR, Birnbaumer L, Putney JW. 2003. Signaling mechanism for receptor-activated canonical transient receptor potential 3 (TRPC3) channels. *J Biol Chem* **278**: 16244-16252

Trevisan G, Hoffmeister C, Rossato MF, Oliveira SM, Silva MA, Silva CR, . . . Ferreira J. 2014. TRPA1 receptor stimulation by hydrogen peroxide is critical to trigger hyperalgesia and inflammation in a model of acute gout. *Free Radical Bio Med* **72**: 200-209

Tsien RY, Pozzan T, Rink TJ. 1982. Calcium homeostasis in intact lymphocytes: Cytoplasmic free calcium monitored with a new, intracellularly trapped fluorescent indicator. *J Cell Biol* **94**: 325 - 334

Tsuchiya M, Hara Y, Okuda M, Itoh K, Nishioka R, Shiomi A, . . . Umeda M. 2018. Cell surface flip-flop of phosphatidylserine is critical for piezo1-mediated myotube formation. *Nat Commun* **9**: 2049

Tsuruda PR, Julius D, Minor DL, Jr. 2006. Coiled coils direct assembly of a cold-activated TRP channel. *Neuron* **51**: 201-212

Tsvilovskyy VV, Zholos AV, Aberle T, Philipp SE, Dietrich A, Zhu MX, . . . Flockerzi V. 2009. Deletion of TRPC4 and TRPC6 in mice impairs smooth muscle contraction and intestinal motility *in vivo*. *Gastroenterology* **137**: 1415-1424

Turner JM, Brodsky MH, Irving BA, Levin SD, Perlmutter RM, Littman DR. 1990. Interaction of the unique N-terminal region of tyrosine kinase $p56^{lck}$ with cytoplasmic domains of CD4 and CD8 is mediated by cysteine motifs. *Cell* **60**: 755-765

Ullrich ND, Voets T, Prenen J, Vennekens R, Talavera K, Droogmans G, Nilius B. 2005. Comparison of functional properties of the Ca^{2+} activated cation channels TRPM4 and TRPM5 from mice. *Cell calcium* **37**: 267-278

Umehara H, Huang JY, Kono T, Tabassam FH, Okazaki T, Gouda S, . . . Domae N. 1998. Co-stimulation of T cells with CD2 augments TCR-CD3-mediated activation of protein tyrosine kinase $p72^{syk}$, resulting in increased tyrosine phosphorylation of adapter proteins, Shc and Cbl. *Int Immunol* **10**: 833-845

Vaca L, Sampieri A. 2002. Calmodulin modulates the delay period between release of calcium from internal stores and activation of calcium influx via endogenous TRP1 channels. *J Biol Chem* **277**: 42178-42187

Vaeth M, Feske S. 2018. Ion channelopathies of the immune system. *Curr Opin Immunol* **52**: 39-50

Vaeth M, Yang J, Yamashita M, Zee I, Eckstein M, Knosp C, . . . Feske S. 2017. Orai2 modulates store-operated calcium entry and T cell-mediated immunity. *Nat Commun* **8**: 14714

van der Wijst J, Blanchard MG, Woodroof HI, Macartney TJ, Gourlay R, Hoenderop JG, . . . Alessi DR. 2014. Kinase and channel activity of TRPM6 are co-ordinated by a dimerization motif and pocket interaction. *Biochem J* **460**: 165-175

van Ewijk W, Hollander G, Terhorst C, Wang B. 2000. Stepwise development of thymic microenvironments *in vivo* is regulated by thymocyte subsets. *Development* **127**: 1583-1591

van Ewijk W, Shores EW, Singer A. 1994. Crosstalk in the mouse thymus. *Immunol Today* **15**: 214-217

van Kooyk Y, Weder P, Heije K, de Waal Malefijt R, Figdor CG. 1993. Role of intracellular Ca^{2+} levels in the regulation of CD11a/CD18 mediated cell adhesion. *Cell Adhes Commun* **1**: 21-32

Van Laethem F, Sarafova SD, Park J-H, Tai X, Pobezinsky L, Guinter TI, . . . Singer A. 2007. Deletion of CD4 and CD8 coreceptors permits generation of αβT

cells that recognize antigens independently of the MHC. *Immunity* **27**: 735-750

Vandewauw I, Owsianik G, Voets T. 2013. Systematic and quantitative mRNA expression analysis of TRP channel genes at the single trigeminal and dorsal root ganglion level in mouse. *BMC Neurosci* **14**: 21

Vannier B, Peyton M, Boulay G, Brown D, Qin N, Jiang M, . . . Birnbaumer L. 1999. Mouse Trp2, the homologue of the human Trpc2 pseudogene, encodes mTrp2, a store depletion-activated capacitative Ca^{2+} entry channel. *Proc Natl Acad Sci USA* **96**:

Varnum MD, Dai G. 2015. Cyclic nucleotide-gated ion channels In *Handbook of ion channels*, ed. J Zheng, MC Trudeau, pp. 361-382. Boca Raton, FL: CRC Press Taylor & Frqancis Group

Vassilieva IO, Tomilin VN, Marakhova I, Shatrova AN, Negulyaev YA, Semenova SB. 2013. Expression of transient receptor potential vanilloid channels TRPV5 and TRPV6 in human blood lymphocytes and Jurkat leukemia T cells. *J Membr Biol* **246**: 131-140

Vazquez G, Bird GSJ, Mori Y, Putney JW. 2006. Native TRPC7 channel activation by an inositol trisphosphate receptor-dependent mechanism. *J Biol Chem* **281**: 25250-25258

Vazquez G, Lievremont JP, St JBG, Putney JW, Jr. 2001. Human trp3 forms both inositol trisphosphate receptor-dependent and receptor-independent store-operated cation channels in DT40 avian B lymphocytes. *Proc Natl Acad Sci USA* **98**: 11777-11782

Vazquez G, Tano JY, Smedlund K. 2010. On the potential role of source and species of diacylglycerol in phospholipase-dependent regulation of TRPC3 channels. *Channels* **4**: 232-240

Vazquez G, Wedel BJ, Kawasaki BT, Bird GS, Putney JW, Jr. 2004. Obligatory role of Src kinase in the signaling mechanism for TRPC3 cation channels. *J Biol Chem* **279**: 40521-40528

Veillette A, Zúñiga-Pflücker JC, Bolen JB, Kruisbeek AM. 1989. Engagement of CD4 and CD8 expressed on immature thymocytes induces activation of intracellular tyrosine phosphorylation pathways. *J Exp Med* **170**: 1671

Veis DJ, Sorenson CM, Shutter JR, Korsmeyer SJ. 1993. Bcl-2-deficient mice demonstrate fulminant lymphoid apoptosis, polycystic kidneys, and hypopigmented hair. *Cell* **75**: 229-240

Venkatachalam K, Montell C. 2007. TRP channels. *Annu Rev Biochem* **76**:

Venkatachalam K, Zheng F, Gill DL. 2003. Regulation of canonical transient receptor potential (TRPC) channel function by diacylglycerol and protein kinase C. *J Biol Chem* **278**: 29031-29040

Verkhratsky A, Trebak M, Perocchi F, Khananshvili D, Sekler I. 2017. Crosslink between calcium and sodium signalling. *Exp Physiol* **103**: 157-169

Vermot-Desroches C, Rigal D, Bernaud J. 1991. Dextran sulfate specifically interacts with the human LFA-1 molecule (leucocyte function associated antigen-1). *Mol Immunol* **28**: 1095-1104

Vielkind S, Gallagher-Gambarelli M, Gomez M, Hinton HJ, Cantrell DA. 2005. Integrin regulation by RhoA in thymocytes. *J Immunol* **175**: 350-357

Vig M, Kinet J-P. 2009. Calcium signaling in immune cells. *Nat Immunol* **10**: 21-27

Viitanen TM, Sukumaran P, Lof C, Tornquist K. 2013. Functional coupling of TRPC2 cation channels and the calcium-activated anion channels in rat thyroid cells: Implications for iodide homeostasis. *J Cell Physiol* **228**: 814-823

Voets T, Janssens A, Prenen J, Droogmans G, Nilius B. 2003. Mg^{2+}-dependent gating and strong inward rectification of the cation channel TRPV6. *J Gen Physiol* **121**: 245-260

Voets T, Nilius B, Hoefs S, van der Kemp AW, Droogmans G, Bindels RJ, Hoenderop JG. 2004. TRPM6 forms the Mg^{2+} influx channel involved in intestinal and renal Mg^{2+} absorption. *J Biol Chem* **279**: 19-25

Vollger LW, Tuck DT, Springer TA, Haynes BF, Singer KH. 1987. Thymocyte binding to human thymic epithelial cells is inhibited by monoclonal antibodies to CD-2 and LFA-3 antigens. *J Immunol* **138**: 358-363

Voolstra O, Huber A. 2014. Post-translational modifications of TRP channels. *Cells* **3**: 258-287

Vrenken KS, Jalink K, van Leeuwen FN, Middelbeek J. 2016. Beyond ion-conduction: Channel-dependent and -independent roles of TRP channels during development and tissue homeostasis. *Biochimica et Biophysica Acta (BBA) - Mol Cell Research* **1863**: 1436-1446

Vriens J, Held K, Janssens A, Toth BI, Kerselaers S, Nilius B, . . . Voets T. 2014. Opening of an alternative ion permeation pathway in a nociceptor TRP channel. *Nat Chem Biol* **10**: 188-195

Vriens J, Owsianik G, Hofmann T, Philipp SE, Stab J, Chen X, . . . Voets T. 2011. TRPM3 is a nociceptor channel involved in the detection of noxious heat. *Neuron* **70**: 482-494

Wacholtz MC, Cragoe EJ, Lipsky PE. 1993. Delineation of the role of a Na^{+}/Ca^{2+} exchanger in regulating intracellular Ca^{2+} in T cells. *Cell Immunol* **147**: 95-109

Wagner TF, Loch S, Lambert S, Straub I, Mannebach S, Mathar I, . . . Oberwinkler J. 2008. Transient receptor potential m3 channels are ionotropic steroid receptors in pancreatic β cells. *Nat Cell Biol* **10**: 1421-1430

Wahl A, Dinet C, Dillard P, Puech P-H, Limozin L, Sengupta K. 2017. Biphasic mechanosensitivity of TCR mediated adhesion of T lymphocytes. *bioRxiv*:

Walk SF, March ME, Ravichandran KS. 1998. Roles of Lck, Syk and ZAP-70 tyrosine kinases in TCR-mediated phosphorylation of the adapter protein Shc. *Eur J Immunol* **28**: 2265-2275

Walser M. 1961. Ion association. Vi. Interactions between calcium, magnesium, inorganic phosphate, citrate and protein in normal human plasma. *J Clin Invest* **40**: 723-730

Wang C. 2006. *Structure, function and regulation of TRP channels*. thesis. The Ohio State University, retrieved from http://citeseerx.ist.psu.edu/viewdoc/download?doi=10.1.1.884.7433&rep=rep1&type=pdf. 171 pp.

Wang D, Zheng M, Lei L, Ji J, Yao Y, Qiu Y, . . . Lu L. 2012. Tespa1 is involved in late thymocyte development through the regulation of TCR-mediated signaling. *Nat Immunol* **13**: 560-568

Wang G, Wang K. 2017. The Ca^{2+}-permeable cation transient receptor potential TRPV3 channel: An emerging pivotal target for itch and skin diseases. *Mol Pharmacol* **92**: 193

Wang H, Wei B, Bismuth G, Rudd CE. 2009. SLP-76-ADAP adaptor module regulates LFA-1 mediated costimulation and T cell motility. *Proc Natl Acad Sci USA* **106**: 12436

Wang J, Richards DA. 2012. Segregation of PIP_2 and PIP_3 into distinct nanoscale regions within the plasma membrane. *Biol Open* **1**: 857

Wang Y, Chi S, Guo H, Li G, Wang L, Zhao Q, . . . Xiao B. 2018. A lever-like transduction pathway for long-distance chemical- and mechano-gating of the mechanosensitive piezo1 channel. *Nat Commun* **9**: 1300

Wang Y, Deng X, Mancarella S, Hendron E, Eguchi S, Soboloff J, . . . Gill DL. 2010. The calcium store sensor, STIM1, reciprocally controls Orai and CaV1.2 channels. *Science* **330**: 105-109

Wang Y, Liang L, Esselman WJ. 2000. Regulation of the calcium/nf-at t cell activation pathway by the d2 domain of CD45. *J Immunol* **164**: 2557

Wang Y, Shibuya K, Yamashita Y, Shirakawa J, Shibata K, Kai H, . . . Shibuya A. 2008. LFA-1 decreases the antigen dose for T cell activation *in vivo*. *Int Immunol* **20**: 1119-1127

Wardenburg JB, Fu C, Jackman JK, Flotow H, Wilkinson SE, Williams DH, . . . Findell PR. 1996. Phosphorylation of SLP-76 by the ZAP-70 protein-tyrosine kinase is required for T-cell receptor function. *J Biol Chem* **271**: 19641-19644

Warren HS, Parish CR. 1990. Mapping the dextran sulfate binding site on CD2. *Immunol Cell Biol* **68**: 199-205

Watanabe H, Vriens J, Janssens A, Wondergem R, Droogmans G, Nilius B. 2003a. Modulation of TRPV4 gating by intra- and extracellular Ca^{2+}. *Cell calcium* **33**: 489-495

Watanabe H, Vriens J, Prenen J, Droogmans G, Voets T, Nilius B. 2003b. Anandamide and arachidonic acid use epoxyeicosatrienoic acids to activate TRPV4 channels. *Nature* **424**: 434-438

Watanabe H, Vriens J, Suh SH, Benham CD, Droogmans G, Nilius B. 2002. Heat-evoked activation of TRPV4 channels in a HEK293 cell expression system and in native mouse aorta endothelial cells. *J Biol Chem* **277**: 47044-47051

Weber KS, Hildner K, Murphy KM, Allen PM. 2010. Trpm4 differentially regulates Th1 and Th2 function by altering calcium signaling and NFAT localization. *J Immunol* **185**: 2836-2846

Wehbi VL, Taskén K. 2016. Molecular mechanisms for cAMP-mediated immunoregulation in T cells- role of anchored protein kinase A signaling units. *Front Immunol* **7**:

Wei C, Wang X, Chen M, Ouyang K, Song L-S, Cheng H. 2009. Calcium flickers steer cell migration. *Nature* **457**: 901-905

Wenning AS, Neblung K, Strauß B, Wolfs M-J, Sappok A, Hoth M, Schwarz EC. 2011. TRP expression pattern and the functional importance of TRPC3 in primary human t-cells. *Biochimica et Biophysica Acta (BBA) - Mol Cell Research* **1813**: 412-423

Wera S, Hemmings BA. 1995. Serine/threonine protein phosphatases. *Biochem J* **311 (Pt 1)**: 17-29

Werneck CC, Cruz MS, Silva LCF, Villa-Verde DMS, Savino W, Mourao PAS. 2000. Is there a glycosaminoglycan-related heterogeneity of the thymic epithelium? *J Cell Physiol* **185**: 68-79

Werneck CC, Oliveira-Dos-Santos AJ, Silva L-CF, Villa-Verde DMS, Savino W, Mourão PAS. 1999. Thymic epithelial cells synthesize a heparan sulfate with a highly sulfated region. *J Cell Physiol* **178**: 51-62

Weston SA, Tellam RL, Parish CR. 1991. Dextran sulfate induces changes in the free intracellular calcium ion concentration of a subpopulation of immature thymocytes. *Immunol Cell Biol* **69 (Pt 6)**: 369-376

Whyte-Fagundes P, Zoidl G. 2018. Mechanisms of pannexin1 channel gating and regulation. *Biochim Biophys Acta* **1860**: 65-71

Wieraszko A. 1986. Evidence that ruthenium red disturbs the synaptic transmission in the rat hippocampal slices through interacting with sialic acid residues. *Brain Res* **378**: 120-126

Wiest DL, Yuan L, Jefferson J, Benveniste P, Tsokos M, Klausner RD, . . . Singer A. 1993. Regulation of T cell receptor expression in immature $CD4^+$ $CD8^+$ thymocytes by $p56^{lck}$ tyrosine kinase: Basis for differential signaling by CD4 and CD8 in immature thymocytes expressing both coreceptor molecules. *J Exp Med* **178**: 1701-1712

Winchester RJ. 2008. The major histocompatibility complex In *Clinical immunology* ed. RR Rich, TA Fleisher, WT Shearer, HW Schroeder, AJ Frew, CM Weyand, pp. 79-90. Edinburgh: Mosby

Winslow MM, Neilson JR, Crabtree GR. 2003. Calcium signalling in lymphocytes. *Curr Opin Immunol* **15**: 299-307

Woo D, H, Jung S, J, Zhu M, H, Park C, Kim Y, H, Oh S, Justin c, L. 2008. Direct activation of transient receptor potential vanilloid 1 (TRPV1) by diacylglycerol (DAG). *Mol Pain* **4**:

Woo S-H, Ranade S, Weyer AD, Dubin AE, Baba Y, Qiu Z, . . . Patapoutian A. 2014. Piezo2 is required for Merkel-cell mechanotransduction. *Nature* **509**: 622

Woudenberg-Vrenken TE, Sukinta A, van der Kemp AW, Bindels RJ, Hoenderop JG. 2011. Transient receptor potential melastatin 6 knockout mice are lethal whereas heterozygous deletion results in mild hypomagnesemia. *Nephron Physiol* **117**: p11-19

Wrenshall LE, Cerra FB, Rubinstein P, Platt JL. 1993. Regulation by heparan sulfate and interleukin 1α of the ontogenic expression of T-cell receptor, CD4, and CD8 in developing thymus. *Hum Immunol* **38**: 165-171

Wu J, Kamimura N, Takeo T, Suga S, Wakui M, Maruyama T, Mikoshiba K. 2000. 2-aminoethoxydiphenyl borate modulates kinetics of intracellular Ca^{2+} signals mediated by inositol 1,4,5-trisphosphate-sensitive Ca^{2+} stores in single pancreatic acinar cells of mouse. *Mol Pharmacol* **58**: 1368-1374

Wu J, Lewis AH, Grandl J. 2017a. Touch, tension, and transduction - the function and regulation of piezo ion channels. *Trends Biochem Sci* **42**: 57-71

Wu J, Young M, Lewis AH, Martfeld AN, Kalmeta B, Grandl J. 2017b. Inactivation of mechanically activated piezo1 ion channels is determined by the C-terminal extracellular domain and the inner pore helix. *Cell Rep* **21**: 2357-2366

Wu JN, Gheith S, Bezman NA, Liu QH, Fostel LV, Swanson AM, . . . Peterson EJ. 2006. Adhesion- and degranulation-promoting adapter protein is required for efficient thymocyte development and selection. *J Immunol* **176**: 6681-6689

Wu L-J, Sweet T-B, Clapham DE. 2010. International union of basic and clinical pharmacology. Lxxvi. Current progress in the mammalian TRP ion channel family. *Pharmacol Rev* **62**: 381-404

Wu Q-y, Sun M-r, Wu C-l, Li Y, Du J-j, Zeng J-y, . . . Sun Y-h. 2015. Activation of calcium-sensing receptor increases TRPC3/6 expression in T lymphocyte in sepsis. *Mol Immunol* **64**: 18-25

Wulfing C, Sjaastad MD, Davis MM. 1998. Visualizing the dynamics of T cell activation: Intracellular adhesion molecule 1 migrates rapidly to the T cell/b cell interface and acts to sustain calcium levels. *Proc Natl Acad Sci USA* **95**: 6302-6307

Xiang M, Feng M, Muend S, Rao R. 2007. A human Na^+/h^+ antiporter sharing evolutionary origins with bacterial nhaa may be a candidate gene for essential hypertension. *Proc Natl Acad Sci USA* **104**: 18677

Xiao B, Coste B, Mathur J, Patapoutian A. 2011. Temperature-dependent STIM1 activation induces ca^{2+} influx and modulates gene expression. *Nat Chem Biol* **7**: 351-358

Xiao R, Tang J, Wang C, Colton CK, Tian J, Zhu MX. 2008. Calcium plays a central role in the sensitization of TRPV3 channel to repetitive stimulations. *J Biol Chem* **283**: 6162-6174

Xie J, Sun B, Du J, Yang W, Chen HC, Overton JD, . . . Yue L. 2011. Phosphatidylinositol 4,5-bisphosphate (PIP_2) controls magnesium gatekeeper TRPM6 activity. *Sci Rep-UK* **1**: 146

Xu C, Gagnon E, Call ME, Schnell JR, Schwieters CD, Carman CV, . . . Wucherpfennig KW. 2008. Regulation of T cell receptor activation by dynamic membrane binding of the CD3ε cytoplasmic tyrosine-based motif. *Cell* **135**: 702-713

Xu H, Fu Y, Tian W, Cohen DM. 2006. Glycosylation of the osmoresponsive transient receptor potential channel TRPV4 on Asn-651 influences membrane trafficking. *Am J Physiol Renal Physiol* **290**: F1103-1109

Xu H, Ramsey IS, Kotecha SA, Moran MM, Chong JA, Lawson D, . . . Clapham DE. 2002. TRPV3 is a calcium-permeable temperature-sensitive cation channel. *Nature* **418**: 181-186

Xu H, Zhao H, Tian W, Yoshida K, Roullet JB, Cohen DM. 2003. Regulation of a transient receptor potential (TRP) channel by tyrosine phosphorylation. Src family kinase-dependent tyrosine phosphorylation of TRPV4 on TYR-253 mediates its response to hypotonic stress. *J Biol Chem* **278**: 11520-11527

Xu S-Z, Zeng F, Boulay G, Grimm C, Harteneck C, Beech DJ. 2005. Block of TRPC5 channels by 2-aminoethoxydiphenyl borate: A differential, extracellular and voltage-dependent effect. *Brit J Pharmacol* **145**: 405-414

Xu XZ, Moebius F, Gill DL, Montell C. 2001. Regulation of melastatin, a TRP-related protein, through interaction with a cytoplasmic isoform. *Proc Natl Acad Sci USA* **98**: 10692-10697

Xue L, Chiang L, Kang C, Winoto A. 2008. The role of the PI_3K-akt kinase pathway in T-cell development beyond the β checkpoint. *Eur J Immunol* **38**: 3200-3207

Yang F, Ma L, Cao X, Wang K, Zheng J. 2014. Divalent cations activate TRPV1 through promoting conformational change of the extracellular region. *J Gen Physiol* **143**: 91-103

Yang J, Cai W, Lu X, Liu S, Zhao S. 2017. Rna-sequencing analyses demonstrate the involvement of canonical transient receptor potential channels in rat tooth germ development. *Front Physiol* **8**: 455

Yang P, Zhu MX. 2014. TRPV3 In *Mammalian transient receptor potential (TRP) cation channels: Volume I*, ed. B Nilius, V Flockerzi, pp. 273-291. Berlin, Heidelberg: Springer Berlin Heidelberg

Yang SL, Cao Q, Zhou KC, Feng YJ, Wang YZ. 2009. Transient receptor potential channel C3 contributes to the progression of human ovarian cancer. *Oncogene* **28**: 1320-1328

Yao J, Liu B, Qin F. 2011. Modular thermal sensors in temperature-gated transient receptor potential (TRP) channels. *Proc Natl Acad Sci USA* **108**: 11109-11114

Yao X, Kwan H-Y, Huang Y. 2005. *Regulation of TRP channels by phosphorylation*. 273-280 pp.

Yuan JP, Kiselyov K, Shin DM, Chen J, Shcheynikov N, Kang SH, . . . Muallem S. 2003. Homer binds TRPC family channels and is required for gating of TRPC1 by IP_3 receptors. *Cell* **114**:

Yuan JP, Zeng W, Huang GN, Worley PF, Muallem S. 2007. STIM1 heteromultimerizes TRPC channels to determine their function as store-operated channels. *Nat Cell Biol* **9**: 636-645

Yue L, Peng J, Hediger M, Clapham D. 2001. Cat1 manifests the pore properties of the calcium-release-activated calcium channel. *Nature* **410**: 705

Zagranichnaya TK, Wu X, Villereal ML. 2005. Endogenous TRPC1, TRPC3, and TRPC7 proteins combine to form native store-operated channels in HEK-293 cells. *J Biol Chem* **280**: 29559-29569

Zambon AC, Wilderman A, Ho A, Insel PA. 2011. Increased expression of the pro-apoptotic protein bim, a mechanism for cAMP/protein kinase A (PKA)-induced apoptosis of immature T cells. *The J Biol Chem* **286**: 33260-33267

Zanou N, Mondin L, Fuster C, Seghers F, Dufour I, de Clippele M, . . . Gailly P. 2015. Osmosensation in TRPV2 dominant negative expressing skeletal muscle fibres. *J Physiol* **593**: 3849-3863

Zarayskiy V, Monje F, Peter K, Csutora P, Khodorov BI, Bolotina VM. 2007. Store-operated Orai1 and IP_3 receptor-operated TRPC1 channel. *Channels* **1**: 246-252

Zayats V, Samad A, Minofar B, Roelofs KE, Stockner T, Ettrich R. 2013. Regulation of the transient receptor potential channel TRPA1 by its N-terminal ankyrin repeat domain. *J Mol Model* **19**: 4689-4700

Zhang F, Swartz KJ, Jara-Oseguera A. 2019. Conserved allosteric pathways for activation of TRPV3 revealed through engineering vanilloid-sensitivity. *eLife* **8**: e42756

Zhang P, Yang C, Delay RJ. 2010. Odors activate dual pathways, a TRPC2 and a AA-dependent pathway, in mouse vomeronasal neurons. *American journal of physiology. Cell physiology* **298**: C1253-C1264

Zhang W, Sloan-Lancaster J, Kitchen J, Trible RP, Samelson LE. 1998. LAT: The ZAP-70 tyrosine kinase substrate that links T cell receptor to cellular activation. *Cell* **92**: 83-92

Zhang X, Li L, McNaughton PA. 2008. Proinflammatory mediators modulate the heat-activated ion channel TRPV1 via the scaffolding protein AKAP79/150. *Neuron* **59**: 450-461

Zhang Z, Tang J, Tikunova S, Johnson JD, Chen Z, Qin N, . . . Zhu MX. 2001. Activation of trp3 by inositol 1,4,5-trisphosphate receptors through displacement of inhibitory calmodulin from a common binding domain. *Proc Natl Acad Sci USA* **98**: 3168-3173

Zhang Z, Tóth B, Szollosi A, Chen J, Csanády L. 2018. Structure of a TRPM2 channel in complex with Ca^{2+} explains unique gating regulation. *eLife* **7**: e36409

Zhao Q, Wu K, Geng J, Chi S, Wang Y, Zhi P, . . . Xiao B. 2016. Ion permeation and mechanotransduction mechanisms of mechanosensitive piezo channels. *Neuron* **89**: 1248-1263

Zhao Y, Iwata M. 1995. Cross-linking of the TCR–CD3 complex with CD4, CD8 or LFA-1 induces an anti-apoptotic signal in thymocytes: The signal is canceled by FK506. *Int Immunol* **7**: 1387-1396

Zheng J. 2013. Molecular mechanism of TRP channels In *Comprehensive physiology*: John Wiley & Sons, Inc.

Zheng M, Li D, Zhao Z, Shytikov D, Xu Q, Jin X, . . . Lu L. 2019. Protein phosphatase 2A has an essential role in promoting thymocyte survival during selection. *Proc Natl Acad Sci USA*: 201821116

Zheng W, Cai R, Hofmann L, Nesin V, Hu Q, Long W, . . . Chen XZ. 2018. Direct binding between pre-S1 and TRP-like domains in TRPP channels mediates gating and functional regulation by PIP_2 *Cell Rep* **22**: 1560-1573

Zhivotovsky B, Orrenius S. 2011. Calcium and cell death mechanisms: A perspective from the cell death community. *Cell calcium* **50**: 211-221

Zholos A. 2010. Pharmacology of transient receptor potential melastatin channels in the vasculature. *Brit J Pharmacol* **159**: 1559-1571

Zholos AV, Tsytsyura YD, Gordienko DV, Tsvilovskyy VV, Bolton TB. 2004. Phospholipase c, but not $InsP_3$ or DAG, -dependent activation of the muscarinic receptor-operated cation current in guinea-pig ileal smooth muscle cells. *Brit J Pharmacol* **141**: 23-36

Zhong F, Davis MC, McColl KS, Distelhorst CW. 2006. Bcl-2 differentially regulates Ca^{2+} signals according to the strength of T cell receptor activation. *J Cell Biol* **172**: 127-137

Zhou Y, Suzuki Y, Uchida K, Tominaga M. 2013. Identification of a splice variant of mouse TRPA1 that regulates TRPA1 activity. *Nat Commun* **4**: 2408

Zhu M, Janssen E, Zhang W. 2003. Minimal requirement of tyrosine residues of linker for activation of T cells in TCR signaling and thymocyte development. *J Immunol* **170**: 325-333

Zhu MX. 2005. Multiple roles of calmodulin and other Ca^{2+}-binding proteins in the functional regulation of TRP channels. *Pflügers Archiv* **451**: 105-115

Zinchenko VP, Antonov SA, Sergeev AI. 2009. Constitutively active calcium channels in plasma membrane of T-lymphocytes. *Biochemistry (Moscow) Supplement Series A: Membrane and Cell Biology* **3**: 286-290

Zitt C, Strauss B, Schwarz EC, Spaeth N, Rast G, Hatzelmann A, Hoth M. 2004. Potent inhibition of Ca^{2+} release-activated Ca^{2+} channels and t-lymphocyte activation by the pyrazole derivative btp2. *J Biol Chem* **279**: 12427-12437

Zubcevic L, Le S, Yang H, Lee S-Y. 2018. Conformational plasticity in the selectivity filter of the TRPV2 ion channel. *Nat Struct Mol Biol* **25**: 405-415

Zurborg S, Yurgionas B, Jira JA, Caspani O, Heppenstall PA. 2007. Direct activation of the ion channel TRPA1 by Ca^{2+}. *Nat Neurosci* **10**: 277

Reference list for Table 3.2

1. Rohacs, T., Phosphoinositide regulation of TRPV1 revisited. *Pflugers Arch*, 2015.**467**(9):p. 1851-69.
2. Zhang, X., J. Huang, and P.A. McNaughton, NGF rapidly increases membrane expression of TRPV1 heat-gated ion channels. *EMBO J*, 2005.**24**(24):p. 4211-23.
3. Tsumura, M., U. Sobhan, T. Muramatsu, M. Sato, H. Ichikawa, Y. Sahara, . . . Y. Shibukawa, TRPV1-mediated calcium signal couples with cannabinoid receptors and sodium-calcium exchangers in rat odontoblasts. *Cell calcium*, 2012.**52**(2):p. 124-36.
4. Sato, M., D.U. Sobhan, M. Tsumura, H. Kuroda, M. Soya, A. Masamura, . . . Y. Shibukawa, Hypotonic-induced stretching of plasma membrane activates transient receptor potential vanilloid channels and sodium–calcium exchangers in mouse odontoblasts. *Journal of Endodontics*, 2013.**39**:p. 779–787.
5. Woo, D., H, S. Jung, J, M. Zhu, H, C. Park, Y. Kim, H, S. Oh, and c. Justin, L, Direct activation of transient receptor potential vanilloid 1 (TRPV1) by diacylglycerol (DAG). *Mol Pain*, 2008.**4**:p.
6. Chuang, H.H., E.D. Prescott, H. Kong, S. Shields, S.E. Jordt, A.I. Basbaum, . . . D. Julius, Bradykinin and nerve growth factor release the capsaicin receptor from PtdIns(4,5)P_2-mediated inhibition. *Nature*, 2001.**411**(6840):p. 957-62.
7. Lukacs, V., B. Thyagarajan, P. Varnai, A. Balla, T. Balla, and T. Rohacs, Dual regulation of TRPV1 by phosphoinositides. *J Neurosci*, 2007.**27**(26):p. 7070-7080.
8. Lishko, P.V., E. Procko, X. Jin, C.B. Phelps, and R. Gaudet, The ankyrin repeats of TRPV1 bind multiple ligands and modulate channel sensitivity. *Neuron*, 2007.**54**(6):p. 905-18.

9. Voolstra, O. and A. Huber, Post-translational modifications of TRP channels. *Cells*, 2014.**3**(2):p. 258-287.
10. Chung, M.-K., H. Lee, A. Mizuno, M. Suzuki, and M.J. Caterina, 2-Aminoethoxydiphenyl borate activates and sensitizes the heat-gated ion channel TRPV3. *J Neurosci*, 2004.**24**(22):p. 5177.
11. Xu, H., I.S. Ramsey, S.A. Kotecha, M.M. Moran, J.A. Chong, D. Lawson, . . . D.E. Clapham, TRPV3 is a calcium-permeable temperature-sensitive cation channel. *Nature*, 2002.**418**(6894):p. 181-6.
12. Doerner, J.F., H. Hatt, and I.S. Ramsey, Voltage- and temperature-dependent activation of TRPV3 channels is potentiated by receptor-mediated PI(4,5)P_2 hydrolysis. *J Gen Physiol*, 2011.**137**(3):p. 271.
13. Fan, H.C., X. Zhang, and P.A. McNaughton, Activation of the TRPV4 ion channel is enhanced by phosphorylation. *J Biol Chem*, 2009.**284**(41):p. 27884-91.
14. Wegierski, T., U. Lewandrowski, B. Muller, A. Sickmann, and G. Walz, Tyrosine phosphorylation modulates the activity of TRPV4 in response to defined stimuli. *J Biol Chem*, 2009.**284**(5):p. 2923-33.
15. Garcia-Elias, A., S. Mrkonjic, C. Pardo-Pastor, H. Inada, U.A. Hellmich, F. Rubio-Moscardo, . . . M.A. Valverde, Phosphatidylinositol-4,5-biphosphate-dependent rearrangement of TRPV4 cytosolic tails enables channel activation by physiological stimuli. *Proc Natl Acad Sci U S A*, 2013.**110**(23):p. 9553-8.
16. Xu, H., H. Zhao, W. Tian, K. Yoshida, J.B. Roullet, and D.M. Cohen, Regulation of a transient receptor potential (TRP) channel by tyrosine phosphorylation. SRC family kinase-dependent tyrosine phosphorylation of TRPV4 on TYR-253 mediates its response to hypotonic stress. *J Biol Chem*, 2003.**278**(13):p. 11520-7.
17. Watanabe, H., J. Vriens, A. Janssens, R. Wondergem, G. Droogmans, and B. Nilius, Modulation of TRPV4 gating by intra- and extracellular Ca^{2+}. *Cell calcium*, 2003.**33**(5):p. 489-495.
18. Garcia-Elias, A., I.M. Lorenzo, R. Vicente, and M.A. Valverde, IP_3 receptor binds to and sensitizes TRPV4 channel to osmotic stimuli via a calmodulin-binding site. *J Biol Chem*, 2008.**283**(46):p. 31284-8.
19. Takahashi, N., S. Hamada-Nakahara, Y. Itoh, K. Takemura, A. Shimada, Y. Ueda, . . . S. Suetsugu, TRPV4 channel activity is modulated by direct interaction of the ankyrin domain to PI(4,5)P_2. *Nat Commun*, 2014.**5**:p. 4994.
20. Peng, H., U. Lewandrowski, B. Muller, A. Sickmann, G. Walz, and T. Wegierski, Identification of a protein kinase C-dependent phosphorylation site involved in sensitization of TRPV4 channel. *Biochem Biophys Res Commun*, 2010.**391**(4):p. 1721-5.

21. Watanabe, H., J. Vriens, J. Prenen, G. Droogmans, T. Voets, and B. Nilius, Anandamide and arachidonic acid use epoxyeicosatrienoic acids to activate TRPV4 channels. *Nature*, 2003.**424**(6947):p. 434-438.
22. Albarran, L., N. Dionisio, E. Lopez, G.M. Salido, P.C. Redondo, and J.A. Rosado, STIM1 regulates TRPC6 heteromultimerization and subcellular location. *Biochem J*, 2014.**463**(3):p. 373-81.
23. Hisatsune, C., Y. Kuroda, K. Nakamura, T. Inoue, T. Nakamura, T. Michikawa, . . . K. Mikoshiba, Regulation of TRPC6 channel activity by tyrosine phosphorylation. *J Biol Chem*, 2004.**279**(18):p. 18887-18894.
24. Meng, F., W.K. To, and Y. Gu, Role of TRP channels and NCX in mediating hypoxia-induced $[Ca^{2+}]_i$ elevation in PC12 cells. *Respir Physiol Neurobiol*, 2008.**164**(3):p. 386-93.
25. Basora, N., G. Boulay, L. Bilodeau, E. Rousseau, and M.D. Payet, 20-hydroxyeicosatetraenoic acid (20-HETE) activates mouse TRPC6 channels expressed in HEK293 cells. *J Biol Chem*, 2003.**278**(34):p. 31709-16.
26. Gottlieb, P., J. Folgering, R. Maroto, A. Raso, T. Wood, A. Kurosky, . . . E. Honoré, Revisiting TRPC1 and TRPC6 mechanosensitivity. *Pflüg Arch Eur J Phy*, 2008.**455**(6):p. 1097-1103.
27. Hofmann, T., A.G. Obukhov, M. Schaefer, C. Harteneck, T. Gudermann, and G. Schultz, Direct activation of human TRPC6 and TRPC3 channels by diacylglycerol. *Nature*, 1999.**397**(6716):p. 259-263.
28. Weber, E.W., F. Han, M. Tauseef, L. Birnbaumer, D. Mehta, and W.A. Muller, TRPC6 is the endothelial calcium channel that regulates leukocyte transendothelial migration during the inflammatory response. *J Exp Med*, 2015.**212**(11):p. 1883-99.
29. Itsuki, K., Y. Imai, H. Hase, Y. Okamura, R. Inoue, and M.X. Mori, PLC-mediated $PI(4,5)P_2$ hydrolysis regulates activation and inactivation of TRPC6/7 channels. *J Gen Physiol*, 2014.**143**(2):p. 183-201.
30. Horinouchi, T., T. Higa, H. Aoyagi, T. Nishiya, K. Terada, and S. Miwa, Adenylate cyclase/cAMP/protein kinase A signaling pathway inhibits endothelin type A receptor-operated Ca^{2+} entry mediated via transient receptor potential canonical 6 channels. *J Pharmacol Exp Ther*, 2012.**340**(1):p. 143-51.
31. Albarrán, L., J.J. Lopez, N. Dionisio, T. Smani, G.M. Salido, and J.A. Rosado, Transient receptor potential ankyrin-1 (TRPA1) modulates store-operated Ca^{2+} entry by regulation of STIM1-Orai1 association. *Biochimica et Biophysica Acta (BBA) - Mol Cell Res*, 2013.**1833**(12):p. 3025-3034.
32. Sura, L., V. Zima, L. Marsakova, A. Hynkova, I. Barvik, and V. Vlachova, C-terminal acidic cluster is involved in Ca^{2+}-induced regulation of human transient receptor potential ankyrin 1 channel. *J Biol Chem*, 2012.**287**(22):p. 18067-77.

33. Doerner, J.F., G. Gisselmann, H. Hatt, and C.H. Wetzel, Transient receptor potential channel A1 is directly gated by calcium ions. *J Biol Chem*, 2007.**282**:p.
34. Bandell, M., G.M. Story, S.W. Hwang, V. Viswanath, S.R. Eid, and M.J. Petrus, Noxious cold ion channel TRPA1 is activated by pungent compounds and bradykinin. *Neuron*, 2004.**41**:p.
35. Dai, Y., S. Wang, M. Tominaga, S. Yamamoto, T. Fukuoka, T. Higashi, . . . K. Noguchi, Sensitization of TRPA1 by PAR2 contributes to the sensation of inflammatory pain. *J Clin Invest*, 2007.**117**(7):p. 1979-87.
36. Hill, K. and M. Schaefer, TRPA1 is differentially modulated by the amphipathic molecules trinitrophenol and chlorpromazine. *J Biol Chem*, 2007.**282**(10):p. 7145-7153.
37. Marcotti, W., F. Sachs, J.F. Ashmore, and C. Kros, Effect of a peptide tarantula toxin on mechano-transduction in neonatal mouse cochlear hair cells. *Int J Audiol*, 2001.**41**:p. 231.
38. Zayats, V., A. Samad, B. Minofar, K.E. Roelofs, T. Stockner, and R. Ettrich, Regulation of the transient receptor potential channel TRPA1 by its N-terminal ankyrin repeat domain. *J Mol Model*, 2013.**19**(11):p. 4689-4700.
39. Planells-Cases, R., N. Garcia-Sanz, C. Morenilla-Palao, and A. Ferrer-Montiel, Functional aspects and mechanisms of TRPV1 involvement in neurogenic inflammation that leads to thermal hyperalgesia. *Pflugers Arch*, 2005.**451**(1):p. 151-9.
40. Penna, A., V. Juvin, J. Chemin, V. Compan, M. Monet, and F.A. Rassendren, PI_3-kinase promotes TRPV2 activity independently of channel translocation to the plasma membrane. *Cell calcium*, 2006.**39**(6):p. 495-507.
41. Nie, L., Y. Oishi, I. Doi, H. Shibata, and I. Kojima, Inhibition of proliferation of MCF-7 breast cancer cells by a blocker of Ca^{2+}-permeable channel. *Cell calcium*, 1997.**22**(2):p. 75-82.
42. Mercado, J., A. Gordon-Shaag, W.N. Zagotta, and S.E. Gordon, Ca^{2+}-dependent desensitization of TRPV2 channels is mediated by hydrolysis of phosphatidylinositol 4,5-bisphosphate. *J Neurosci*, 2010.**30**(40):p. 13338.
43. Senning, E.N., M.D. Collins, A. Stratiievska, C.A. Ufret-Vincenty, and S.E. Gordon, Regulation of TRPV1 Ion channel by phosphoinositide (4,5)-bisphosphate: The role of membrane asymmetry. *J Biol Chem*, 2014.**289**(16):p. 10999-11006.
44. Park, C.W., H.J. Kim, Y.W. Choi, B.Y. Chung, S.Y. Woo, D.K. Song, and H.O. Kim, TRPV3 channel in keratinocytes in scars with post-burn pruritus. *Int J Mol Sci*, 2017.**18**(11):p.
45. Rampino, M.A.F. and S.A. Nawy, Relief of Mg^{2+}-dependent inhibition of TRPM1 by PKCα at the rod bipolar cell synapse. *J Neurosci*, 2011.**31**(38):p. 13596-13603.

46. Tang, J., Y. Lin, Z. Zhang, S. Tikunova, L. Birnbaumer, and M.X. Zhu, Identification of common binding sites for calmodulin and inositol 1,4,5-trisphosphate receptors on the carboxyl termini of TRP channels. *J Biol Chem*, 2001.**276**(24):p. 21303-21310.
47. Lucas, P., K. Ukhanov, T. Leinders-Zufall, and F. Zufall, A diacylglycerol-gated cation channel in vomeronasal neuron dendrites is impaired in TRPC2 mutant mice: mechanism of pheromone transduction. *Neuron*, 2003.**40**(3):p. 551-61.
48. Kwon, Y., T. Hofmann, and C. Montell, Integration of phosphoinositide- and calmodulin-mediated regulation of TRPC6. *Mol Cell*, 2007.**25**(4):p. 491-503.
49. Kashio, M., T. Sokabe, K. Shintaku, T. Uematsu, N. Fukuta, N. Kobayashi, . . . M. Tominaga, Redox signal-mediated sensitization of transient receptor potential melastatin 2 (TRPM2) to temperature affects macrophage functions. *Proc Natl Acad Sci U S A*, 2012.**109**(17):p. 6745-50.
50. Hara, Y., M. Wakamori, M. Ishii, E. Maeno, M. Nishida, T. Yoshida, . . . Y. Mori, LTRPC2 Ca^{2+}-permeable channel activated by changes in redox status confers susceptibility to cell death. *Mol Cell*, 2002.**9**(1):p. 163-173.
51. McHugh, D., R. Flemming, S.Z. Xu, A.L. Perraud, and D.J. Beech, Critical intracellular Ca^{2+} dependence of transient receptor potential melastatin 2 (TRPM2) cation channel activation. *J Biol Chem*, 2003.**278**(13):p. 11002-6.
52. Vazquez, G., G.S.J. Bird, Y. Mori, and J.W. Putney, Native TRPC7 channel activation by an inositol trisphosphate receptor-dependent mechanism. *J Biol Chem*, 2006.**281**(35):p. 25250-25258.
53. Zhang, W., Q. Tong, K. Conrad, J. Wozney, J.Y. Cheung, and B.A. Miller, Regulation of TRP channel TRPM2 by the tyrosine phosphatase PTPL1. *Am J Physiol Cell Physiol*, 2007.**292**(5):p. C1746-58.
54. Togashi, K., Y. Hara, T. Tominaga, T. Higashi, Y. Konishi, Y. Mori, and M. Tominaga, TRPM2 activation by cyclic ADP-ribose at body temperature is involved in insulin secretion. *EMBO J*, 2006.**25**(9):p. 1804-15.
55. Thebault, S., R.T. Alexander, W.M. Tiel Groenestege, J.G. Hoenderop, and R.J. Bindels, EGF increases TRPM6 activity and surface expression. *J Am Soc Nephrol*, 2009.**20**(1):p. 78-85.
56. Xie, J., B. Sun, J. Du, W. Yang, H.C. Chen, J.D. Overton, . . . L. Yue, Phosphatidylinositol 4,5-bisphosphate (PIP_2) controls magnesium gatekeeper TRPM6 activity. *Sci Rep-UK*, 2011.**1**:p. 146.
57. Nair, A.V., B. Hocher, S. Verkaart, F. van Zeeland, T. Pfab, T. Slowinski, . . . J.G. Hoenderop, Loss of insulin-induced activation of TRPM6 magnesium channels results in impaired glucose tolerance during pregnancy. *Proc Natl Acad Sci U S A*, 2012.**109**(28):p. 11324-9.

58. Martinac, B., The ion channels to cytoskeleton connection as potential mechanism of mechanosensitivity. *Biochim Biophys Acta*, 2014.**1838**(2):p. 682-91.
59. Vriens, J., G. Owsianik, T. Hofmann, S.E. Philipp, J. Stab, X. Chen, . . . T. Voets, TRPM3 is a nociceptor channel involved in the detection of noxious heat. *Neuron*, 2011.**70**(3):p. 482-94.
60. Tóth, B.I., M. Konrad, D. Ghosh, F. Mohr, C.R. Halaszovich, M.G. Leitner, . . . T. Voets, Regulation of the transient receptor potential channel TRPM3 by phosphoinositides. *J Gen Physiol*, 2015.**146**(1):p. 51-63.
61. Numata, T., T. Shimizu, and Y. Okada, TRPM7 is a stretch- and swelling-activated cation channel involved in volume regulation in human epithelial cells. *Am J Physiol Cell Physiol*, 2007.**292**(1):p. C460-7.
62. Numata, T., T. Shimizu, and Y. Okada, Direct mechano-stress sensitivity of TRPM7 channel. *Cell Physiol Biochem*, 2007.**19**(1-4):p. 1-8.
63. Runnels, L.W., L. Yue, and D.E. Clapham, The TRPM7 channel is inactivated by PIP_2 hydrolysis. *Nat Cell Biol*, 2002.**4**(5):p. 329-336.
64. Gwanyanya, A., K.R. Sipido, J. Vereecke, and K. Mubagwa, ATP and PIP_2 dependence of the magnesium-inhibited, TRPM7-like cation channel in cardiac myocytes. *Am J Physiol Cell Physiol*, 2006.**291**(4):p. C627-35.
65. Okada, T., R. Inoue, K. Yamazaki, A. Maeda, T. Kurosaki, T. Yamakuni, . . . Y. Mori, Molecular and functional characterization of a novel mouse transient receptor potential protein homologue TRP7. . *J Biol Chem*, 1999.**274**(39):p. 27359-70.
66. Zhang, X. and M. Trebak, Transient receptor potential canonical 7: a diacylglycerol-activated non-selective cation channel. *Handb Exp Pharmacol*, 2014.**222**:p. 189-204.
67. Kawasaki, B.T., Y. Liao, and L. Birnbaumer, Role of Src in C3 transient receptor potential channel function and evidence for a heterogeneous makeup of receptor- and store-operated Ca^{2+} entry channels. *Proc Natl Acad Sci USA*, 2006.**103**(2):p. 335-40.
68. Tu, C.L., W. Chang, and D.D. Bikle, Phospholipase Cγ1 is required for activation of store-operated channels in human keratinocytes. *J Invest Dermatol*, 2005.**124**(1):p. 187-97.
69. Zeng, W., J.P. Yuan, M.S. Kim, Y.J. Choi, G.N. Huang, P.F. Worley, and S. Muallem, STIM1 gates TRPC channels, but not Orai1, by electrostatic interaction. *Mol Cell*, 2008.**32**(3):p. 439-48.
70. Jardin, I., J.J. Lopez, G.M. Salido, and J.A. Rosado, Functional relevance of the *de novo* coupling between hTRPC1 and type II IP_3 receptor in store-operated Ca^{2+} entry in human platelets. *Cell Signal*, 2008.**20**(4):p. 737-47.
71. DeHaven, W.I., B.F. Jones, J.G. Petranka, J.T. Smyth, T. Tomita, G.S. Bird, and J.W. Putney, Jr, TRPC channels function independently of STIM1 and Orai1. *J Physiol*, 2009.**587**(Pt 10):p. 2275-98.

72. Borbiro, I., D. Badheka, and T. Rohacs, Activation of TRPV1 channels inhibits mechanosensitive Piezo channel activity by depleting membrane phosphoinositides. *Sci Signal*, 2015.**8**(363):p. ra15.
73. Bae, C., F. Sachs, and P.A. Gottlieb, The mechanosensitive ion channel Piezo1 is inhibited by the peptide GsMTx4. *Biochemistry*, 2011.**50**(29):p. 6295-6300.

6 Appendices

6.1 Appendix 1: Heparan sulfate binding proteins

List of proposed HSBP that show an increase in expression in the αβ DP thymocyte populations. The functions of these proteins are described in the Immunological Genome Project (*M. musculus)* database (ImmGen) http://www.immgen.org/databrowser/index.html. In general, data available on the ImmGen website has been derived by profiling gene expression on Affymetrix microarrays using cells from five-week-old C57Bl/6J mice. The DP thymocyte populations of interest are described in the "abT cell" data group.

Gene	Title	Proposed function: from ImmGen data base and, as described in the protein knowledge database UniProtKB: https://www.uniprot.org/uniprot/
Cd8b1	CD antigen, β chain 1	Coreceptor binds MHC class I; T cell signalling pathway
Cd4	CD4 antigen	Coreceptor binds MHC class II; T cell signalling pathway
Fas	TNF receptor family member	Receptor activity MAPK signalling pathway, mediator of apoptosis
Adgre5 (Cd97)	Adhesion G protein coupled receptor (GPCR) E5	Transmembrane signalling receptor
Insr	Insulin receptor	Protein kinase activity; Negative regulation of protein phosphorylation. In response to insulin leads to activation of PI_3K-AKT/PKB signalling pathway
Anxa2	Annexin A2	Phospholipase inhibitor activity; Ca^{2+} dependent PIP_2 binding; raft assembly. Ca^{2+} regulated membrane-binding protein who affinity for calcium is greatly enhanced by anionic phospholipids. May cross link PM phospholipids with actin and the cytoskeleton
Anxa5	Annexin A5	Ca^{2+} dependent phospholipid binding; receptor tyrosine kinase binding
Ptprc (Cd45)	Protein tyrosine phosphatase receptor type C	T cell receptor signalling pathway; interacts with Src family kinases. Acts as a positive regulator of T cell coactivation
Cd47	Rh-related antigen	Cell adhesion; co-stimulates T cell activation. Has a role in cell adhesion and modulation of integrins, may play a role in integrin dependent signal transduction
Lrrc8b	Leucine rich repeat Volume regulating anion channel subunit B	Key player in regulation of cytosolic calcium, make act as leak channel in the ER (Ghosh *et al.* 2017)

6.2 Appendix 2: Expression of HSBP in the abT cell group

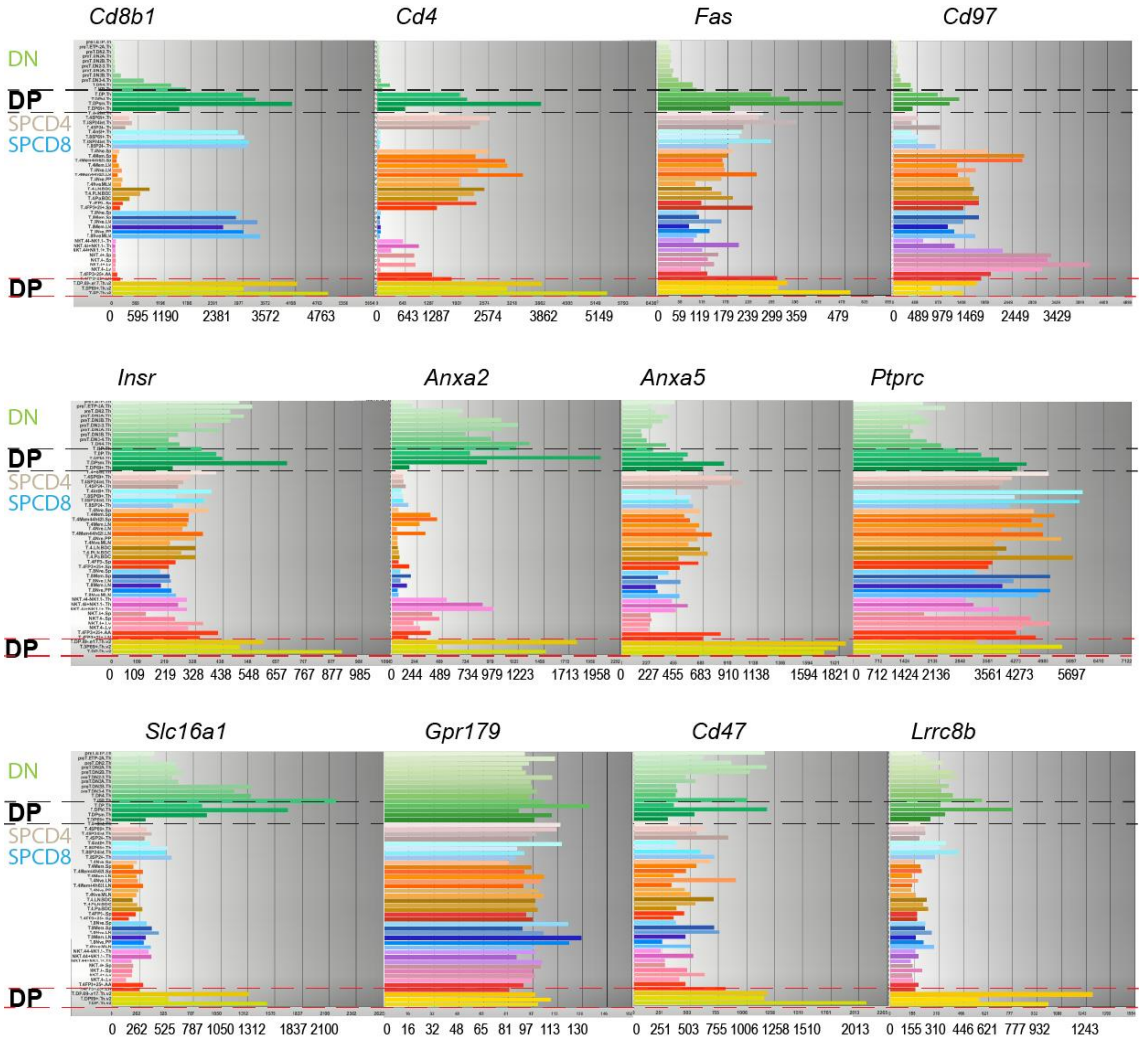

mRNA expression levels of HSBP in the abT cell group as made available in the Immunological Genome Project (*M. musculus)* database (ImmGen). In general, data provided by the ImmGen website has been derived by profiling gene expression on Affymetrix microarrays using cells from five-week-old C57Bl/6J mice. The DP thymocyte populations of interest are described in the "abT cell" data group. http://www.immgen.org/databrowser/index.html. In descending order, the four DP populations framed by the dashed black lines are All; Blasts; Small resting; 69^{+} Early Positive selection. The three DP subpopulations framed by the dashed red lines are DP 69^{-} preselection, DP 69^{+} early positive selection and DP early positive selection.

6.3 Appendix 3: Previously investigated channels

The following channels were investigated to determine if they were required in facilitating the Ca^{2+} influx observed following the addition of DxS to a thymocyte suspension. In the case of all target channels, in the presence of the inhibitory or activating chemicals and DxS, there was no significant change in the time course or amplitude of the DxS induced $[Ca^{2+}]_i$ rise when compared to DxS only treated samples. None of these channels appeared to have a crucial role in facilitating the DxS induced $[Ca^{2+}]_i$ rise.

Target	Chemical	μM	antagonist	agonist
VDCC	Cd^{2+}	200	$Ca_v1.1$, $Ca_v1.2$ $Ca_v1.3$, $Ca_v2.3$	
	Ni^{2+}	30	$Ca_v2.3$, $Ca_v3.2$ $Ca_v3.3$	
CNGA	dequalinium	1	CNGA1, CNGA2	
P2XR	NF449	1 100	P2x1 P2x7	
	Suramin	10 100	P2x1 P2x7	
	PPADs	10 100	P2X1,2,3,5 P2x7	
	ATP	100		P2xR
IP_3R (PM)	TEA	20 mM	IP_3R3	
iGluR	D-AP5	50	NMDAR	
	NBQX	20	AMPAR	
nAChR	atropine	30	nAChRα9, nAChRα8	
	nicotine	100	nAChRα9, nAChRα10	nAChRα4

6.4 Appendix 4: Phylogenetic relationship between TRP genes

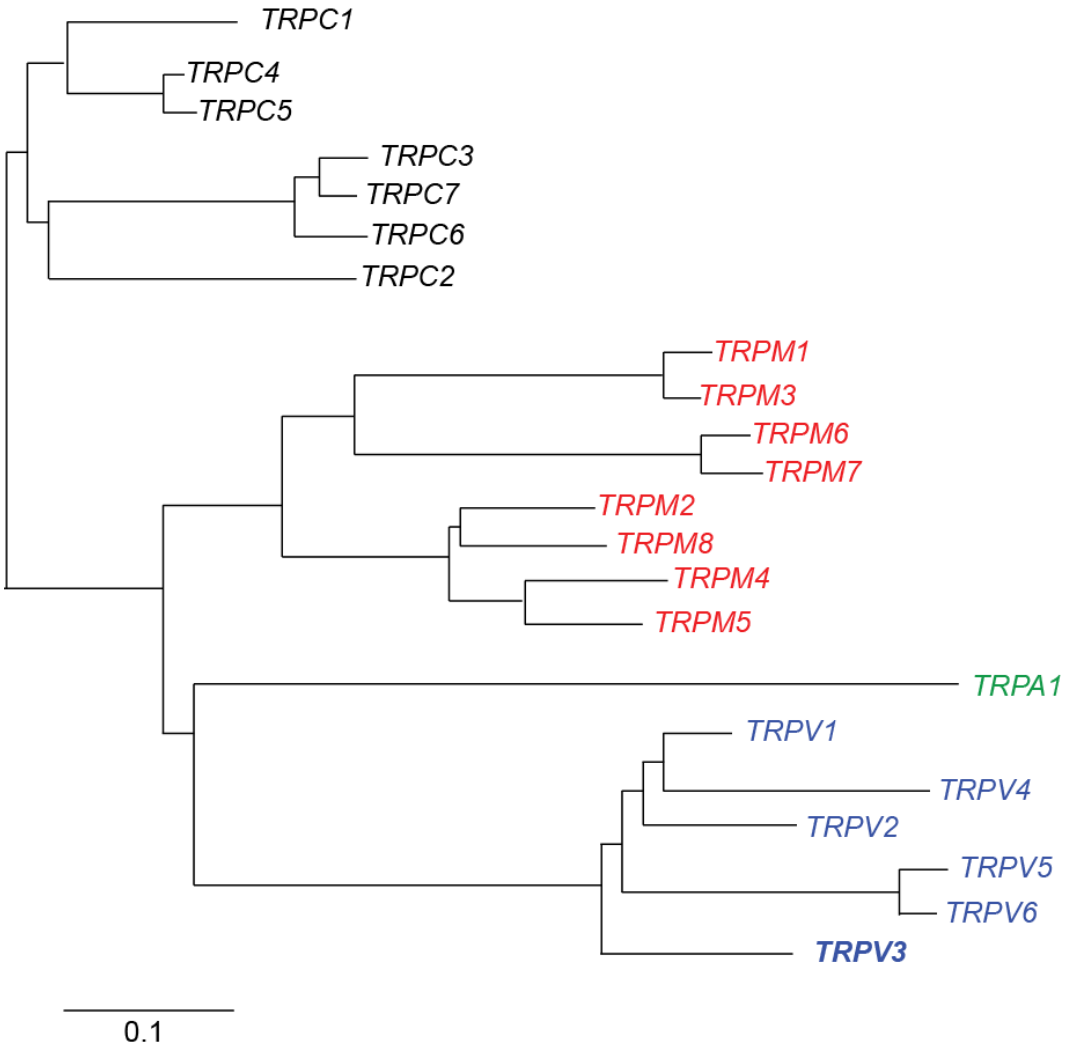

Schematic illustration of the phylogenetic relationship between TRPC, TRPV, TRPA1 and TRPM. Bar represents approximate 10 % variation. Adapted from Minke (2006), and Nilius *et al.* (2014)

6.5 Appendix 5: Commonly used chemicals

Chemical (Cat. No.)	Sourced from
Bovine serum albumin (BSA)	
$CaCl_2.2H_2O$	Merck Pty. Ltd. Vic. AUS
D-glucose	Gibco BRL Life technologies
Donkey serum	Santa Cruz Biotechnology, Inc Dallas TX 75220
Dimethyl sulfoxide (DMSO)	Sigma-Aldrich Gmbh St Louis, MO, USA
F15 Minimum essential media (MEM) powder # 41500-018	lot 1649212x Gibco® Life technologies Carlsbad, CA
Hydrochloric acid (HCl)	Diggers Australia Pty. Ltd. Maddington WA 6109
HEPES	Sigma Aldrich Gmbh St Louis, MO, USA. Santa Cruz Biotechnology, Inc Dallas TX 75220
KCl	Merck Pty. Ltd. Vic. AUS
$MgCl_2.6H_2O$	Ajax Chemicals Pty. Ltd. NSW AUS
NaCl	Merck Pty. Ltd. Vic. AUS
$NaHCO_3$	Merck Pty. Ltd. Vic. AUS
$Na_2HPO_4.H_2O$	Ajax Chemicals Pty. Ltd. NSW AUS
NaOH	Ajax Chemicals Pty. Ltd. NSW AUS
Paraformaldehyde (SLP1627)	ScienceLab.com Inc. Houston TX 77396 USA

6.6 Appendix 6: Orai/STIM gene expression profile

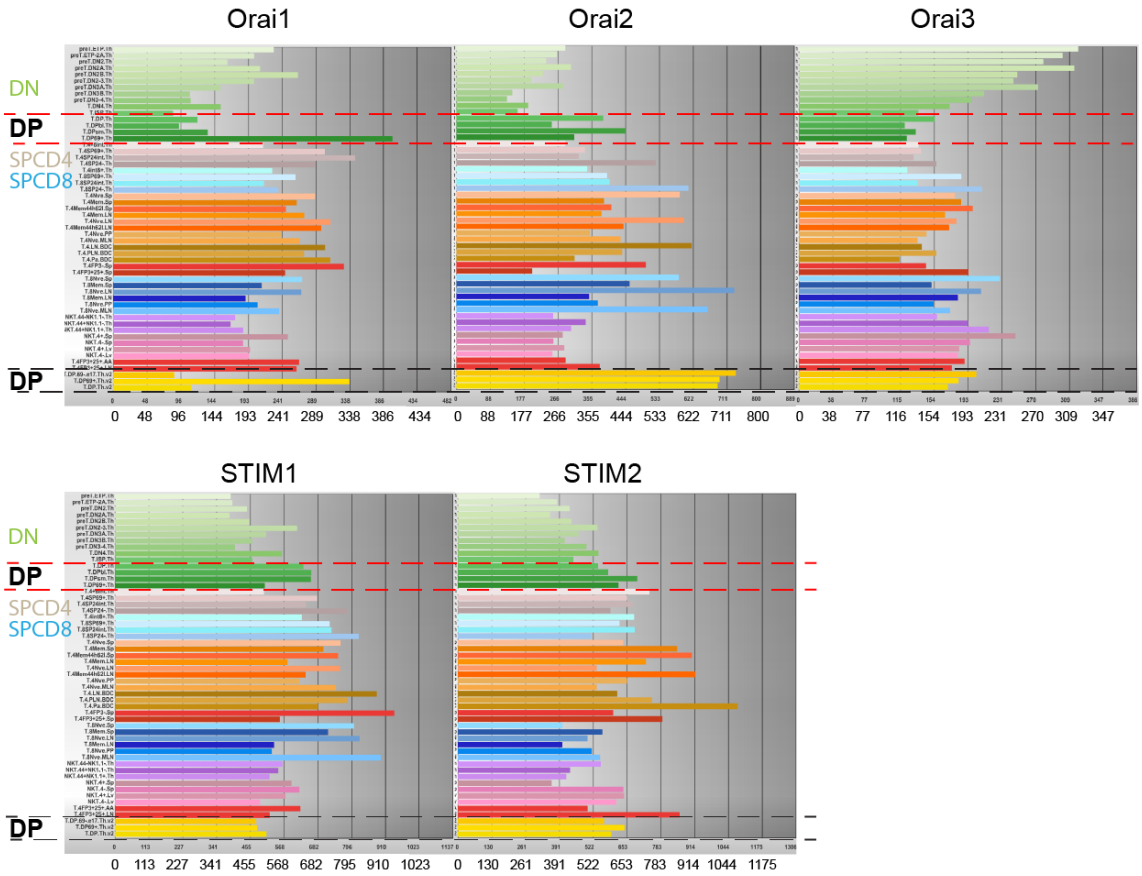

From the Immunological Genome Project (*M. musculus)* (ImmGen) database. The DP thymocyte populations of interest are described in the "abT cell" data group. The four DP populations enclosed by the red broken lines are in descending order: All; Blasts; Small resting; 69+ Positive selection transitional intermediate. In the DP populations Orai2 has the highest expression levels. Although notably, there is an ~ 3-fold increase in Orai1 expression in the "69+ Positive selection transitional intermediate DP" (green) and "DP 69^{+} early selection" (yellow) population. The three DP subpopulations framed by the dashed black lines are in descending order DP 69^{-} preselection, DP 69^{+} early selection, DP early selection. The overall relative transcription level is indicated by the arbitrary numbers below each plot. http://www.immgen.org/databrowser/index.html Probesets: 10525464; 10534570; 10557754; 10555681; 10521950